# LONG-TERM PERFORMANCE OF GEOSYNTHETIC LINER MATERIALS IN LOW-LEVEL RADIOACTIVE WASTE DISPOSAL FACILITIES

By

Kuo Tian

A dissertation submitted in partial fulfillment of the requirements for the degree of Doctor of Philosophy

Civil and Environmental Engineering

At the

UNIVERSITY OF WISCONSIN-MADISON

2015

Date of final oral examination: 6/22/2015

The dissertation is approved by the following members of the Final Oral Committee:

Craig H. Benson, Professor, Civil and Environmental Engineering James M. Tinjum, Associate Professor, Engineering Professional Development Tuncer B. Edil, Professor, Civil and Environmental Engineering Samuel Kung, Professor, Soil Science Douglass Henderson, Professor, Engineering Physics

#### **ABSTRACT**

# LONG-TERM PERFORMANCE OF GEOSYNTHETIC LINER MATERIALS IN LOW-LEVEL RADIOACTIVE WASTE DISPOSAL FACILITIES

#### **KUO TIAN**

Under the Supervision of Professors Craig H. Benson and James M. Tinjum at the University of Wisconsin-Madison

Low-level radioactive waste (LLW) disposal facilities employ geosynthetic liner materials [e.g., high-density polyethylene (HDPE) geomembrane (GM) and geosynthetic clay liner (GCL)] in multilayer barrier systems to control the flux of contaminants into the environment. Long-term durability of geosynthetics in contact with LLW leachate is of particular importance because the design life of LLW barrier systems is commonly 1000 yr.

This study focused on antioxidant depletion in 2-mm-thick HDPE GM immersed in synthetic radioactive leachate (RSL) with chemistry representative of leachate in LLW disposal facilities operated by the U.S. Department of Energy's environmental restoration programs. HDPE GMs were immersed in RSL at elevated temperature (25, 50, 70, and 90 °C), and antioxidant depletion rates were measured by oxidation induction time. Based on Arrhenius modeling, results demonstrate that antioxidant depletion time in 2-mm-thick HDPE GM is approximately 649 yr if correlated to an average field temperature of 15 °C. In separate experimentation, the radiation (e.g., alpha and beta) from LLW leachate had a negligible effect on antioxidant depletion in HDPE GM due to low dosage (2.3 Gy) over the 1000-yr service life and the surface effect of alpha and beta radiation on GM.

This study also evaluated hydraulic conductivity of two conventional sodium-bentonite (CS and GS) and six polymer-bentonite (CPL, GPL, GPM, CPM, GPH, and BPC) GCLs permeated with RSL. *In situ* conditions were simulated with an elevated stress level to mimic a waste body

ii

mass and prehydration of GCLs from subgrade soil. For the CS, GS, CPL, GPL, and GPM GCLs, the hydraulic conductivity permeated with RSL gradually increased by a factor of 5–25 times, with final hydraulic conductivities ranging from 1.3 x  $10^{-10}$  to 7.5 x  $10^{-10}$  m/s at 20 kPa effective stress. In contrast, hydraulic conductivity of the CPM, GPH, and BPC GCLs were very low to RSL ( $\approx 3 \times 10^{-12}$  to 8 x  $10^{-12}$  m/s) due to polymer hydrogel blocking. Increasing the confining stress from 20 kPa to 450 kPa reduced the hydraulic conductivity of CS GCL by approximately two orders of magnitude and eliminated preferential flow for CS GCL hydrated on a subgrade prior to permeation.

8/13/15

Signature

Date

Craig H. Benson, Professor

8/13/15

Signature

Date

James M. Tinjum, Associate Professor

#### **ACKNOWLEDGEMENTS**

First of all, I would like to thank my advisors, Professors Craig Benson and James Tinjum for their guidance and mentorship through my study at University of Wisconsin Madison. Also many thanks to my committee: Professor Tuncer Edil, Professor Samuel Kung, Professor Douglass Henderson, and Professor Grace Hsuan.

I also want to thank Xiaodong Wang and Jackie B. Cooper for their assistance in the lab. Appreciation is also extended to Victor Goretsky and Yuliya Henes from the Department of Environment, Health, and Safety with assistance in the protocols associated with use of radionuclides in the laboratory.

I would like to acknowledge Jiannan Chen and Erin Hunter for their help and friendship during my studies. Thanks are extended to all GLE friends who made my enjoyable experience in Madison.

Most importantly, I would like to express gratitude to my parents Guozhu Tian and Chunfeng Wei, and my fiancée Qian Zhao for their love and support.

The research described in this document was conducted under the sponsorship of the US Department of Energy under Cooperative Agreement Number DE-FC01-06EW07053 entitled The Consortium for Risk Evaluation with Stakeholder Participation III awarded to Vanderbilt University. The opinions, findings, conclusions, or recommendations expressed herein are solely those of the authors and do not necessarily represent the views of the US Department of Energy.

## **TABLE OF CONTENTS**

ABS	TRACT		I
ACK	NOWLED	GEMENTS	
TAB	LE OF CC	NTENTS	IV
LIST	OF FIGU	RES	VIII
LIST	OF TABL	ES	XIV
1	INTROD	UCTION	1
2		CAL CHARACTERISTICS OF LEACHATE IN LOW-LEVEL RADIOACTIVE DISPOSAL FACILITIES	10
	2.1 II	NTRODUCTION	11
	2.2 N	//ETHODS	15
	2.2.1	Leachate Data Collection	15
	2.2.2	Leachate Chemical Analysis	16
	2.3 F	RESULTS AND DISCUSSION	17
	2.3.1	Inorganic Macro-components	20
	2.3.2	Trace Heavy Metals	21
	2.3.3	Radionuclides	23
	2.3.4	Ionic Strength and RMD	26
	2.4	SUMMARY	27
3		ROUND: MECHANISMS FOR THE DEGRADATION OF HIGH-DENSITY THYLENE GEOMEMBRANE	52
	3.1 II	NTRODUCTION	52
	3.2	DEGRADATION MECHANISMS IN GEOMEMBRANE	53
	3.2.1	Degradation due to Swelling	55
	3.2.2	Extraction	55
	3.2.3	Oxidative Degradation	55
	3.2.4	Radiation Effect	57
	3.2.5	UV Degradation	57
	3.3 F	FACTORS AFFECTING THE OXIDATIVE DEGRADATION	58
	331	GM Properties	58

٠	
О	

		`
	3.3.2 Exposure Medium	59
	3.3.3 External Mechanical Stresses	60
	3.4 ANTIOXIDANT DEPLETION	60
	3.5 LIFE TIME PREDICTION METHODS	61
	3.6 LABORATORY STUDIES OF GM DURABILITY	63
	3.7 LIFE TIME PREDICTION STUDIES	66
	3.8 SUMMARY	68
4	ANTIOXIDANT DEPLETION IN HDPE GEOMEMBRANES EXPOSED TO LO RADIOACTIVE WASTE LEACHATE	
	4.1 INTRODUCTION	87
	4.2 BACKGROUND	89
	4.2.1 Degradation of HDPE via Oxidation	90
	4.2.2 Effect of Radiation on Polymer Degradation	91
	4.2.3 Depletion of Antioxidants	
	4.2.4 Arrhenius Model	94
	4.3 MATERIALS AND METHODS	94
	4.3.1 Geomembrane and Exposure Liquids	94
	4.3.2 Immersion Test	95
	4.3.3 Oxidation Induction Time (OIT)	96
	4.3.4 Melt Flow Index (MFI) Test	97
	4.3.5 Crystallinity	97
	4.4 RESULTS AND DISCUSSION	98
	4.4.1 Depletion of Antioxidant	98
	4.4.2 Effect of Radiation on Antioxidant Depletion	102
	4.4.3 Lifetime Prediction	103
	4.4.4 Melt Flow Index (MFI)	104
	4.4.5 Crystallinity	105
	4.5 SUMMARY	106
5	EFFECT OF RADIATION FROM LOW-LEVEL RADIOACTIVE LEACHATE OF ANTIOXIDANT DEPLETION IN HDPE GM	
	5.1 INTRODUCTION	126
	5.2 BACKGROUND	128
	5.2.1 Effect of Radiation on Polymer Degradation	129

	5.2.2	Degradation of HDPE GM in LLW Disposal Facilities	131
	5.3 N	MATERIALS and METHODS	132
	5.3.1	GEANT4 Monte Carlo Simulation Toolkit	133
	5.3.2	HDPE GM Exposed to Sealed Source	134
	5.3.3	OIT Measurement	135
	5.3.4	Multiple-Layer Model for Antioxidant Depletion in HDPE GM	135
	5.4 F	RESULTS and DISCUSSION	137
	5.4.1	Dose Deposition in HDPE GM from Sealed Source	137
	5.4.2	OIT Measurement Results	137
	5.4.3	Dose Deposition in HDPE GM under In Situ Condition	139
	5.5	CONCLUSION	141
6		ROUND: COMPATIBILITY OF GEOSYNTHETIC CLAY LINER IN NMENT APPLICATION	155
	6.1 I	NTRODUCTION	155
	6.2	CONVENTIONAL BENTONITE	156
	6.2.1	Swelling of Conventional Bentonite	156
	6.2.2	Compatibility Study of Conventional GCL	158
	6.2.3	Compatibility of GCLs under In Situ Conditions	159
	6.3 N	MODIFIED BENTONITE	161
	6.3.1	Swell of Modified Bentonite	162
	6.3.2	Compatibility Study of Modified GCL	163
	6.3.3	Compatibility of GCLs under In Situ Conditions	168
	6.4	SUMMARY	168
7		ULIC CONDUCTIVITY OF GEOSYNTHETIC CLAY LINERS PERMEATED EVEL RADIOACTIVE WASTE LEACHATE	
	7.1 I	NTRODUCTION	180
	7.2 E	BACKGROUND	182
	7.2.1	Effect of Ionic Strength and Cation Abundance	182
	7.2.2	Composition of LLW Leachate	183
	7.2.3	Polymer-Bentonite	183
	7.3 N	MATERIALS AND METHODS	185
	7.3.1	Geosynthetic Clay Liner (GCL)	185
	732	Permeant Liquids	187

# **LIST OF FIGURES**

Fig. 2.1.	Top panel: Typical lower layer cross-section for LLW disposal facilities. (Modified from
	Powell et al. 2011). Lower panel: Rodney A. Baltzer, president of Waste Control
	Specialists, with a model of the installed barrier system at the Andrews, TX LLW facility
	(Stravato 2014)40
Fig. 2.2.	Comparison of (a) pH values across LLW sites and (b) pH variation with time. (ERDF:
	the Environmental Restoration Disposal Facility at Hanford, WA; OSDF: the On Site
	Disposal Facility at Fernald, OH; ICDF: the Idaho CERCLA Disposal Facility at Idaho
	Falls, ID; EMWMF: Environmental Management Waste Management Facility at Oak
	Ridge; All LLW contains data for all four LLW sites)41
Fig. 2.3	. Comparison of major cation concentrations at LLW sites. LLW concentrations of
	calcium, Ca (a), magnesium, Mg (b), potassium, K (c), and sodium, Na (d), are
	compared to MSW concentrations42
Fig. 2.4	. Major cation concentrations over time: (a) calcium, Ca; (b) magnesium, Mg; (c)
	potassium, K; and (d) sodium, Na
Fig. 2.5.	Comparison of major anion concentrations in LLW and MSW leachates: (a) sulfate,
	SO <sub>4</sub> <sup>2-</sup> ; (b) chloride, Cl <sup>-</sup> ; and (c) nitrate/nitrite, NO <sub>3</sub> <sup>-</sup> /NO <sub>2</sub> <sup>-</sup> 44
Fig. 2.6.	Changes in major anion concentrations with time: (a) sulfate, SO <sub>4</sub> <sup>2-</sup> ; (b) chloride, Cl <sup>-</sup> ;
	and (c) nitrate/nitrite, NO <sub>3</sub> -/NO <sub>2</sub> 45
Fig. 2.7.	Comparison of trace heavy metal concentrations in LLW and MSW leachates: (a) iron,
	Fe; (b) manganese, Mn; (c) copper, Cu; and (d) barium, Ba46
Fig. 2.8.	Change of trace heavy metal concentrations with time: (a) iron, Fe; (b) manganese,
	Mn; (c) copper, Cu; and (d) barium, Ba47
Fig. 2.9.	Gross alpha and beta activity (in Bq/L) versus time48

Fig. 2.10. Comparison of specific radionuclide concentrations across LLW sites and in MSW,
where applicable: (a) Total Uranium, U; (b) Technetium-99, Tc-99; (c) Strontium-90, Sr-
90; and (d) Tritium, H-349
Fig. 2.11. Change in concentration for specific radionuclides with time: (a) Total Uranium, U; (b)
Technetium-99, Tc-99; (c) Strontium-90, Sr-90; and (d) Tritium, H-350
Fig. 2.12. Comparison of RMD to ionic Strength (I) for LLW and MSW leachates51
Fig. 3.1. Backbone and branches for polyethylene (Note: Figure form Cheng et al. 2011)79
Fig. 3.2. (a) Crystal and Amorphous Region (surface view) (b) Crystal and Amorphous Region
(Cross-section view) (c) Three types of inter-crystalline chains (Note: Figure (a) form
http://web.utk.edu/~mse/Textiles/Polymer%20Crystallinity.htm)80
Fig. 3.3. Oxidation cycles in polyethylene (modified form Grassie and Scott 1985) (Rowe and
Sangam 2002)81
Fig. 3.4. The name of hydrogen and carbon atom: a) primary hydrogen, b) secondary hydrogen,
and c) tertiary hydrogen, and d) name of carbon atom
(http://www.masterorganicchemistry.com)82
Fig. 3.5. The three conceptual stages in chemical aging of HDPE GMs (modified from Rowe and
Sangam 2002)83
Fig. 3.6. Apparatus used for immersion incubation testing of GM (Koerner 2005)84
Fig. 3.7. Apparatus used for column incubation testing of GM (Rowe et al. 2010)85
Fig. 4.1. Oxidation loops for polyethylene [modified from Grassie and Scott (1985) and Rowe
and Sangam (2002)]118
Fig. 4.2. Std-OIT vs. HP-OIT for HDPE geomembranes immersed in DI water (the sample aged
in DI water from right to left: 1 month at 50 °C, 1 month at 70 °C, 2 months at 90 °C,
and 6 months at 90 °C) and initial condition.

Fig. 4.3	. Std-OIT of GM immersed in RSL vs. time and In[OIT] vs. Time; (a) and (b) are 2-
	parameter fitting, (c) and (d) are 3-parameter fitting
Fig. 4.4.	Std-OIT depletion of GM exposed to DI, NSL and RSL as a function of aging time121
Fig. 4.5	. Arrhenius plot of antioxidant depletion for (a) DI water (Current and other studies). (b)
	DI, NSL, and RSL122
Fig. 4.6	Predicted antioxidant depletion time as a function of temperature and immersion liquid.
	123
Fig. 4.7	. Melt Flow Index (a) and Crystallinity (b) of HDPE GM exposed to RSL and NSL at 90
	°C as a function of aging time124
Fig. 5.1	. Oxidation loops for polyethylene [modified from Grassie and Scott (1985) and Rowe
	and Sangam (2002)]146
Fig. 5.2	. GEANT4 Monte Carlo simulation geometry for sealed-source experiments (Note, the
	dimension of the sealed source was based on information provided by the
	manufacturer.)147
Fig. 5.3	. GEANT4 Monte Carlo Simulation geometry for in situ condition, consisting of HDPE
	polymer sandwiched between water and sand. A region in the water is defined to be
	the source of particles
Fig. 5.4.	Multiple-layer model for antioxidant depletion in HDPE GM exposure to radiation149
Fig. 5.5.	. Monte Carlo simulation for dose deposition in HDPE GM with sealed source of (a) Am-
	241 and (b) Tc-99 as a function of depth150
Fig. 5.6	. Dose deposition in HDPE GM exposed to sealed source of 241Am sealed source (a)
	and 99Tc (b) for 1 h, 10 h, and 50 h151
Fig. 5.7	. Oxidation induction time of HDPE GM specimens exposed to sealed sources of (a)
	241Am and (b) 99Tc, along with the fitting curve based on multiple-layer model. (Note:
	the error represents one standard deviation based on three measurement)152

Fig. 5.8. Monte Carlo simulation for dosage deposition from low-level radioactive waste
HDPE GM over 1000 yr as a function of depth1
Fig. 5.9. Prediction of antioxidant depletion in HDPE GM over 1000-yr service life caused by (
alpha radiation and (b) beta radiation1
Fig. 6.1. Swelling index vs. Ionic Strength (Mix cations include monovalent and divalent cation
Data derived from Jo et al. 2001, 2005; Kolstad et al. 2004b; Lee and Shackelfo
2005.)1
Fig. 6.2. Hydraulic conductivity of GCLs permeated with solutions of varying ionic strength a
various valent cations. (Mix cations include monovalent and divalent cations. Da
derived from Jo et al. 2001, 2005; Kolstad et al. 2004b; Lee and Shackelford 2005.)1
Fig. 6.3. Hydraulic conductivity of GCLs permeated with solutions of varying ionic streng
versus swell index test of bentonite derived from the permeated GCLs. (Mix catio
include monovalent and divalent cations. Data derived from Jo et al. 2001, 200
Kolstad et al. 2004b; Lee and Shackelford 2005.)1
Fig. 6.4. Influence of ionic strength on the swell index of natural Na-bentonite and modific
bentonites Literature data for Na-B GCLs are provided for comparison (data derive
from Jo et al. 2001, 2005; Kolstad et al. 2004b; Lee and Shackelford 2005)1
Fig. 6.5. Influence of ionic strength on the hydraulic conductivity of natural Na-bentonite a
modified bentonites for hydraulic compatibility. Literature data for Na-B GCLs a
provided for comparison (data derived from Jo et al. 2001, 2005; Kolstad et al. 2004
Lee and Shackelford 2005)1
Fig. 6.6. Hydraulic conductivity versus swell index for natural Na-bentonite and modific
bentonites. Literature data for Na-B GCLs are provided for comparison (data derive
from Jo et al. 2001, 2005; Kolstad et al. 2004b; Lee and Shackelford 2005)1

Fig. 7.1. RMD vs. ionic strength for LLW and MSW leachates. RSL is shown with diamond
symbol
Fig. 7.2. Grain size distribution for GCLs used in this study (the amount of GPH GCLs was not
sufficient to conduct test for grain size distribution)
Fig. 7.3. Data from hydraulic conductivity test on CS GCL using NSL as the permeant liquid. 208
Fig. 7.4. Concentration of major cations in influent and effluent for test conducted
withconventional CS GCL permeated with NSL: (a) Na, (b) Ca, (c) Mg, and (d) K209
Fig. 7.5. Hydraulic conductivity of GCLs permeated with radioactive synthetic leachate (RSL) vs.
hydraulic conductivity to non-radioactive synthetic leachate (NSL)210
Fig. 7.6. Swell index of bentonite from each GCL in RSL, NSL, and DI water211
Fig. 7.7. Hydraulic conductivity of GCLs to RSL or NSL vs. hydraulic conductivity to DI water.
212
Fig. 7.8. Hydraulic conductivity of polymer-bentonite GCLs as a function of polymer loading213
Fig. 7.9. Image of polymer-bentonite from CPM GCL at 20 x using optical microscope (a) and
SEM image of freeze-dry polymer-bentonite from CPM permeated with DI water (b).
214
Fig. 7.10. Conceptual models for mechanism controlling hydraulic conductivity of sodium
bentonite GCL: (a) bentonite granular, (b) osmotic swelling of sodium bentonite in
dilute solution reduce flow between montmorillonite plate and decrease hydraulic
conductivity215
Fig. 7.11. Conceptual models for mechanism controlling hydraulic conductivity of polymer-
bentonite GCL: (a) hydrogel with bound water, (b) hydrogel clogs intergranular flow
path and yields to low hydraulic conductivity when reduction of swell of bentonite in
leachate216
Fig. 8.1. Data from hydraulic conductivity test on GCL using NSL as the permeant liquid233

Fig.	8.2.	Concentration of (a) Na and (b) Ca and Mg in effluent of GCL permeated with NSL.	234
Fig.	8.3.	Hydraulic conductivity of GCL to DI water, NSL, and RSL at 20 kPa effective st	ress
		after direct permeation or permeation after subgrade hydration.	.235
Fig.	8.4.	Swell index of bentonite in DI water, NSL, and RSL before and after direct permea	ation
		with NSL	.236
Fig.	8.5	. Dye marking preferential flow path in GCL specimen hydrated on subgrade	and
		permeated with RSL	.237
Fig.	8.6.	Hydraulic conductivity vs. effective stress for GCL specimens directly permeated	with
		DL RSL and NSL or permeated with RSL after subgrade hydration	238

## **LIST OF TABLES**

Table 2.1. Radionuclides classified for low-level radioactive waste	32
Table 2.2. Analytical methods used in collection and analysis of LLW, based on inf	ormation
provided by the DOE	33
Table 2.3. Measured parameters of LLW leachate	34
Table 2.4. Radionuclides measured at study LLW sites	37
Table 2.5. Detectable radionuclides at study LLW sites	38
Table 3.1. Geomembrane composition	72
Table 3.2. Type of antioxidants	73
Table 3.3. Arrhenius equation in the literature	74
Table 3.4. Prediction antioxidant depletion times of GM	75
Table 3.5. Estimated of induction time for GM	76
Table 3.6. Estimated GM degradation time for 50% degradation of GMs	77
Table 3.7. Estimated total service lifetime of GM	78
Table 4.1. Properties of HDPE GM	112
Table 4.2. Composition of radioactive synthetic leachate (RSL)	113
Table 4.3. Antioxidant depletion rates in DI, NSL, and RSL leachate	114
Table 4.4. List of antioxidant depletion rate in the literature for different exposure cond	itions for
HDPE geomembrane	115
Table 4.5. Arrhenius equation and activation energies from Fig. 4.6	116
Table 4.6. Prediction of antioxidant depletion time	117
Table 5.1. Oxidation induction time of HDPE specimens with various thickness	145
Table 7.1. Polymer loading, swell index, and concentrations of bound cations in the e	xchange
complex of bentonite in GCLs	201
Table 7.2. Mineralogy of bentonite in GCLs (trc = trace amount)	202

Table 7.3. C	Characteristics of synthetic LLW leachates used in the study2	203
Table 7.4. F	Hydraulic conductivity of GCLs permeated with RSL, NSL, and DI water2	204
Table 7.5. S	Swell index and concentrations of bound cations in the exchange complex2	205
Table 8.1. C	Characteristics of synthetic LLW leachates used in study	230
Table 8.2. F	Hydraulic conductivity of GCLs permeated with RSL, NSL, and DI water2	231
Table 8.3. N	Mole fractions of bound cations of bentonite from GCL initially, after direct permeat	ion
W	vith NSL, and after subgrade hydration2	232

#### 1 INTRODUCTION

In U.S., low-level radioactive waste (LLW) disposal facilities are required to function effectively for at least 1000 yrs (U.S. NRC 2000). Many of these disposal facilities employ multilayer barrier systems to control the flux of contaminants into the surrounding environment. LLW leachate is formed when precipitation flows through waste and dissolves chemical elements by chemical and physical processes. LLW leachate is characterized by near neutral pH and elevated concentration of metals, and radionuclides. LLW leachate is a potential threat to ground and surface water proximate to the landfill area. There is the potential for long-term risks to groundwater stemming from placement of LLW near the ground surface in engineered waste containment facilities that are designed similar to municipal solid waste landfills (MSW). A multilayer liner typically consists of (from top to bottom) a leachate collection layer, primary high-density polyethylene (HDPE) geomembrane (GM), primary geosynthetic clay liner (GCL), leak detection layer, secondary HDPE GM, secondary GCL, and a compacted clay liner. HDPE GM is considered as an impermeable layer to advective flow and, combined with a GCL, provides very low hydraulic conductivity (<10<sup>-10</sup> m/s) and effectively impedes advective contaminate flux. Geosynthetic liner materials play a pivotal role in the overall effectiveness of a barrier system. Long-term performance of geosynthetic materials in contact with LLW leachate is of particular importance because design life may approach 1000 yr (U.S. NRC 2000). This study focuses on antioxidant depletion of 2-mm-thick HDPE GM immersed in synthetic LLW leachate with chemistry representative of leachate in LLW disposal facilities operated by the U.S. Department of Energy's (DOE) environmental restoration programs. Moreover, this study evaluates hydraulic barrier behaviors of conventional and modified GCLs when permeated with synthetic LLW leachate.

HDPE GMs deteriorate due to oxidative degradation, thus degrading over long time frames and losing effectiveness as a contaminate barrier. The most reliable way of assessing non-mechanical degradation is to exhume samples of GM from the field at different time intervals during the service life. However, the first generation of GMs was installed circa 1980, making long-term (100+ yr) field data non-existent. Consequently, accelerated aging tests conducted in the laboratory are used to estimate the service lifetime of HDPE GMs, with particular focus on antioxidant depletion (Hsuan and Koerner 1998, Sangam and Rowe 2002, Gulec et al. 2004, Rowe and Rimal 2008, Rowe et al. 2009). To date, examination of antioxidant depletion in GMs installed in LLW composite liner system is very limited. A primary objective of this research was thus to estimate the rate of antioxidant depletion in 2-mm-thick HDPE GM exposed to radioactive synthetic leachate (RSL) through immersion testing. Additionally, the effects of alpha and beta radiation from LLW were examined to provide a better prediction of the service life of the HDPE GM installed at LLW disposal facilities.

A main concern of GCL barrier performance is the hydraulic conductivity change over the service life. The primary function of GCLs is to limit the advective flow of contaminate liquid due to its low hydraulic conductivity (<10<sup>-10</sup> m/s). GCLs are thin, prefabricated, composite liners consisting of a layer of granular or powdered sodium bentonite (Na-B) sandwiched between two geotextiles. The swelling and hydraulic conductivity of bentonite are sensitive to the chemical characteristics of the liquid that hydrates the bentonite and the permeant liquid. To data, few studies have focused on GCL behavior exposed to LLW leachate. The first objective of this study is to investigate the hydraulic conductivity of GCLs exposed to LLW leachate. Another objective of this research was to compare hydraulic barrier behaviors between conventional Na-B GCLs and P-B GCL to LLW leachate.

This dissertation thesis includes 7 chapters. Chapter 2, titled "Chemical Characteristics of Leachate in Low-level Radioactive Waste Disposal Facilities," presents the composition and characteristics of LLW leachate. This summary is based on leachate data collected by four DOE LLW sites: Environmental Restoration Disposal Facility (ERDF) in Hanford, WA; the On-Site Disposal Facility (OSDF) in Fernald, OH; the Idaho CERCLA Disposal Facility (ICDF) in Idaho Falls, ID; and the Environmental Management Waste Management Facility (EMWMF) in Oak Ridge, TN. Existing data show LLW leachate components can be divided into three groups: 1) inorganic macrocomponents, 2) trace heavy metals, and 3) radionuclides (e.g., uranium, <sup>99</sup>Tc, and <sup>3</sup>H). The LLW leachate contains very low concentration of organic compounds. Summarization of this information provides an approach to predict the behavior of geosynthetic liner materials in LLW disposal facilities. For example, how does HDPE GM deteriorate when in contact with LLW leachate, and how does the hydraulic conductivity of GCL change when exposed to LLW leachate?

Chapter 3, titled "Background: Mechanisms for the Degradation of High-Density Polyethylene Geomembrane," discusses the degradation mechanism of GM and laboratory aging tests that predict the service lifetime of HDPE GM. The degradation of GM can be divided into three stages: 1) antioxidant depletion, 2) induction time to the onset of polymer degradation, and 3) polymer property degradation, which can be affected by different degradation mechanisms (e.g., thermo-oxidation, radiation effect, and ultraviolet light exposure). Many studies have predicted the service lifetime of HDPE GM in barrier liner systems, with particular focus on antioxidant depletion (Hsuan and Koerner 1998, Sangam and Rowe 2002, Gulec et al. 2004, Rowe et al. 2009). The effects of exposure to a chemical environment on GM are generally in accordance with an exposure test. The common approach is to expose the geomembrane to specific synthetic leachate (e.g., synthetic MSW leachate and synthetic acidic mine drainage) at elevated temperature through column or

immersion testing. A comparison of GM properties (e.g., tension properties and stress crack resistance) is then made between original and exposed GM. Antioxidant depletion is sensitive to the leachate composition. Metals in the leachate can lead to increased antioxidant consumption (Osawa and Ishizuka 1973). In addition, a higher concentration of surfactant results in increased of wettability of GM, thus leading to higher diffusive loss of antioxidants (Rowe and Rimal 2008). Without protection of antioxidants, a GM is vulnerable to oxidative degradation and rapidly progresses into the second and third stages of degradation (Grassie and Scott 1985).

Chapter 4, titled "Antioxidant Depletion in HDPE Geomembranes Exposed to Low-Level Radioactive Waste Leachate," predicts antioxidant depletion time of 2-mm-thick HDPE GM through immersion testing. GMs were immersed in three different media: radioactive synthetic leachate (RSL), non-radioactive synthetic leachate (NSL), and deionized water (DI) at 25, 50, 70, and 90 °C. Characteristics of the leachates were based on a review of leachate analysis compiled with data from the DOE (Chapter 2). The synthetic leachates used in the experiments were chemically identical, except one leachate was prepared without radionuclides (NSL) and the other with radionuclides (RSL). The concentrations of radionuclides in the LLW leachate resemble the highest concentrations observed at the DOE facilities and are intended to represent a worst-case scenario. Change in properties of HDPE GM was examined by periodic testing of the aged sample and comparison to the original properties. Comparing the antioxidant depletion rates between the RSL and NSL groups leads to a conclusion that low radiation activity may have negligible effects on antioxidant depletion. Depletion of antioxidant is the main focus in this chapter. Arrhenius modeling was used to predict antioxidant depletion by extrapolating experimental data at high temperature to at a specific field temperature. The antioxidant depletion time of the 2-mm-thick HDPE GM is approximately 649 yr at 15 °C under in situ condition.

Chapter 5, titled "Effect of Alpha and Beta Radiation from Low-Level Radioactive Waste Leachate on Antioxidant Depletion in HDPE GM," investigates the effect of radiation on antioxidant depletion in 2-mm-thick HDPE GM. The HDPE GM specimens were exposed to <sup>241</sup>Am (alpha particles) and <sup>99</sup>Tc (beta particles) from a sealed sources to simulate radiation from LLW leachate (e.g., <sup>234</sup>U, <sup>235</sup>U, <sup>238</sup>U and <sup>99</sup>Tc). GM specimens were prepared using a Dayton #6536 Model film-blowing machine to thickness of 0.04 mm, 0.1 mm, 0.2 mm, and 2 mm. The specimens were exposed to sealed sources for 1-50 h, followed by OIT testing to determine the depletion of antioxidant. A GEANT4 model was built to investigate the dose deposition in HDPE GM when exposed to sealed sources. Alpha particles from <sup>241</sup>Am can penetrate about 28 µm into HDPE GM, whereas beta particles from <sup>99</sup>Tc can penetrate 0.48 mm into HDPE GM. The surface dosages in HDPE GM were approximately 50000 Gy and 0.3 Gy after exposure to <sup>241</sup>Am and <sup>99</sup>Tc, respectively from sealed sources for 50 h. The physical dose deposition for both particles largely occurred on the superficial layers and decreased monotonically with depth to a negligible dose. The OIT of 0.04-mmthick GM decreased from 185 min to 158 min after exposure to a sealed source of <sup>241</sup>Am for 50 h, whereas the OIT of 2-mm-thick GM had no change after exposure. Similar OIT results were observed for HDPE GM exposed to a sealed source of 99Tc. Thus, alpha and beta radiation likely only affects antioxidant at the surface of HDPE GM. The effect of radiation from LLW leachate was modeled using GEANT4. The total dosage was approximately 2.4 Gy over the 1000-yr life cycle. This relatively low dosage is likely to have a negligible effect on antioxidant depletion in HDPE GM installed in LLW disposal facilities.

Chapter 6, titled "Background: Compatibility of Geosynthetic Clay Liner in Containment Application," summarizes previous study on hydraulic barrier behavior of GCL for waste containment applications. The hydraulic conductivity of GCLs can be affected by chemical interactions between the bentonite and contained liquid. GCLs permeated with more

aggressive leachates having higher ionic strength and/or a predominance of polyvalent cations can be orders of magnitude more permeable than GCLs permeated with deionized (DI) or tap water (Petrov and Rowe 1997, Jo et al. 2001, Kolstad et al. 2004, Jo et al. 2005). Limited information in the literature discusses the hydraulic barrier behavior of GCL exposed to LLW leachate; thus, reviews of *in situ* studies of the hydraulic conductivity of GCLs exposed to MSW leachate (Petrov and Rowe 1997) have been used as an indicator, as LLW leachate has similar inorganic salts (e.g. Ca²+, Mg²+, K+, and Na+) to MSW leachate (see Chapter 2). Recognizing this deficiency for long-term applications, many researchers has been investigate modified bentonite with organic molecules (Onikata et al. 1996, Tranger and Darlington 2000, Di Emidio et al 2010). Organic molecules are intercalated in the interlayer of montmorillonite to increase the adjacent platelet space, thus increasing the swelling of montmorillonite. In addition, some organic molecules are superabsorbent and clog the flowpaths. The modified GCLs exhibited better hydraulic barrier performance than conventional GCLs (Onikata et al. 1996, Katsumi et al. 2008)

Chapter 7, titled "Hydraulic Conductivity of Geosynthetic Clay Liner Exposed to Low-Level Radioactive Leachate," evaluates how typical LLW leachates in facilities operated by the U.S. Department of Energy's Environmental Management Division affect the swelling of bentonite and the hydraulic conductivity of GCLs. Experiments were conducted to evaluate the hydraulic conductivity of geosynthetic clay liners (GCLs) to leachate from low-level radioactive waste (LLW). Eight commercially available GCLs were evaluated. Two of the GCLs (CS and GS) contained conventional Na-B and the others contained P-B mixture and composite (CPL, CPM, BPC, GPL, GPM, and GPH). All GCLs (except CPL and GPL) were permeated directly with two synthetic LLW leachates that are chemically identical, except one leachate was prepared without radionuclides (non-radioactive synthetic leachate, or NSL) and the other with radionuclides (radioactive synthetic leachate, or RSL). Control tests were

conducted with deionized (DI) water. Hydraulic conductivities of the GCLs permeated with RSL and NSL were identical. For the CS and GS GCLs permeated with RSL and NSL, the hydraulic conductivity gradually increased by a factor ranging between 5–25 times than DI water at 20 kPa due to divalent cations in synthetic leachate replacing the native sodium. The CPL, GPL, and GPM GCLs with low polymer loading (1.6–3.3%) had similar hydraulic conductivity as the conventional GCLs. In contrast, the CPM, GPH, and BPC GCLs with high polymer loading (>5%) had low hydraulic conductivity (~10<sup>-12</sup> m/s) to all permeant liquids.

Chapter 8, titled "Effect of Low-Level Radioactive Waste Leachate on Hydraulic Conductivity of a Geosynthetic Clay Liner", investigates the effect of effective stress and subgrade soil hydration on hydraulic conductivity of a GCL exposed to LLW leachate. Experiments were conducted to evaluate how permeation with leachate from low-level radioactive waste (LLW) disposal facilities affects the hydraulic conductivity of a geosynthetic clay liner (GCL) with conventional sodium bentonite. GCL specimens were permeated with RSL and NSL, which representative of leachates in LLW disposal facilities operated by the U.S. Department of Energy. NSL is identical to RSL, but contains no radionuclides. Control tests were conducted with DI water. GCLs permeated directly with RSL and NSL (no prehydration step) had near-identical hydraulic conductivity (~ 3 x 10<sup>-10</sup> m/s) at 20 kPa effective stress and were approximately 10 times more permeable to leachate than to DI water. Hydrating the GCL on a subgrade soil resulted in higher hydraulic conductivity at lower stresses, primarily due to a reduction in swell potential of the bentonite due to cation exchange from the subgrade. GCLs hydrated on subgrades exhibited preferential flow through localized areas. Increasing the confining stress from 20 to 450 kPa reduced the hydraulic conductivity by approximately two orders of magnitude for both leachates, and eliminated preferential flow for GCLs hydrated on a subgrade prior to permeation.

#### REFERENCE

- Benson, C., Wang, X., Gassner, F., and Foo, D. (2008). Hydraulic conductivity of two geosynthetic clay liners permeated with an aluminum residue leachate. *GeoAmericas* 2008, International Geosynthetics Society.
- Di Emidio, G., Van Impe, W., and Mazzieri, F. (2010). A polymer enhanced clay for impermeable geosynthetic clay liners. *Proceedings of Sixth International Conference on Environmental Geotechnics*, International Society for Soil Mechanics and Geotechnical Engineers, New Delhi, India, 963–967.
- Farquhar C. and Rovers, F. (1973). Gas production during refuse decomposition. *Water Air Soil Pollut.*, 2, 483–495.
- Gulec, S., Edil, T., and Benson, C. (2004). Effect of acidic mine drainage on the polymer properties of an HDPE geomembrane. *Geosynthet. Int.*, 11(2), 60–72.
- Grassie, N. and Scott, G. (1985). *Polymer Degradation and Stabilization*. Cambridge University Press, New York, USA, 222.
- Hsuan, Y., and Koerner, R. (1998). Antioxidant depletion lifetime in high density polyethylene GMs. *J. of Geotech. and Geoenviron. Engr.*, 124(6), 532–541.
- Katsumi, T., Ishimori, Ho, Onikata, M., and Fukagawa, R. (2008). Long-term barrier performance of modified bentonite materials against sodium and calcium permeant solutions. *Geotextiles and Geomembranes*, 26(1), 14–30.
- Kolstad, D., Benson, C., and Edil, T. (2004). Hydraulic conductivity and swell of nonprehydrated GCLs permeated with multi-species inorganic solutions. *J. of Geotech. and Geoenviron. Engr.*, 130(12), 1236–1249.
- Jo, H., Katsumi, T., Benson, C., and Edil, T. (2001). Hydraulic conductivity and swelling of non-prehydrated GCLs permeated with single species salt solutions. *J. of Geotech. and Geoenviron. Engr.*, 127(7), 557–567.
- Jo, H., Benson, C., Shackelford, C., Lee, J., and Edil, T. (2005). Long-term hydraulic conductivity of a non-prehydrated geosynthetic clay liner permeated with inorganic salt solutions. *J. of Geotech. and Geoenviron. Engr.*, 131(4), 405–417.
- Meer, S. and Benson, C. (2007). Hydraulic conductivity of geosynthetic clay liners exhumed from landfill final covers. *J. of Geotech. and Geoenviron. Engr.*, 133(5), 550–563.
- Onikata, M., Kondo, M., and Kamon, M. (1996). Development and characterization of a multiswellable bentonite. *Environmental Geotechnics*. *Taylor and Francis, Rotterdam*, 587–590.
- Petrov, R. and Rowe, R. (1997). Geosynthetic clay liner (GCL)-chemical compatibility by hydraulic conductivity testing and factors impacting its performance. *Canadian Geotechnical J.*, 34, 863–885.
- Ruhl, J. and Daniel, D. (1997). Geosynthetic clay liners permeated with chemical solutions and leachates. *J. of Geotech. and Geoenviron. Engr.*, 123(4), 369–381.
- Rowe, R., Islam, M. and Hsuan, Y. (2009). Ageing of HDPE geomembrane exposed to air, water and leachate at different temperatures. *Geotextiles and Geomembranes*, 27, 137–151

- Rowe, R. and Rimal, S. (2008). Depletion of antioxidants from an HDPE geomembrane in a composite liner. *J. of Geotech. and Geoenviron. Engr.*, 134 (1), 68–78.
- Sangam, H., and Rowe, R. (2002). Effects of exposure conditions on the depletion of antioxidants from high-density polyethylene (HDPE) geomembrane. *Can. Geotech. J.*, 39, 1221–1230.
- Shackelford, C., Sevick, G., and Eykholt, G. (2010). Hydraulic conductivity of geosynthetic clay liners to tailings impoundment solutions. *Geotextiles and Geomembranes*, 28(2), 206–218
- Trauger, R. and Darlington, J. (2000). Next-generation geosynthetic clay liners for improved durability and performance. *TR-220*. Colloid Environmental Technologies Company, Arlington Heights, 2–14.
- U.S. Nuclear Regulatory Commission (U.S. NRC). (Oct. 2000). Assessment Methodology for Low Level Radioactive Waste Disposal Facilities.

2 CHEMICAL CHARACTERISTICS OF LEACHATE IN LOW-LEVEL RADIOACTIVE
WASTE DISPOSAL FACILITIES

ABSTRACT

Leachate from low-level radioactive waste (LLW) is a potential pollutant to groundwater and surface water due to the presence of heavy metals and radionuclides. Many LLW disposal facilities have been built in the U.S.; however few studies have focused on the composition and characteristics of LLW leachate. Leachate data presented in this paper were collected at and analyzed by four LLW disposal facilities associated with the U.S. Department of Energy (DOE). Pollutants in LLW leachate can be categorized into three groups: inorganic macro-components, trace heavy metals, and radionuclides. As municipal solid waste (MSW) leachate has been thoroughly investigated in prior studies, cross-comparison allows more detailed characterization of LLW. LLW leachate contains little organic carbon and concentrations of inorganic macro-components and trace heavy metals that remain relatively constant over time. However, the concentrations of certain radionuclides (total uranium, tritium, technetium-99, and strontium-90) are significant in LLW leachate. Characterization of LLW leachate provides critical base-line information for design of future LLW containment structures.

**Keywords:** radioactive wastes, landfills, waste management, leachate

#### 2.1 INTRODUCTION

Low-level radioactive waste (LLW) is nuclear waste primarily generated by government facilities, industries, and medical diagnostic processes. LLW is distinguished from waste materials incidental to processing, high-level waste, and uranium mill tailings (U.S. NRC 2002). LLW typically contains waste items such as contaminated protective shoe covers and clothing, reactor water treatment residues, equipment and tools, luminous dials, medical tubes, and other items incidental to radioactive work (U.S. NRC 2002). LLW, like all radioactive waste, is characterized by radioactive decay, a process in which an unstable atomic nucleus loses energy by emitting ionizing particles. The half-life (t<sub>1/2</sub>), or the time required for half of the original radioactive material to decay, of some radionuclides requires hundreds, or even millions of years. As examples of radionuclides potentially present in LLW, the t<sub>1/2</sub> of <sup>90</sup>Sr is 28.8 years while the t<sub>1/2</sub> of <sup>79</sup>Se is 0.327 million years. The radioactivity of LLW can range from just above natural background levels to highly radioactive levels in certain cases (e.g., parts from inside reactor vessels at nuclear power plants).

LLW is generally disposed in near-surface facilities designed and constructed to prevent contamination to the surrounding environment. A multi-liner system is typically used to isolate LLW. Similar to municipal solid waste (MSW) landfill facilities, multi-layer systems for LLW consist of low permeability liners, a leachate collection system (LCS), a leak detection system (LDS), and a groundwater monitoring system, as shown in Fig. 2.1. Additionally, LLW is commonly packaged in steel, concrete, lead, or other encased disposal containers (U.S. NRC 2002). Based on reports from the U.S. Department of Energy (DOE), DOE disposal facilities received over 3.3 × 10<sup>6</sup> m³ of LLW through 1997 (U.S. DOE OEM 2000). Further, an estimated 8.1 x 10<sup>6</sup> m³ of additional LLW will be disposed in DOE facilities by 2070 (U.S. DOE OEM 2000). DOE disposal facilities include those associated with the

Waste Management Program (1.5  $\times$  10<sup>6</sup> m³), current Comprehensive Environmental Response, Compensation, and Liability Act (CERCLA) sites (5.4  $\times$  10<sup>6</sup> m³), and planned future CERCLA facilities (3.9  $\times$  10<sup>5</sup> m³) (U.S. DOE OEM 2000).

The containment and isolation of LLW over a design lifetime that may exceed 1000 yr is procedurally different than that of MSW disposal and containment. LLW barrier systems are expected to provide low permeability, low diffusivity, and effective retardation to minimize long-term contaminant migration. Grambow (2008) identified the need for characterizing the stability of radioactive waste forms on a three-fold basis: homogeneity of the waste, low long-term dissolution rates, and low interfacial solution concentrations of mobile radionuclides. These factors can be contextualized in the short-term by evaluating the composition of leachate from LLW disposal facilities.

During the operational life of a LLW facility, leachate originates as precipitation that subsequently travels through the waste layers and the containment system. Solid contaminants dissolve in the infiltrating water through a combination of physical, chemical, and microbial processes and interactions within the waste (Christensen and Kjeldsen 1989). The leachate poses a potential risk to groundwater and surface water, dependent on the chemical composition. Specific radionuclides identified by the NRC Regulation 10 CFR 61.55 (2001), Inyang et al. (2009), and Kaplan et al (1998) and noted for their inclusion in LLW are highlighted in Table 2.1.

Two main factors control the transport of radionuclides: radionuclide speciation and barrier attenuation processes. Radionuclides can display both cationic ( $^{60}$ Co,  $^{137}$ Cs, and  $^{90}$ Sr) and anionic ( $^{129}$ I,  $^{79}$ Se, and  $^{99}$ Tc) tendencies as a consequence of speciation (Wang et al. 2010). Cationic behavior, where the species of interest has a positive charge, is typically characterized by increasing sorption with increasing system pH, while anionic species, those with negative charge stemming from excess electrons, have decreasing sorption with

increasing system pH. The opposing pH and ionic tendencies exhibited by various radionuclides create difficulties in finding methods and materials to address full suites of behaviors resulting from mixed waste streams. Um and Serne (2005) reported that 99Tc and <sup>125</sup>I, acting as anions, had no or little sorption affinity, respectively, across a range of pH values for sediments from the Hanford LLW disposal facility site, suggesting ease of transport outside of containment. 75Se, although also an anion, demonstrated increased sorption affinity, indicating intermediate retention to the Hanford soils, while 90Sr, acting as a cation, had significant sorption affinity, suggesting strong retention (Um and Serne 2005). The high mobility of <sup>99</sup>Tc in soils arises in part from repulsion of its anionic species (<sup>99</sup>TcO<sub>4</sub>-) to the increasing negative surface charge of soils above neutral pH (Zachara et al. 2007), while <sup>90</sup>Sr can be strongly retarded due to having similar chemical properties and behaviors as Ca (Rimstidt et al. 1998). In addition to the influence of speciation on sorption behavior, radionuclides, like other metals, can display multiple sorption mechanisms, often dependent on the pH of the system. As an example, Missana et al. (2004) indicated that Cs sorption typically results from ion exchange for molecules of higher affinity, while U experiences both ion exchange at low pH and surface complexation above pH 6. Consequently, even though many radionuclides may be present in LLW, there is the possibility that some may not be present in LLW leachate due to low initial concentrations and attenuation processes occurring during transport through the waste. Further, the presence of additional materials (such as calcium, carbonate, and organics), coupled with interactions between multiple radionuclides can alter the potential sorption mechanisms. Viable mechanisms affecting sorption may differ between radionuclide and barrier material combinations, but the potential for sorption is primarily controlled by factors influenced directly by the leachate composition and chemistry. Truly effective systems must account for all facets affecting sorption within a disposal system to understand relational impacts between components.

Few studies have been published summarizing the concentration of radionuclides and other chemical components in LLW leachate. Without this baseline information, the impact of LLW leachate on the surrounding environment would be difficult to estimate in the event of a disposal facility leakage. Moreover, limited information is available in the literature focused on the behavior of barrier system components in contact with LLW leachate, such as the long-term durability of HDPE geomembranes, hydraulic conductivity of geosynthetic clay liners (GCLs), and sorption capacity of barrier soils exposed to LLW leachate. Many studies have evaluated natural and geosynthetic material behavior in containment applications. For example, Rowe et al. (2009) conducted a ten-year study on the durability of HDPE geomembrane in MSW barrier systems through immersion testing with synthetic MSW leachate based on the Keele Valley Landfill leachate, while Gulec et al. (2004) studied the effects of acid mine drainage (AMD) on HDPE geomembrane properties with synthetic AMD leachate. Studies have determined the hydraulic conductivity of GCLs exposed to inorganic salt solutions (Jo et al. 2005), aluminum residue leachate (Benson et al. 2008a), alkaline solutions (Gates and Bouazza 2010), and MSW leachate (Rosin-Paumier and Touze-Foltz 2012), as well as in composite liner systems (Rowe 2005). Compared with these solutions, LLW leachate has an important additional component — radionuclides, where the implication for radiation affects on the long-term behaviors of geosynthetic materials remains unclear.

The primary objective of this paper is thus to analyze the leachate composition from four LLW disposal facilities associated with the DOE, as described in the following section. Based on data from the four disposal facilities, LLW leachate composition was divided into three categories. To better understand the materials present in LLW, LLW leachate was compared to MSW leachate. As MSW leachate has been extensively studied (Christensen and Kjeldsen 1989, 1995, Christensen et al. 1998, Fatta et al. 1999, Saarela 2003, Mor et al. 2006), the range of chemicals present in MSW have been summarized and temporal

concentration changes comprehensively discussed. Comparison between LLW and MSW leachates can provide an approach to better understanding both the inert and radioactive components of LLW leachate. Further, understanding of LLW leachate composition can be used to help predict natural and geosynthetic liner material behavior in LLW disposal facilities.

### 2.2 METHODS

#### 2.2.1 Leachate Data Collection

Leachate was collected at four DOE-operated LLW disposal facilities: the Environmental Restoration Disposal Facility (ERDF) in Hanford, WA; the On-Site Disposal Facility (OSDF) in Fernald, OH; the Idaho CERCLA Disposal Facility (ICDF) in Idaho Falls, ID; and the Environmental Management Waste Management Facility (EMWMF) in Oak Ridge, TN.

Built in 1996, ERDF only accepts LLW generated from environmental restoration activities pertaining to CERCLA requirements at the Hanford site (U.S. DOE 2012). The capacity of ERDF increased to  $1.64 \times 10^7$  tons of waste with the addition of two disposal cells completed in January 2011. LLW at the site includes contaminated soil, waste, and debris generated from building demolition. Monitoring of the LLW leachate began in 1999.

OSDF was designed for the cleanup of the Fernald, Ohio, site on behalf of the DOE and occupies approximately 36 ha (Powell et al. 2011). OSDF comprises eight individual cells, with the last cell closed in 2006 (Powell et al. 2011). The project was completed in 2006. Approximately  $2.25 \times 10^6$  m³ of contaminated soil and foundations were excavated to achieve cleanup levels established by the U.S Environmental Protection Agency (EPA). The leachate data in this paper were collected from 2005 to 2010.

ICDF is a disposal facility accepting both LLW and mixed low-level radioactive waste (MLLW) generated from remediation activities at the Idaho National Laboratory (Benson et al.

2007). ICDF's first landfill cell and the evaporation pond were completed in September 2003.

A second cell began receiving waste in February 2006. The included leachate data represent only the LLW portions of the facility and were collected from 2003 to 2010.

EMWMF, with a total capacity of approximately  $1.3 \times 10^6$  m³, is approved for disposal of LLW as defined in Subtitle C of the Resource Conservation and Recovery Act, as well as hazardous wastes defined by the Toxic Substances Control Act (Benson et al. 2008b). Contaminated soils and demolition debris dominate the waste stream at EMWMF. EMWMF began to accept LLW in 2003, and the leachate data discussed covers the years from 2003-2010.

LLW leachate samples are collected from the LCS installed at each of the 4 sites. Samples were collected in plastic or glass bottles that have been cleaned and rinsed with reagent water, following the EPA's SW 846. At OSDF, samples were collected from sample ports at the bottom of the LCS. If the volume of a sample from the discharge lines was insufficient, the samples were collected from LCS tanks using dedicated Teflon bailers.

### 2.2.2 Leachate Chemical Analysis

Various analytical methods, as deemed appropriate by the separate facilities, were used to determine the chemical composition of the leachates. Table 2.2 lists the specific analytical methods that were used in analyzing the leachate at each site. EPA methods 9060 and 415.1 were used to analyze total organic carbon (TOC) in LLW leachate at the OSDF and EMWMF sites, respectively. Inductively coupled plasma-atomic emission spectrometry (ICP-AES) was used per EPA method 6010C as part of SW-846 to determine metals in solution at all four LLW sites. Sulfate and chloride were measured via ion chromatography through EPA method 300.0.

Standardized methodology was not used for the radiological analyses at all four sites. For uranium, both alpha spectroscopy and relevant methods within EPA SW-846 were used for analysis. Beta-emitting isotopes were detected by liquid scintillation counting at all four sites, and different gamma rays were collected and analyzed by a gamma-ray spectroscopy system.

#### 2.3 RESULTS AND DISCUSSION

The concentration of LLW leachate compositions varied significantly between the 4 disposal facilities. In general, LLW leachate components can be grouped into three categories (accompanying tables are listed):

- i) Inorganic macro-components including major cations ( $Ca^{2+}$ ,  $Mg^{2+}$ ,  $K^+$ , and  $Na^+$ ) and major anions ( $Cl^-$ ,  $SO_4^{2-}$ ,  $HCO_3^-$ , and  $NO_3^-/NO_2^-$  (Table 2.3)
- ii) Trace heavy metals, such as Al, As, Ba, Cu, Fe, Li, Mn, Ni, Sr, and Zn (Table 2.3)
- iii) Radionuclides (Tables 2.4 and 2.5).

Kjeldsen et al. (2002) divided MSW leachate compositions into four categories: dissolved organic matter, inorganic macro-components, heavy metals, and xenobiotic organic compounds. Two of the three groups are common to both MSW and LLW leachate (namely inorganic macro-components and heavy metals); however, LLW leachate contains higher radionuclide concentrations and lacks xenobiotic organic compounds due to a lack of organic wastes within the overall waste composition. Other elements, such as Se, Hg, Ag, and Co, may be found in LLW leachate, but are generally at concentrations near or below method detection limits (MDLs), and are therefore less important for understanding the overall leachate composition. Volatile organic compounds were also measured at the LLW sites, but concentrations were below MDLs.

Total organic carbon (TOC) is an important MSW leachate parameter dependent on the presence of organic degradation products, as indicated by Kjeldsen et al. (2002) with the inclusion of dissolved organic matter as a MSW leachate category. The decomposition of organic matter generates components with varying molecular weight, ranging from small volatile acids to refractory fulvic- and humic-like compounds (Chian and Dewalle 1977). Low concentrations of total organic carbon were measured at the three reporting LLW sites (ICDF data did not contain TOC measurements), ranging from 0.86 to 48.1 mg/L, with a mean of 7.78 mg/L (Table 2.3). Comparatively, Kjeldsen et al. (2002) reported that the concentration of total organic matter in MSW was between 30 and 29000 mg/L. The very low TOC concentrations in LLW leachate are likely a result of waste composition. As mentioned previously, LLW is generated by government, industries, and medical facilities and contains a high percentage of inorganic components and very little organic matter, due to the significant presence of contaminated soil and debris. Alternatively, MSW waste includes organic rubbish, such as food, yard trimmings, cloth, and leather items (Daskalopoulos et al. 1998). Due to the low concentrations of TOC in LLW, organic matter has been not been considered a significant component of the leachate. Therefore, the composition of LLW leachate is divided into three categories, similar to those described for MSW, with the third category comprised of radionuclides.

Table 2.3 presents the measured leachate parameters based on field data from the four LLW sites as well as comparisons to MSW sites. LLW leachate data from OSDF, ERDF, and ICDF exhibit relatively constant component concentrations over time, while the leachate components at EMWMF temporally vary. Across the 4 sites, LLW leachate contains very low concentrations of organic carbon, low heavy metal concentrations, and concentrations of inorganic macro-components comparable to MSW leachates. The concentrations of all

detected radionuclides at the four LLW sites are shown in Table 2.4; however, only four isotopes are considered to be significant: total Uranium, <sup>3</sup>H, <sup>90</sup>Sr and <sup>99</sup>Tc.

Few studies have focused on the decay processes of LLW leachate, and no clear decomposition phases have been observed. However, the decomposition mechanisms and leachate composition of MSW have been comprehensively studied for several decades (Farquhar and Rovers 1973, Ehrig 1988, Christensen and Kjeldsen 1989, Kjeldsen et al. 2002). Comparisons are made between the chemical composition of LLW leachate and MSW leachate, in order to provide better context to understand LLW leachate composition.

The pH for LLW leachate changes over a relatively small range (5.7-9.1) and most pH data only range from 6-8 (Fig. 2.2 (a)). Fig. 2.2(b) shows that pH for LLW leachate did not change with time at any of the four sites. The pH temporal consistency may be due to the lack of organic materials found in LLW, leading to little pH change expected during the waste stabilization process. Zachara et al. (2007) found that for natural sediments in the Hanford vadose zone the pH range is approximately 7 to 8.5. Since the major waste source at ERDF is contaminated Hanford soil, the pH of the LLW leachate mirrors that of the waste. In contrast, the pH of MSW leachate changes significantly during landfill decomposition, described by Farquhar and Rovers (1973) as involving an aerobic phase, an anaerobic acid phase, an initial methanogenic phase, and a stable methanogenic phase. Ehrig (1988) indicated that pH decreases during the anaerobic acid phase, when easily degradable organic compounds are highly concentrated. In the later stable methanogenic phase, pH increases and the ratio of biological oxygen demand to chemical oxygen demand (BOD/COD) decreases, indicating that the most easily degradable organic carbon has decomposed. Therefore, the concentration of certain inorganic chemical compositions in MSW leachate changes with landfill decomposition phases. Due to the lack of organic carbon present in LLW, no pH change with decomposition is expected when compared to MSW landfills.

## 2.3.1 Inorganic Macro-components

The concentrations of inorganic macro-components, including major cations and anions, are listed in Table 2.3 with total concentration ranges and average concentrations based on the collected LLW leachate data. The concentrations of many dissolved inorganic macro-components in LLW leachate could be controlled by dissolution and precipitation of mineral phases from contaminated soils (e.g., Ca<sup>2+</sup>, Mg<sup>2+</sup>, and CO<sub>3</sub><sup>2-</sup> in calcite and dolomite) and sorption and desorption from the surface of clay minerals.

The concentrations of major cations (Ca<sup>2+</sup>, Mg<sup>2+</sup>, K<sup>+</sup>, and Na<sup>+</sup>) are shown in Fig. 2.3. Ca<sup>2+</sup> and Mg<sup>2+</sup> levels in LLW and MSW leachate are comparable (Fig 2.3 (a) and (b)), while the concentrations of K<sup>+</sup> and Na<sup>+</sup> in LLW are an order of magnitude lower than MSW leachate (Fig. 2.3 (c) and (d)). Fig. 2.4 presents the change in concentration of major cations with time at the four LLW disposal sites. The concentrations of all major cations are relatively constant at OSDF, ERDF, and ICDF, but vary over time at EMWMF. The concentration of Mg2+ at the EMWMF site increases linearly during all recorded years, while the concentration of the other major cations (Ca<sup>2+</sup>, K<sup>+</sup>, and Na<sup>+</sup>) increase slowly in the first six years and then sharply for the following four. Since EMWMF is still operating, new disposed waste sources might be influencing the varying trend. The concentrations of Ca<sup>2+</sup> and Mg<sup>2+</sup> are much higher at OSDF than at the other three LLW sites. Gravel used to construct the LDS and LCS at OSDF consisted of crushed limestone, making carbonate minerals (such as calcite and dolomite) the dominant solids in contact with atmospheric precipitation at OSDF (U.S. DOE OLM 2008). Moreover, the majority of waste at OSDF is contaminated soils comprised of glacial tills, which contain 40% to 70% carbonate on average (U.S. DOE OLM 2008). These factors may explain why the leachate from OSDF has higher Ca<sup>2+</sup> and Mg<sup>2+</sup> concentrations than the other sites. Christensen et al. (2001) indicated that Ca2+ and Mg2+ are lower in the

methanogenic phase of MSW decomposition due to the higher pH and lower concentration of dissolved organic matter present. However, the pH of LLW leachate is relatively constant over time and the concentration of TOC remains at a low level. Therefore, the concentrations of major cations do not change significantly with time.

Fig. 2.5 shows the concentrations of major anions: sulfate  $(SO_4^2)$ , chloride  $(Cl^2)$ , and nitrate/nitrite  $(NO_3^2/NO_2^2)$ . All four LLW sites have higher average concentrations of  $SO_4^{2^2}$  and  $NO_3^2/NO_2^2$  than MSW leachate. The concentrations of  $Cl^2$  at the four sites are between one and two orders of magnitude lower than those for MSW leachate. Due to the characteristics of their waste streams, OSDF and ERDF in particular have high concentrations of  $SO_4^{2^2}$  (Fig. 2.5 (a)). At both sites, large amounts of drywall and concrete debris were disposed, which may contribute to the high concentration of  $SO_4^{2^2}$ . Fig. 2.6 demonstrates the concentration change with time for the major anions. In general, similar to the major cations, the concentrations of anions at OSDF, ERDF, and ICDF remain relatively constant, but vary over time at EMWMF. The concentration of sulfate at the EMWMF site increased sharply in the first two recorded years then decreased from the second to fourth year, and finally increased slightly from the fourth through the sixth year. Sulfate's changing trend is additionally mirrored by the concentration of radionuclides in LLW leachate at the EMWMF site.

## 2.3.2 Trace Heavy Metals

The concentration of heavy metals varies widely at the four LLW sites, but the average trace metal concentrations are very low when compared with MSW leachate (Fig. 2.7). Average concentrations for Al, As, Ba, Cu, Fe, Li, Mn, Sr, and Zn can be found in Table 2.3. Additional elements, including Co, Cd, and Cr, are also found in LLW leachate, but at concentrations at or below minimum detection levels and are of less relative importance. Fig.

2.8 shows the changing concentration of trace metals at each site, in general, no obvious trends are observed

Heavy metal concentrations in LLW leachate can be explained by the limited sources of metal in LLW. Kjeldsen et al. (2002) indicated that Fe and Mn can be considered to be inorganic macro-components in MSW leachate due to their higher concentration level. The high level of Fe in the MSW leachate may be a result of the large amount of iron and steel scrap disposed with MSW. However, while LLW contains potential sources of iron, especially from disposed soils at the ERDF site, the low solubility of Fe(III) in soil controls Fe availability in LLW leachate, leading to low Fe concentrations. In LLW leachate, Fe is still present at high concentrations compared with other trace metals, but significantly lower concentrations than the major cations and anions; thus, Fe is included with the trace heavy metals rather than the inorganic macro-components. Zn and Pb typically have low concentrations in LLW leachate due to a lack of waste sources. High concentrations of Zn in MSW leachate are attributed to the inclusion of waste from batteries and fluorescent lamps (Mor et al. 2006). Similarly, Moturi et al. (2004) indicated that the presence of Pb in MSW leachate is from the disposal of Pb batteries, chemicals for photograph processing, Pb-based paints, and pipes in MSW landfills. LLW sites might receive limited wastes that contain large amounts of Zn and Pb as a consequence of LLW composition. Metal attenuation may be another reason for the low concentrations of metals in LLW leachate. Kjeldsen et al. (2002) indicated that sorption and precipitation are significant mechanisms for metal immobilization in MSW leachate, resulting in fairly low heavy metal concentrations. The same attenuation processes occur at LLW sites due to similar barrier systems used at both of LLW and MSW.

#### 2.3.3 Radionuclides

Many radionuclides could potentially be found in LLW leachate due to varying waste compositions. The composition of LLW was distinct at each of the four sites, leading to multiple potentially present radionuclides in LLW. Table 2.4 lists the specific radionuclides monitored in the LLW leachate at each site. However, most radionuclides are present in concentrations at or below method detection limits. As such, the detectable radionuclides and their corresponding concentrations are listed in Table 2.5. This paper focuses on four specific radionuclides that represent the most widely prevalent and consistently measured species: total Uranium, <sup>3</sup>H, <sup>90</sup>Sr, and <sup>99</sup>Tc.

# 2.3.3.1 Gross Alpha and Beta Activity

Two LLW landfill sites measure the gross alpha and beta activity in leachate (Fig. 2.9). Increasing alpha and beta activity are discernible at ERDF for the first ten years of measurement, with a slight decrease in activity during the last two years. At EMWMF, beta activity trends upward with time; however, the alpha activity increases sharply for the first three years, decreases in the following two years, and then increases thereafter. In general, most alpha particles were emitted from uranium, while <sup>99</sup>Tc, <sup>90</sup>Sr, and <sup>3</sup>H are the dominant sources for beta activity. The gross alpha trend corresponded to the change in uranium concentration, while the gross beta trend corresponded to the combined concentrations of <sup>99</sup>Tc and <sup>90</sup>Sr. The increasing trend of radionuclides in leachate may be a unique characteristic at the ERDF site. Since EMWMF is still operating, the complex variation in activity might be a result of new waste sources actively being disposed.

# 2.3.3.2 Total Uranium

Uranium is an element found naturally occurring with three isotopes:  $^{238}$ U with  $t_{1/2}$  approximately  $4.47 \times 10^9$  yrs;  $^{235}$ U with  $t_{1/2}$  =  $7.04 \times 10^8$  yrs; and  $^{234}$ U with  $t_{1/2}$  =  $2.46 \times 10^5$  yrs.

Uranium was measured in µg/L at the OSDF, ERDF, and EMWMF sites. The uranium concentration present in natural waters depends upon the surrounding geology (Bakaç and Kumru 2000). Langmuir (1997) indicated that the concentrations of uranium in natural waters range from 0.1 µg/L to 7 µg/L, while concentrations in seawater are higher, ranging from 2 μg/L to 4 μg/L. Another study found that the median concentration of uranium is 20 μg/L in Russian lake water and 41 µg/L in Norwegian lakes (Reimann et al. 1999). Øygard and Gjengedal (2009) found uranium concentrations less than 3.1 µg/L in MSW landfill leachate, similar to concentrations expected for naturally occurring water around the landfill. However, uranium occurs at significantly higher concentrations in LLW leachate (Fig. 2.10) as a consequence of the disposed wastes. For example, a significant amount of contaminated soil, waste, and debris were disposed at the OSDF, ERDF and EMWMF sites due to CERCLA cleanup actions. Dong et al. (2005) indicated that uranium (VI) adsorption in a calcitesaturated solution increases as a function of pH from 7.2 to 8.5, and then the adsorption decreases as the pH increase from 8.5 to 10. Since the pH at each of the four LLW sites is close to neutral, retardation of uranium may be limited, particularly below pH 7.2. Additionally, the presence of Ca-carbonate can reduce the sorption of uranium because calcite coatings can block the highly reactive surface sorption sites and a strong aqueous complex (Ca-U-CO<sub>3</sub>) can form in solution (Um et al. 2007). Ca-carbonate occurs in the LLW leachate at all LLW sites, potentially resulting in enhanced U transport through barrier systems. At OSDF and ICDF, the concentrations of uranium are relatively constant (Fig. 2.10 (a)); however, uranium concentrations increased from 212 μg/L to 3060 μg/L at ERDF from 1999 to 2009, and then dropped to 1480 µg/L in 2010. The average uranium concentration was 780 µg/L across the four LLW sites.

### 2.3.3.3 Technetium-99

<sup>99</sup>Tc is the primary radioactive isotope of technetium with a half-life of 2.11 × 10<sup>5</sup> years. Another important species of technetium is the metastable isomer <sup>99m</sup>Tc, which is used in nuclear medicine, and is produced from molybdenum-99. <sup>99m</sup>Tc is a short-lived isotope with a half-life of around 6 h, which decays by isomeric transition to <sup>99</sup>Tc. <sup>99</sup>Tc is one of the more problematic components of nuclear waste due to its long half-life and significant mobility as an anionic species in the environment. Um and Serne (2005) concluded that <sup>99</sup>Tc, as pertechnetate, TcO<sub>4</sub>\*, is largely not adsorbed onto Hanford sediments. Consequently, <sup>99</sup>Tc is expected to be highly mobile in LLW disposal facilities, making <sup>99</sup>Tc a risk for the long-term disposal of LLW. <sup>99</sup>Tc ranges from 0.24 Bq/L to over 47.87 Bq/L among the four LLW sites. The OSDF, ERDF, and ICDF sites show a relatively constant concentration of <sup>99</sup>Tc. Similar to Uranium, <sup>99</sup>Tc concentrations are highest (18.05 Bq/L to 37 Bq/L) at ERDF. EMWMF showed high concentrations of <sup>99</sup>Tc at the beginning of data collection (47.88 Bq/L), but decreased to 0.24 Bq/L in the subsequent seven years, potentially due to a limited <sup>99</sup>Tc waste source. Much of the original <sup>99</sup>Tc was likely washed out by rainwater in a short time period, resulting in the decreased concentration over time.

#### 2.3.3.4 Strontium-90

Natural strontium is nonradioactive, but the <sup>90</sup>Sr isotope constitutes a radioactive hazard. <sup>90</sup>Sr is a byproduct of nuclear fission and present in significant quantities in spent nuclear fuel and radioactive waste from nuclear reactor. Ion exchange is a dominant mechanism for <sup>90</sup>Sr attenuation processes (Zachara et al. 2007). Rimstidt et al. (1998) indicated that Sr has similar chemical properties to Ca. Both Sr and Ca are divalent cations in solution and have similar atomic radii (1.0 and 1.12 nm for Ca and Sr, respectively). Therefore Sr can substitute for Ca in calcite and aragonite (polymorphs of CaCO<sub>3</sub>) to form

strontianite (SrCO<sub>3</sub>) (Faure 2001; Rimstidt et al. 1998). Um and Serne (2005) found a high  $K_d$  value for  $^{90}$ Sr on Hanford sediments. The concentration of  $^{90}$ Sr in LLW leachate was monitored at the EMWMF and ICDF sites (Fig. 2.10(c)). Fig. 2.11(c) shows the change in  $^{90}$ Sr concentration, which is similar to uranium at EMWMF and ICDF.  $^{90}$ Sr increases from 0.03 Bq/L to 12.43 Bq/L at the ICDF site over the observation period. The concentration of  $^{90}$ Sr appears to stabilize at EMWMF with a concentration around 3.7 Bq/L.

# 2.3.3.5 *Tritium* (<sup>3</sup>H)

Tritium is another major radionuclide found in LLW leachate and is typically produced in nuclear reactors or high-energy accelerators. Fig. 2.10(d) shows the concentrations of tritium at three LLW landfill sites as well as 35 MSW landfill sites. U.S. drinking water standards stipulate a maximum contaminant level of 740 Bq/L for tritium. The concentrations of tritium at EMWMF and ICDF are lower than the drinking water standard; however, the limited data for tritium concentrations at ERDF show much higher concentrations, ranging from 3589-4625 Bq/L. The average concentrations of tritium are higher at MSW sites than LLW sites.

## 2.3.4 Ionic Strength and RMD

The ratio of monovalent to divalent cations (RMD) characterizes the relative abundance of monovalent and multivalent cations in leachate. Kolstad et al. (2004) defined RMD as  $M_m/\sqrt{M_d}$ , where  $M_m$  is the total molarity of monovalent cations in solution and  $M_d$  is the total molarity of multivalent cations in solution. Fig. 2.12 compares RMD to ionic strength for MSW and LLW leachates. MSW shows a linear relationship between ionic strength and RMD. Three of the LLW leachates display similar behavior of RMD to ionic strength as the MSW leachates. The exception is OSDF, where the lower RMD value is due to high Ca and Mg concentrations. Additionally, the high sulfate concentration present at OSDF raises the

ionic strength at the site. The low concentrations of inorganic macro-components at EMWMF during the earliest measurements and continuous upward growth lead to an increased ionic strength over time.

#### 2.4 SUMMARY

LLW leachate data from four DOE sites display varying compositions in terms of inorganic macro-components, trace heavy metals, and radionuclides. Dissolved organic matter concentrations in LLW leachate are a non-critical leachate component when compared with MSW leachate. Concentrations of inorganic macro-components are similar between LLW and MSW leachate. For major cations, the concentrations of Ca and Mg are similar at LLW and MSW sites, while K and Na concentrations are higher at MSW landfill sites. For major anions, the sulfate concentration is much higher at LLW sites, particularly OSDF and ERDF, due to large amounts of disposed drywall and concrete debris. Trace heavy metals in LLW leachate show relatively lower concentrations compared with MSW leachate. The concentration of heavy metals is relatively constant over time at OSDF, ERDF, and ICDF. At EMWMF, the trace heavy metal concentration began to increase after 6 years of data collection.

Many radionuclides are measured at the analyzed LLW sites, but the concentrations for most are near or below method detection limits. Exceptions are the concentrations of total Uranium, <sup>3</sup>H, <sup>90</sup>Sr, and <sup>99</sup>Tc. Different radionuclide concentrations show varying trends at different LLW sites. The leachate from ERDF has the highest uranium and <sup>99</sup>Tc concentrations among the four sites. The uranium concentration has increased sharply over time at ERDF. The concentration of <sup>90</sup>Sr at EMWEF and ICDF has also increased over time. Total alpha and beta activity in leachate increases with time at ERDF and EMWMF. In summary, the measured radioactivity of the analyzed LLW leachate is increasing with time.

#### REFERENCE

- 10 CFR pt.61.55. (2001). Waste classification. *Code of Federal Regulations* Title 10, Pt. 61.55, 2001 ed.
- Bacaç, M. and Kumru, M. (2000). Uranium, radium and field measurements in the water of Gediz river. *Turk. J. Eng. Env. Sci.*, *24*, 229–236.
- Benson, C., Albright, W., Ray, D, and Smegal, J. (2007). Review of the Idaho CERCLA Disposal Facility (ICDF) at Idaho National Laboratory, Independent Technical Review Report: Idaho Operations. Office of Engineering and Technology (EM-20), U.S. Department of Energy, Washington, DC, 5 December 2007.
- Benson, C., Wang, X., Gassner, F., and Foo, D. (2008a). Hydraulic conductivity of two geosynthetic clay liners permeated with an aluminum residue leachate. *GeoAmericas* 2008 The First Pan American Geosynthetics Conference and Exhibition, Industrial Fabrics Association International (IFAI), Roseville, MN, 94–101.
- Benson, C., Albright, W., Ray, D., and Smegal, J. (2008b). Review of the Environmental Management Waste Management Facility (EMWMF) at Oak Ridge, Independent Technical Review Report: Oak Ridge Reservation. Office of Engineering and Technology (EM-20), U.S. Department of Energy, Washington, DC, 1 February 2008.
- Chian, E. and DeWalle, F. (1977). Characterization of soluble organic matter in leachate. *Environ. Sci. Tech.*, 11, 158–163.
- Christensen, J., Jensen, D., Gron, C., Filip, Z., and Christensen, T. (1998). Characterization of the dissolved organic carbon in landfill leachate-polluted groundwater. *Water Res.*, 32, 125–135.
- Christensen, T. and Kjeldsen, P. (1989). Basic biochemical processes in landfills. *Sanitary Landfilling: Process, Technology and Environimental Impact*, T.H. Christensen, R. Cossu, and R. Stegmann, eds. Academic Press, London, UK, chap 2.1, 29–49.
- Christensen, T. and Kjeldsen, P. (1995). Landfill emissions and environmental impact: An introduction. *Proceedings of Sardinia '95 Fifth International Landfill Symposium, CISA., T.H. Christensen, R. Cossu, and R. Stegmann, eds.,* Cagliari: Environmental Sanitary Engineering Centre, Cagliari, Italy, 3, 3–12.
- Christensen, T., Kjeldsen, P., Bjerg, P., Jensen, D., Christensen, J., Baun, A., Albrechtsen, H., and Heron, G., (2001). Biogeochemistry of landfill leachate plumes. *Appl. Geochem.*, 16, 659–718.
- Daskalopoulos, E., Bader, O., and Probert, S. (1998). Municipal solid waste: a prediction methodology for the generation rate and composition in the European Union countries and the United States of America. *Resources, Conservation and Recycling*, 24, 155–166.
- Dong, W., Ball, W., Liu, C., Wang, Z., Stone, A., Bai, J., and Zachara, J. (2005). Influence of calcite and dissolved calcium on uranium(VI) sorption to a Hanford subsurface sediment. *Environ. Sci. Technol.*, 39, 7949–7955.
- Ehrig, H. (1988). Water and element balances of landfills. *Lecture Notes in Earth Sciences* 20: The landfill reactor and final storage, P. Baccini, ed., Springer-Verlag, Berlin, Germany, 83–115.

- Farquhar C. and Rovers, F. (1973). Gas production during refuse decomposition. *Water Air Soil Pollut.*, 2, 483–495.
- Fatta, D., Papadopoulos, A., and Loizidou, M. (1999). A study on the landfill leachate and its impact on the groundwater quality of the greater area. *Environ. Geochem. Health*, 21(2), 175–190.
- Faure, G. (2001). Chemical properties of Rb and Sr. *Origin of igneous rocks: The isotopic evidence*, Springer, New York, NY, 1–2.
- Gates, W. and Bouazza, M. (2010). Bentonite transformations in strongly alkaline solutions. *Geotextiles and Geomembranes*, 28(2), 219–225.
- Grambow, B. (2008). Mobile fission and activation products in nuclear waste disposal. *Journal of Contaminant Hydrology*, 102, 180–186.
- Gulec, S., Edil, T., and Benson, C. (2004). Effect of acidic mine drainage on the polymer properties of an HDPE geomembrane. *Geosynthetics International*, 11(2), 60–72.
- Inyang, H., Wachsmuth, P., and Menezes, G. (2009). Georadiological barrier gamma attenuation model for waste containment. II: Model implementation. *Journal of Environmental Engineering*, 135(4), 234–242.
- Jo, H., Benson, C., Shackelford, C., Lee, J., and Edil, T. (2005). Long-term hydraulic conductivity of a geosynthetic clay liner (GCL) permeated with inorganic salt solutions. *Journal of Geotechnical and Geoenvironmental Engineering*, 131(4), 405–417.
- Kaplan, D., Parker, K., and Ritter, J. (1998). Effects of aging quartz sand and Hanford sediment with sodium hydroxide on radionuclide sorption coefficients and sediment physical and hydrologic properties: Final report for Subtask 2a. Pacific Northwest National Laboratory, PNNL-11965, Richland, Washington.
- Kjeldsen, P., Morton, A., Rooker A., Baun A., Ledin A., and Christensen, T. (2002). "Present and long-term composition of MSW landfill leachate: A review." *Critical Reviews in Environmental Science and Technology*, 32(4), 297–336.
- Kolstad, D., Benson, C., and Edil, T. (2004). Hydraulic conductivity and swell of nonprehydrated GCLs permeated with multi-species inorganic solutions. *J. Geotech. Geoenviron. Eng.*, 130(12), 1236–1249.
- Langmuir, D. (1997). Aqueous geochemistry of uranium. *Aqueous environmental geochemistry*, Prentice Hall, Upper Saddle River, NJ, 495–501.
- Missana, T., Garcia-Gutierrez, M., and Alonso, U. (2004). Kinetics and irreversibility of cesium and uranium sorption onto bentonite colloids in a deep granitic environment. *Applied Clay Science*, 26, 137–150.
- Mor, S., Ravindra, K., Dahiya, R., and Chandra, A. (2006). "Leachate characterization and assessment of groundwater pollution near municipal solid waste landfill site." *Environmental Monitoring and Assessment*, 118, 435–456.
- Moturi, M., Rawat, M. and Subramanian, V. (2004). Distribution and fractionation of heavy metals in solid waste from selected sites in the industrial belt of Delhi, India. *Environ. Monit. Assess.* 95, 183–199.
- Øygard, J. and Gjengedal, E. (2009). Uranium in municipal solid waste landfill leachate. *Int. J. Environ. Res.*, 3(1), 61–68.

- Powell, J., Abitz, R., Broberg, K., Hertel, W., and Johnston, F. (2011). Status and performance of the On-Site Disposal Facility Fernald Preserve, Cincinnati, Ohio. *Proceedings, Waste Management Symposia 2011*, WM Symposia, Ref. 11137, accessed via: http://www.wmsym.org/archives/2011/papers/11137.pdf
- Reimann, C., Banks, D., Bogatyrev, I., de Caritat, P., Kashulina G., and Niskavaara, H. (1999). Lake water geochemistry on the western Kola Peninsula, northwest Russia. *Appl. Geochem.*, 14, 787–805.
- Rimstidt, J., Balog, A., and Webb, J. (1998). Distribution of trace elements between carbonate minerals and aqueous solutions. *Geochim. Cosmochim. Acta* 62, 1851–1863.
- Rosin-Paumier, S. and Touze-Foltz, N. (2012). Hydraulic and chemical evolution of GCLs during filter press and oedopermeametric tests performed with real leachate. *Geotextiles and Geomembranes*, 33, 15–4.
- Rowe, R. (2005). Long-term performance of containment barrier systems. *Géotechnique*, 55(9), 631–678.
- Rowe, R., Rimal, S., and Sangam, H. (2009). Ageing of HDPE geomembrane exposed to air, water and leachate at different temperatures. *Geotextiles and Geomembranes*, 27(2), 137–151.
- Saarela, J. (2003). Pilot investigations of surface parts of three closed landfills and factors affecting them. *Environ. Monit. Assess.*, 84, 183–192.
- Stravato, M. (2014). Rodney A. Baltzer, president of Waste Control Specialists, showing a model of the engineered bed that containers of radioactive waste sit on. There is a base layer of nearly waterproof clay, a layer of concrete reinforced with steel and three layers of plastic. Photograph. *The New York Times*, January 20, 2014, <a href="http://www.nytimes.com/2014/01/21/business/energy-environment/texas-company-alone-in-us-cashes-in-on-nuclear-waste.html">http://www.nytimes.com/2014/01/21/business/energy-environment/texas-company-alone-in-us-cashes-in-on-nuclear-waste.html</a> (Jan. 29, 2014).
- Um, W. and Serne R. (2005). Sorption and transport behavior of radionuclides in the proposed low-level radioactive waste disposal facility at the Hanford site, Washington. *Radiochim. Acta*, 93(1), 57–63.
- Um, W., Serne R., and Krupka, K. (2007). Surface complexation modeling of U(VI) sorption to Hanford sediment with varying geochemical conditions. *Environ. Sci. Technol.*, 41(10), 3587–3592.
- U.S. Department of Energy (U.S. DOE). (2012). Environmental Restoration Disposal Facility. *Hanford*, <a href="https://www.hanford.gov/page.cfm/erdf">www.hanford.gov/page.cfm/erdf</a>> (Oct. 29, 2013).
- U.S. Department of Energy Office of Environmental Management (U.S. DOE OEM). (2000). The current and planned low-level waste disposal capacity report revision 2. Office of Environmental Management, U.S. Department of Energy, Washington, DC. Available via: <a href="http://energy.gov/sites/prod/files/em/llwrev2.pdf">http://energy.gov/sites/prod/files/em/llwrev2.pdf</a>>
- U.S. Department of Energy Office of Legacy Management (U.S. DOE OLM) (2008). Fernald Site: Evaluation of aqueous ions in the monitoring systems of the On-site Disposal Facility. DOE-LM/1591-2008. Office of Legacy Management, U.S. Department of Energy, Grand Junction, Colorado, March 2008.

- U.S. Nuclear Regulatory Commission (U.S. NRC). (2002). Radioactive waste: Production, storage, disposal (NUREG/BR-0216, Revision 2). Office of Public Affairs, U.S. Nuclear Regulatory Commission, Washington DC, 20555-0001. Available via: <a href="http://www.nrc.gov/reading-rm/doc-collections/nuregs/brochures/br0216/">http://www.nrc.gov/reading-rm/doc-collections/nuregs/brochures/br0216/</a>>
- Wang, T., Hsieh, C., Lin, S, Wu, D, Li, M, and Teng, S. (2010). Effect of alkyl properties and head groups of cationic surfactants on retention of cesium by organoclays. *Environmental Science and Technology*, 44, 5142–5147.
- Zachara, J., Serne, J., Freshley, M., Mann, F., Anderson, F., Wood, M., Jones, T., and Myers, D. (2007). Geochemical processes controlling migration of tank wastes in Hanford's vadose zone. *Vadose Zone Journal*, 6(4), 985–1003

Table 2.1. Radionuclides classified for low-level radioactive waste

NRC 10 CFR 61.55	Inyang et al. (2009)	Kaplan et al (1998)
<sup>90</sup> Sr	<sup>90</sup> Sr	<sup>90</sup> Sr
<sup>137</sup> Cs	<sup>137</sup> Cs	<sup>137</sup> Cs
<sup>99</sup> Tc		<sup>99</sup> Tc
129		<sup>129</sup>
<sup>60</sup> Co	<sup>60</sup> Co	
<sup>3</sup> H	<sup>3</sup> H	
<sup>63</sup> Ni	<sup>63</sup> Ni	
<sup>14</sup> C	<sup>144</sup> Ce	<sup>90</sup> Se
<sup>242</sup> Cm	<sup>58</sup> Co	<sup>237</sup> Np
<sup>59</sup> Ni	<sup>51</sup> Cr	U
<sup>94</sup> Nb	<sup>134</sup> Cs	
<sup>241</sup> Pu	<sup>55</sup> Fe	
Alpha emitting transuranic	<sup>54</sup> Mn	
nuclides with half-life greater than 5 years	<sup>95</sup> Nb	
Total of all nuclides with less than 5 year half-life	<sup>65</sup> Zn	

Note: Bold species are common across multiple sources, while undifferentiated species are unique to a specific ruling or source.

Table 2.2. Analytical methods used in collection and analysis of LLW, based on information provided by the DOE

Radionuclides           Technetium-99         Liquid Scint.a         N.A.         Liquid Scint.a         N.A.         N.A.         P.A.         E906.0           Uranium         SW-846b         N.A.         SW-846b         ALPHASPEC         N.A.         SW-846b	Parameter	OSDF	ERDF	EMWMF	ICDF
Technetium-99         Liquid Scint.a         N.A.         Liquid Scint.a         N.A.         N.A.         E906.0           Uranium         SW-846b         N.A.					
Tritium         Liquid Scint.a         N.A.         N.A.         E906.0           Uranium         SW-846b         N.A.         SW-846b         ALPHASPEC           Strontium-90         N.A.         N.A.         N.A.           Inorganic Cations         N.A.         N.A.         N.A.           Aluminum         SW-846b         SW-846b         SW-846b         SW-846b           Arsenic         Barium         Barium         SW-846b         SW-846b<		Liquid Scint a	NΑ	Liquid Scint a	Liquid Scint a
Uranium         SW-846b         N.A.         SW-846b         ALPHASPEC           Strontium-90         N.A.         N.A.         N.A.           Inorganic Cations         N.A.         N.A.         N.A.           Aluminum         SW-846b         SW-846b         SW-846b         SW-846b           Arsenic         Barium         Boron         SW-846b         SW-					
Strontium-90					
Inorganic Cations		<u> </u>			
Aluminum         SW-846b         <					
Arsenic		SW-846b	SW-846b	SW-846b	SW-846b
Barium   Boron   Calcium   Cobalt   Copper   Iron   Lithium   Magnesium   Manganese   Nickel   Potassium   Selenium   Sodium   Vanadium   Zinc   General Chemistry   Total Organic Halogens   9020Bb   N.A.   N.A.   N.A.   N.A.   Total Organic Carbon   9060b   Blank   415.1c   N.A.   N.A.   Chloride   325.2c, 300(all)c   300c   300c   300c   300c   300c   Sulfate   375.2c, 300.0c, 4500Ed   300.0c   300.0c   300.0c   300.0c   300.0c   Total Dissolved Solids   160.1c, 2540Cd   160.1c   N.A.   N.A.		011 0100	011 0100	311 3 102	011 0 102
Boron   Calcium   Cobalt   Copper   Iron   Lithium   Magnesium   Manganese   Nickel   Potassium   Selenium   Sodium   Vanadium   Zinc   General Chemistry   Total Organic Halogens   9020Bb   N.A.   N.A.   N.A.   Total Organic Carbon   9060b   Blank   415.1c   N.A.   Total Organic Carbon   9060b   Blank   415.1c   N.A.   Chloride   325.2c, 300(all)c   300c   300c					
Calcium           Copper         Iron           Lithium         Magnesium           Manganese         Nickel           Potassium         Selenium           Sodium         Vanadium           Zinc         General Chemistry           Total Organic Halogens         9020Bb         N.A.         N.A.           Total Organic Carbon         9060b         Blank         415.1c         N.A.           Chloride         325.2c, 300(all)c         300c         <					
Copper   Iron					
Copper					
Iron					
Lithium         Magnesium         Manganese         Nickel         Potassium         Selenium         Sodium         Vanadium         Zinc         General Chemistry         Total Organic Halogens       9020Bb       N.A.       N.A.       N.A.         Total Organic Carbon       9060b       Blank       415.1c       N.A.         Chloride       325.2c, 300(all)c       300c       300c       300c         Nitrate/Nitrite       353.1c,353.2c, 4500Dd,4500Ed       353.2c       353.2c       353.2c         Sulfate       375.2c, 300.0c, 4500Ed       300.0c       300.0c       300.0c         Total Dissolved Solids       160.1c, 2540Cd       160.1c       N.A.       N.A.					
Magnesium           Manganese           Nickel           Potassium           Selenium           Sodium           Vanadium           Zinc           General Chemistry           Total Organic Halogens         9020Bb         N.A.         N.A.         N.A.           Total Organic Carbon         9060b         Blank         415.1c         N.A.           Chloride         325.2c, 300(all)c         300c         300c         300c           Nitrate/Nitrite         353.1c,353.2c, 4500Dd,4500Ed         353.2c         353.2c         353.2c           Sulfate         375.2c, 300.0c, 4500Ed         300.0c         300.0c         300.0c           Total Dissolved Solids         160.1c, 2540Cd         160.1c         N.A.         N.A.					
Manganese           Nickel           Potassium           Selenium           Sodium           Vanadium           Zinc           General Chemistry           Total Organic Halogens         9020Bb         N.A.         N.A.         N.A.           Total Organic Carbon         9060b         Blank         415.1c         N.A.           Chloride         325.2c, 300(all)c         300c         300c         300c         300c           Nitrate/Nitrite         353.1c,353.2c, 4500Dd,4500Ed         353.2c         353.2c         353.2c         353.2c           Sulfate         375.2c, 300.0c, 4500Ed         300.0c         300.0c         300.0c         300.0c           Total Dissolved Solids         160.1c, 2540Cd         160.1c         N.A.         N.A.					
Nickel           Potassium           Selenium           Sodium           Vanadium           Zinc           General Chemistry           Total Organic Halogens         9020Bb         N.A.         N.A.         N.A.           Total Organic Carbon         9060b         Blank         415.1c         N.A.           Chloride         325.2c, 300(all)c         300c         300c         300c         300c           Nitrate/Nitrite         353.1c,353.2c, 4500Dd,4500Ed         353.2c         353.2c         353.2c         353.2c           Sulfate         375.2c, 300.0c, 4500Ed         300.0c         300.0c         300.0c         300.0c           Total Dissolved Solids         160.1c, 2540Cd         160.1c         N.A.         N.A.	<u> </u>				
Selenium           Sodium           Vanadium           Zinc           General Chemistry           Total Organic Halogens         9020Bb         N.A.         N.A.         N.A.           Total Organic Carbon         9060b         Blank         415.1c         N.A.           Chloride         325.2c, 300(all)c         300c         300c         300c           Nitrate/Nitrite         353.1c,353.2c, 4500Dd,4500Ed         353.2c         353.2c         353.2c           Sulfate         375.2c, 300.0c, 4500Ed         300.0c         300.0c         300.0c           Total Dissolved Solids         160.1c, 2540Cd         160.1c         N.A.         N.A.					
Sodium           Vanadium           Zinc           General Chemistry           Total Organic Halogens         9020Bb         N.A.         N.A.         N.A.           Total Organic Carbon         9060b         Blank         415.1c         N.A.           Chloride         325.2c, 300(all)c         300c         300c         300c           Nitrate/Nitrite         353.1c,353.2c, 4500Dd,4500Ed         353.2c         353.2c         353.2c           Sulfate         375.2c, 300.0c, 4500Ed         300.0c         300.0c         300.0c           Total Dissolved Solids         160.1c, 2540Cd         160.1c         N.A.         N.A.	Potassium				_
Vanadium           Zinc           General Chemistry           Total Organic Halogens         9020Bb         N.A.         N.A.         N.A.           Total Organic Carbon         9060b         Blank         415.1c         N.A.           Chloride         325.2c, 300(all)c         300c         300c         300c           Nitrate/Nitrite         353.1c,353.2c, 4500Dd,4500Ed         353.2c         353.2c         353.2c           Sulfate         375.2c, 300.0c, 4500Ed         300.0c         300.0c         300.0c           Total Dissolved Solids         160.1c, 2540Cd         160.1c         N.A.         N.A.	Selenium				
Zinc   General Chemistry   Total Organic Halogens   9020Bb   N.A.   N.A.   N.A.   N.A.   N.A.   Total Organic Carbon   9060b   Blank   415.1c   N.A.   N.A	Sodium				
General Chemistry           Total Organic Halogens         9020Bb         N.A.         N.A.         N.A.           Total Organic Carbon         9060b         Blank         415.1c         N.A.           Chloride         325.2c, 300(all)c         300c         300c         300c           Nitrate/Nitrite         353.1c,353.2c, 4500Dd,4500Ed         353.2c         353.2c         353.2c           Sulfate         375.2c, 300.0c, 4500Ed         300.0c         300.0c         300.0c           Total Dissolved Solids         160.1c, 2540Cd         160.1c         N.A.         N.A.	Vanadium				
Total Organic Halogens         9020Bb         N.A.         N.A.         N.A.           Total Organic Carbon         9060b         Blank         415.1c         N.A.           Chloride         325.2c, 300(all)c         300c         300c         300c           Nitrate/Nitrite         353.1c,353.2c, 4500Dd,4500Ed         353.2c         353.2c         353.2c           Sulfate         375.2c, 300.0c, 4500Ed         300.0c         300.0c         300.0c           Total Dissolved Solids         160.1c, 2540Cd         160.1c         N.A.         N.A.	Zinc				
Total Organic Carbon         9060b         Blank         415.1c         N.A.           Chloride         325.2c, 300(all)c         300c         300c         300c           Nitrate/Nitrite         353.1c,353.2c, 4500Dd,4500Ed         353.2c         353.2c         353.2c           Sulfate         375.2c, 300.0c, 4500Ed         300.0c         300.0c         300.0c           Total Dissolved Solids         160.1c, 2540Cd         160.1c         N.A.         N.A.	General Chemistry				
Total Organic Carbon         9060b         Blank         415.1c         N.A.           Chloride         325.2c, 300(all)c         300c         300c         300c           Nitrate/Nitrite         353.1c,353.2c, 4500Dd,4500Ed         353.2c         353.2c         353.2c           Sulfate         375.2c, 300.0c, 4500Ed         300.0c         300.0c         300.0c           Total Dissolved Solids         160.1c, 2540Cd         160.1c         N.A.         N.A.	Total Organic Halogens	9020Bb	N.A.	N.A.	N.A.
Nitrate/Nitrite         353.1c,353.2c, 4500Dd,4500Ed         353.2c         353.2c         353.2c         353.2c           Sulfate         375.2c, 300.0c, 4500Ed         300.0c         300.0c         300.0c         300.0c           Total Dissolved Solids         160.1c, 2540Cd         160.1c         N.A.         N.A.		9060b	Blank	415.1c	N.A.
Nitrate/Nitrite         4500Dd,4500Ed         353.2c         353.2c         353.2c           Sulfate         375.2c, 300.0c, 4500Ed         300.0c         300.0c         300.0c           Total Dissolved Solids         160.1c, 2540Cd         160.1c         N.A.         N.A.	Chloride	325.2c, 300(all)c	300c	300c	300c
Suifate         4500Ed         300.0c         300.0c         300.0c           Total Dissolved Solids         160.1c, 2540Cd         160.1c         N.A.         N.A.	Nitrate/Nitrite		353.2c	353.2c	353.2c
,	Sulfate		300.0c	300.0c	300.0c
Total Alkalinity 310.1c, 2320Bd N.A. N.A. N.A. N.A.	Total Dissolved Solids	160.1c, 2540Cd	160.1c	N.A.	N.A.
	Total Alkalinity	310.1c, 2320Bd	N.A.	N.A.	N.A.

#### Notes:

<sup>&</sup>lt;sup>a</sup>Performance-based analytical specifications for these parameters are provided in Fernald Preserve Quality Assurance Project Plan. (Liquid Scint. = Liquid Scintillation)

<sup>&</sup>lt;sup>b</sup>Test Methods for Evaluating Solid Waste, Physical/Chemical Methods (EPA 1998).

<sup>&</sup>lt;sup>c</sup>Methods for Chemical Analysis of Water and Wastes (EPA 1983).

<sup>&</sup>lt;sup>d</sup>Standard Methods for Analysis of Water and Wastewater, 17th edition (APHA 1989).

<sup>e</sup>Industry standard method, laboratory-specific, based on acceptance by Washington Closure Hanford

Table 2.3. Measured parameters of LLW leachate

Parameters	Sites	No. of Meas.	Ave.	Range	COV
	OSDF	42	6.87	6.07-7.86	0.06
ml l	ERDF	36	7.57	7.1-8.2	0.04
рН	EMWMF	84	7.32	5.69-9.13	0.08
	ICDF	160	7.08	6.11-8.51	0.05
Oxidation	OSDF	228	72.09	-94.4-321.1	1.08
Reduction	ERDF	-	-	-	-
Potential	EMWMF	102	144.52	14-252.3	0.38
(mv)	ICDF	126	128.05	-193-344	1.06
	OSDF	32	4.75	1.9-22.9	1.37
Total	ERDF	20	14.17	4.1-48.1	0.81
Organic Carbon (mg/L)	EMWMF	31	4.28	0.86-10.4	0.52
	ICDF	-	-	-	-
	MSW <sup>a</sup>			30-29000	

	Inorganic Macro-components (mM)								
Parameters	Sites	No. of Meas.	Ave.	Range	COV				
Ca	OSDF	73	12.2	1.64-24.9	0.28				
	ERDF	33	5.06	3.95-6.5	0.14				
	EMWMF	97	3.27	0.77-8.05	0.59				
	ICDF	33	5.28	1.26-10.05	0.37				
	MSW	201b	5.02	0.0035- 346.82					
Mg	OSDF	74	11.2	0.913-30.2	0.49				
	ERDF	22	2.85	1.99-3.74	0.21				
	EMWMF	97	0.89	0.20-1.43	0.31				
	ICDF	33	3.03	0.84-6.33	0.38				
	MSW	211b	6.72	0.0012-204.93					
Na	OSDF	74	1.85	0.40-4.17	0.51				
	ERDF	33	7.31	8.52-14.1	0.12				
	EMWMF	97	1.08	0.19-3.08	0.62				
	ICDF	33	10.85	4.87-38.13	0.51				
	MSW	198b	49.48	0.00053-1926.23					
K	OSDF	74	0.58	0.13-1.94	0.43				
	ERDF	33	0.61	0.43-0.72	0.13				
	EMWMF	82	0.12	0.04-0.28	0.41				
	ICDF	33	0.22	0.11-0.36	0.25				

	MSW	173b	10.05	0.00036-1458.17	
Sulfate	OSDF	74	18.5	1.52-29.6	0.36
	ERDF	49	5.26	3.38-8.65	0.19
	EMWMF	30	1.88	0.39-7.20	0.89
	ICDF	32	2.79	1.10-15.4	0.87
	MSW	193b	2.16	0.0021-82.23	
Chloride	OSDF	74	2.04	0.33-6.17	0.55
	ERDF	47	7.31	4.93-14	0.23
	EMWMF	31	0.54	0.12-0.97	0.42
	ICDF	32	8.9	1.71-19.27	0.47
	MSW	189b	22.81	0.036-236.38	
Nitrate/ Nitrite	OSDF	74	0.0766	0.000048-1.20	2.43
	ERDF	49	5.26	2.02-8.65	0.28
	EMWMF	30	0.012	0.0019-0.024	0.52
	ICDF	33	0.35	0.15-0.88	0.38
	MSW	44	0.057	0.00032-1.77	
Alkalinity	OSDF	31	3.99	2.19-5.57	0.2
	ERDF	-	-	-	-
	EMWMF	2	1.35	1.31-1.39	0.05
	ICDF	48	4.91		
		Tra	ace Metals (mM	1)	
Parameters	Sites	No. of Meas.	Ave.	Range	COV
Al	OSDF	74	0.0766	0.000048-1.20	2.43
	ERDF	22	0.0014	0.00046-0.0025	0.47
	EMWMF	97	0.0088	0.00078-0.087	1.48
	ICDF	19	3.3E-05	0.0000041-0.00012	1.08
	MSW	50b	0.37	0.0037-33.3	
As	OSDF	18	0.00027	0.000033-0.00189	1.75
	ERDF	45	0.00012	0.000067-0.00021	0.31
	EMWMF	-	-	-	-
	ICDF	33	9.3E-05	0.00002-0.00029	0.49
	MSW	187b	0.00086	0.000013-0.068	
Ва	OSDF	74	0.00037	0.00016-0.00075	0.41
	ERDF	49	0.00067	0.00047-0.00093	0.17
	EMWMF	97	0.0057	0.00021-0.0033	0.52
	ICDF	19	0.0016	0.00029-0.0032	0.46
	MSW	145b	0.0077	0.000065-3.46	
Cu	OSDF	72	0.00019	0.000039-0.00054	0.54

	ERDF	22	0.00011	0.000039-0.00016	0.34
	EMWMF	76	3.5E-05	0.0000064-0.000085	0.62
	ICDF	19	9.1E-05	0.000023-0.00023	0.46
	MSW	172b	0.001	0.0000173-0.11	
Fe	OSDF	74	0.119	0.0022-1.02	1.73
	ERDF	8	0.0005	0.00022-0.000893	0.55
	EMWMF	97	0.0041	0.000204-0.043	1.49
	ICDF	17	0.0056	0.00023-0.034	1.71
	MSW	120b	0.25	0.0018-10.92	
Li	OSDF	58	0.029	0.0010-0.139	1.2
	ERDF	-	-	-	
	EMWMF	82	0.0007	0.00009-0.0022	0.68
	ICDF	-	-	-	-
	MSW	6b	0.092	0.0076-0.29	
Mn	OSDF	74	0.023	0.000091-0.132	1.51
	ERDF	-	-	-	-
	EMWMF	97	0.0015	0.000016-0.024	2.7
	ICDF	33	0.00011	0.000022-0.00074	1.2
	MSW	131b	0.043	0.00023-2.73	
Sr	OSDF	42	0.028	0.00279-0.055	0.43
	ERDF	-	-	-	-
	EMWMF	97	0.0036	0.00092-0.026	0.94
	ICDF	5	0.015	0.012-0.019	0.22
	MSW	7b	0.021	0.00083-0.051	
Zn	OSDF	68	0.00048	0.000074-0.0023	1.01
	ERDF	49	0.00015	0.0000077-0.00054	0.76
	EMWMF	97	0.00015	0.0000081-0.0015	1.18
	ICDF	33	0.00043	0.000031-0.0026	1.1
	MSW	207b	0.013	0.000061-3.82	

Notes: '-' means not measured at the site

<sup>&#</sup>x27;ND' means not detected

<sup>&</sup>lt;sup>a</sup>Data from Kjeldsen et al., 2002. <sup>b</sup>Values represent the number of MSW sites sampled.

Table 2.4. Radionuclides measured at study LLW sites

OSDF	ERDF	IC	ICDF EMWMF				
U	U	U	<sup>54</sup> Mn	U	<sup>251</sup> Cf	<sup>237</sup> Np	<sup>226</sup> Ra
<sup>99</sup> Tc	<sup>99</sup> Tc	<sup>99</sup> Tc	<sup>237</sup> Np	<sup>99</sup> Tc	<sup>252</sup> Cf	<sup>59</sup> Ni	<sup>228</sup> Ra
	<sup>129</sup>	<sup>129</sup>	<sup>95</sup> Nb	<sup>129</sup>	<sup>135</sup> Cs	<sup>63</sup> Ni	<sup>108m</sup> Ag
	<sup>3</sup> H	$^3H$	<sup>238</sup> Pu	$^3H$	<sup>137</sup> Cs	<sup>94</sup> Nb	<sup>89</sup> Sr
	<sup>14</sup> C	<sup>14</sup> C	<sup>239,240</sup> Pu	<sup>14</sup> C	<sup>36</sup> CI	<sup>236</sup> Pu	<sup>227</sup> Th
	<sup>40</sup> K	<sup>90</sup> Sr	226Ra	<sup>90</sup> Sr	<sup>60</sup> Co	<sup>238</sup> Pu	<sup>228</sup> Th
	<sup>60</sup> Co	<sup>241</sup> Am	<sup>103</sup> Ru	<sup>225</sup> Ac	<sup>242</sup> Cm	<sup>239,240</sup> Pu	<sup>229</sup> Th
	<sup>137</sup> Cs	<sup>125</sup> Sb	<sup>106</sup> Ru	<sup>227</sup> Ac	<sup>245</sup> Cm	<sup>241</sup> Pu	<sup>230</sup> Th
	<sup>152</sup> Eu	<sup>144</sup> Ce	<sup>108m</sup> Ag	<sup>26</sup> AI	<sup>246</sup> Cm	<sup>242</sup> Pu	<sup>232</sup> Th
	<sup>154</sup> Eu	<sup>134</sup> Cs	<sup>110m</sup> Ag	<sup>241</sup> Am	<sup>247</sup> Cm	<sup>244</sup> Pu	<sup>234</sup> Th
	<sup>155</sup> Eu	<sup>137</sup> Cs	<sup>65</sup> Zn	<sup>243</sup> Am	<sup>248</sup> Cm	<sup>210</sup> Po	<sup>126</sup> Sn
	<sup>226</sup> Ra	<sup>58</sup> Co	<sup>95</sup> Zr	<sup>126</sup> Sb	<sup>152</sup> Eu	$^{40}$ K	<sup>90</sup> Y
	<sup>228</sup> Ra	<sup>60</sup> Co		<sup>133</sup> Ba	<sup>154</sup> Eu	<sup>231</sup> Pa	
	<sup>228</sup> Th	<sup>152</sup> Eu		<sup>207</sup> Bi	<sup>155</sup> Eu	<sup>234m</sup> Pa	
	<sup>232</sup> Th	<sup>154</sup> Eu		<sup>249</sup> Cf	<sup>210</sup> Pb	<sup>223</sup> Ra	
	<sup>241</sup> Am	<sup>155</sup> Eu		<sup>250</sup> Cf	<sup>212</sup> Pb	<sup>225</sup> Ra	

Table 2.5. Detectable radionuclides at study LLW sites

Radionuclides	Site	No of Meas.	Ave.	Range	(Bq/L)	COV
Radionuclides	Sile	(Above MDL/ Total)	(Bq/L)	Low	High	COV
U (µg/L)	OSDF	74/74	121.2	35.2	285	0.41
	ERDF	38/38	1488.7	212	3060	0.55
	EMWMF	104/104	69.52	6.4	388	1.45
	ICDF	31/31	67	10.26	387	0.93
<sup>99</sup> Tc	OSDF	27/27	0.591	0.254	1.991	0.88
	ERDF	37/38	27.701	18.056	37	0.18
	EMWMF	94/107	2.452	0.152	47.88	2.87
	ICDF	15/33	0.297	0.163	0.577	0.39
<sup>3</sup> H	ERDF	10/10	4266.1	3589	4625	0.11
	EMWMF	101/106	71.991	13.109	341.69	0.95
	ICDF	19/31	40.204	0.74	75.85	0.75
	MSW	33a	682.28	0.017	7955	
<sup>90</sup> Sr	EMWMF	108/108	3.837	0.109	17.427	0.91
	ICDF	31/33	2.194	0.03	12.432	1.2
<sup>225</sup> Ac	EMWMF	8/28	0.017	0.006	0.053	0.97
<sup>227</sup> Ac	EMWMF	11/105	0.015	0.006	0.036	0.62
<sup>26</sup> AI	EMWMF	1/64	0.272			
<sup>241</sup> Am	EMWMF	22/108	0.012	0.004	0.054	0.87
<sup>249</sup> Cf	EMWMF	2/30	0.006	0.003	0.009	0.38
<sup>250</sup> Cf	EMWMF	1/30	0.002			
<sup>251</sup> Cf	EMWMF	3/30	0.007	0.005	0.011	0.48
<sup>36</sup> Cl	EMWMF	69/105	0.427	0.093	2.802	1.01
<sup>60</sup> Co	EMWMF	4/85	0.261	0.13	0.345	0.35
<sup>245</sup> Cm	EMWMF	19/75	0.011	0.004	0.017	0.24
<sup>246</sup> Cm	EMWMF	19/76	0.011	0.004	0.017	0.24
<sup>247</sup> Cm	EMWMF	6/76	0.01	0.003	0.019	0.68
<sup>248</sup> Cm	EMWMF	22/105	0.01	0.001	0.036	0.26
152Eu	EMWMF	1/85	1.606	0.001	0.000	0.20
129 <b> </b>	EMWMF	17/107	0.094	0.014	0.474	1.1
1	ICDF	56/110	0.094	0.014	0.474	0.48
210Pb						
	EMWMF	9/55	0.043	0.025	0.084	0.43
<sup>237</sup> Np	EMWMF	14/108	0.016	0.014	0.084	1.05
<sup>59</sup> Ni	EMWMF	2/30	7.659	7.4	7.918	0.048
<sup>63</sup> Ni	EMWMF	5/75	3.45	3.45	10.804	1.2
<sup>236</sup> Pu	EMWMF	1/62	0.013			

Dadianualidaa	Cito	No. of Meas. (Above	Ave.	Range	(Bq/L)	COV
Radionuclides	Site	MDL/ Total )	(Bq/L)	Low	High	COV
<sup>238</sup> Pu	EMWMF	2/88	0.006	0.004	0.009	0.61
	ICDF	2/33	0.006	0.001	0.011	1.14
<sup>239,240</sup> Pu	EMWMF	4/108	0.009	0.003	0.014	0.51
	ICDF	1/15	0.005			
<sup>241</sup> Pu	EMWMF	1/74	1.11			
<sup>242</sup> Pu	EMWMF	36/74	0.013	0.004	0.04	0.58
<sup>244</sup> Pu	EMWMF	5/74	0.006	0.004	0.01	0.46
<sup>210</sup> Po	EMWMF	4/28	0.013	0.009	0.021	0.46
<sup>40</sup> K	EMWMF	9/73	2.715	1.226	6.771	0.59
<sup>234m</sup> Pa	EMWMF	105/106	1.149	0.14	5.779	1.22
<sup>223</sup> Ra	EMWMF	1/35	0.007			
<sup>225</sup> Ra	EMWMF	8/35	0.017	0.006	0.053	0.97
<sup>226</sup> Ra	EMWMF	21/93	0.016	0.004	0.043	0.65
<sup>228</sup> Ra	EMWMF	30/92	0.09	0.016	0.337	1.05
<sup>89</sup> Sr	EMWMF	1/29	0.992			
<sup>227</sup> Th	EMWMF	7/78	0.01	0.006	0.017	0.4
<sup>228</sup> Th	EMWMF	9/105	0.021	0.003	0.108	1.54
<sup>229</sup> Th	EMWMF	12/73	0.07	0.006	0.655	2.65
<sup>230</sup> Th	EMWMF	73/105	0.024	0.004	0.131	0.89
<sup>232</sup> Th	EMWMF	26/106	0.021	0.004	0.206	1.82
<sup>234</sup> Th	EMWMF	56/74	0.545	0.14	5.18	1.71
90 <b>Y</b>	EMWMF	74/74	4.751	0.182	17.427	0.67
			• .	J	• • • • • • •	

Notes: "MDL" means: Method Detection Limit

Table only presents detectable radionuclides at each site – not .every measured radionuclide.

aData from Kjeldsen et al. 2002.

Protective Layer

Leachate collection system (LCS)

Leachate Detection system (LDS)

Leachate Detection system (LDS)

Los Pipe
Supplemental Geotextile Cushion
Primary Geomembrane Liner
Primary Geosynthetic Clay Liner

LDS Pipe
Supplemental Geotextile Cushion



Fig. 2.1. Top panel: Typical lower layer cross-section for LLW disposal facilities. (Modified from Powell et al. 2011). Lower panel: Rodney A. Baltzer, president of Waste Control Specialists, with a model of the installed barrier system at the Andrews, TX LLW facility (Stravato 2014).

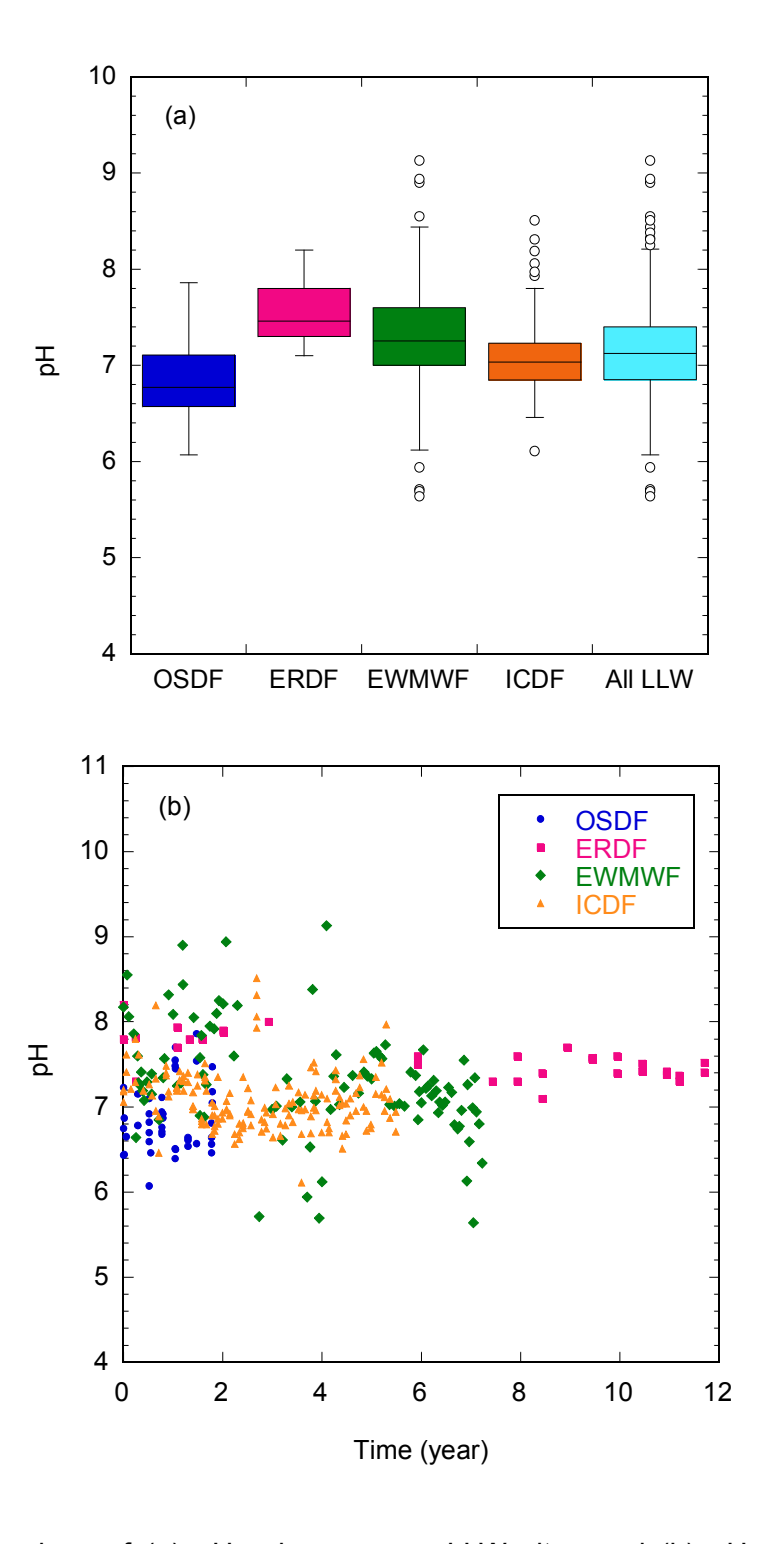


Fig. 2.2. Comparison of (a) pH values across LLW sites and (b) pH variation with time. (ERDF: the Environmental Restoration Disposal Facility at Hanford, WA; OSDF: the On Site Disposal Facility at Fernald, OH; ICDF: the Idaho CERCLA Disposal Facility at Idaho Falls, ID; EMWMF: Environmental Management Waste Management Facility at Oak Ridge; All LLW contains data for all four LLW sites).

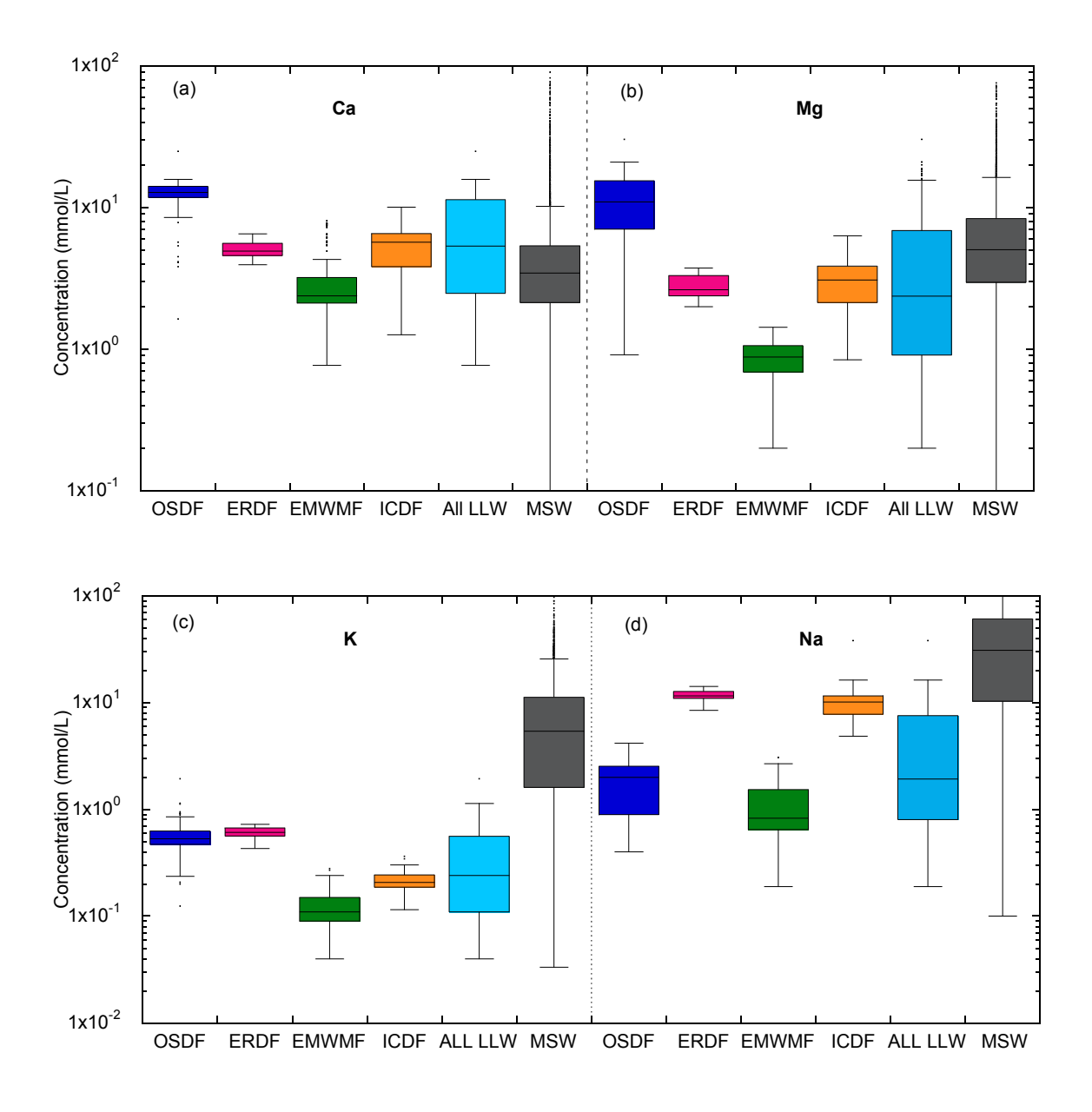


Fig. 2.3. Comparison of major cation concentrations at LLW sites. LLW concentrations of calcium, Ca (a), magnesium, Mg (b), potassium, K (c), and sodium, Na (d), are compared to MSW concentrations.

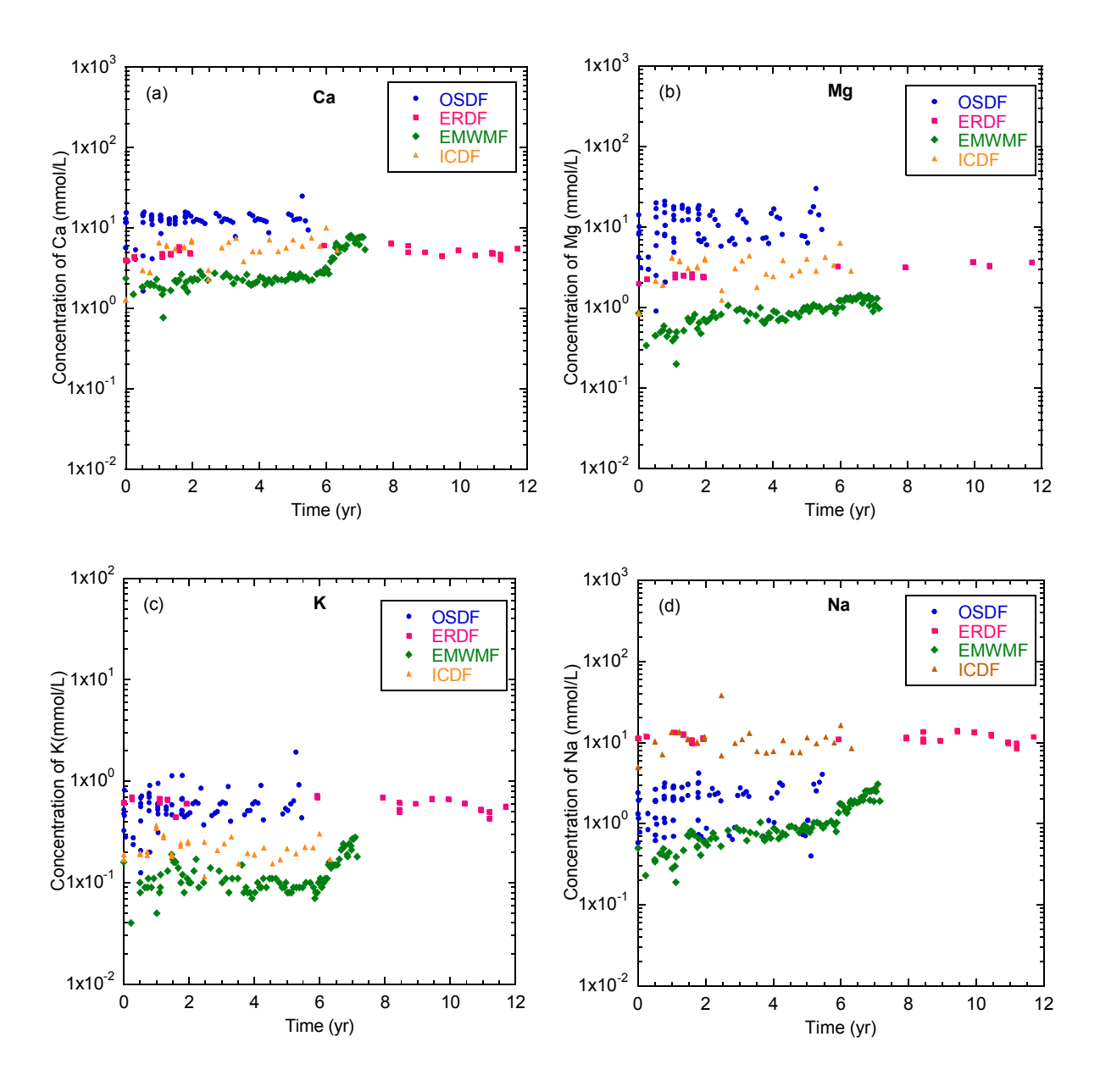


Fig. 2.4. Major cation concentrations over time: (a) calcium, Ca; (b) magnesium, Mg; (c) potassium, K; and (d) sodium, Na.

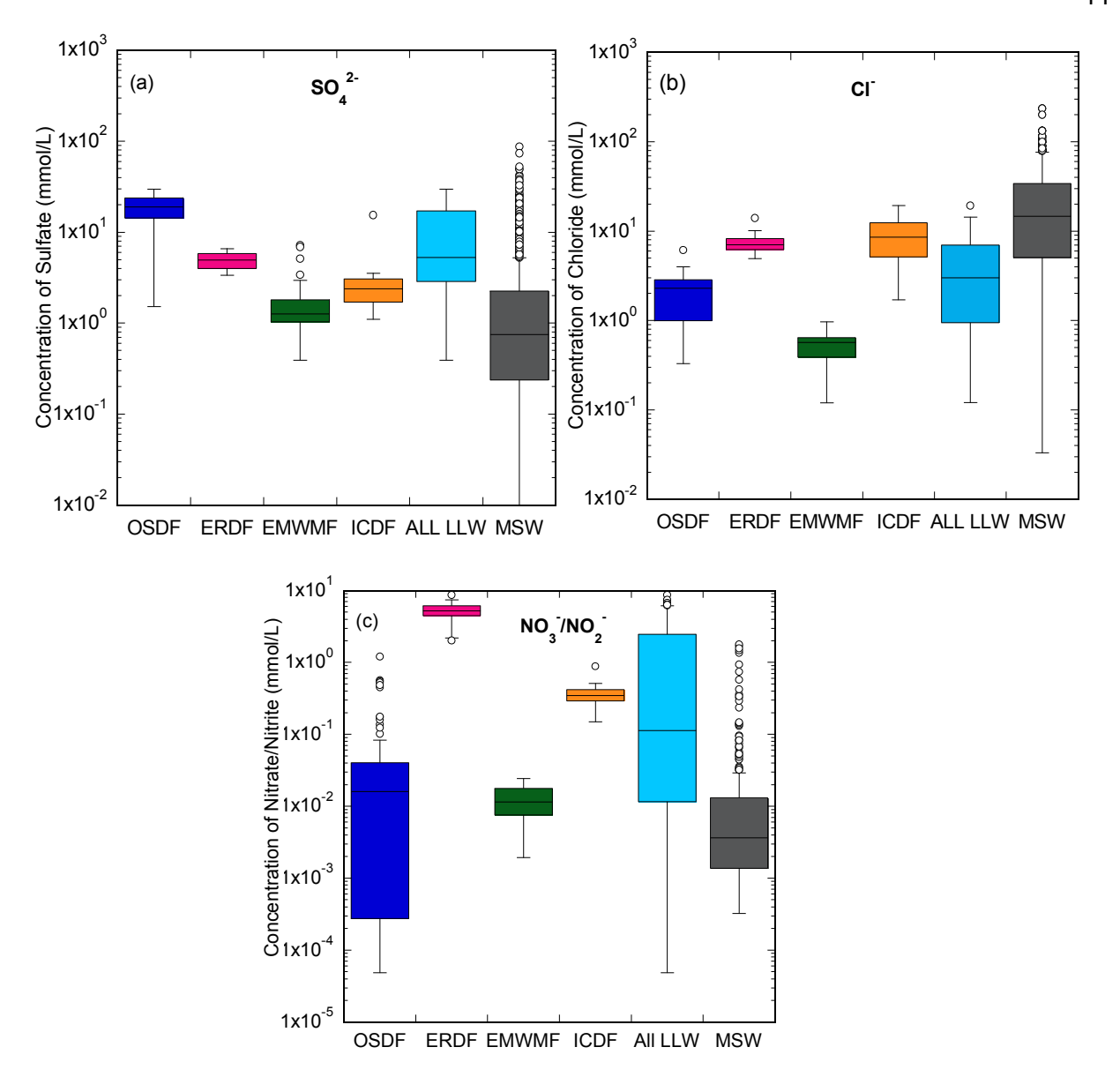


Fig. 2.5. Comparison of major anion concentrations in LLW and MSW leachates: (a) sulfate,  $SO_4^{2-}$ , (b) chloride,  $CI^-$ , and (c) nitrate/nitrite,  $NO_3^-/NO_2^-$ .

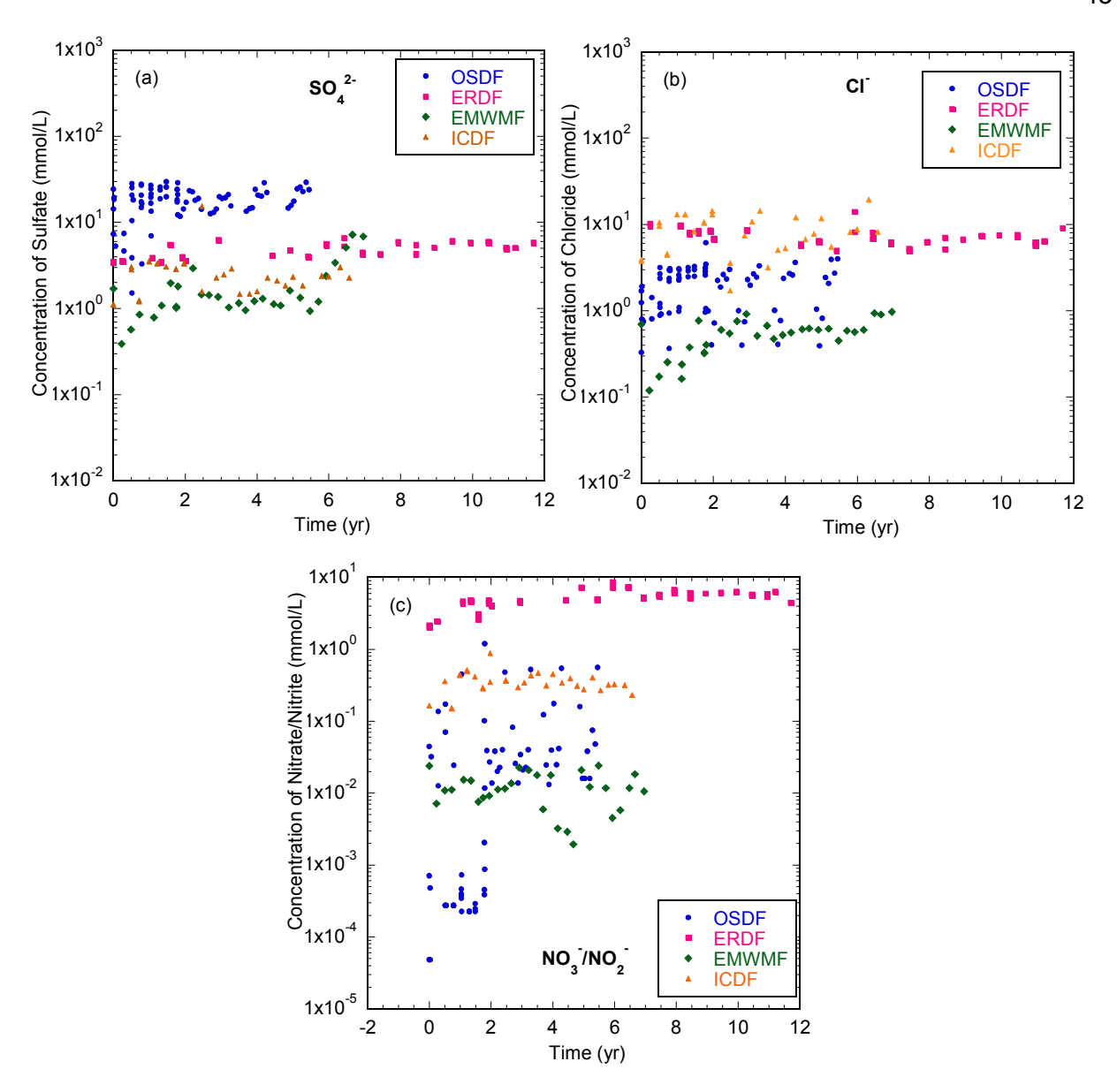


Fig. 2.6. Changes in major anion concentrations with time: (a) sulfate,  $SO_4^{2-}$ , (b) chloride,  $CI^-$ , and (c) nitrate/nitrite,  $NO_3^-/NO_2^-$ .

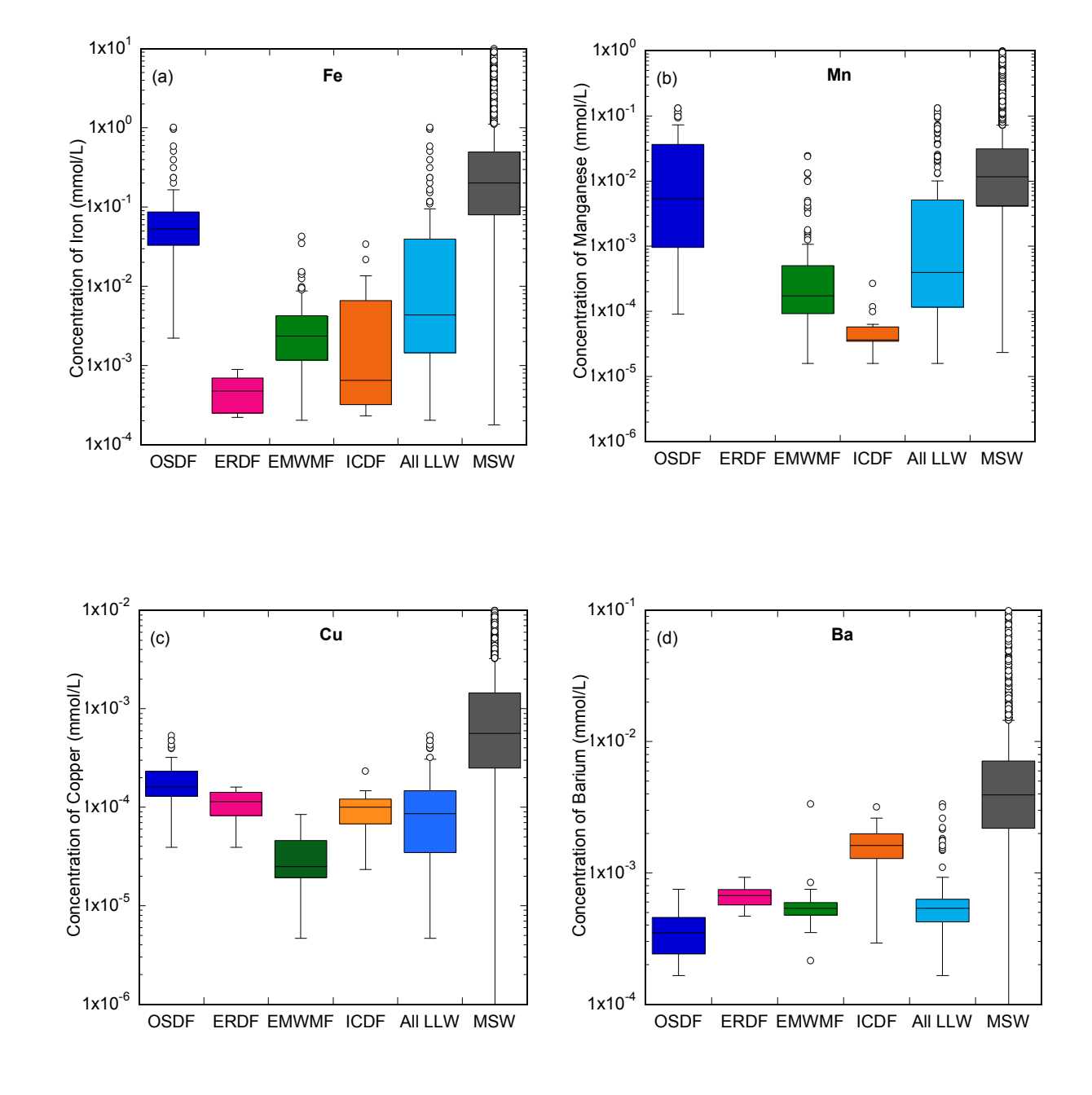


Fig. 2.7. Comparison of trace heavy metal concentrations in LLW and MSW leachates: (a) iron, Fe; (b) manganese, Mn; (c) copper, Cu; and (d) barium, Ba.

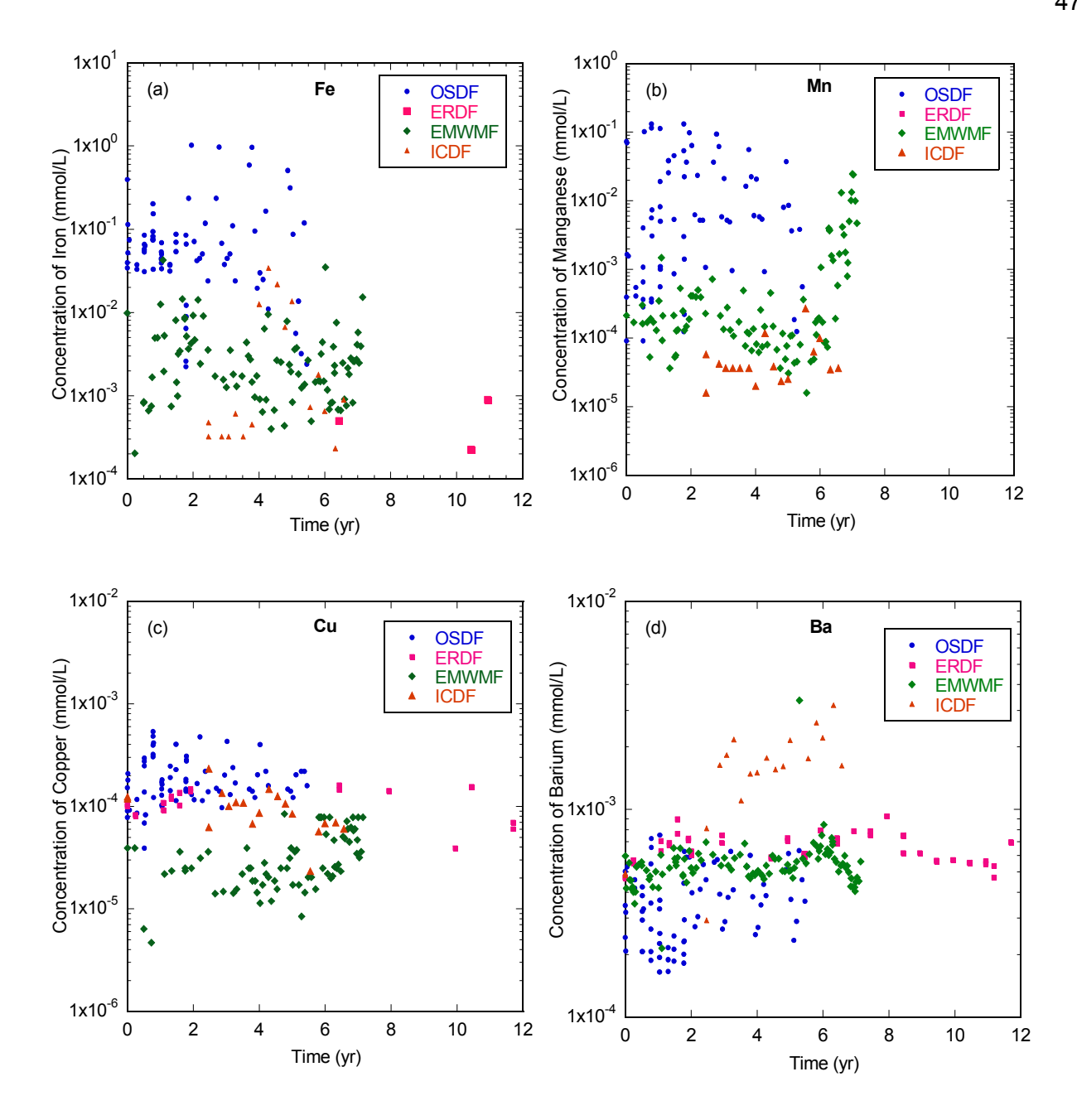


Fig. 2.8. Change of trace heavy metal concentrations with time: (a) iron, Fe; (b) manganese, Mn; (c) copper, Cu; and (d) barium, Ba.

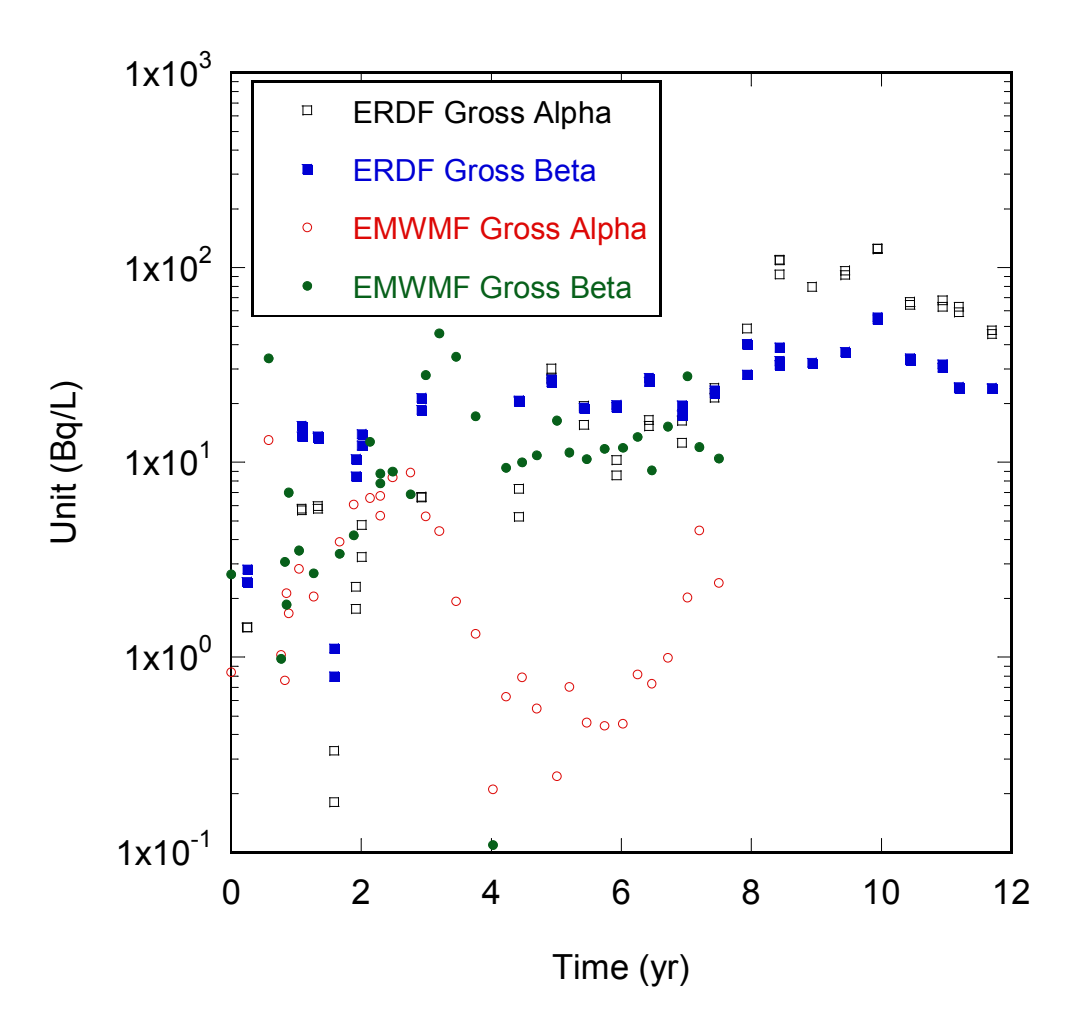


Fig. 2.9. Gross alpha and beta activity (in Bq/L) versus time.

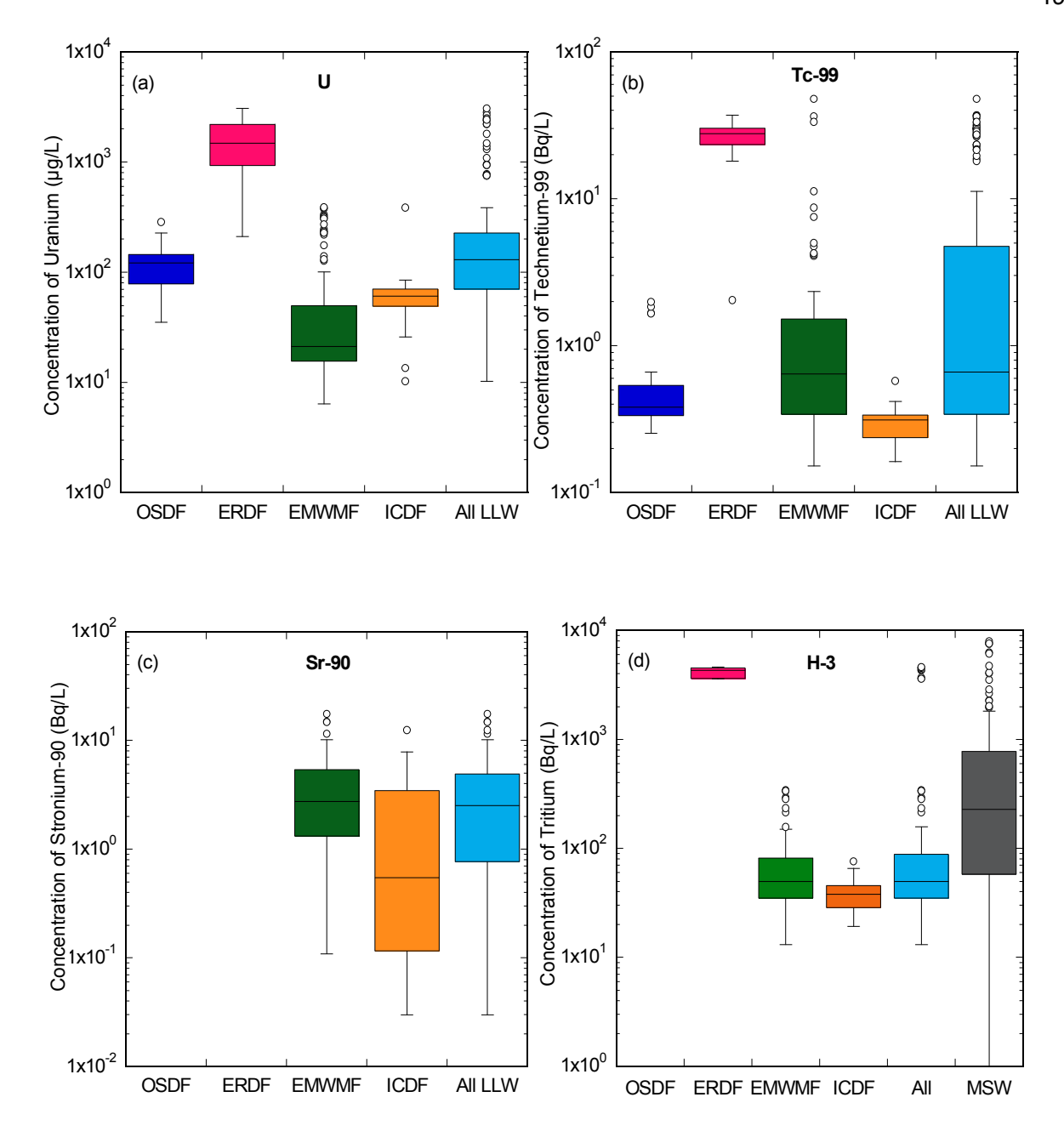


Fig. 2.10. Comparison of specific radionuclide concentrations across LLW sites and in MSW, where applicable: (a) Total Uranium, U; (b) Technetium-99, Tc-99; (c) Strontium-90, Sr-90; and (d) Tritium, H-3.

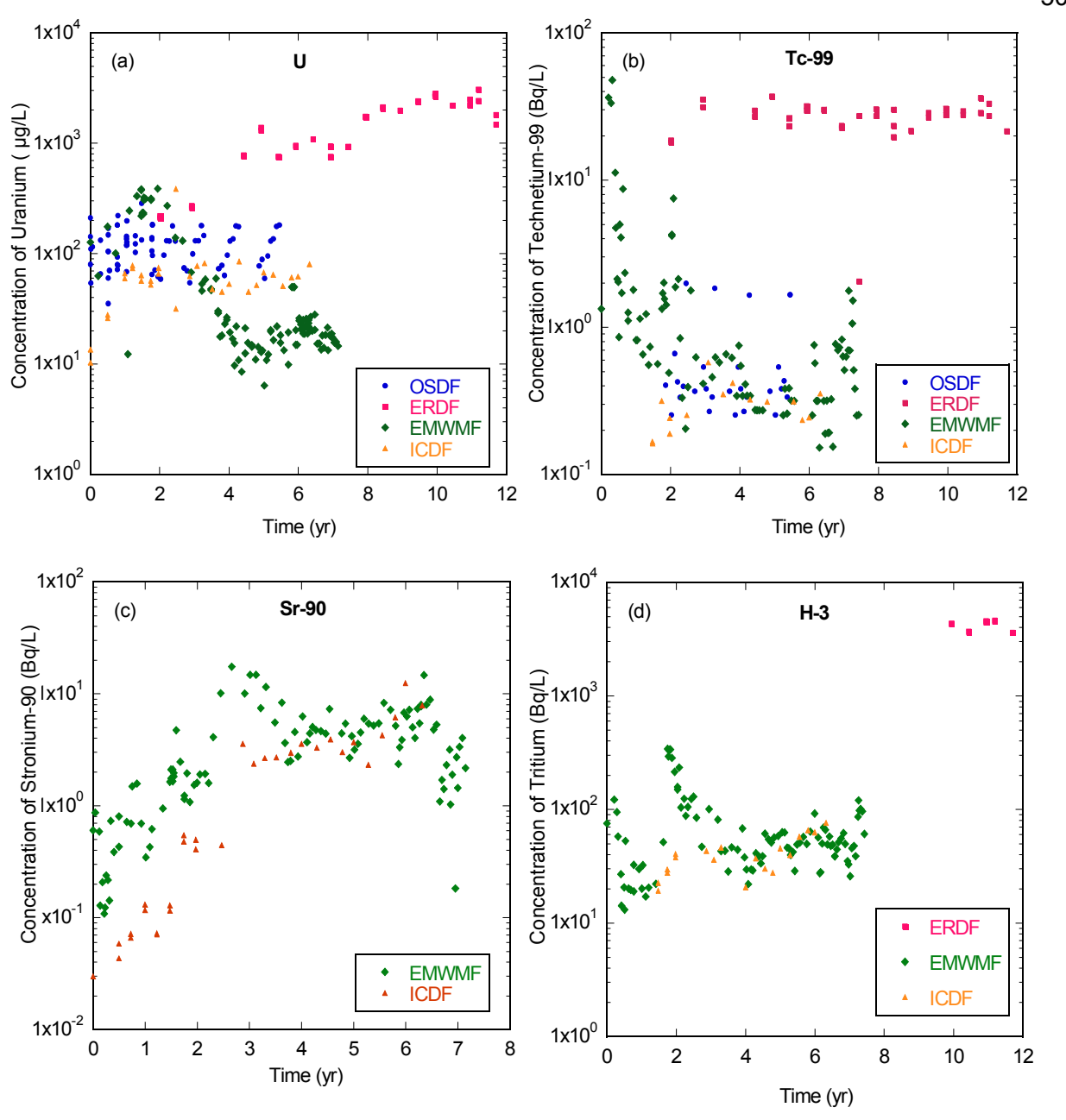


Fig. 2.11. Change in concentration for specific radionuclides with time: (a) Total Uranium, U; (b) Technetium-99, Tc-99; (c) Strontium-90, Sr-90; and (d) Tritium, H-3.

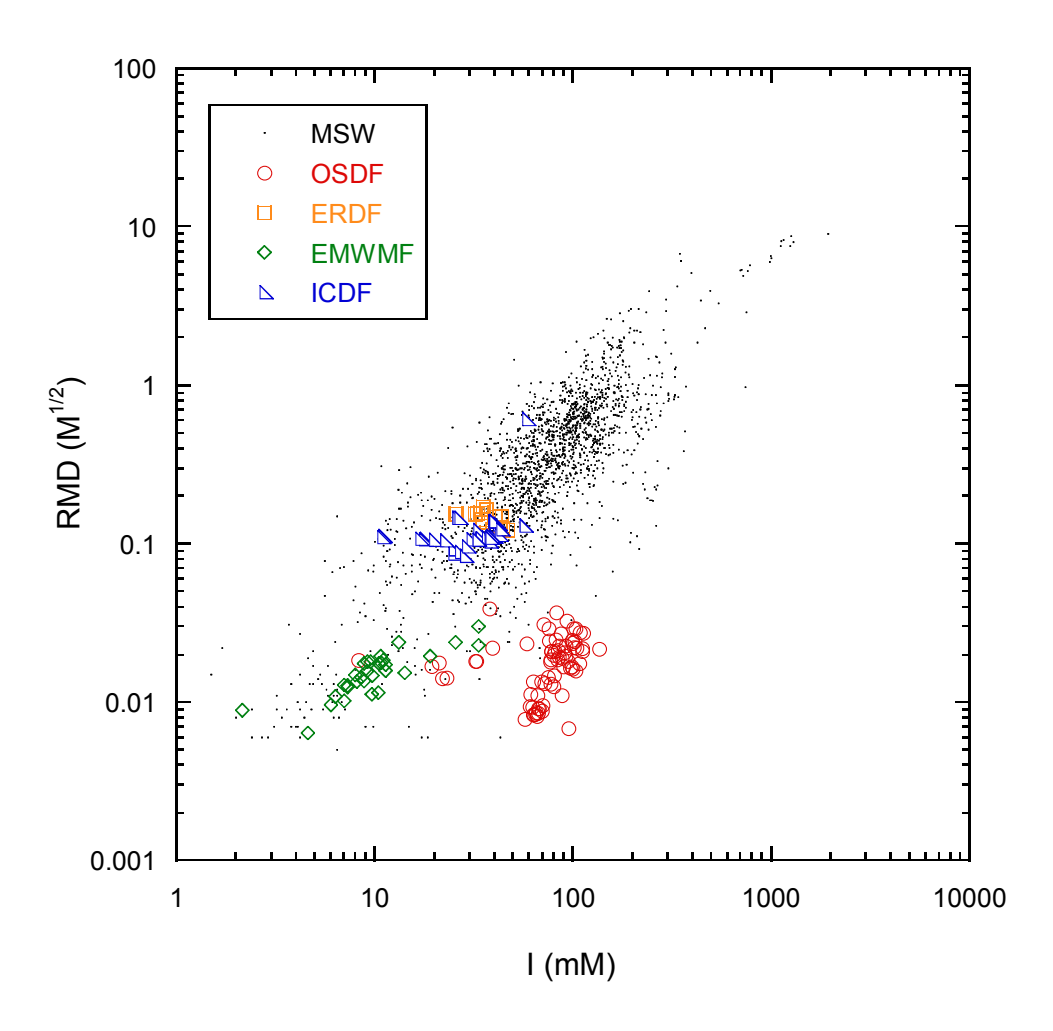


Fig. 2.12. Comparison of RMD to ionic Strength (I) for LLW and MSW leachates.

# 3 BACKGROUND: MECHANISMS FOR THE DEGRADATION OF HIGH-DENSITY POLYETHYLENE GEOMEMBRANE

## 3.1 INTRODUCTION

Geomembranes (GMs) are used in landfill liner systems due to their very low permeability to advective fluid flow. Various types of GMs are used including polyvinyl chloride (PVC), ethylene propylene rubber (EPDM), polypropylene (PP), linear low-density polyethylene (LLDPE), medium-density polyethylene (MDPE) (Rowe and Sangam 2002). High-density polyethylene (HDPE) GMs are used extensively in landfill applications, especially for bottom liners, because of their relatively high resistance to corrosive leachate components.

GMs are composed of varying components, such as resins (> 95%), antioxidants (~ 0.5–1%), and carbon black (~2%) that work to increase the lifetime or effectiveness of the GM. The compositions of several popular GMs are shown in Table 3.1. The basic component of a GM is the resin, such as linear copolymer in HDPE geomembrane. Carbon black is added to the GM formulation to mainly block ultraviolet light from penetrating into the polymer structure (Koerner et al. 1990). Plasticizers are added to the polymer to increase the stiffness of the GM. In addition, a low percentage of antioxidants are introduced to the GM formulation to prevent oxidation and thus provide for a longer service life of the product.

Considering that the first generation of GM barrier liners used in waste facilities is approximately 30-yr old, existing data are insufficient to estimate the service life of a GM. For this reason, many studies have focused on predicting the lifetime of a GM in the laboratory to understand degradation mechanism of the GM and to ensure that GM can work sufficiently for design requirement (Hsuan and Koerner 1998, Gulec et al. 2004, Rowe et al. 2009). The GM degradation includes three stages: (1) antioxidant depletion, (2) induction time, and (3)

decreasing of polymer properties. This chapter provides a review of the existing literature relevant to the durability and degradation mechanisms of HDPE GMs.

## 3.2 DEGRADATION MECHANISMS IN GEOMEMBRANE

Composite barrier systems are used in landfill disposal facilities due to their ability to limit contaminant transport to very low rates. These liner systems often consist (from top to bottom of): a geotextile protection layer, a leachate collection layer, a geotextile protection layer, a 1.5- or 2-mm-thick HDPE GM, and either a geosynthetic clay liner (GCL) or a compacted clay liner (CCL). HDPE GMs have been widely used due to good chemical resistance to many contaminants found in landfill leachate (Tisinger et al. 1991, Eith and Koerner 1997). Typical lifetimes for solid waste landfills are as follows (Hsuan and Koerner 1998):

- Regulatory minimum (e.g., post closure) = 30 years
- Typical nonhazardous waste = 100 years
- Low level radioactive waste = 1000 years

Prediction of the long-term behavior of GM is important to judge the possibility that the material does not degrade below required performance levels over these life spans. GMs in a barrier system undergo degradation in three stages: antioxidant depletion (Stage I), induction time to the onset of polymer degradation (Stage II), and degradation of polymer properties (Stage III). GM degradation is initially controlled by consumption of antioxidants. This process involves the oxidative reaction of antioxidants at the surface of the GM and loss of antioxidants by diffusion (Rowe et al. 2009, 2010). Without protection of antioxidants, a GM becomes vulnerable to oxidative degradation and rapidly undergoes the second and third stages of degradation (Grassie and Scott 1985).

Polyethylene resin is the major part of HDPE GM. Polyethylene is comprised of polymer chains (see Fig. 3.1). Short chain branches are attached to the main carbon backbone (C-C bond) of the polyethylene chain. Lustiger (1985) provided a model to explain the microscopic structure of polyethylene (Fig. 3.2). HDPE consists of a crystalline region and an amorphous region. The crystalline region consists of packs of folded polymer chains named lamella, which are interconnected by the amorphous region. There are three types of intercrystalline chains in the amorphous region:

- 1) Cilia—chains suspended from the end of a crystalline chain
- 2) Loose loops—chains that begin and end in the same lamella
- 3) Tie molecules—chains that begin and end in adjacent lamellae

The intercrystalline polymer chains are named tie molecules and play an important role in the amorphous region. Tie molecules are polymer chains that connect two or more crystalline lamellae (Soares et al. 2000). Lack of tie molecules can lead to a crack in the polymer.

The degradation process of a GM is considered to be a combination of physical and chemical aging of polyethylene (Hsuan and Koerner 1998). Physical aging begins as a slow process with the polymer attempting to reach equilibrium from its manufactured state. During the physical aging process, no covalent bonds are broken in semicrystalline polymers like HDPE GM; however, the process involves a slight increase in the crystallinity of the material (Petermann et al. 1976). Augmentation of crystallinity leads the polymer to increase in stiffness and brittleness. Chemical aging involves bond scission (e.g., C-C or C-H) in the polymer. Bond scission can potentially generate new intermolecular cross-linking, which means that one broken bond connects with another broken bond belonging to a different polymer chain (Schnabel 1981). Chemical aging eventually leads to a decrease in engineering properties and ultimately failure (Rowe and Sangam 2002). Therefore, from an application perspective, chemical aging is the more important degradation mechanism in

comparison to physical aging. Rowe and Sangam (2002) provided a specific discussion of the various types of degradation mechanisms to which an HDPE GM may be subjected by considering its environmental exposure. The degradation mechanisms include swelling, UV degradation, degradation by extraction, biological degradation, oxidative degradation, and radiation degradation.

# 3.2.1 Degradation due to Swelling

Degradation by swelling occurs when the volume of the GM increases due to sorption after exposure to a liquid such as water or leachate (Rowe and Sangam 2002). This type of degradation is reversible after the GM is removed from a liquid, as some desorption of the sorbed chemicals occurs. This type of degradation is generally not a concern for HDPE GMs in landfill applications since swelling does not break chemical bonds (Koerner et al. 1990).

#### 3.2.2 Extraction

Extraction is a type of degradation where several components are removed from the GM due to long-term exposure to liquids. Polymer additives may be extracted after long-term exposure (Koerner et al. 1990). The consequences of extraction become significant when stabilizers and antioxidants are leached out, thus subjecting the GM to other degradation mechanisms (e.g., oxidative degradation).

## 3.2.3 Oxidative Degradation

The essential oxidation process of a polymeric material like HDPE follows free radical chain mechanism (Kelen 1983, Grassie and Scott 1985). Polymer chains react with oxygen thus causing changes in molecular structure, such as breakage of covalent bonds and generation of more cross-linking. Grassie and Scott (1985) described the oxidation mechanism as two interacting cyclical processes, as shown in Fig. 3.3. The loop A is the

alkyl (R•)/hydroperoxy radical (ROO•) chain reaction and the loop B involves the decomposition of hydroperoxides (ROOH), which feeds the chain reaction with two free radicals.

The reaction starts when polymer chain (RH) obtains enough activation energy to form a free radical polymer chain (R•) and H• as shown in Eq. 1 (Koerner et al. 1990):

$$RH \to R \bullet + H \bullet \tag{1}$$

Then, oxygen  $(O_2)$  reacts with a free radical in the polymer  $(R \bullet)$ , thus forming a hydroperoxy free radical  $(ROO \bullet)$  as shown in Eq. 2:

$$R \bullet + O_2 \to ROO \bullet \tag{2}$$

The hydroperoxy free radical reacts with a polymer chain (RH) forming a hydroperoxides (ROOH) and another free radical (R●) as shown in Eq. 3:

$$ROO \bullet + RH \rightarrow ROOH + R \bullet \tag{3}$$

As oxidation continues, additional ROOH molecules are formed. Once the concentration of ROOH overcomes a threshold level, decomposition of ROOH begins, leading to a substantial increase in the amount of free radicals, as indicated in Eq (4)–(6) (Hsuan and Koerner 1998), which is an auto-accelerated process:

$$ROOH \rightarrow RO \bullet + OH \bullet \tag{4}$$

$$RO \bullet + RH \to ROH + R \bullet \tag{5}$$

$$OH \bullet + RH \rightarrow H_2O + R \bullet \tag{6}$$

As hydroperoxide decomposes to RO• and OH•, the oxidation reaction rate increases as a result of more free radicals induced to the oxidation reaction. The sequence of oxidation reactions in HDPE GMs indicated by Eq. (1)-(6) are the interconnected cycles A and B shown in Fig. 3.3. There are four important links in these two cycles, designated (a)-(e). As

oxidative degradation continues, critical mechanical properties start to change, such as yield stress, ultimate breaking elongation, and stress crack resistance (Rowe et al. 2009).

## 3.2.4 Radiation Effect

Exposure to radiation can lead to degradation of a GM. Neutron and  $\gamma$ -rays are uncharged and can penetrate several meters into polymer, whereas  $\alpha$  and  $\beta$  particles are charged and their penetration is limited (Koerner et al. 1990). The  $\alpha$  particles can be shielded by the surface of polymer (micrometer level) and  $\beta$  particles can penetrate into polymer on the order of millimeters. Therefore,  $\alpha$  and  $\beta$  radiation have a surficial effect, whereas neutron and  $\gamma$ -rays homogeneously affect the entire thickness of polymers (Koerner et al. 1990). When radiation penetrates a GM and liberates free radicals, causing broken of covalent bonds in the polymer (Koerner et al. 1990). Typically, one high-molecular weight polymer chain contains thousands of carbon atoms. Thus a cross-linking between two separated polymer chains leads to a significant change of molecular weight. (Phillips 1988).

# 3.2.5 UV Degradation

Irradiation with UV light can cause GM degradation (Rowe and Sangam 2002), which is defined as natural photodegradation. Similar to the radiation effect, UV light can cause photooxidation and bonds break inner structure of polymers, such as reduces the molecular weight of the polymer or generate cross-linking. Long-term exposure to UV induces surface cracks and brittleness of GMs (Schnabel 1981). Carbon black is added to HDPE GM to prevent UV light from penetrating the polymer structure, thus reducing susceptibility to UV degradation. Koerner et al. (1990) indicated that a 15-cm-thick soil above the GM provide adequate protection from UV light.

Hamid (2000) indicated that degradation of polymer can be accelerated with a combination of degradation mechanisms. For example, the ultraviolet radiation effect from

sunlight combines with the oxidative effect from atmospheric oxygen to accelerate the rate of oxidation. UV light contains sufficiently energy to break some bonds directly or to liberate electrons (Suits and Hsuan 2003), and these excited radicals are readily reacted in the presence of oxygen, then the degradation process will be accelerated.

## 3.3 FACTORS AFFECTING THE OXIDATIVE DEGRADATION

Geomembrane durability has been historically addressed in terms of field performance and laboratory testing results under various conditions. The oxidative degradation of HDPE GMs is affected by several factors including the properties of the GM, exposure medium, exposure conditions, and applied mechanical stress field (Rowe and Sangam 2002).

# 3.3.1 GM Properties

The ability of a polymer to resist oxidative degradation largely depends on its chemical structure. Polyethylene chains with fewer branches form less free radicals than those with more branches under the same site conditions (Hsuan and Koerner 1995), because tertiary hydrogens that possess lower dissociation energy (measurement of the strength in a chemical bond, defined as the standard enthalpy change when a bond is broken) than primary or secondary hydrogen atoms (shown in Fig. 3.4), thus making it easier to be converted to free radicals (Kelen, 1983).

Polymer is not susceptible to oxidative degradation in the crystalline phase of semicrystalline polymers because crystalline regions are sufficiently dense, thus restricting oxygen diffusion (Kelen 1983). However, amorphous regions display more susceptibility to oxygen diffusion. This indicates that a GM with high crystallinity is less vulnerable to oxidative degradation than a GM with low crystallinity. Michael and Bixler (1961) stated that the diffusion of oxygen in polyethylene depends not only on the volume fraction of the amorphous region but also on the size, shape, and distribution of crystallites. Likewise, GM

thickness has a significant effect on oxidative degradation. Rowe et al. (2010) reported that the depletion rate of antioxidants decreases with increasing GM thickness and that thicker GMs display longer oxidation induction time than thinner ones. Since the main loss of antioxidant was caused by dissolution to surrounding liquid, outward migration of antioxidants is slower for a thick GM than a thin GM (Rowe et al. 2010). The longer induction time also stems from oxidation rate, which is a function of the number of oxygen molecules available to attack the polymer chains (Kelen 1983). The presence of oxygen in a GM is diffusion controlled, increasing thickness reduces the potential for oxygen to attack the inner polymer. A thicker GM increases the diffusion path of antioxidants, thus inducing a longer period for antioxidant depletion.

## 3.3.2 Exposure Medium

The medium (soil or liquid) in direct contact with a GM can significantly affect the oxidation rate. The chemical compositions of leachate influence the oxidation rate in GMs. The presence of trace metals, either in soil or leachate exposed to the GM, can cause decomposition of hydroperoxides, resulting in accelerating consumption of antioxidants in HDPE GM (Hsuan and Koerner 1995). Metal components such as Cu, Mn, and Fe in leachate can significantly enhance the breakdown of hydroperoxide (ROOH), thus creating free radicals and accelerating the oxidative reduction of the GM (Osawa 1992). Surfactant present in leachate also affects the oxidation rate in GM. Since surfactant can increase the wettability of a GM by decreasing its surface tension, the antioxidant on the GM surface can more easily dissolve into the leachate (Rowe and Islam 2008). Thus, diffusion increases the rate of antioxidant consumption.

#### 3.3.3 External Mechanical Stresses

A large external stress or loading on a GM decreases its service lifetime, primarily through physical creep (Horrocks and D'Souza 1992). Oxidative degradation is the dominant factor at low stress conditions, mechanical stress accelerates oxidative degradation at intermediate stresses, and mechanical breakage of stressed bonds is dominate at high stresses. Accordingly, the stress levels used in accelerated laboratory aging tests is an important factor that requires consideration (Rowe and Sangam 2002).

# 3.4 ANTIOXIDANT DEPLETION

Hsuan and Koerner (1998) summarized two categories of antioxidants used for commercial GM as primary and secondary antioxidants (shown in Table 3.2). Different types of antioxidant display various effective temperatures. For example, hindered phenol can work efficiently from 0 to 300 °C, while hindered amine loses its ability at temperature over 150 °C. Primary antioxidants, such as hindered phenol and hindered amine, stabilize the polymer by reacting directly with free radicals and creating inert species after formulation; e.g., breaking links (a), (b), and (e) (shown in Fig. 3.3). There are five important links in these two cycles, designated (a)–(e). If any of the links are broken, the oxidation rate of the polymer is halted. If all five links are intercepted, then oxidation is stopped. Therefore, the purpose of adding antioxidants in the GM formulation is to halt these reactions and thus stop the oxidative degradation. The antioxidants intercept the link (b) and (e) by donating an electron, which reacts with free radicals ROO•, RO• and •OH by converting them to ROOH, ROH, and H<sub>2</sub>O, respectively. Another type of antioxidant intercept link (a) by accepting an electron, which converts alkyl free radicals (R.) to a stable polymer chain. Secondary antioxidants are designed to intercept links (c) and (d) in the B cycle (see in Fig. 3.3). Their function is to react with hydroperoxides (ROOH) to form a stable alcohol (ROH), which prevents the formation of more free radicals in Eq. 4, 5, and 6 and impedes oxidation. Typically, in a commercial GM, antioxidant packages, including two or more types of antioxidant, are used to protect GM from oxidation. The antioxidant packages should not only protect the GM from high temperature due to extrusion processes but also should prevent oxidation at lower temperatures during its service lifetime.

### 3.5 LIFE TIME PREDICTION METHODS

The oxidative degradation of HDPE GMs can be divided into three relatively distinct stages (Hsuan and Koerner 1995 and 1998) as shown in Fig. 3.5. The depletion of antioxidants (Stage A) is due either to their consumption as a result of their chemical reactions with oxygen, free radicals, and hydroperoxides or to their physical loss by diffusion. The antioxidant depletion rate is highly dependent on the type, amount, and distribution of antioxidants, temperature, and environmental conditions (Koerner et al. 2005). Antioxidant depletion is measured by oxidation induction time (OIT) following ASTM D3895. Longer OIT time indicates that a high amount of antioxidants remains in the GM.

In the induction period (Stage B), the polymer reacts with oxygen and forms hydroperoxide, as indicated in Eq. (1)–(3). However, the concentration of ROOH is so low in this stage that the hydroperoxide does not decompose into other free radicals. The engineering properties of GM do not change in this stage. During Stage C (see Fig. 3.5), hydroperoxides start to decompose free alkyl radicals, which leads to accelerated oxidation (Hsuan and Koerner 1995). As oxidation continues, more ROOH molecules are formed. Once the concentration of ROOH reaches a critical level, decomposition of ROOH begins, leading to a substantial increase in the amount of free radicals, as indicated in Eq. (4)–(6). In the early stage of this acceleration, the molecular weight remains the same, while mechanical properties appear relatively unchanged (Rowe and Islam 2010). As oxidation

advances further, the reaction of oxygen degradation occurs as chain scission (C-C bond breakage) causing a reduction in molecular weight or cross-linking increasing molecular weight. Such changes in molecular size can be detected by the melt flow index (MFI) test because the MFI is inversely related to molecular weight. A direct consequence of the degradation that occurs during Stage C is the decrease of both stress and strain at break; however, stress crack resistance (SCR) is far more significant than tensile modulus and yield stress in assessing GM service life (Rowe et al. 2009).

Stress cracking is very important because even short cracks can allow large leachate flux through the GM. Moreover, short cracks grow with time, eventually allowing excessive leakage through the GM even in areas of good contact with the clay (Rowe and Sangam 2002). According to ASTM D883, stress cracking is "an external or internal rupture in a plastic caused by tensile stress less than its short term mechanical strength." One concern of HDPE GMs is their susceptibility to stress cracking as a consequence of their high crystallinity (typically about 40-50%). There are three stages in crack development (Peggs and Carlson 1989): crack is (1) initiated at a scratch that is a planar defect, (2) opened in the presence of tensile stress, and (3) propagated through the GM. The molecular structure of the polymer controls its susceptibility to stress cracking. Lustiger and Corneliussen (1986) summarized that lack of tie molecules might lead to failure in long service lifetime. Fig. 3.2 shows that tie molecules are abundant in the amorphous zone, which controls the stresscrack behavior. Consequently, HDPE GM with a high degree of crystallinity is prone to stress cracking due to lack of tie molecules. Other polymer properties, such as molecular weight and comonomer content, also affect its resistance to stress cracking ability (Lu and Brown 1990 and 1991). Higher molecular weight corresponds to longer chains resulting in more tie molecules and more effective tie molecule entanglements, providing better cracking resistance.

The service lifetime of GM is taken as the sum of the duration of the three stages (Fig. 3.5). Stage C is characterized by significant changes to the physical and mechanical properties that lead to GM failure. The end of the GM service lifetime is defined as the point in Stage C when the mechanical properties of the GM are reduced below a critical level. The two most commonly used approaches to define service life correspond to 50% of the initial property (Hsuan and Koerner 1998) or 50% of the specified property value (Rowe et al. 2009). The latter approach is reasonable for products whose initial value of properties significantly exceeds the minimum specified value (Rowe and Sangam 2002).

### 3.6 LABORATORY STUDIES OF GM DURABILITY

Laboratory testing involves incubating and aging the GM samples under an ambient surrounding that is designed to simulate to typical field conditions (Hsuan and Koerner 1998). The degradation reaction under incubating conditions is accelerated by using elevated test temperatures, which results in degradation of the sample in a relatively short period of time (e.g., a few months under accelerated conditions in comparison to many years under actual site conditions).

Two methods (immersion and column tests) are widely used for incubation testing of GMs. Immersion tests involve submerging GMs in a fluid within a temperature-controlled apparatus (shown in Fig. 3.6) for extended lengths of time. Samples are removed periodically to determine change in antioxidant quantity or physical and mechanical properties. The typical mediums used in immersion tests are air, water, and synthetic leachate, which is commonly used to mimic the conditions expected in the field (Gulec et al. 2004, Rowe et al. 2009). Exposing both sides of a GM is not the same as the exposure condition in the field, so these tests provide a conservative prediction of service lifetime of GMs (Rowe et al. 2010).

Column testing is another method used for incubation testing for the prediction of GM lifetime. A diagram of a typical column incubation test apparatus is shown in Fig. 3.7. The advantage of column testing is that an analog to field conditions is created with a specific subgrade and overburden material (e.g., gravel, geotextile, and geosynthetic clay liner). Liquids are applied to one side of the GM, and controlling equivalent pressure (simulate 20-or 30-m-thick waste pressure) to the GM (Koerner 2005). The service lifetime of the GM at a site-specific temperature can then be predicted by using the Arrhenius extrapolation method based on data obtained from the elevated temperature tests.

Stage A of service life of a GM is highly dependent on the depletion rate of antioxidants. During Stage A, OIT of the GM decreases as antioxidants are depleted with time (Hsuan and Koerner 1998). Thus, the standard OIT (ASTM D3895) and high pressure OIT (ASTM D5885) test are used to monitor the depletion of antioxidants from a GM using differential scanning calorimeters (DSC).

Standard OIT testing involves testing a GM at 200 °C and 35 kPa in an inert gas environment (e.g., nitrogen) until equilibrium, then oxygen gas is introduced to attack the HDPE GM specimens. The GM specimen is held isothermally in an oxygen environment until the exothermic peak is detected. The time span from the moment the oxygen is introduced until the beginning of the exothermic reaction is the OIT. A high pressure OIT (HP-OIT) can be performed at higher pressure (3400 kPa) and relatively lower temperature (150 °C) than the standard OIT test because several types of antioxidants can volatilize and deactivate at temperatures greater than 150 °C, thus providing conservative estimates of the GM lifetime (Hsuan and Koerner 1998).

Depletion of antioxidant from a HDPE GM follows the frist order decay (Sangam and Rowe 2002). At aging time, the OIT representing the total amount of antioxidant remaining in the GM can be expressed as:

$$OIT(t) = OIT_0 \exp(-st)$$
 (7)

Or, taking logarithm of both sides:

$$ln(OIT(t)) = ln(OIT_0) - st$$
 (8)

where OIT is the measured oxidation induction time,  $OIT_0$  is the initial oxidation induction time, s is the antioxidant depletion rate, and t is the incubation time.

The antioxidant depletion rate can be described by the Arrhenius equation:

$$s = A \exp(-E_a/RT) \tag{9}$$

where A is a constant (month<sup>-1</sup>), E<sub>a</sub> is the activation energy in kJ/mol, R is the universal gas constant, and T is the absolute temperature. The Arrhenius model commonly used to extrapolate the experimental data obtained at high aging temperature to a specific site temperature (Hsuan and Koerner 1995, Hsuan and Koerner 1998, Sangam and Rowe 2002, Gulec et al. 2004, Rowe et al. 2009). Three assumptions are required for use of the Arrhenius equations: (1) antioxidant depletion only depends on temperature, (2) A is constant with various temperatures, (3) the activation energy remains the same through the temperature range (Rowe et al. 2009).

The site-specific antioxidant depletion rate can be used in Eq. 8 along with the OIT of unstabilized GM, which is usually taken to be 0.5 min (Hsuan and Koerner 1998). The use of 1.0 min as the OIT of unstabilized GM is also common due to uncertainty in the measurement of unstabilized OIT. Rowe et al. (2009) showed that uncertainty due to using 0.5 min or 1.0 min as the unstabilized OIT is negligible.

Durations of Stage C determined from incubation testing must also be adjusted for sitespecific temperatures (Rowe et al. 2009). The duration of stage C can be established using Eq. 10,

$$\frac{t_{T1}}{t_{T2}} = \exp\left(-\frac{E_a}{R} \left[ \frac{1}{T_1} - \frac{1}{T_2} \right] \right)$$
 (10)

where  $t_{T1}$  is the time for 50% degradation of the engineering property at the elevated testing temperature,  $t_{T2}$  is the estimated time for 50% degradation of the property at the site-specific temperature,  $T_1$  is the testing temperature,  $T_2$  is the expected site-specific temperature, and  $E_a/R$  is the slope of the Arrhenius plot.

The Arrhenius equations (Eq. 8 and 9) can be used to estimate the antioxidant depletion rate at typical MSW landfill liner temperatures. Based on currently available data, the primary liner temperatures are expected to be between 30 °C and 40 °C, and 35 °C can be taken as the median temperature (Rowe 2005). In some landfills with leachate recirculation and/or moisture augmentation systems designed to accelerate biodegradation of organic waste, the liner temperature may exceed 40 °C (Koerner and Koerner 2006) and could in some circumstances reach 60 °C (or even higher in some unpublished cases). Liner temperatures of 40–60 °C have been observed in municipal solid waste landfills where there is a significant leachate mound (Rowe 2005).

# 3.7 LIFE TIME PREDICTION STUDIES

Many investigators have conducted laboratory tests to examine durability and degradation mechanisms related to GM liners for landfills (e.g., Hsuan and Koerner 1998, Sangam and Rowe 2002, Gulec et al. 2004). Studies commonly focused on the antioxidant depletion rate of Stage A, with relatively few studies focusing on stages B and C.

Immersion testing is one of the most common methods for GM service lifetime predictions because it is relatively simple and less time consuming. Sangam and Rowe (2002) conducted a series of laboratory-accelerated aging tests for HDPE GM. 2.0-mm-thick GM was exposed to air, water, and synthetic leachate at temperature of 22, 40, 55, 70, and

85 °C. Antioxidant depletion rate was fastest in leachate and slowest in air. Arrhenius modeling used to determine the estimated duration of stage A resulted in 12–40 years in leachate, 44–190 years in water, and 90–390 years in air for temperatures ranging from 13–33 °C. This paper also estimated the antioxidant depletion rate for a GM exposed to leachate on one side and unsaturated soil on another, and the measurement of antioxidant depletion times 160 years at 13 °C and 40 years at 33 °C. A general summary of antioxidant depletion rates depending on temperature (based on Arrhenius model) are shown in Table 3.3.

The experiments reported by Sangam and Rowe (2002) were continued following the publication of the preliminary results, with updated results reported by Rowe et al. (2009). After an additional seven years, the updated antioxidant depletion times for specimens immersed in leachate ranged from 5–25 years for temperatures between 20 °C and 50 °C (shown in Table 3.4). In addition, the testing focused on Stage B and C. The GM, incubated at 85 °C, passed from Stage B to C (shown in Table 3.5 and Table 3.6), with an observed decrease in MFI with time attributed to the oxidative cross-linking. Three main properties dominated the lifetime prediction of GM: (1) tensile break strength, (2) tensile break strain, and (3) stress crack resistance. The properties of tensile break strength lead to the longest service lifetime prediction, while stress crack resistance provides a relative short estimation. The estimated total service lifetime is shown in Table 3.7

Column testing provides a more accurate prediction of the GM lifetime because field conditions can be simulated more precisely, such as one side exposure of GM and undersimulated stress. The antioxidants diffuse out from both sides of a GM dissolve into the leachate immersion testing, which causes a relatively high concentration gradient and a short outward diffusive flux path from the centroid to surface. Only one side of the GM installed in landfill liner contacts with leachate. Therefore, a simulated liner test can provide more accurate prediction for antioxidants depletion (Rowe and Rimal 2008, Rowe et al. 2010 and

Rowe et al 2013). Rowe and Rimal (2008) conducted a comparison test between simple immersion test and simulated composite liner condition aging test by using 1.5-mm-thick HDPE GM. The antioxidant depletion rate obtained from immersed test was 3.5 times higher than the one based on a simulated liner test. In addition, Rowe et al. (2010) measured antioxidant depletion of HDPE GM under simulated landfill liner conditions with applied pressure of 250 kPa. The predicted antioxidant depletion time based on this improved simulation test was approximately 3 times longer than the one from simple immersion testing.

## 3.8 SUMMARY

GM lifetime is influent by various degradation mechanisms including swelling, UV light degradation, and degradation by extraction, biological degradation, oxidative degradation, and radiation degradation. These degradation factors can combine together to accelerate the overall degradation rate.

Immersion incubation tests and column incubation tests were both used to predict the service lifetime of GM. Comparing with immersion test, column incubation tests provide a more realistic simulation of field conditions. Thus, accurate estimates of GM service lifetime can be obtained based on the data from column testing.

The antioxidant depletion follows first-order decay. Then Arrhenius modeling is used to extrapolate the experimental data obtained at higher temperature to the *in situ* environment at lower temperature. Based on Arrhenius modeling, GM lifetimes have been estimated to be as high as 1905 years at 20 °C, or as low as 50 years when the temperature is elevated to 50 °C (Rowe et al. 2009).

#### REFERENCE

- Bacaç, M., and Kumru, M. (2000). Uranium, radium and field measurements in the water of Gediz river. *Turk. J. Eng. Env. Sci.*, 24, 229–236.
- Cheng, J., Polak, M., and Penlidis, A. (2011), Influence of micromolecular structure on environmental stress cracking resistance of high density polyethylene. *Tunnelling and Underground Space Technology*, 26, 582–593
- Farquhar C. and Rovers, F. (1973). Gas production during refuse decomposition. *Water Air Soil Pollut.*, 2, 483–495.
- Flory, P. and Vrij, A. (1963). Melting points of linear-chain homologs. The normal paraffin hydrocarbons. *Journal of the American Chemical Society* 85, 3548–3553.
- Grassie, N. and Scott, G. (1985). *Polymer Degradation and Stabilization.*" Cambridge University Press, New York, USA, 222.
- Gulec, S., Edil, T., and Benson, C. (2004). Effect of acidic mine drainage on the polymer properties of an HDPE geomembrane. *Geosynthet. Int.*, 11(2), 60–72.
- Hamid, S. (2000). *Handbook of polymer degradation-second edition*. Marcel Dekker, Inc, New York.
- Hsuan, Y. and Koerner, R. (1998). Antioxidant depletion lifetime in high density polyethylene GMs. *Journal of Geotechnical and Geoenvironmental Engineering*, 124(6), 532–541.
- Hsuan, Y. and Guan, Z. (1997). Evaluation of the antioxidant behavior of polyethylene geomembranes using oxidative induction time tests. *Oxidative behavior of materials by thermal analytical techniques*, ASTM STP1326, A. T. Riga and G. H. Patterson, eds., ASTM, Philadelphia, 76–90.
- Hsaun, Y. and Koerner, R. (1995). Long term durability of HDPE GM: Part I depletion of antioxidant. *GRI Report* 16, 35.
- Horrocks, A. and D'Souza, J. (1992). Degradation of polymers in geomembranes and geotextiles. In:Hamid, A.H., Amin, M.B., Maadhah, A.G., (Eds.), *Handbook of Polymer Degradation*, 434–505.
- Islam, M. and Rowe, R. (2007). Leachate composition and antixoxidant depletion from HDPE geomembranes. *Proc., Geosynthetics 2007 Conf. CD-ROM*, Washington D.C.
- Kelen, T. (1983). Polymer Degradation. Van Nostrand Reinhold, New York, NY, 211.
- Koerner, R., Hsuan, Y., and Koerner, G. (2005). Geomembran lifetime prediction: unexposed and exposed conditions. *GRI White Paper* 6, 19.
- Koerner, R. M. (2005). Designing with geosynthetics. *Pearson Education, Inc.,* Upper Saddle River, NJ, 796p.
- Koerner, R., Lord, A., and Hsuan, Y. (1992). Arrhenius modeling to predict geosynthetic degradation. *Journal of Geotextiles and GMs*, 11(2), 151–183.
- Koerner, R., Halse, Y., and Lord, A, (1990). Long-term durability and aging of geomembrane. In:Bonaparte, R.(Ed.), *Waste Containment Systems: Construction, Regulation, and Performance. ASCEGeotechnical Special Publication No.26, New York*, 106–134.

- Kong, Y. and Hay, J. (2002). The measurement of the crystallinity of polymers by DSC. *Polymer* 43, 3873–3878.
- Lu, X. and Brown, N. (1990). The transition from ductile to slow crack growth failure in a copolymer of polyethylene. *Journal of Materials Science*, 25, 411–416.
- Lu, X., and Brown, N. (1991). Unification of ductile failure and slow growth in an ethylene–octene copolymer. *Journal of Materials Science*, 26, 612–620.
- Lustiger, A. and Corneliussen, R. (1986), *Modern Plastics*. 74–82.
- Lustiger, A. (1985). The molecular mechanism of slow crack growth in polyethylene. *Ph.D dissertation*, Drexel Unviersity.
- Michaels, A., and Bixler, H. (1961), Solubility of gases in polyethylene. *J. Polym. Sci.* 50, 393–412
- Osawa, Z., and Ishizuka, T. (1973). Catalytic action of metal salts in autoxidation and polymerization. *Journal of Applied Polymer Science*, 17, 2897–2907.
- Osawa, Z. (1992). Photo-induced degradation of polymers." In: Hamid, A.H., Amin, M.B., Maadah, A.G. (Eds.), *Handbook of Polymer Degradation*. Marcel Dekker Inc., New York, 169–217.
- Peacock, A. (2000). Handbook of Polyethylene: Structures. *Properties and Application*. Marcel Dekker Inc., New York. 534.
- Petermann, J., Miles, M., and Gleiter, H. (1976). Growth of polymer crystals during annealing. *Journal of Macromolecular ScienceFPhysics B* 12(3), 393–404.
- Peggs, I., and Carlson, D. (1989). Stress cracking of polyethylene geomembrane: field experience. In: Koerner, R.M. (Ed.), *Durability and Aging of Geosynthetics*, Elsevier Applied Science Publishers Ltd., Amsterdam, Netherlands, 195–211.
- Phillips, D. (1988). Effects of Radiation on Polymers. *Materials Sciense and Technology*, 4, 85–91.
- Rowe, R., Islam, M., and Hsuan, Y. (2010), Effects of thickness on the aging of HDPE GMs. *J. Geotech. Geoenviron.*, 136 (2), 299–309.
- Rowe, R., Islam, M. and Hsuan, Y. (2009). Ageing of HDPE geomembrane exposed to air, water and leachate at different temperatures. *Geotextiles and Geomembranes*, 27, 137–151
- Rowe, R., Islam, M. and Hsuan, Y. (2008). Leachate chemical compositioneffects on OIT depletion in an HDPE geomembranes. *Geosynthetics International*, 15(2), 136–151.
- Rowe, R. and Rimal, S. (2008b). Depletion of antioxidants from an HDPE geomembrane in a composite liner. *Journal of Geotechnical and Geoenvironmental Engineering*, 134(1), 68–78.
- Rowe, R. (2005). Long-term performance of containment barrier systems. *Geotechnique*, 55(9), 631–678.
- Rowe, R., Sangam, H., and Lake, C. (2003). Evaluation of an HDPE GM after 14 years as a leachate lagoon liner. *Can. Geotech J.*, 40, 536–550.
- Rowe, R. and Sangam, H. (2002), Durability of HDPE geomembranes. *Geotextiles and geomembranes*, 20, 77–95.

- Sangam, H. and Rowe, R. (2002). Effects of exposure conditions on the depletion of antioxidants from high-density polyethylene (HDPE) geomembrane. *Can. Geotech. J.*, 39, 1221–1230.
- Schnabel, W. (1981). Polymer Degradation: Principles and Practical Applications. *Hanser International, Toronto,* 227.
- Singh, A. (1999). Irradiation of polyethylene: Some aspects of crosslinking and oxidative degradation. *Radiation Physics and Chemistry*, 56, 375–380
- Sperling, L. (1992). Introduction to Physical Polymer Science, 2nd ed. Wiley, New York, 880.
- Wisse, J., Broos, C., and Boels, W. (1990). Evaluation of the Life expectancy of polypropylene geotextiles used in bottom protection structures around the Ooster Schelde storm surge barrier: a case study. *In: Proceedings of the fourth International Conference on Geotextiles. Geomembranes and Related Products*, 2, 697–702.
- Viebke, J., Elble, E., Ifwarson, M., and Gedde, U. (1994). Degradation of unstabilized medium-density polyethylene pipes in hot-waterapplications. *Polym. Eng. Sci.*, 34(17), 1354–1361.
- U.S. Nuclear Regulatory Commission (U.S. NRC), (Oct. 2000). Assessment Methodology for Low Level Radioactive Waste Disposal Facilities

Table 3.1. Geomembrane composition

Туре	Resin %	Antioxidants %	Carbon Black %	Plasticizer %
High-density polyethylene	95-98	0.25-3	2-3	0
Linear low density polyethylene	94-96	0.25-3	2-3	0
Flexible polyethylene	85-98	0.25-2	2-4	0
Polyvinyl chloride	50-70	2-5	2-5	25-35

Note: Percentage by weight

.

Table 3.2. Type of antioxidants

Category	Chemical Type	Example	Effective Temperature (°C)
Drimon	Hindered phenol	Irganox 1076 Irganox 1010. Santowhite Crystals	0-300
Primary Hindered amines		Various types of Tinuvin. Chimassorb 944	0-150
	Phosphites	Irgafos 168	145-300
Secondary	Sulfur compounds	Dilauryl thiodipropionate (DLTDP),di-stearyl thiodipropionate (DSTDP)	0-200
	Hindered amines	Various types of Tinuvin, Chimassorb 944	0-150

Note: Modified from Hsuan and Koerner (1998)

Table 3.3. Arrhenius equation in the literature

Exposure condition	Arrhenius equation	Ea (kJ/mol)
Leachate immersed GM (Rowe et al. 2005)	In(s) = 19.85–7084/T	58.9
Composite liner GM (Rowe et al. 2005)	In(s) = 20.06–7540/T	62.7
2 mm thick GM immersed in synthetic MSW leachate (Sangam and Rowe 2002)	In(s) = 13.768–5213/T	43.3
2 mm thick GM immersed water (Sangam and Rowe 2002)	In(s) = 16.054–6305/T	52.4
1.5 mm GM immersed in AMD (Gulec et al. 2004)	In(s) = 19.16–7099/T	58.9

Note: T represents absolute temperature (°K)

Table 3.4. Prediction antioxidant depletion times of GM

Source	Test Apparatus	Exposure condition	Temperature(°C)	Estimated Lifetime (years)
Hsuan and Koerner (1998)	Column	Water	20	200
	Immersion	Air	13	390
	Immersion	Air	15	330
	Immersion	Air	20	230
	Immersion	Air	25	160
	Immersion	Air	33	90
	Immersion	Water	13	190
	Immersion	Water	15	160
Sangam and Rowe	Immersion	Water	20	120
(2002)	Immersion	Water	25	80
	Immersion	Water	33	44
	Immersion	Leachate	13	40
	Immersion	Leachate	15	36
	Immersion	Leachate	20	26
	Immersion	Leachate	25	22
	Immersion	Leachate	33	12
	Immersion	AMD	15	119
Gulec et al. (2004)	Immersion	AMD	20	78
,	Immersion	AMD	25	15
	Immersion	Water	20	200
	Immersion	Water	25	135
Koerner (2005)	Immersion	Water	30	95
	Immersion	Water	35	65
	Immersion	Water	40	45
	Column	Leachate	20	135
Rowe and Rimal (2008)	Column	Leachate	35	40
	Column	Leachate	50	10
	Immersion	Leachate	20	35
	Immersion	Leachate	35	10
	Immersion	Leachate	50	4
	Immersion	Leachate	20	25
Rowe et al. (2009)	Immersion	Leachate	35	10
	Immersion	Leachate	50	5

Note: AMD = Synthetic Acid Mine Drainage

Leachate= Keele Valley Landfill Synthetic Leachate

Table 3.5. Estimated of induction time for GM

Source	Temperature (°C)	Estimate of induction times (years)
	20	30
	25	25
Koerner 2005	30	20
	35	15
	40	10
Down at al. 2000 (based on	20	120-255
Rowe et al. 2009 (based on tensile break strength)	35	30-45
terisile break strength)	50	8-9
Rowe et al. 2009 (based on tensile break strain)	20	20-30
	35	10-15
	50	6-7

Notes: Lower values in a range were based on the author's interpretation of data, and higher values were based on best fit.

Table 3.6. Estimated GM degradation time for 50% degradation of GMs

Source	Temperature (°C)	Degradation time of Stage C (years)
Koerner 2005	20	149-255
	25	77-132
	30	41-70
	35	22-38
	40	12-21
Rowe et al. 2009 (based on tensile break strength)	20	1455-1625
	35	295-330
	50	70-75
Rowe et al. 2009 (based on tensile break strain)	20	840-1125
	35	170-225
	50	40-55

Table 3.7. Estimated total service lifetime of GM

Source	Temperature (°C)	Degradation time of Stage C (years)
	20	449
	25	279
Koerner 2005	30	173
	35	111
	40	73
Rowe et al. 2009	20	1605-1905
(based on tensile break	35	335-380
strength)	50	80-90
Rowe et al. 2009	20	885-1180
(based on tensile break strain)	35	190-250
	50	50-65
Rowe et al. 2009	20	685-1180
(based on stress crack	35	150-225
resistance)	50	40-50

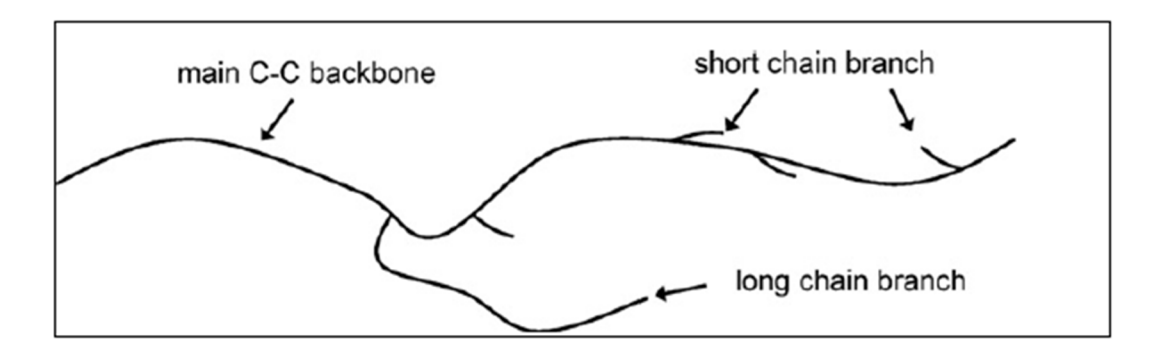


Fig. 3.1. Backbone and branches for polyethylene (Note: Figure form Cheng et al. 2011).

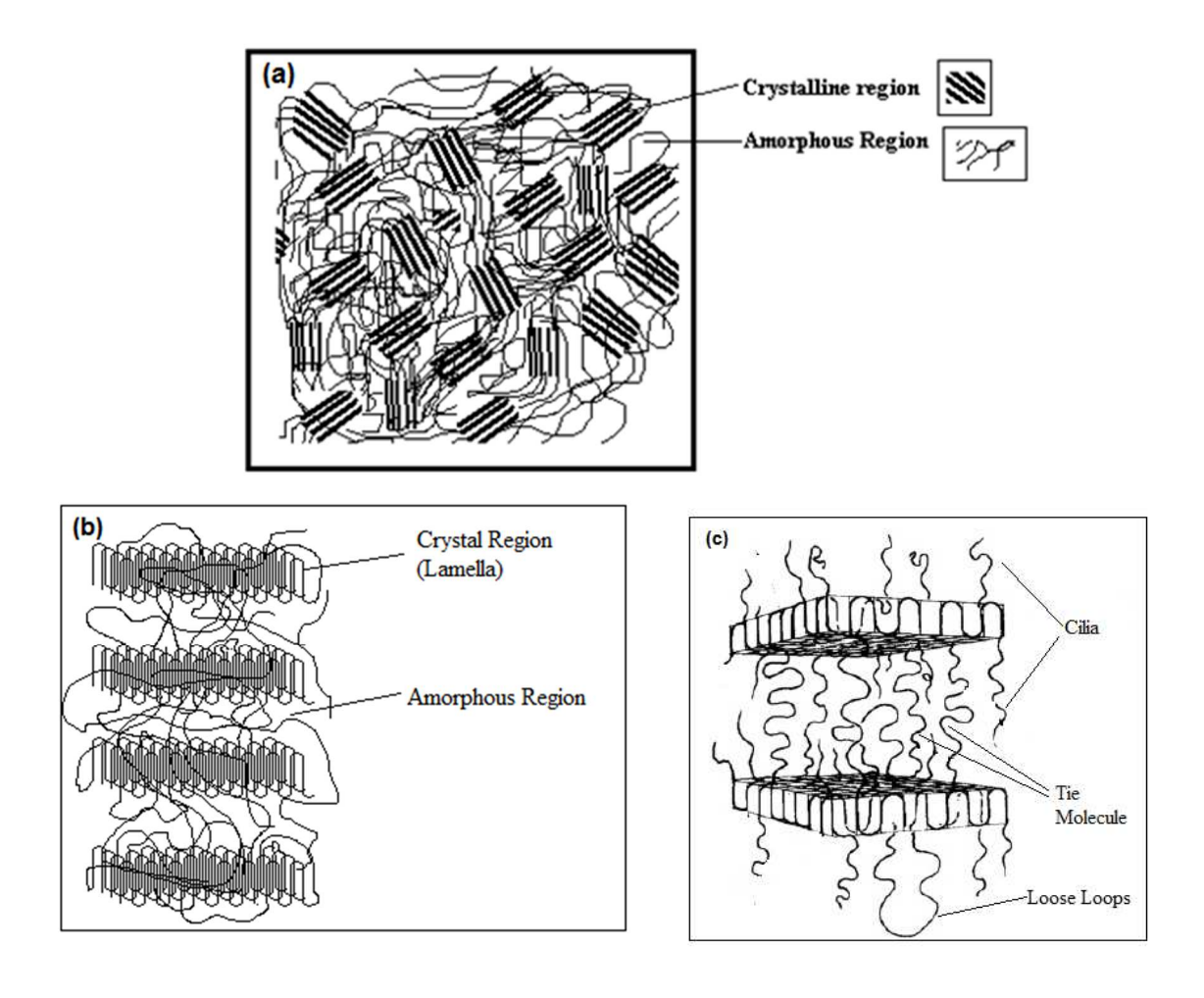
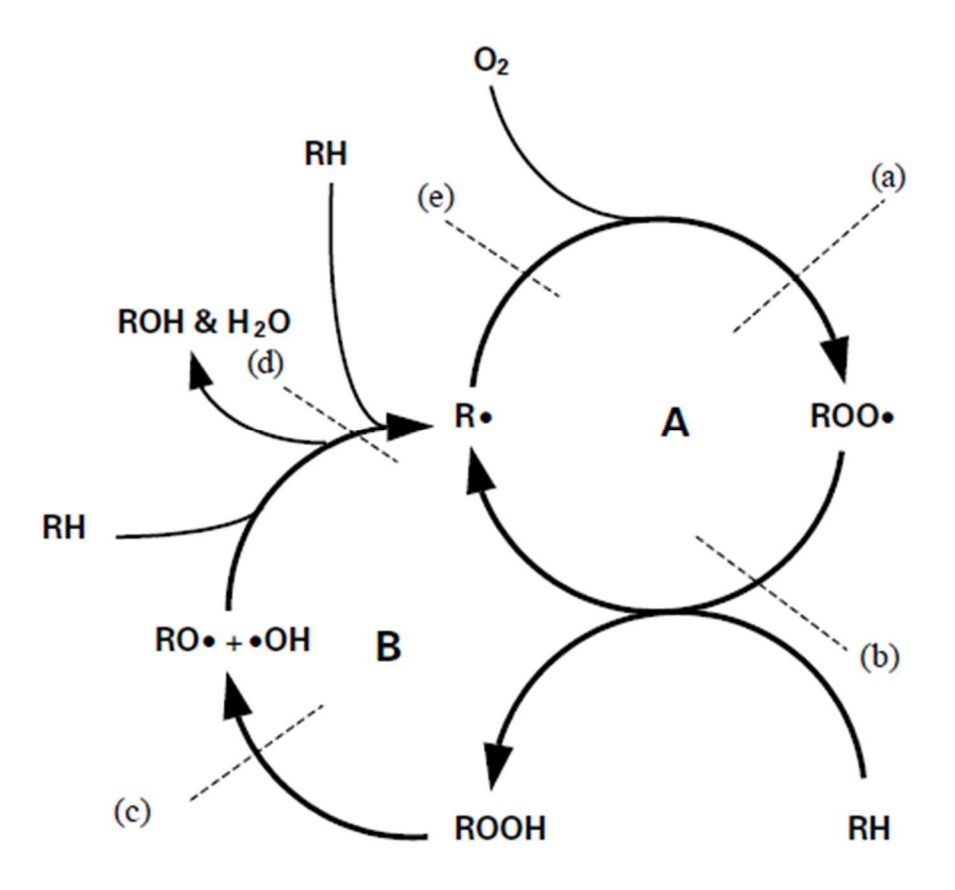


Fig. 3.2. (a) Crystal and Amorphous Region (surface view) (b) Crystal and Amorphous Region (Cross-section view) (c) Three types of inter-crystalline chains (Note: Figure (a) form http://web.utk.edu/~mse/Textiles/Polymer%20Crystallinity.htm).



RH: Polyethylene polymer chain

Roo•: Reactive free radical Hydroperoxy radical

ROOH: Hydroperoxid

(a) (b) (e): Primary antioxidants (c) (d): Secondary antioxidants

Fig. 3.3. Oxidation cycles in polyethylene (modified form Grassie and Scott 1985) (Rowe and Sangam 2002).

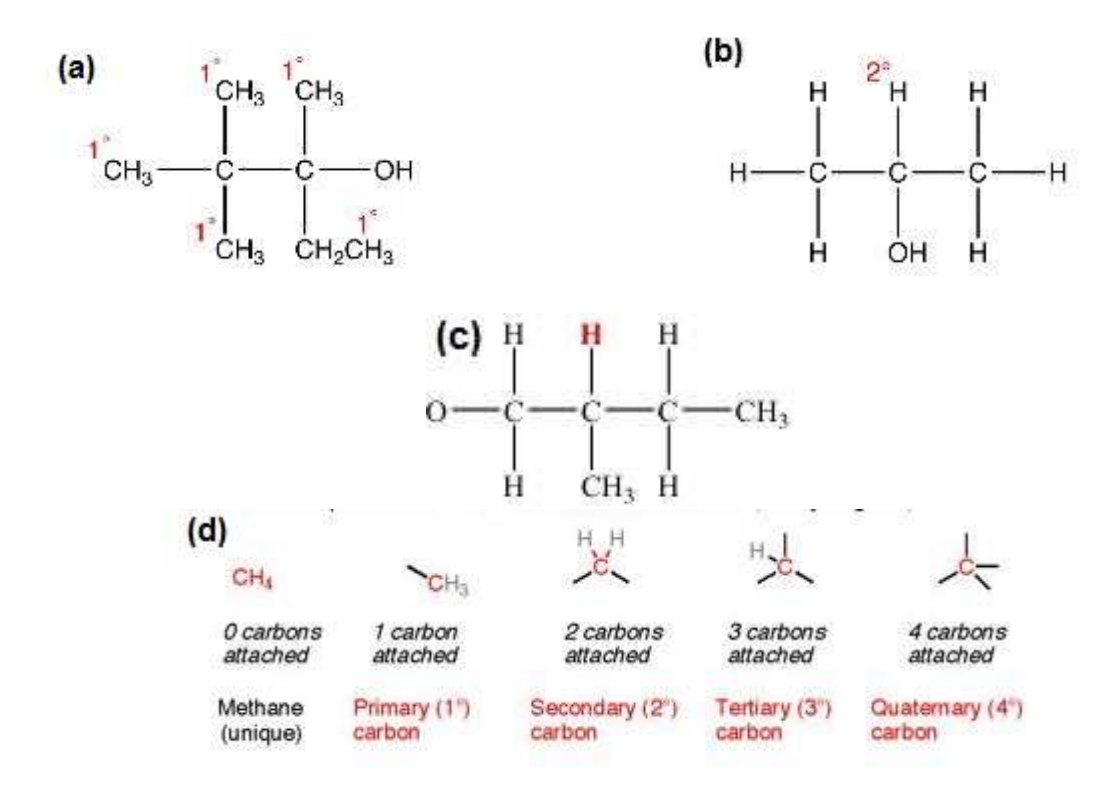


Fig. 3.4. The name of hydrogen and carbon atom: a) primary hydrogen, b) secondary hydrogen, and c) tertiary hydrogen, and d) name of carbon atom (http://www.masterorganicchemistry.com).

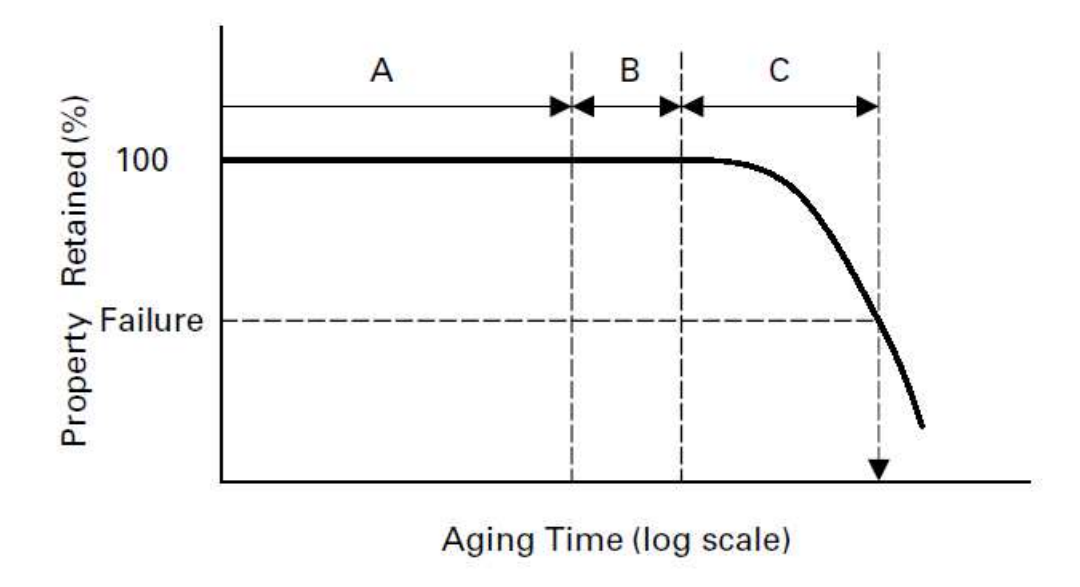


Fig. 3.5. The three conceptual stages in chemical aging of HDPE GMs (modified from Rowe and Sangam 2002).

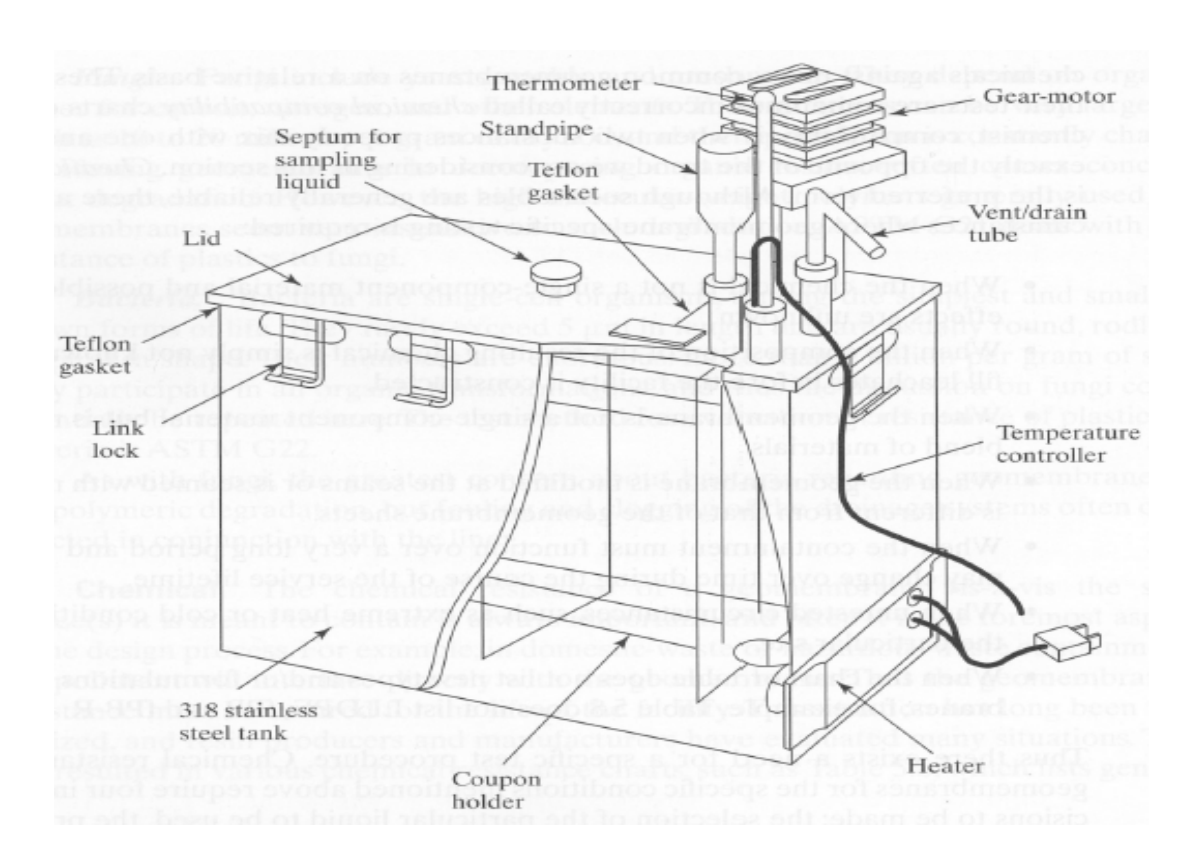


Fig. 3.6. Apparatus used for immersion incubation testing of GM (Koerner 2005).

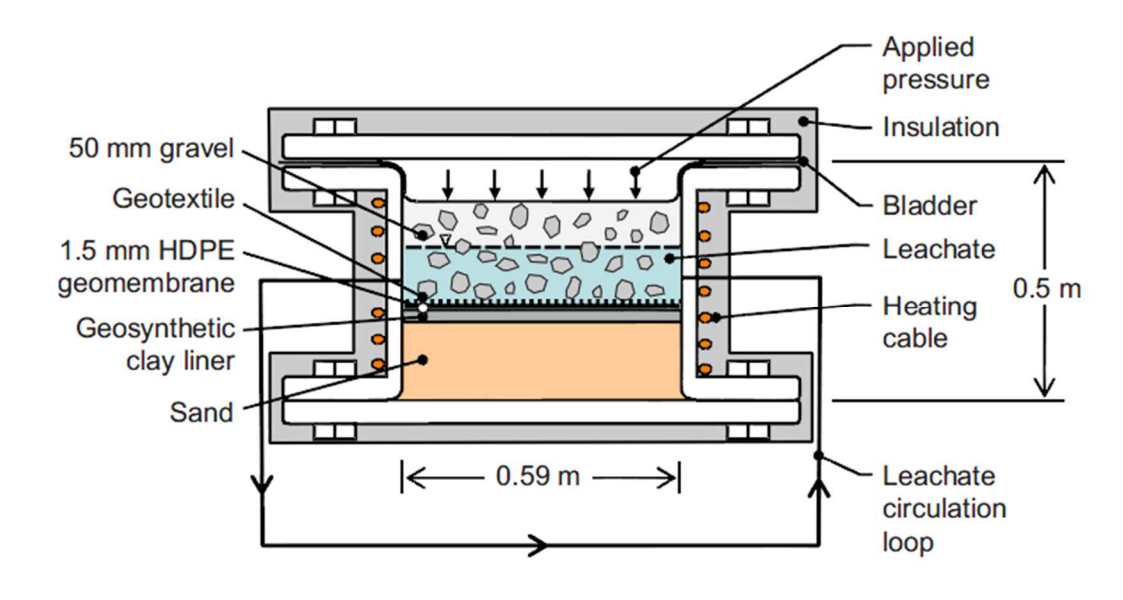


Fig. 3.7. Apparatus used for column incubation testing of GM (Rowe et al. 2010).

# 4 ANTIOXIDANT DEPLETION IN HDPE GEOMEMBRANES EXPOSED TO LOW-LEVEL RADIOACTIVE WASTE LEACHATE

ABSTRACT: Low-level radioactive waste (LLW) and mixed waste (MW) disposal facilities in the US are required to have a service life in excess of 1000 yr. Understanding the rate of degradation of high-density polyethylene (HDPE) geomembranes (GM) used in LLW and MW facilities is necessary to assess their service life. This paper focuses on Stage I, i.e., antioxidant depletion in GM in contact with LLW leachate. HDPE GM coupons (2-mm-thick) were immersed in radioactive synthetic leachate (RSL) with chemistry representative of leachate in LLW disposal facilities operated by the US Department of Energy's environmental restoration programs. Depletion was assessed at four temperatures (25, 50, 70, and 90 °C). To identify the effect of radionuclides on antioxidant depletion, comparative tests were conducted with non-radioactive synthetic leachate (NSL) having the same chemistry as the RSL leachate, except radionuclides were excluded. Control tests were conducted with deionized water. Specimens were removed periodically and tested to determine the mechanical and chemical properties. Antioxidant depletion was measured by both standard and high-pressure oxidative induction time (OIT) tests. The antioxidant depletion rate increased with exposure temperature and aging time. The antioxidant deletion rate of HDPE GM in RSL were no different than NSL at 25, 50, 70, and 90 °C, respectively, which indicated that radiation from LLW leachate had limited effect on antioxidant depletion. Arrhenius modeling was used to extrapolate the laboratory data at elevated temperatures to a typical LLW liner at 15 °C. The predicted time to antioxidant depletion for a GM in a composite liner in contact with LLW leachate is estimated to be 649 yr.

**Keywords:** radioactive waste, mixed waste, geomembrane, degradation, antioxidant, high-density polyethylene.

#### 4.1 INTRODUCTION

Composite barrier systems are used in low-level radioactive waste (LLW) and mixed waste (MW) disposal facilities due to their ability to limit contaminant transport to very low rates. Composite barriers typically consist of a geomembrane (GM) overlying a geosynthetic clay liner or a compacted clay liner. High-density polyethylene (HDPE) is the most common polymer used for GMs in landfill facilities to prevent advective migration of contaminants (Foose et al. 2002, Rowe et al. 2004, Gulec et al. 2004, Rowe 2005, Take et al. 2007, Andrejkovicova et al. 2008, Bouazza et al. 2008, Saidi et al. 2008, Vukelić et al. 2008). A typical HDPE GM consists of polymer resin (>95%), carbon black (2–3%), and antioxidant (0.5–1%) (Hsuan and Koerner 1998). Carbon black is added to protect GM from UV light, and an antioxidant package is used to prevent GM from oxidation.

A major issue in the application of HDPE GMs in a landfill liner system is to predict the service lifetime to resist degradation. The service lifetime is defined as the length of time that a GM liner can act as an effective hydraulic barrier layer (Needham et al. 2006). HDPE GM undergoes degradation in three stages: antioxidant depletion (Stage I), induction time to the onset of polymer degradation (Stage II), and polymer property degradation (Stage III) (Viebke et al. 1994, Hsuan and Koerner 1998, Rowe and Sangam 2002, Gulec et al. 2004, Rowe et al. 2009). GM degradation is initially controlled by consumption of antioxidants. The process involves oxidation of antioxidants at the surface of the GM and loss of antioxidants by diffusion (Hsuan and Koerner 1998, Sangam and Rowe 2002, Rowe at al. 2009, Rowe et al. 2010a, 2013). Without protection of antioxidants, a GM becomes vulnerable to degradation via oxidation and rapidly starts stages II and III of degradation (Grassie and Scott 1985, Rowe et al. 2009).

The most reliable way of assessing antioxidant degradation of a GM is to exhume samples from the field at different time intervals during its service life. Rowe et al. (2003) evaluated a 14-year-old 1.5-mm-thick HDPE GM used as a lagoon liner to store nonhazardous leachate from industrial, municipal, and commercial landfills. The amount of antioxidant remaining in the GM was measured via the standard oxidation induction time (OIT) test. The results showed low OIT (less than 7 min) for GM samples exhumed from the lagoon. Yako et al. (2010) evaluated a 20-year-old 2.0-mm HDPE GM used in the liner of an ash surface impoundment. The OIT for the buried GM was 80 min, whereas the OIT was only 35 min for the GM exposed to the ash. These studies are valuable in understanding degradation of GM in containment applications. However, the first generation of GMs was installed circa 1980, making long-term (100+ yr) field data non-existent. Consequently, accelerated aging tests conducted in the laboratory are used to estimate the service lifetime of HDPE GMs exposed to municipal solid waste (MSW) leachate (Sangam and Rowe 2002, Rowe and Rimal 2008, Rowe et al. 2009, Rowe et al. 2013), exposed to acidic miner drainage (AMD) (Gulec et al. 2004), or exposed to synthetic LLW leachate with high pH (Rowe et al. 2015) with particular focus on antioxidant depletion. Rowe et al. (2010b) tested a HDPE GM (initial OIT = 115 min) under a simulated MSW liner system. The antioxidant depletion in HDPE GM was estimated to last 6-120 yr depend on field temperature (20-60 °C). Gulec et al. (2004) concluded that AMD accelerated the depletion of antioxidants in HDPE GM due to low pH (2.1) and high heavy metal concentration (Fe = 1500 mg/L, Zn = 350 mg/L). The antioxidant was projected to protect HDPE GM (initial OIT=200 min) in AMD for 46-426 years depending on field temperature (15-25 °C). These results indicate that the antioxidant depletion in HDPE GM is affected by leachate composition (e.g., surfactant, heavy metals, extreme pH). The antioxidant depletion rate in HDPE GM increased as increasing concentration of surfactant up to 5 mL/L (Rowe et al. 2008). Gulec et al. (2004) reported that heavy metals in AMD can accelerate decomposition of hydroperoxides, thus resulting in a higher antioxidant consumption rate. Additionally, HDPE GM exposed to leachate with extreme pH (e.g., < 3, or > 11) had a higher antioxidant depletion rate (Gulec et al. 2004, Rowe et al. 2015).

HDPE GM installed in a LLW disposal system is desired to work as an effective barrier for contaminant flux for 1000 yr. The service life of HDPE GM may be affect by the LLW leachate. The composition of LLW leachate, described in Tian (2012), includes trace heavy metals (e.g., Fe, Cu), and radionuclides (e.g., uranium, <sup>99</sup>Tc). Trace heavy metals may affect the antioxidant depletion of HDPE GM installed in a LLW liner system, as described in Osawa and Ishizuka (1973) and Gulec et al. (2004). In addition, alpha and beta radiation emitted from uranium (U) and <sup>99</sup>Tc may affect the antioxidant depletion in HDPE GM (Klemchuck 2000). Thus, the question remains: how long will HDPE GM effectively function as a barrier in a liner system.

To date, examination of service lifetime of GMs installed in LLW composite liner systems has been limited. Rowe et al. (2015) examine the antioxidant depletion in HDPE GM exposed to synthetic LLW leachate with high pH but without radionuclides. The objective of this study is to estimate the service life of a typical commercial HDPE GM (2-mm-thick) exposed to LLW leachate through immersion testing, with particular focusing on antioxidant depletion. The synthetic LLW leachate in this study consists inorganic metals, organic compound, and radionuclides with a near neutral pH.

## 4.2 BACKGROUND

The main component of GM is polymer resin (95% by mass). Polymer degradation largely depends on polymer type and exposure environment, such as UV light, radiation, elevated temperature, and chemical disintegration (Koerner et al. 1990, Rowe and Sangam

2002). Degradation initially changes the polymer structure and, eventually, changes the engineering properties of the GM (Hsuan and Koerner 1998, Rowe and Sangam 2002, Gulec et al. 2005, Rowe et al. 2009). Identification of one dominant factor that governs the degradation of GM installed in a LLW disposal facility is difficult because, typically, more than one effective factor is encountered through *in situ* exposure.

LLW leachate may have high pH (Rowe et al. 2015), numerous metal components (e.g., Ca, Mg, Fe, Al, and Sr), and radionuclides (e.g., U, <sup>3</sup>H, and <sup>99</sup>Tc) (Tian 2012). Chemical degradation occurs in GM exposed to strong chemicals (e.g., extreme pH or high ionic strength) and causes polymer swelling or extraction of additives (Rowe and Sangam 2002). Radiation impingement on a polymer can liberate electrons and generate free radicals, (Costa et al 2008, Yong et al. 2010), thus leading to antioxidant consumption. Oxidative degradation in a GM happens in the presence of oxygen (Grassie and Scott 1985). Even trace amounts of oxygen are sufficient to generate hydroperoxide (Klemchuck 2000). The decomposition of hydroperoxide can accelerate the consumption of antioxidant (Hsuan and Koerner 1998). Free radicals caused by irradiation may also participate in the oxidation reaction, which is defined as radiation-induced oxidation (Costa et al. 2008, Bracco et al. 2006, Klemchuck 2000). Thus, oxidation appears to be the fundamental degradation mechanism for GM.

## 4.2.1 Degradation of HDPE via Oxidation

The oxidation of polyethylene follows the free-radical reactions as shown in Fig. 4.1 (Grassie and Scott 1985, Rowe and Sangam 2002), which can be represented through Eqs. 1–6. Loop A consists of the formation of hydroperoxides (ROOH) and free radicals. Loop B displays the auto-accelerating process that is caused by decomposition of ROOH, which increases the amount of free radicals that attack the original polymer chain and accelerate

the chain reactions. The first cyclical reaction occurs when the polymer chain (RH) obtains the necessary activation energy (e.g., radiation and thermal effect) to form a free radical polymer chain (R•) and hydrogen (H•).

$$RH \to R \bullet + H \bullet \tag{1}$$

Then, oxygen (O₂) reacts with a free radical in the polymer (R•), thus forming a hydroperoxy free radical (ROO•), which is represented as

$$R \bullet + O_2 \to ROO \bullet \tag{2}$$

The hydroperoxy free radical reacts with a polymer chain (RH) to form ROOH and another free radical, as follows

$$ROO \bullet + RH \rightarrow ROOH + R \bullet \tag{3}$$

As oxidation continues, additional ROOH molecules are formed. As ROOH accumulates, decomposition begins, leading to a substantial increase in the amount of free radicals, as indicated in Eqs. 4–6 (Hsuan and Koerner 1998). The degradation of polyethylene then transitions into stage II or III.

$$ROOH \rightarrow RO \bullet + OH \bullet \tag{4}$$

$$RO \bullet + RH \to ROH + R \bullet \tag{5}$$

$$OH \bullet + RH \rightarrow H_2O + R \bullet \tag{6}$$

## 4.2.2 Effect of Radiation on Polymer Degradation

Long molecular chains of polymers of HDPE GM can be broken into free radicals through the absorption of ionizing radiation that carries energy above the energy of the covalent bond energy in the polymer; i.e., the bond energy of carbon-carbon typically is in the range of 5–10 eV (Czvikovszky 2004). The radionuclides in LLW leachate include  $^{3}$ H ( $^{3}$ H radiation: 18.4 keV),  $^{99}$ Tc ( $^{3}$ P radiation: 294 keV), and uranium ( $^{3}$ P radiation:  $^{4}$ P-5.4 MeV). The energy of these  $^{3}$ P and  $^{3}$ P particles surpasses the minimum dissociation carbon-carbon

bond energy of the polymer chain, which is indicative of potential risk of degradation to HDPE GM used in LLW liner systems.

The effect of radiation on polymer degradation depends on radiation type (Phillips 1988, Czvikovszky 2004). Charged  $\alpha$  particles only penetrate a polymer on the order of micrometers, charged  $\beta$  particles on the order of hundreds of micrometers, whereas uncharged particles, neurons and  $\gamma$  ray, can penetrate meters into a polymer. Therefore,  $\alpha$  and  $\beta$  particles can potentially affect the surface of GM, whereas the  $\gamma$  ray can affect the overall thickness of GM. The radiation can break original bonds, resulting in chain scission. In PE material, chain scission includes main chain rupture (i.e., C-C bond) or side chain rupture (i.e., C-H bond), and these broken bonds with an excited electron can form a new chemical bond with an adjacent free radical, defined as cross-linking (Phillips 1988, Peacock 2000). Moreover, in the presence of oxygen, free radicals formed by irradiation can react with oxygen to form peroxide, hydroperoxide, resulting in accelerating degradation process, as proposed in Eqs 2–6 (Costa et al. 2008, Phillips 1988). This process is defined as radiation-induced oxidation (Costa et al. 2008, Bracco et al. 2006).

Previous studies have investigated the radiation effect on the degradation of polymer (Costa et al. 2008, Phillips 1988, Whyatt and Farnsworth 1990). Costa et al. (2008) irradiated a PE material with an electron beam at dosage up to 50 kGy. The concentration of hydroperoxide in PE displayed an increasing trend with higher irradiation dosage. Whyatt and Farnsworth (1990) conducted a compatibility test of 1.5-mm HDPE GM used in LLW disposal facilities. The HDPE GMs were immersed in high pH (>14) inorganic solution at 90 °C for 120 d, and samples were irradiated with gamma rays up to doses up to 3.89 ×10<sup>5</sup> Gy to simulate a 30-yr-equivalent dosage. The results displayed a decreasing strength and elongation and increasing puncture force and hardness after aging for 120 d. Another test

conducted by Phillips (1988) showed that polymer properties (e.g., elongation) start to change at a total exposed gamma radiation dose between 10 kGy to 100 kGy.

# 4.2.3 Depletion of Antioxidants

Antioxidants are added to polymeric materials to prevent oxidative degradation (Grassie and Scott 1985). Manufacturers generally use an antioxidant package with a combination of two or more types of antioxidants to provide overall stability. Hsuan and Koerner (1998) indicate that four temperature-specific categories are commonly used: hindered phenols (0–300 °C), hindered amines (0–150 °C), phosphites (150–300 °C), and thiosynergists (0–200 °C). These four categories of antioxidants can be divided into primary and secondary groups based on their mechanisms. The primary antioxidant acts by accepting or donating an electron. Antioxidants intercept the links (b) and (d) in Fig. 4.1 by donating an electron to react with the free radicals (ROO•, RO•, and OH•) and converting them to ROOH, ROH, and H<sub>2</sub>O, respectively (Hsuan and Koerner 1998, Rowe and Sangam 2002). Another type of antioxidant performs as an electron acceptor. Electron acceptors break links (a) and (e) by converting alkyl free radicals (R•) to a stable polymer chain. Secondary antioxidants are designed to intercept link (c) to prevent ROOH from becoming a free radical by changing the ROOH to a stable alcohol (ROH) (Hsuan and Koerner 1998).

Rowe et al. (2008) investigate the effect of leachate composition on antioxidant depletion in HDPE GM. Surfactant in the synthetic leachate accelerates diffusion loss of antioxidant by increasing the wetting ability of the GM (Rowe and Rimal 2008). Surfactant can reduce the surface tension of a GM and turn the GM from hydrophobic to hydrophilic materials. Increasing wetting ability lead to increase the contact area between leachate and the GM, which cause a higher outflowing rate through diffusion. Osawa and Ishizuka (1973) indicated that metals can catalyze the decomposition of hydroperoxide, thus increasing the

rate of generation of free radicals and the consumption of antioxidants. Moreover, GM thickness has a significant impact on the depletion of antioxidants, with thinner GMs having shorter antioxidant depletion times (Rowe et al. 2010a).

#### 4.2.4 Arrhenius Model

Higher temperatures are used in the laboratory to accelerate GM degradation processes. The Arrhenius equation is commonly used to extrapolate experimental data obtained at high temperatures to the specific *in situ* temperature (Hsuan and Koerner 1995, Hsuan and Koerner 1998, Müller and Jakob 2003, Gulec et al. 2004, Rowe and Rimal 2008, Rowe et al. 2009, 2010a, 2013). The Arrhenius equation is

$$s=Ae^{-(E_a/RT)}$$
 (7)

which can be rewritten as

$$ln(s) = lnA - \left(\frac{E_a}{R}\right) \left(\frac{1}{L}\right)$$
 (8)

where s is the depletion rate, A is a constant, E<sub>a</sub> is the activation energy, R is the universal gas constant, and T is absolute temperature (°K). Three assumptions are inherent when applying Eqs. 7 and 8, as described in Rowe et al. (2009): (1) s is a function of temperature, (2) A does not influence the temperature sensitivity of the reaction, and (3) E<sub>a</sub> remains constant over time and is independent of temperature.

# 4.3 MATERIALS AND METHODS

## 4.3.1 Geomembrane and Exposure Liquids

A commercially available 2-mm-thick smooth HDPE GM was used in the experimental program. The initial standard oxidation induction time was 197 min, and the high-pressure oxidation induction time was 831 min. Table 4.1 lists other properties of the 2-mm-thick HDPE GM used in this study. To simulate the field scenario of a LLW disposal facility, RSL

was synthetically composed to be representative of field leachate at LLW disposal facilities, as identified by analysis of the data from sites operated by the US Department of Energy (Tian 2012). Mean concentrations as reported by Tian (2012) were used for most chemical components, except for radionuclides, which had concentrations near the upper bound, thus representing a worst-case scenario. The composition of the RSL is given in Table 4.2. Another immersion liquid, referred to as NSL, was prepared having an identical composition as RSL, but without radionuclides. Finally, deionized water (DI) was used as the reference liquid. The leachate was refreshed every month to maintain constant leachate compositions.

#### 4.3.2 Immersion Test

Insulated stainless steel tanks (380 mm x 380 mm x 840 mm) filled with DI water were equipped with heaters and mixers for use in the immersion tests with the objective of maintaining an elevated-temperature environment (Tian 2012). Exposure temperatures were set at 25, 50, 70, and 90 °C to accelerate aging (Hsuan and Koerner 1998, Gulec et al. 2004, Rowe et al. 2009) and controlled to within  $\pm$  0.1 °C. GM coupons (12 x 24 cm in size) were placed in sealed polypropylene plastic boxes (150 mm x 150 mm x 300 mm). The plastic box were sealed with rubber gasket and filled with synthetic leachate or DI water and were placed in the stainless steel tanks. The sealing was necessary to minimize the diffusion of oxygen into the liquid and to prevent evaporation of leachate. Diffusion of oxygen into the synthetic LLW leachate was minimized to simulate the base liner condition. Another reason to minimize oxygen intrusion is that the precipitation of some metals can occurs in the presence of oxygen (such as iron oxides) (Gulec et al. 2004). Moreover, the sealed plastic boxes also limit the evaporation of leachate due to the high aging temperatures employed. Evaporation of leachate would cause an increase in salt concentration and radionuclide concentration (e.g.,  $^{99}$ Tc and U), which could potentially affect the antioxidant depletion rate.

## 4.3.3 Oxidation Induction Time (OIT)

Oxidation induction time was measured with differential scanning calorimetry (DSC), a common thermo-analytical method used to indirectly determine antioxidant content (Hsuan and Koerner 1995, 1998, Sangam and Rowe 2002, Gulec et al. 2004, Rowe et al. 2010b, 2013). The measurement of OIT is proportional to the total amount of antioxidant remaining in the HDPE GM and thus provides a measure of antioxidant content. Standard OIT (Std-OIT) tests were conducted in accordance with ASTM D3895 and high-pressure testing (HP-OIT) was conducted in accordance with ASTM D5885. Std-OIT was measured at the Soft Material Laboratory at the University of Wisconsin-Madison (UW-Madison) using a TA Instruments Q100 DSC. A 5-mg specimen was heated to 200 °C with an incremental rate of 20 °C/min in a nitrogen atmosphere. After reaching 200 °C, the specimen was maintained in an isothermal stage for 5 min. Then the gas was changed to oxygen, and the enthalpy change of the specimen was recorded. The test was terminated when an exothermal peak was detected. The results were validated by having independent tests conducted on the same GM at the TRI Institution. TRI reported a Std-OIT measurement of 187  $\pm$  4 min for unexposed GM, whereas the Std-OIT tested at the UW-Madison was 197  $\pm$  5 min—are in reasonable agreement with each other.

Additional tests were conducted with HP-OIT to investigate antioxidants in the GM, which could be destroyed and ignored in the Std-OIT tests due to higher temperature. For example, Hsuan and Guan (1997) indicated that hindered amines with effective temperature 0–150 °C volatilized or degraded in an Std-OIT test at 200 °C. HP-OIT testing is similar to Std-OIT testing, except that higher gas pressure (3500 kPa) and lower temperature (150 °C) are applied during the test. Samples were sent to TRI Institution to measure the HP-OIT for GM used in this study.

The HP-OIT increased from 0 to 1 month of aging, and then decreased (shown in Fig. 4.2). The mechanism behind this unusual behavior is not clear. However, when this initial point (~ 200 min in Std-OIT) is ignored, a linear relationship exists between the Std-OIT and HP-OIT. Hsuan and Koerner (1998), Sangam and Rowe (2002), Gulec at al. (2004) report similar linear relationships, which indicates that the high temperature of the Std-OIT test did not destroy or mask the antioxidants. Therefore, hindered amines were unlikely to be present in the tested HDPE GM, and the antioxidant package used in the GM production is likely to be phosphite- and phenol-based, which have effective temperature ranges of 150–300 °C and 0–300 °C, respectively (Hsuan and Koerner 1998). The following discussion is thus based on Std-OIT results, which are simply referred to as OIT.

#### 4.3.4 Melt Flow Index (MFI) Test

Melt Flow Index (MFI) testing is a simple method to obtain the molecular weight of polymer materials, following ASTM D1238. The MFI measures the amount of molten polymer extruded through an orifice in 10 min under a constant load of 2.16 kg at elevated temperature (190 °C). As the antioxidant deplete completely, the degradation of GM turns to stage II and III - chain scission and cross-linking reactions start to occur during the aging process (Peacock 2000, Rowe et al. 2009). Chain scission produces smaller polymer molecules, which is reflected as higher MFI, whereas cross-linking generates larger polymer molecules, which is displayed as lower MFI. The MFI tests were conducted at UW-Madison using a Dynisco LMI4001 Model (shown in Table 4.1). Independent tests conducted on the unexposed GM at the TRI Institution displayed the same MFI.

#### 4.3.5 Crystallinity

The degree of crystallinity indicates the amount of crystalline region in polymer. Kong and Hay (2002) and Sperling (1992) indicate that crystallinity influences physical and

mechanical properties such as stress cracking resistance, yield stress, modulus of elasticity, impact resistance, density, permeability, and melting point. The crystallinity of HDPE GM can be obtained by using a DSC following the procedure given in ASTM E794. Higher crystallinity displays a relatively higher stiffness in HDPE GM; however, higher crystallinity decreases the stress cracking resistance (Rowe et al. 2009). GM specimens ranging in mass from 10 to 15 mg were placed in the DSC and heated at a rate of 10 °C/min through the melting range until the baseline reoccurs above the melting endotherm. Flory and Vrij (1963) indicated that the crystallinity percentage is defined as a ratio between the measured heat of fusion and the heat of fusion of 100% crystalline HDPE (i.e., 290 J/g). The measurement of crystallinity can reflect the changing of polymer structure in HDPE GM.

#### 4.4 RESULTS AND DISCUSSION

# 4.4.1 Depletion of Antioxidant

The most common approach used to predict antioxidant depletion rates at different temperatures is based on the OIT test. Assuming that the antioxidants deplete completely and that the final OIT measurement is equal to zero, first-order exponential decay model with two-parameters ( $OIT_0$  and s) can be fitted to the experimental OIT data (Rowe et al. 2009, 2010a,b, Gulec et al 2004, Hsuan and Koerner 1995, 1998), as follows

$$OIT_t = OIT_0 \exp(-st)$$
 (9)

which can be linearized as

$$ln(OIT_t) = ln(OIT_0) - st$$
 (10)

where  $OIT_t = OIT$  (min) aging as a function of time,  $OIT_0 = initial OIT$  (min), s = antioxidant depletion rate (month<sup>-1</sup>), and t = time (months).

However, the antioxidant in GM will not deplete completely during the aging time, as described in Rowe at al. (2010a). To better predict the antioxidant depletion rate, another

approach to analyze the data involves three parameters (OIT<sub>0</sub>, OIT<sub>r</sub>,and s). Residual time (OIT<sub>r</sub>) is considered as the third parameter in exponential decay, and use of OIT<sub>r</sub> may provide a better prediction (Rowe et al. 2013):

$$OIT_t = OIT_t + OIT_0 \exp(-st)$$
 (11)

which can be linearized as

$$ln(OIT_t^*) = ln(OIT^*) - st$$
 (12)

where  $OIT_t = OIT$  (min) aging with time,  $OIT_0 = initial\ OIT$  (min),  $OIT_r = residual\ OIT$  (min),  $OIT^* = OIT_0 - OIT_r$ ,  $OIT_t^* = OIT_t - OIT_r$ ,  $s = antioxidant\ depletion\ rate\ (month^{-1})$ , and  $t = time\ (month)$ .

Fig. 4.3 displays first-order decay fitting for antioxidant depletion of GM exposed to RSL based on two/three-parameter fitting. The curve based on two-parameter fitting does not perfectly match the experimental data, especially exposure temperatures of 90 °C (shown in Fig. 4.3a). The disagreement between the two-parameter fitting and experimental data was due to the residual time of HDPE GM immersed in RSL at 90 °C. Three-parameter exponential decay fitting and experiment data was shown in Fig. 4.3c. The residual time (11 min) was determined by least-square fitting cross-antioxidant depletion of HDPE GM exposed to RSL at 25, 50, 70, and 90 °C. The residual OIT (described in Rowe at al. 2013) is defined as a relative constant, for which the remaining antioxidants are no longer effective in preventing oxidation. In other words, the physical and chemical properties of the GM start to change (e.g., molecular weight and tension properties) before the antioxidants completely deplete, this OIT value constant is defined as residual time. Hsuan and Koerner (1998) defined the residual time of Std-OIT and HP-OIT as 0.5 min and 20 min for a 1.5-mm-thick GM after a 24-month aging test. Rowe at al. (2010a) reported the residual time of 1.5-mmthick GM immersed in synthetic MSW leachate as 1.5 min for Std-OIT and 80 min for HP-OIT after 15-month aging. The Std-OIT time ranged from 9-12 min for HDPE GM immersed in

RSL from 10 to 22 month, with similar trends for HDPE GM immersed in NSL and DI (Fig. 4.4). Depletion of antioxidant was considered to slow down when the Std-OIT reached 11 min. The residual time for the HDPE GM used in this study was much higher when compared with other studies by Rowe et al. (2010a), Hsuan and Koerner (1998), which may be attributed to different antioxidant packages of the studied GMs. Additionally, a thicker GM gives a lower antioxidant depletion rate due to the longer diffusion path for antioxidant to migrate to the surface of the GM. Thus, the high residual time of GM used in this study may be due to 2-mm thickness in contrast to 1.5-mm thickness of GM tested by Rowe et al. (2010) and Hsuan and Koerner (1998).

The antioxidant depletion rate (s) for each condition was obtained by linear regression, as shown in Fig. 4.3b and d. The slope of each line represents the antioxidant depletion rate exposed to RSL/NSL at each temperature (Table 4.3). Three-parameter fitting displays better agreement to antioxidant depletion when residual time was considered. The following discussion is based on the antioxidant depletion rate obtained from the three-parameter model.

OIT decreases with aging time and decreases at a higher rate when exposed to high temperature (Fig. 4.3c) – similar results had been reported by Hsuan and Koerner (1998), Sangam and Rowe (2002), Gulec et al. (2004), Rowe et al. (2010a, 2013). The depletion rate for RSL at 90 °C was 0.4569 month<sup>-1</sup>, which is approximately 2.5 times higher than that at 70 °C (0.1862 month<sup>-1</sup>), 16 times higher than that at 50 °C (0.0277 month<sup>-1</sup>), and 97 times higher than that at 25 °C (0.0047 month<sup>-1</sup>). Furthermore, the fastest depletion occurs in the RSL, followed by NSL and DI (Table 4.3). At 90 °C, the antioxidant depletion rate in RSL (0.4569 month<sup>-1</sup>) is 1.06 times faster compared to the rate in NSL (0.4319 month<sup>-1</sup>), and 1.31 times faster compared to the depletion rate in DI water (0.3472 month<sup>-1</sup>).

The higher depletion rate for GM immersed in NSL relative to that for DI water is attributed to the metals and surfactant in the leachate. Rowe and Rimal (2008) indicate that surfactant can increase the wetting ability of the GM, resulting in rapid loss of antioxidants via diffusion into the leachate. Moreover, Osawa and Ishizuka (1973) indicate that the presence of transition metals (e.g., Co, Mn, Cu, AI, Fe, and Mg) can break down hydroperoxides via redox reactions and create additional free radicals. The depletion rate increases because antioxidants are consumed by reaction with free radicals.

Table 4.4 lists the antioxidant depletion rates published in the literature for various HDPE GMs. Rowe et al. (2009) reported that the antioxidant depletion rate of GM immersed in synthetic MSW leachate was 1.6–3.2 times faster than in water, whereas antioxidant depletion rate of RSL/NSL was only approximately 1.3 times than that in DI. The ratio of antioxidant depletion rate in RSL/NSL to that in DI water were smaller than the ratio of antioxidant depletion rate in MSW to that in DI water, which is probably due to a lower surfactant concentration in NSL (0.005 mL/L) than in synthetic MSW leachate (5 mL/L). Increasing surfactant concentration from 1 mL/L to 5 mL/L led to an increased antioxidant depletion rate of HDPE GM (Rowe et al. 2008).

Gulec et al. (2004) showed that the antioxidant depletion rate for a 1.5-mm HDPE GM is 1.2 times higher in synthetic acid mine drainage containing a variety of metals than in acidic water without metals. The high antioxidant depletion rates of HDPE GM exposed to acid mine drainage agreed with Osawa and Ishizuka's (1973) conclusion that heavy metals can accelerate decomposition of hydroperoxides, thus resulting in a higher antioxidant consumption rate. Thus, the metal components in RSL/NSL increase the consumption of antioxidant and result in a higher depletion rate than in DI water.

## 4.4.2 Effect of Radiation on Antioxidant Depletion

The antioxidant depletion rate can potential be accelerated due to the effect of radiation on GM. The energy of  $\alpha$  and  $\beta$  particles emitted from U, <sup>99</sup>Tc, and <sup>3</sup>H can generate free radicals by breaking the carbon-carbon bond of the polymer chain (Czvikovszky 2004). The oxygen can react with free radicals to generate peroxide and hydroperoxide; i.e., radiation-induced oxidation (Costa et al. 2008). The antioxidant deletion rate was only 9%, 4%, and 6% faster when immersed in RSL than in NSL at 25, 70, and 90 °C (Table 4.3), respectively, and same antioxidant depletion rate was observed at 50 °C. The slightly increased antioxidant depletion rate in RSL can potentially be explained by the following hypothesis: 1) alpha and beta radiation can penetrate short distance in water, thus only the radioactive decay occur close to the GM surface may affect the antioxidant depletion, and 2) alpha and beta radiation only penetrate a short distance into the polymer, thus only affecting the surface of HDPE GM.

The radionuclides in RSL were <sup>238</sup>U, <sup>99</sup>Tc and <sup>3</sup>H. An alpha particle with 4.2 MeV (Alpha decay form <sup>238</sup>U) can transport through approximately 20 µm of water, whereas a beta particle with 294 keV (Beta decay from <sup>99</sup>Tc) may penetrate approximately 0.5 mm in water (Turner 2007). Thus, only the radiation within a narrow zone adjacent to the GM can potentially reach the surface of HDPE GM. As a result, radiation decay must occur close to the surface of a GM to affect the degradation of the GM, which further weakens the radiation effect.

To investigate effect of alpha and beta radiation emitted from U and  $^{99}$ Tc on GM, a simple model simulated by GEANT4 was used to test  $\alpha$  and  $\beta$  radiation penetration in GM. The results indicate that alpha radiation emitted form  $^{238}$ U is shielded by 40  $\mu$ m of GM (2% of 2-mm-thick HDPE GM), while beta radiation emitted from  $^{99}$ Tc penetrates approximately 500  $\mu$ m (25% of 2-mm-thick HDPE GM) into GM. Thus, only the antioxidant close to the surface

of GM may be affected by alpha and beta radiation from LLW leachate, and thus the radiation has a limited effect on antioxidant depletion. Further research is needed to support and quantify these hypotheses.

#### 4.4.3 Lifetime Prediction

Lifetime predictions of GMs are typically made using the Arrhenius modeling and accelerated laboratory antioxidant depletion tests. To reduce the testing time, antioxidant depletion rates at elevated temperatures are obtained in laboratory experiments in a much shorter period (Hsuan and Koerner 1998, Sangam and Rowe 2002). Arrhenius modeling is then used to extrapolate the antioxidant depletion rates obtained at elevated temperatures to *in situ* temperature for the lifetime prediction (Hsuan and Koerner 1998, Sangam and Rowe 2002, Gulec et al. 2004, Rowe and Rimal 2008, Rowe et al. 2010a, 2013).

Arrhenius graphs (In(s) vs. 1/T) for the GM tested in the three leaching liquids are shown in Fig. 4.5. The data in Fig. 4.5a for DI water immersion are consistent with the data from Gulec et al. (2004) and Rowe et al. (2009) after taking into account the difference in antioxidant packages and thickness of the HDPE GMs tested. Activation energies calculated from the data in Fig. 4.5b using Eq. 8 and the depletion rates given in Table 4.3 are summarized in Table 4.5. The activation energy is deduced from the slopes of the Arrhenius graphs by applying least-squares fitting to the data (shown in Fig 4.5b). The antioxidant depletion rate at different temperature can be determined using the Arrhenius equations shown in Table 4.5. The time to antioxidant depletion at site-specific temperatures is then estimated as

$$t=[\ln(OIT^*)]/s \tag{13}$$

Antioxidant depletion times are shown in Fig. 4.6 as a function of temperature and the different liquids used for immersion. The immersion test provides an estimate of antioxidant

depletion time for the 2-mm-thick HDPE GM exposed to RSL on both sides: 216 yr at a field temperature of 15 °C (shown in Table 4.6), which is typical of liner temperatures at LLW facilities operated by the DOE (Tian 2012).

However, immersion testing is considered to be conservative (Rowe and Rimal 2008, Rowe et al. 2010). In immersion testing, antioxidants diffuse out from both sides of the GM, which causes a relatively high concentration gradient and outward diffusive flux. In contrast, the leachate is only in contact with one side of the GM in a landfill liner the outward diffusive antioxidant concentration gradient is lower, thus reducing the outward diffusive flux (Rowe and Rimal 2008). Therefore, simulated liner tests provide for a more accurate prediction of antioxidant depletion (Rowe and Rimal 2008, Rowe et al. 2010b, 2013). Rowe et al. (2010b) compared results between immersion testing and simulated composite liner testing by using 1.5-mm-thick HDPE GM. The antioxidant depletion of a GM was tested under simulated landfill liner condition, with applied pressure of 250 kPa. The antioxidant depletion rates for both testing conditions were listed in Table 4.4. The predicted antioxidant depletion time based on simulation testing was approximately 3 times longer than that from immersion testing.

To provide a more representative prediction of antioxidant depletion rates in LLW liner, a correction factor (1/3) was applied to the times computed using Eq. 13 to estimate the antioxidant depletion rate in a composite liner (i.e., one-sided depletion), as suggested by Rowe et al. (2010b). Applying this correction factor, the antioxidant depletion time for RSL was computed as 649 yr under field conditions (Fig. 4.6).

## 4.4.4 Melt Flow Index (MFI)

The measurement of MFI can obtain the molecular weight of polymer materials (e.g., chain scission and cross-linking), which is an indicator to determine the beginning of

degradation stage II or III. The MFI for GM exposed to RSL and NSL at 90 °C was presented in Fig. 4.7a. The mean MFI of the unexposed GM is shown as the solid line and the dashed lines are one and two standard deviations from the mean in Fig. 4.7a. For normally distributed data, one standard deviation from the mean encompasses 68% of the dispersion in the data and 95% is encompassed within two standard deviations. The MFIs for different specimen fall within two standard deviations from 1 to 16 months aging time, regardless of the exposed liquid. A clear decreasing trend of MFIs occurs after 17-month aging time. The decrease in MFIs reflects the molecular weight increase of the GM, which indicates that cross-linking occurs in the GM during the aging process. The decreasing of MFIs display that the degradation of GMs immersed in RSL/NSL at 90 °C has completed degradation stage I-antioxidant depletion and turns to the degradation stage II or stage III, as described in Rowe et al. (2009). Thus, the remaining antioxidants (reflect as OIT<sub>r</sub>) in GM exposed to RSL/NSL at 90 °C cannot protect the polymer from oxidation. Further measurement of MFI is needed to monitor this trend to predict the longevity of stage II and III.

## 4.4.5 Crystallinity

Degree of crystallinity indicates the ratio of crystalline region and amorphous region in polymer, which can be used to determine the change of polymer structure. The crystallinity of the GMs immersed in RSL and NSL at 90 °C was shown in Fig. 4.7b. The crystallinity increased during the early stages of aging (up to 12 month) and then slowly decreased approximately 1% from the peak crystallinity during 15–21 month, respectively. The crystallinity increased from the initial value of 42.4% to 45.5–46.5%. Petermann et al. (1976) and Wrigley (1989) defined this increasing trend of crystallinity as a physical aging process in which the GM attempts to establish equilibrium from its non-equilibrium state. Recrystallization and/or post-crystallization of polyethylene occurs mostly during the initial aging

time (Dörner and Lang 1998). Similar observation of increase in crystallinity of HDPE GM immersed in leachate at 85 °C was reported by Islam and Rowe (2008) and Rowe et al. (2009). Rowe et al. (2009) observed a drop of crystallinity of GM exposed to leachate at 85 °C after the antioxidant was completely depleted and cross-linking started to occur. The cross-linking can reduce the degree of freedom of molecular segments to form crystallites, resulting decrease in crystallinity (Peacock 2000). The slightly decrease of crystallinity of GM exposed to RSL and NSL indicated that the degradation of HDPE GM (Rowe et al. 2009), which was consistent with MFI results.

#### 4.5 SUMMARY

This paper has described results of immersion tests conducted to evaluate how exposure to LLW leachate affects antioxidant depletion in high-density polyethylene (HDPE) geomembrane (GM). Specimens were exposed to radioactive synthetic leachate (RSL) and non-radioactive synthetic leachate (NSL) at 25, 50, 70, and 90°C. DI water testing was conducted as a control. Aged samples were periodically removed to determine oxidation induction time (OIT), melt flow index (MFI), and crystallinity.

The antioxidant depletion rates of the 2-mm-thick HDPE GM exposed to RSL were 0.0047, 0.0277, 0.1862, and 0.4569 month<sup>-1</sup> at 25 50, 70, and 90°C, respectively, based on 3-parameter fitting. The antioxidant depletion rates were faster at higher aging temperature and higher when immersed in synthetic leachate as compared to DI water control. Arrhenius modeling was used to extrapolate the laboratory immersion data at elevated temperatures to a typical low-level radioactive waste (LLW) liner temperature of 15 °C. The predicted time to antioxidant depletion based on immersion test is 216 yr. Considering a correction factor of 3, as suggested by Rowe et al. (2010a) for a liner with one-sided exposure to RSL, the predicted *in situ* antioxidant depletion time of HDPE GM in low-level radioactive waste liner

system was 649 yr. The actual service lifetime will be longer than this with considering the additional degradation Stages II and III.

The antioxidant depletion rate of HDPE GM exposed to radioactive synthetic leachate was 9%, 4%, and 6% higher than that exposed to non-radioactive synthetic leachate at 25, 70, and 90 °C, respectively and similar at 50 °C. The slightly increasing of antioxidant depletion rate in RSL may be caused by radiation effect. The limited effect of radiation on antioxidant depletion in HDPE GM was hypothesized on the basis that alpha and beta radiation can only penetrate short distance (e.g., 0.02 mm and 0.2 mm) in water, resulting in low radiation dosage. Additionally, the alpha and beta radiation cannot penetrate through GM, which may cause surface effect on antioxidant depletion in HDPE GM. Another study will be continued to clarify this.

Melt flow index and crystallinity testing were applied to monitor the degradation process of HDPE GM immersed in RSL/NSL at 90 °C. The melt flow index of HDPE GM immersed in RSL/NSL displayed a decreasing trend after 16-month aging time, which indicated that the completed the degradation stage I and move to stage II and stage III. The crystallinity increased from 42.4% to 45.5–46.5% in the early (0-12 month) stages of immersion test due to physical aging process, and followed by approximately 1% decreasing form 15 to 21 month. The decreasing of crystallinity indicated that the GM went through the first-degradation stage. The analysis of MFI supported the judgment that remaining antioxidant cannot protect the degradation of HDPE GM, which is reflected as residual OIT. Thus, these two index tests valid to monitor the degradation of HDPE GM.

#### REFERENCE

- Andrejkovicova, S., Rocha, F., Janotka, I., and Komadel, P. (2008). An investigation into the use of blends of two bentonites for geosynthetic clay liners. *Geotextiles and Geomembranes*, 26 (5), 236–445.
- ASTM D1238. Standard test method for melt flow rates of thermoplastics by extrusion plastometer, Annual Book of ASTM Standards.
- ASTM D3895. Standard test method for oxidative-induction time of polyolefins by differential scanning calorimetry Annual Book of ASTM Standards.
- ASTM. D5885. Standard test method for oxidative induction time of polyolefin geosynthetics by high-pressure differential scanning calorimetry, Annual Book of ASTM Standards.
- ASTM E794. Standard test method for melting and crystallization temperatures by thermal analysis, Annual Book of ASTM Standards.
- Bouazza, A., Vangpaisal, T., Abuel-Naga, H., and Kodikara, J. (2008). Analytical modelling of gas leakage rate through a geosynthetic clay liner–geomembrane composite liner due to a circular defect in the geomembrane. *Geotextiles and Geomembranes*, 26(2), 122–129
- Bracco, P., Brach del Prever, E., Cannas, M., Luda, M., and Costa, L. (2006). Oxidation behaviour in prosthetic UHMWPE components sterilised with high energy radiation in a low oxygen environment. *Polymer Degradation and Stability*, 91(9), 2030–2038.
- Costa, L., Carpentieri, I., and Bracco, P. (2008). Post electron-beam irradiation oxidation of orthopaedic UHMWPE. *Polymer Degradation and Stability*, 93(9), 1695–1703.
- Czvikovszky, T. (2004). Degradation effects in polymers. *Proceeding of International Atomic Energy Agency Meeting,* Notre Dame, Indiana, U.S.
- Dörner, G. and Lang, R. (1998). Influence of various stabilizer systems on the ageing behavior of PE-ME-I. Hot water ageing compression molding plaques. *Polymer Degradation and Stability*, 62, 421–430.
- Flory, P. and Vrij, A. (1963). Melting points of linear-chain homologs. The normal paraffin hydrocarbons. *Journal of the American Chemical Society*, 85, 3548–3553.
- Foose, G., Benson, C., and Edil, T. (2002). Comparison of solute transport in three composite liners. *Journal of Geotechnical and Geoenvironmental Engineering*, 128(5), 1–13.
- Grassie, N. and Scott, G. (1985). *Polymer Degradation and Stabilization*. Cambridge University Press, New York, USA.
- Gulec, S., Edil, T., and Benson, C. (2004). Effect of acidic mine drainage on the polymer properties of an HDPE geomembrane. *Geosynthetic International*, 11(2), 60–72.
- Gulec, S., Benson, C., and Edil, T. (2005). Effect of Acidic Mine Drainage on the Mechanical and Hydraulic Properties of Three Geosynthetics. *Journal of Geotechnical and Geoenvironmental Engineering*, 131(8), 937–950.
- Hsuan, Y. and Koerner, R. (1998). Antioxidant depletion lifetime in high density polyethylene geomembranes. *Journal of Geotechnical and Geoenvironmental Engineering*, 124(6), 532–541.

- Hsuan, Y. and Guan, Z. (1997). Evaluation of the antioxidant behavior of polyethylene geomembranes using oxidative induction time tests. *Oxidative behavior of materials by thermal analytical techniques*, ASTM STP1326, A. T. Riga and G. H. Patterson, eds., ASTM, Philadelphia, 76–90.
- Hsuan, Y. and Koerner, R. (1995). Long term durability of HDPE GM: Part I depletion of antioxidant. *GRI Report*, 16, 35.
- Islam, M., and Rowe, R. (2008). Effect of geomembrane ageing on the diffusion of VOCs through HDPE geomembranes. *In: GeoAmericas 2008*, Cancun, Mexico. 459–467.
- Klemchuck, P. (2000). *Environmental degradation of polymers. Handbook of Polymer Degradation*. Hamid, S., Editor, Marcel Dekker, New York.
- Koerner, R., Halse, Y., and Lord, A. (1990). Long-term durability and aging of geomembranes. Waste Containment Systems: Construction, Regulations, and Performance, GSP 26, Bonaparte, R., Editor, ASCE, New York, 106–134.
- Kong, Y., and Hay, J. (2002). The measurement of the crystallinity of polymers by DSC. *Polymer*, 43(14), 3873–3878.
- Kulshreshtha, A. (1992). *Chemical degradation. Handbook of Polymer Degradation.* Hamid, S. H., Amin, M. B. & Maadhah, A. G., Editors, Marcel Dekker, New York, 55–95.
- Müller, W. and Jakob, I. (2003). Oxidative resistance of high-density polyethylene geomembranes. *Polymer Degradation and Stability*, 79, 161–172.
- Needham, A., Smith, J., and Gallagher, E. (2006). The service life of polyethylene geomembrane barriers. *Engineering Geology*, 85, 82–90.
- Osawa, Z. and Ishizuka, T. (1973). Catalytic action of metal salts in autoxidation and polymerization. *Journal of Applied Polymer Science*, 17, 2897–2907.
- Peacock, A., (2000). *Handbook of Polyethylene: Structures, Properties and Application.*Marcel Dekker Inc., New York.
- Petermann, J., Miles, M., and Gleiter, H. (1976). Growth of polymer crystals during annealing. *Journal of Macromolecular Science – Physics B*, 12(3), 393–404.
- Phillips, D. (1988). Effect of radiation on poplymers. *Materials Science and Technology*, 4, 85–91.
- Rowe, R., Abdelaal, F., and Brachman, R. (2013). Antioxidant depletion of HDPE geomembrane with sand protection layer. *Geosynthetic International*, 20(1), 73–89.
- Rowe R., Islam, M., and Hsuan, Y. (2010a). Effect of thickness on the ageing of HDPE geomembranes. *Journal of Geotechnical and Geoenvironmental Engineering*, 136(2), 299–309.
- Rowe R., Islam, M., Brachman, R., Arnepalli, D., and Ewais, A. (2010b). Antioxidant depletion from a high density polyethylene geomembrane under simulated landfill conditions. *Journal of Geotechnical and Geoenvironmental Engineering*, 136(7), 930–939.
- Rowe, R., Islam, M., and Hsuan, Y. (2009). Ageing of HDPE geomembrane exposed to air, water and leachate at different temperatures. *Geotextiles and Geomembranes*, 27(2), 137–151

- Rowe, R. and Rimal, S. (2008). Depletion of antioxidants from an HDPE geomembrane in a composite liner. *Journal of Geotechnical and Geoenvironmental Engineering*, 134(1), 68–78.
- Rowe, R., Islam, M., and Hsuan, Y. (2008). Leachate chemical composition effects on OIT depletion in an HDPE geomembrane. *Geosynthetics International*, 15(2), 136–151.
- Rowe, R. (2005). Long-term performance of contaminant barrier systems. *Geotechnique*, 55 (9), 631–678.
- Rowe, R., Quigley, R., Brachman, R., and Booker, J. (2004). *Barrier Systems for Waste Disposal Facilities, 2nd ed.* Spon Press. 587.
- Rowe, R., Sangam, H., and Lake, C. (2003). Evaluation of an HDPE geomembrane after 14 years as a leachate lagoon liner. *Canadian Geotechnical Journal*, 40, 536–550.
- Rowe, R. and Sangam, H. (2002). Durability of HDPE geomembranes. *Geotextiles and Geomembranes*, 20, 77–95
- Sangam, H. and Rowe, R. (2002). Effects of exposure conditions on the depletion of antioxidants from high-density polyethylene (HDPE) geomembrane. *Canadian Geotechnical Journal*, 39, 1221–1230.
- Saidi, F., Touze-Foltz, N., and Goblet, P. (2008). Numerical modelling of advective flow through composite liners in case of two interacting adjacent square defects in the geomembrane. *Geotextiles and Geomembranes*, 26(2), 196–204.
- Sperling, L. (1992). *Introduction to Physical Polymer Science, 2nd ed.* Wiley, New York.
- Take, W., Chappel, M., Brachman, R., and Rowe, R. (2007). Quantifying geomembrane wrinkles using aerial photography and digital image process. *Geosynthetics International*, 14(4), 219–227.
- Tian, K. (2012). Durability of high-density polyethylene geomembrane in low-level radioactive waste leachate. *MS thesis*, Univ. of Wisconsin-Madison, Madison, Wisconsin.
- Turner, J. (2007). *Atoms, Radiation, and Radiation Protection*. WILEY-VCH Verlag GmbH & Co. KGaA, Weinheim.
- Whyatt, G. and Farnsworth, R. (1989). The high pH chemical and compatibility of various liner materials. *Geosynthetic Testing for Waste Containment Applications*, ASTM STP 1081, Robert M. Koerner, editor, American Society for Testing and Materials, Philadelphia, 1990.
- Wrigley, N. (1989). The durability and aging of geogrids. In: Koerner, R.M. (Ed.), Durability and Aging of Geosynthetics. Elsevier, New York, 110–134.
- Viebke, J., Elble, E., Ifwarson, M., and Gedde, U. (1994). Degradation of unstabilized medium-density polyethylene pipes in hot-water applications. *Polymer Engineering & Science*, 34(17), 1354–1361.
- Vukelić, A., Szavits-Nossan, A., and Kvasnička, P. (2008). The influence of bentonites extrusion on shear strength of GCL/geomembrane interface. *Geotextiles and Geomembranes*, 26 (1), 82–90.
- Yako M., Koerner G., Koerner R., and Hsuan Y. (2010). Case History of a 20-Year Old Exposed HDPE Surface Impoundment Liner. *Proceedings of 9th International Conference on Geosynthetics*, Guarujá, Brazil, 805–808.

Yong, N. R., Pusch, R., and Nakano, M. (2010). Containment of High-level Radioactive and Hazardous Solid Wastes with Clay Barrier. Spon Press, London, New York.

Table 4.1. Properties of HDPE GM

Property	Method (ASTM)	Average
Density (g/cm <sup>3</sup> )	D 1505	0.946ª
Average Thickness (mm)	D 5199	2ª
Carbon black content (%)	D 4218/1603	2.62 <sup>a</sup>
Standard Oxidation Induction Time (min)	D 3895	197 <sup>b</sup>
High-Pressure Oxidation Induction Time (min)	D 5885	831°
Crystallinity (%)	E 794	43.4 <sup>a</sup>
Melt Flow Index (g/10 min)	D 1238	0.081 <sup>a,c</sup>

Note: <sup>a</sup>Measured by the manufactory (GSE), <sup>b</sup>Measured by UW-Madiosn, <sup>c</sup>Measured by TRI

Table 4.2. Composition of radioactive synthetic leachate (RSL)

Inorganic Components (mmol/L)				
Ca	4	As	0.001	
Mg	6	Ва	0.002	
Na	7	Cu	0.0002	
K	0.7	Fe	0.04	
Sulfate	7.5	Li	0.02	
CI	8	Mn	0.01	
Nitrate/Nitrite	1.5	Ni	0.0003	
Alkalinity	3.5	Sr	0.02	
Al	0.03	Zn	0.0005	
Radionuclides		Chemical Characteristics		
U-238 (µg/L)	1500	TOC	5 mg/L surfactant and	
			3 mg/L acetic acid	
H-3 (Bq/L)	4400	OPR	120	
Tc-99 (Bq/L)	29.6	рН	7.2	

Note:  $H_2SO_4$  used to adjust pH  $\approx 7.2$ ,  $Na_2S$  used to adjust oxidation reduction potential (ORP) to  $\approx 120$  mV, and TOC is short for total organic carbon.

Table 4.3. Antioxidant depletion rates in DI, NSL, and RSL leachate

Two-Parameter Fitting [In(min)/month]			ıg	Three-Parameter Fitting [In(min)/month]				
Temp.	Antioxidant Depletion Rate Ratio		Antioxidant Depletion Rate			Ratio		
( 0)	DI	NSL	RSL	RSL/ NSL	DI	NSL	RSL	RSL/ NSL
25	0.0024	0.0043	0.0047	1.09	0.0025	0.0043	0.0047	1.09
50	0.0230	0.0255	0.0253	1.00	0.0244	0.0278	0.0277	1.00
70	0.1340	0.1609	0.1670	1.04	0.1344	0.1789	0.1862	1.04
90	0.2545	0.3683	0.3858	1.05	0.3472	0.4319	0.4569	1.06

Table 4.4. List of antioxidant depletion rate in the literature for different exposure conditions for HDPE geomembrane

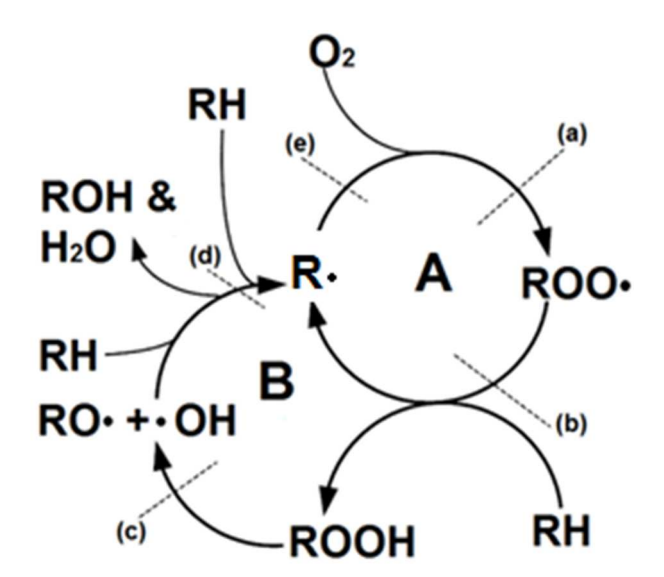
Exposure Condition	Incubation temperature (°C)	Antioxidant depletion rate (month <sup>-1</sup> )
1.5-mm thick geomembrane with saturated	85	0.1404
sand on the top with static compressive	75	0.0798
stress of 260 kPa and dry sand on the bottom. Initial Std-OIT=80.5 min; HP-	65	0.0589
OIT=210 min. (Hsuan and Koerner 1998)	55	0.0217
4.5	80	1.2056
1.5-mm thick geomembrane immersed in AMD. Initial Std-OIT=208 min; HP-OIT=484	60	0.0906
min. (Gulec et al. 2004)	40	0.0480
(	20	0.0051
4.5	85	1.2423
1.5-mm thick geomembrane immersed in synthetic MSW leacahte. Intial Std-OIT = 135	70	0.4809
min, HP-OIT = 660 (Rowe and Rimal 2008)	55	0.1183
	26	0.0253
1.5-mm thick geomembrane aged under a	85	0.2750
simulate liner with gravel and geotextile on	70	0.2123
the top and geosytnthetic clay liner at the bottom. Intial Std-OIT = 135 min, HP-OIT =	55	0.0539
660 (Rowe and Rimal 2008)	26	0.0053
	85	0.1724
2-mm thick geomembrane immersed water.	70	0.1097
Initial Std-OIT=133 min; HP-OIT=380 min. (Rowe et al. 2009)	55	0.0357
(110WC Ct al. 2000 )	40	0.0233
	22	0.0048
	85	0.4341
2-mm thick geomembrane immersed in	55	0.1438
synthetic MSW leachate. Initial Std-OIT =133 min; HP-OIT=380 min. (Rowe et al. 2009)	40	0.0586
, 3.1 333 11 (1.040 31 41. 2000)	22	0.0185

Table 4.5. Arrhenius equation and activation energies from Fig. 4.6

Group	roup Arrhenius Equation		Activation Energy (kJ/mol)
RSL	In(s) = 21.043 - 7879 / K	0.99	65.4
NSL	In(s) = 20.193 - 7922 / K	0.99	65.8
DI	In(s) = 22.203 - 8383 / K	0.99	69.7

Table 4.6. Prediction of antioxidant depletion time

Temp.	DI	NSL	RSL	LLW
°C	(Immersion Test)	(Immersion Test)	(Immersion Test)	(Composite Liner)
5	1130	646	563	1690
10	672	396	346	1038
15	407	247	216	649
20	251	157	137	412
25	157	101	89	266
30	100	66	58	174
35	65	44	38	115
40	42	29	26	78
45	28	20	18	53
50	19	14	12	36
55	13	9	8	25
60	9	7	6	18
65	6	5	4	13



RH: Polyethylene polymer chain R•: Reactive free radical ROO+: Hydroperoxy radical ROOH: Hydroperoxide

Fig. 4.1. Oxidation loops for polyethylene [modified from Grassie and Scott (1985) and Rowe and Sangam (2002)].

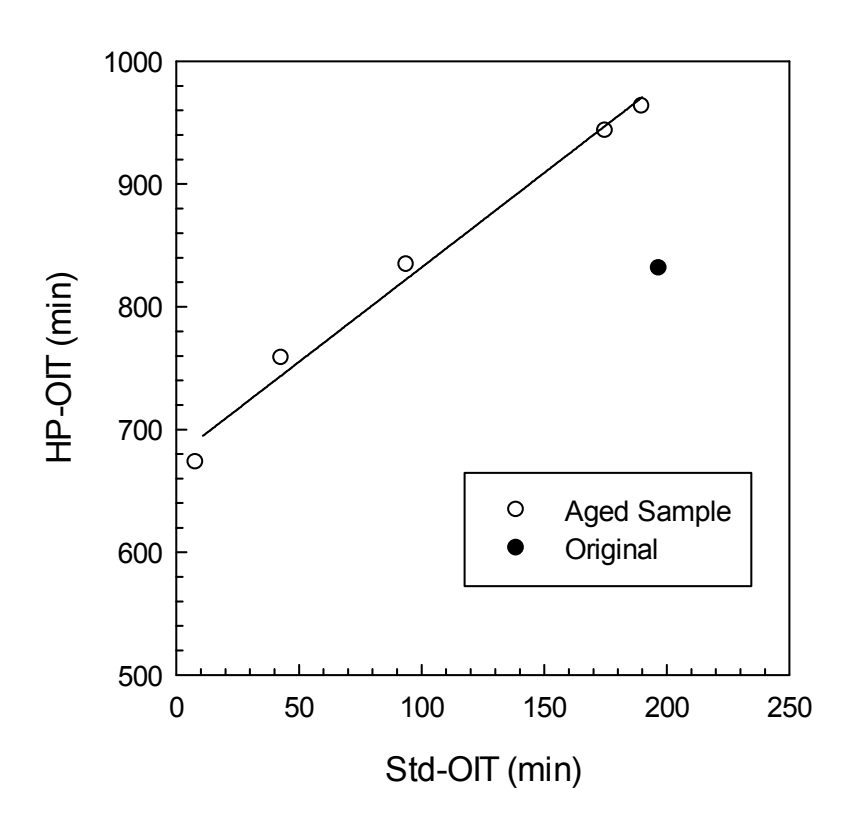


Fig. 4.2. Std-OIT vs. HP-OIT for HDPE geomembranes immersed in DI water (the sample aged in DI water from right to left: 1 month at 50 °C, 1 month at 70 °C, 2 months at 90 °C, and 6 months at 90 °C) and initial condition.

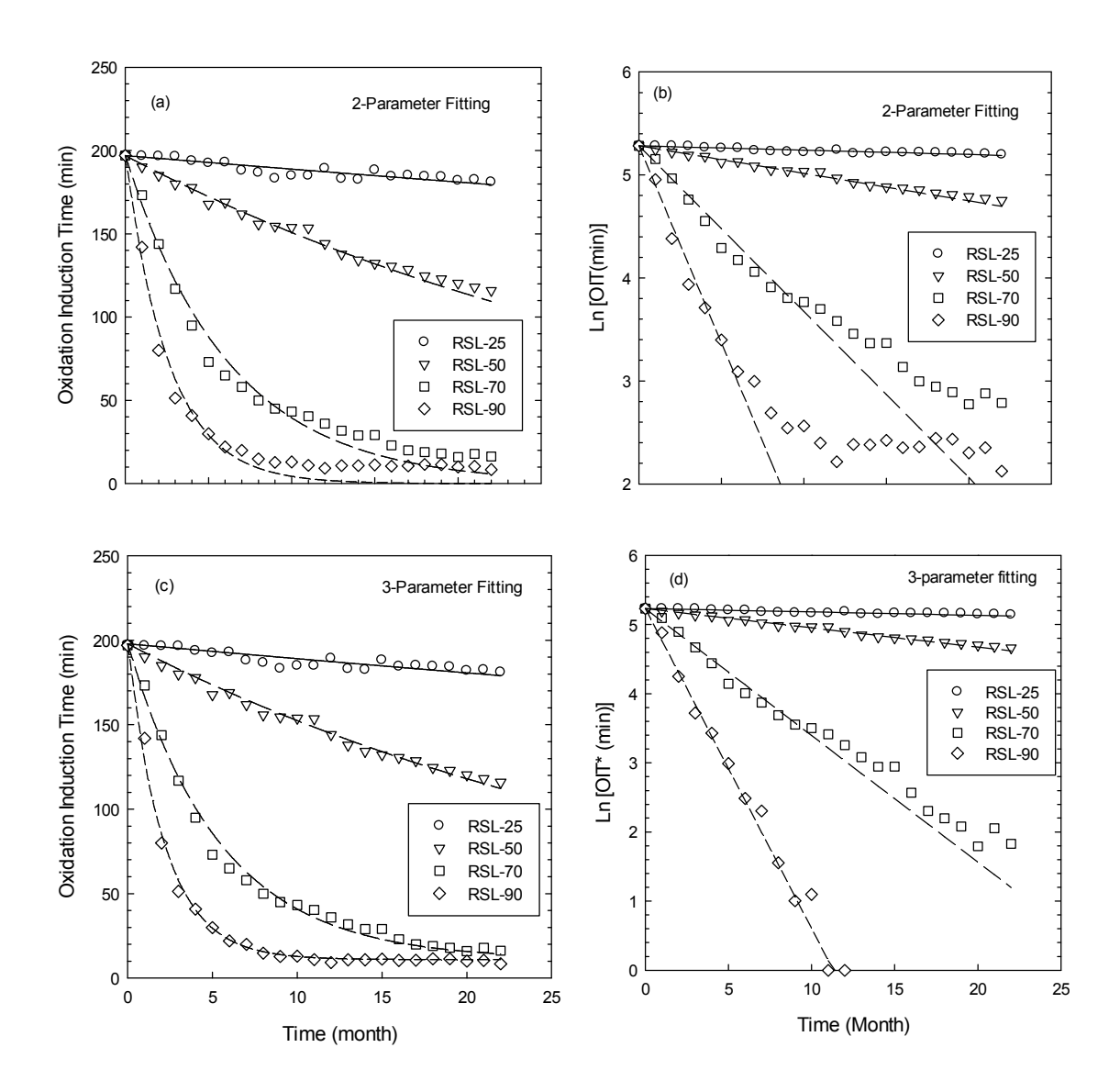


Fig. 4.3. Std-OIT of GM immersed in RSL vs. time and In[OIT] vs. Time; (a) and (b) are 2-parameter fitting, (c) and (d) are 3-parameter fitting.

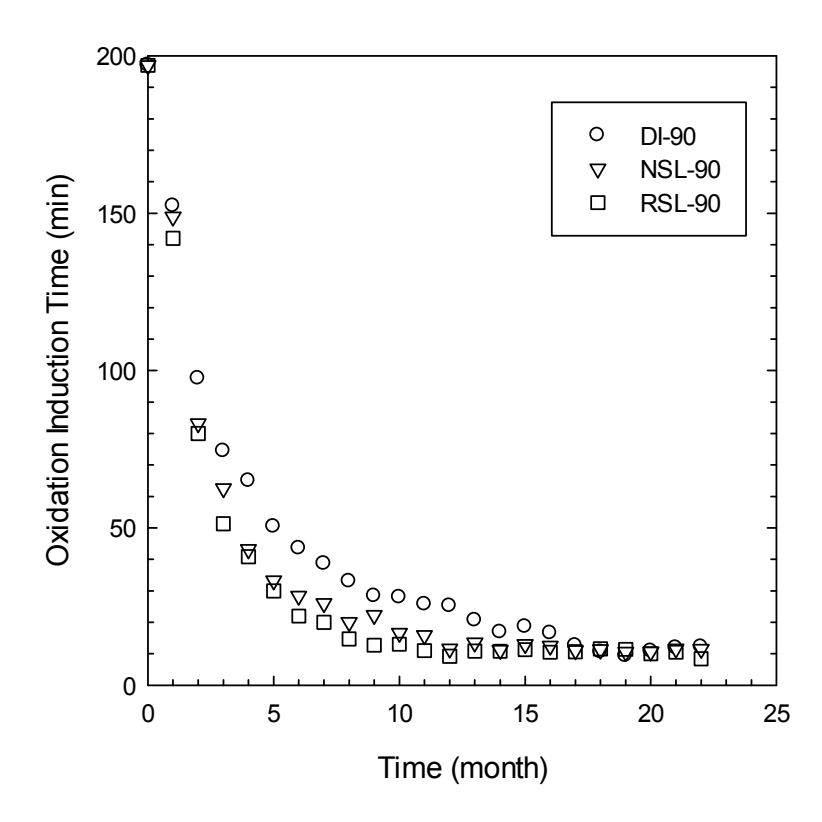


Fig. 4.4. Std-OIT depletion of GM exposed to DI, NSL and RSL as a function of aging time.

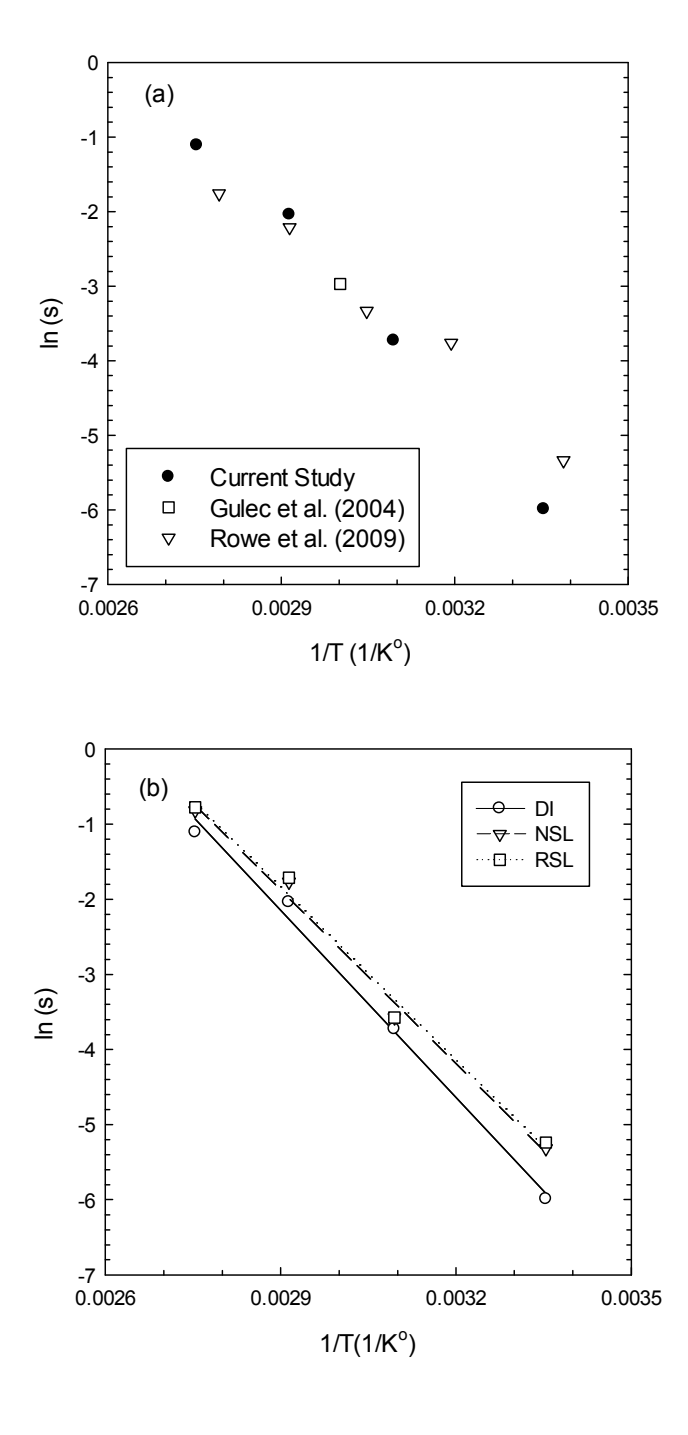


Fig. 4.5. Arrhenius plot of antioxidant depletion for (a) DI water (Current and other studies). (b) DI, NSL, and RSL.

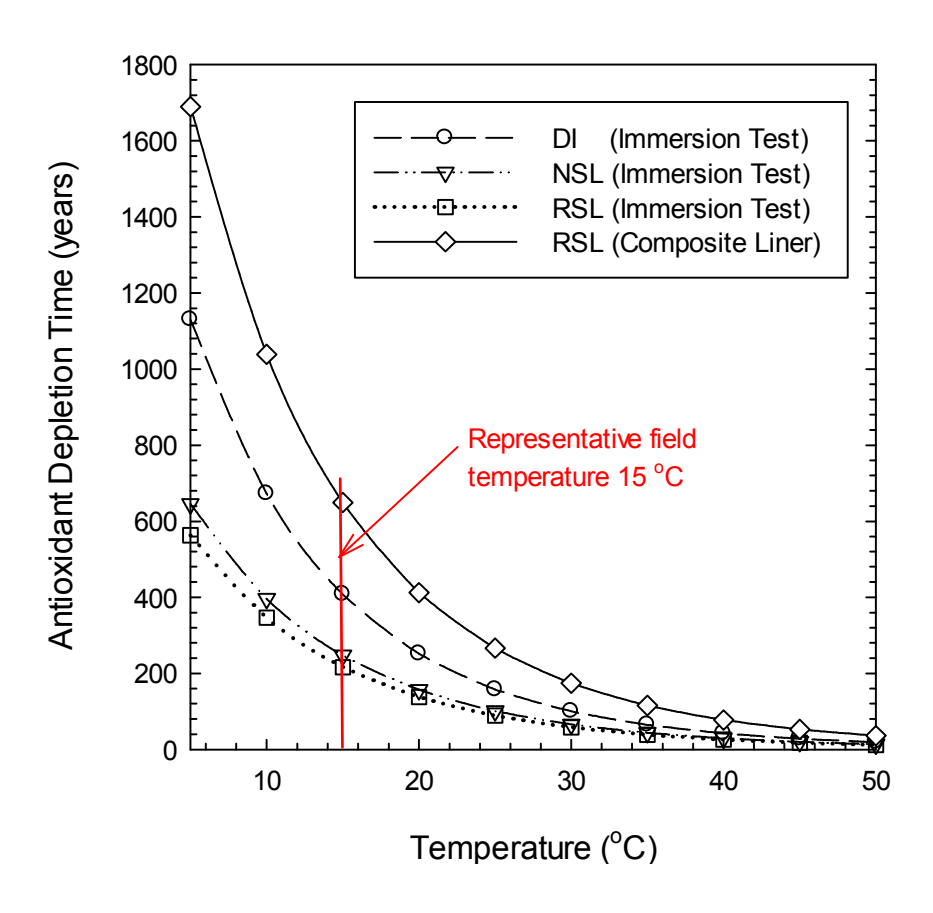
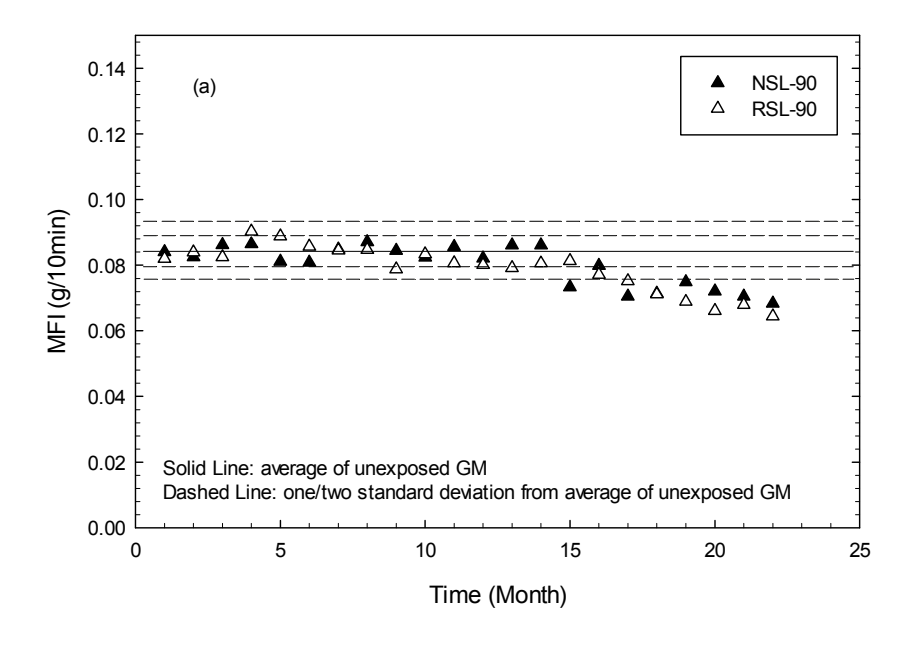


Fig. 4.6 Predicted antioxidant depletion time as a function of temperature and immersion liquid.



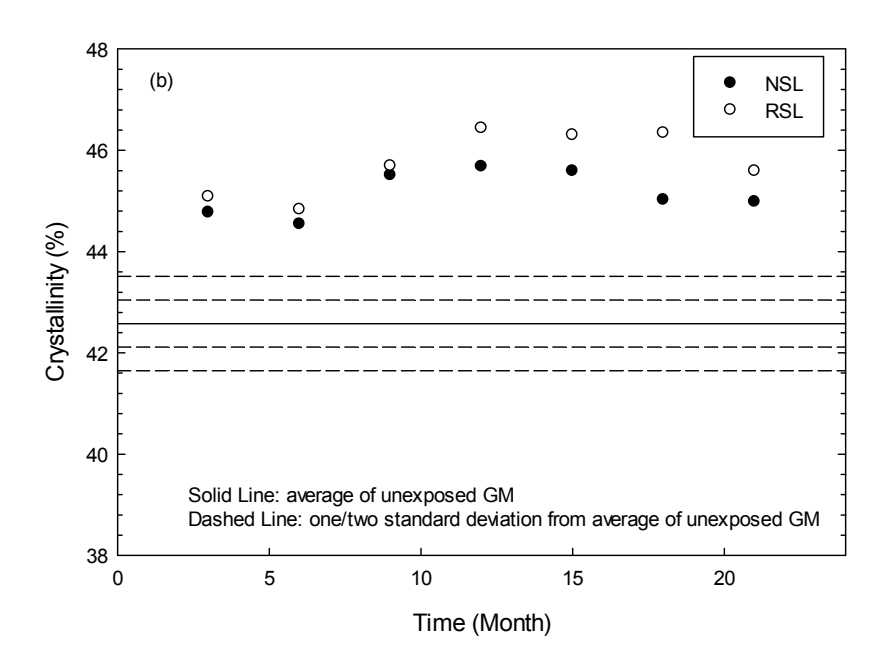


Fig. 4.7. Melt Flow Index (a) and Crystallinity (b) of HDPE GM exposed to RSL and NSL at  $90\,^{\circ}\text{C}$  as a function of aging time.

# 5 EFFECT OF RADIATION FROM LOW-LEVEL RADIOACTIVE LEACHATE ON ANTIOXIDANT DEPLETION IN HDPE GM

# ABSTRACT:

High-density polyethylene (HDPE) geomembrane (GM) specimens were exposed to <sup>241</sup>Am (alpha particles) and <sup>99</sup>Tc (beta particles) from sealed sources to simulate radiation from low-level radioactive waste (LLW) leachate (e.g., 234U, 235U, 238U and 99Tc). Sealed source of <sup>241</sup>Am and <sup>99</sup>Tc were used to simulate alpha (uranium and <sup>226</sup>Ra) and beta (<sup>99</sup>Tc) radiation from LLW leachate. The dosage deposition in HDPE GM from sealed sources was simulated with the GEANT4 Monte Carlo (MC) simulation Toolkit. The results from Monte Carlo simulation can be used to investigate the impact zone for alpha and beta radiation. Additionally, HDPE GM specimens of various thickness (e.g., 0.04-mm, 0.1-mm, 0.2-mm and 2-mm) were exposed to sealed sources of <sup>241</sup>Am (alpha particles) and <sup>99</sup>Tc (beta particles) from 1-50 h. Antioxidant depletion in HDPE GM post irradiation was monitored by Std-OIT testing following ASTM D3895. Multiple-layer model was created to simulation the antioxidant depletion in HDPE GM. Another simulation was conducted with GEANT4 to mimic the HDPE GM under the in situ condition, which can predict the total dosage deposition in HDPE GM installed in LLW liners over a 1000-yr service life. Based on the dosage, the impact of radiation from LLW leachate on antioxidant depletion in HDPE GM can be estimated over 1000 yr using multiple-layer model. The results indicate that low dosage from LLW leachate would have a negligible effect on antioxidant depletion in HDPE GM installed in LLW disposal facilities.

#### 5.1 INTRODUCTION

High-density polyethylene (HDPE) geomembranes (GMs) are used in composite barrier system at waste disposal facilities including low-level radioactive waste (LLW) and mixed waste (MW). HDPE GM is considered as an impermeable layer to advective flow (Foose et al. 2002, Gulec et al. 2004, Take et al. 2007, Saidi et al. 2008, Vukelić et al. 2008, Abdelaal and Rowe 2015). HDPE GMs are now used in applications at

LLW is a class of radioactive waste that is produced alongside spent nuclear fuel, high-level waste, transuranic waste, and uranium and thorium mill tailings (U.S. Environmental Protection Agency 2012). LLW is disposed within disposal facilities using a composite liner system (Powell et al. 2011). Composite barriers typically consist of a 2-mm-thick HDPE GM overlying a geosynthetic clay liner or a compacted clay liner (Powell et al. 2011). A typical HDPE GM consists of polymer resin (>95%), carbon black (2–3%), and antioxidant (0.5–1%) (Hsuan and Koerner 1998). Carbon black is added to protect the GM from ultraviolet light, and an antioxidant package is used to prevent oxidation within the GM.

Degradation of HDPE GM undergoes three stages: antioxidant depletion (Stage I), induction time to the onset of polymer degradation (Stage II), and degradation of polymer properties (Stage III) (Viebke et al. 1994, Hsuan and Koerner 1998, Rowe and Sangam 2002, Gulec et al. 2004, Rowe et al. 2009). The degradation of HDPE GM is initially limited through the consumption of antioxidants. Without protection of antioxidants, a GM becomes vulnerable to degradation via oxidation and rapidly progresses through stages II and III of degradation (Grassie and Scott 1985, Rowe et al. 2009). Previous studies have reported that antioxidant depletion in HDPE GM is affected by leachate composition (e.g., surfactant, heavy metals, extreme pH) in municipal solid waste (MSW) leachate or in acidic mine

drainage (Gulec et al. 2004, Rowe et al. 2008, 2009). However, LLW leachate has a unique component (e.g., radionuclides) that may affect the antioxidant depletion in HDPE GM.

The composition of LLW leachate can generally be divided into three categories: 1) macro inorganic components, 2) trace heavy metals, and 3) radionuclides (Tian 2012). Little dissolved organic compound (i.e., < 30 mg/L TOC) is commonly observed in LLW leachate. The pH of LLW leachate ranged from 5.7 to 9.1, with an average pH of 7.2. Abdelaal and Rowe (2015) presented an analysis of leachate data from six different LLW disposal sites located in North America. The radionuclides in LLW leachate contained <sup>226</sup>Ra (3.9–50 Bq/L) and <sup>236</sup>U (6–1500 µg/L), whereas other radionuclides (e.g., <sup>210</sup>Pb, <sup>232</sup>Th, <sup>230</sup>Th, and <sup>235</sup>U) were present at low concentrations. The pH of the six LLW leachates ranged from 8–12.3, where the high pH may be due to treatment to increase the pH and result in reducing the leaching of metals and radionuclides (Abdelaal and Rowe 2015). Based on the leachate data from these 10 sites, HDPE GMs installed in LLW disposal facilities may encounter radionuclides, heavy metals, and high pH conditions, all of which may affect antioxidant depletion in a HDPE GM (Abdelaal and Rowe 2015, Tian 2012).

Abdelaal and Rowe (2015) addressed the antioxidant depletion of HDPE GM exposed to synthetic LLW leachate with high pH (9.5–13.5). The antioxidant depleted faster in synthetic LLW leachate with higher pH. Tian et al. (2014) investigated antioxidant depletion in HDPE GM in synthetic LLW leachate with neutral pH and radionuclides. The impact of radiation on antioxidant depletion in the HDPE GM was insignificant. Whyatt and Farnsworth (1989) investigated the longevity of 1.5-mm-thick HDPE GM used in LLW disposal facilities by considering the effect of gamma radiation. HDPE GM becomes more rigid after irradiation; i.e., the elongation of HDPE GM decreased and the hardness of HDPE GM increased. Mason et al. (1993) investigated the effect of gamma radiation on antioxidant depletion in

cross-linked PE. The depletion of antioxidant followed first-order decay as a function of radiation dosage.

In LLW leachate, alpha (e.g., uranium and <sup>226</sup>Ra) and beta (e.g., <sup>99</sup>Tc) radiation are the predominant forms of radiation. Limited studies have thoroughly investigated the effect of alpha and beta particles from LLW leachate on antioxidant depletion in HDPE GM to date. Thus, the objective of this study was to examine the effect of radiation from LLW leachate on antioxidant depletion in HDPE GM. Multiple-layer model was created to simulate the antioxidant depletion in HDPE GM exposed to alpha and beta radiation. Understanding the effect of radiation on antioxidant depletion can provide a better prediction of the service life of the HDPE GM installed at LLW disposal facilities.

#### 5.2 BACKGROUND

The degradation of HDPE GM follows the free radical mechanism as shown in Fig. 5.1 (Grassie and Scott 1985, Rowe and Sangam 2002). The HDPE polymer chain (RH) can break into a free radical polymer chain (R•) and hydrogen (H•) after obtaining the necessary activation energy (e.g., from radiation or thermal). R• can react with oxygen (O₂) to form a hydroperoxy free radical (ROO•). The ROO• attacks the polymer backbone (RH) to form hydroperoxide (ROOH) and another free radical polymer chain. As oxidation continues, accumulation of ROOH results in decomposition into RO• and OH• and the generation of more free radicals that may attack the original polymer chain. This process is defined as an auto-accelerating process (Hsuan and Koerner 1998, Rowe and Sangam 2002).

To protect a GM from oxidation, an antioxidant package with a combination of two or more types of antioxidants is commonly added to the polymer resin (Hsuan and Koerner 1998, Rowe and Sangam 2002). Primary antioxidants interrupt the reaction by donating an electron to convert free radicals (ROO•, RO•, and OH•) to form stable compounds (ROOH,

ROH, and H<sub>2</sub>O), as indicated by dashed lines (b) and (d) in Fig. 5.1. Another type of antioxidant performs as an electron acceptor to break links (a) and (e) by converting alkyl free radicals (R•) to a stable polymer chain. Secondary antioxidants react with ROOH to form a stable alcohol, which is indicated as dashed line (c) in Fig. 5.1. Overall, the antioxidants intercept the loops in Fig. 5.1 to protect the HDPE GM from degradation.

# 5.2.1 Effect of Radiation on Polymer Degradation

HDPE GM installed in LLW disposal facilities may experience radiation damage due to the decay of radionuclides (e.g., uranium, <sup>226</sup>Ra, and <sup>99</sup>Tc) (Abdelaal and Rowe 2015, Tian 2012). Alpha (e.g., uranium and <sup>226</sup>Ra) and beta (e.g., <sup>99</sup>Tc) radiation can dissociate the polymer chain, which accelerates the degradation rate of HDPE GM. Therefore, the effect of radiation on the degradation of HDPE GMs in LLW liner should be considered in the prediction of service life.

Different types of radiation have various effects on polymer degradation (Phillips 1988, Czvikovszky 2004, Turner 2007). Charged alpha particles may penetrate into polymer on the order of micrometers, charged beta particles on the order of millimeters, whereas uncharged particles (e.g., neurons and gamma ray) can penetrate meters into a polymer. Therefore, alpha and beta particles potentially will affect the surface of a GM, whereas gamma ray can affect the entire thickness of a GM. LLW leachate contains uranium and <sup>99</sup>Tc, which emit alpha (exceeding 4.2 MeV) and beta particles (294 keV). The energy of these alpha and beta particles are high enough to be categorized as ionizing radiation—ionizing radiation carries energy above the energy of the covalent bond energy in the polymer chain that leads to random scission of carbon-carbon bonds and carbon-hydrogen bonds, resulting in the free radicals (R• and H•). The bond energy of carbon-carbon typically is in the range of 5–10 eV

(Czvikovszky 2004). Thus, alpha and beta particles from LLW leachate can potentially break the bonds in HDPE GMs.

Previous studies have investigated the effect of radiation on the degradation of polymers (Phillips 1988, Whyatt and Farnsworth 1989, Sohma et al. 1991, Mason et al. 1993, Singh 1999, Costa et al. 2008, Sugimoto et al. 2013). The original polymer chain can dissociate to a free radical chain (R•) and hydrogen (H•) under gamma radiation. The free radical polymer chain (R•) can form a new chemical bond with an adjacent free radical (e.g., R-R)—defined as crosslinking—which makes the polyethylene more rigid and easy to crack (Phillips 1988, Peacock 2000). Additionally, the hydrogen (H•) can attack the RH to form hydrogen gas and R•.

In the presence of oxygen, oxidative degradation becomes a dominant degradation mechanism for polymer exposed to gamma or beta radiation (Sugimoto et at. 2013, Sohma et al. 1991, Singh 1999). The free radicals can react with oxygen to form peroxide and hydroperoxide, accelerating the degradation process, schematically shown in Fig. 5.1. This process is defined as radiation-induced oxidation (Costa et al. 2008, Bracco et al. 2006). Costa et al. (2008) irradiated PE with an electron beam at dosages up to 50 kGy. The change in polymer structure was monitored using fourier transform infrared spectroscopy (FTIR). The concentration of hydroperoxides in PE displayed an increasing trend with higher irradiation dosage. The decomposition of hydroperoxides happened immediately and formed ketones. Overall, the products induced by oxidative degradation includes water molecules, carbon dioxide, alcohols, ketones, hydroperoxides, and carboxylic acid (Singh 1999, Sugimoto et al. 2013).

Mason et al. (1993) investigated the effect of gamma radiation on antioxidant depletion in cross-linked polyethylene materials. The consumption of antioxidant was determined by standard oxidation inducting time (Std-OIT) following ASTM D3895. Since the gamma

radiation can penetrate meters in polymer (Phillips 1988), the dosage distribution is nearly uniform in the PE materials. Thus, the antioxidant decreased uniformly through in the PE material. The depletion of Std-OIT followed first-order decay as a function of exposure dosage, which indicated that the antioxidant was consumed post irradiation.

# 5.2.2 Degradation of HDPE GM in LLW Disposal Facilities

Abdelaal and Rowe (2015) investigated antioxidant depletion in HDPE GM in synthetic LLW leachate over a range of pH (e.g., 9.5, 11.5, and 13.5). GM coupons (190 mm × 100 mm) were immersed in synthetic LLW leachate and incubated at temperatures of 40, 65, 75, 85, and 95 °C for 3 yr. The antioxidant depletion in GMs was monitored by Std-OIT and high-pressure oxidation induction time (HP-OIT). Increasing pH in the leachate from 9.5 to 13.5 resulted in an increase of the antioxidant depletion rate. The antioxidant depletion time ranged from 17–81 yr at temperature ranging from 20 to 40 °C.

Tian et al. (2014) investigated the antioxidant depletion in HDPE GM exposed to synthetic LLW leachate with various inorganics, neutral pH, and radionuclides (238U, 99Tc, and 3H) HDPE GM coupons (2-mm-thick) were immersed in radioactive synthetic leachate (RSL) with chemistry representative of LLW leachate. Based on immersion testing, the antioxidant can protect the HDPE GM from oxidation for approximated 89–216 yr at temperatures ranging from 15 to 30 °C. To identify the effect of radionuclides on antioxidant depletion, comparative tests were conducted with NSL, which was chemically identical to RSL but excluded radionuclides. Antioxidant deletion in HDPE GM in RSL was no different than that in NSL, which indicated that radiation from LLW leachate may have a limited effect on antioxidant depletion. Two hypotheses are proposed for this limited radiation effect from LLW leachate: (1) alpha and beta radiation from uranium and 99Tc can only penetrate a short distance in water (i.e., less than millimeter), thus only the radioactive decay occurring close

to the GM surface may affect the degradation of HDPE GM; and (2) alpha and beta radiation only penetrate a short distance into the polymer, thus only affecting the surface of HDPE GM.

Whyatt and Farnsworth (1989) investigated the compatibility of 1.5-mm-thick HDPE GM used in LLW disposal facilities. The HDPE GMs were irritated with gamma rays up to 389 µGy to simulate a 30-yr-equivalent dosage in LLW disposal facilities and then immersed in high pH (>14) inorganic solution at 90 °C for 120 d. The strength and elongation of HDPE GM decreased after aging, whereas the puncture force and hardness of HDPE GM increased.

#### 5.3 MATERIALS AND METHODS

Sealed sources of <sup>241</sup>Am and <sup>99</sup>Tc were used to simulate alpha (uranium and <sup>226</sup>Ra) and beta (<sup>99</sup>Tc) radiation from LLW leachate. The dosage deposition in HDPE GM from sealed sources was simulated with the GEANT4 Monte Carlo (MC) simulation Toolkit. The results from Monte Carlo simulation can be used to investigate the impact zone for alpha and beta radiation. Additionally, HDPE GM specimens of various thickness (e.g., 0.04-mm, 0.1-mm, 0.2-mm and 2-mm) were exposed to sealed sources of <sup>241</sup>Am (alpha particles) and <sup>99</sup>Tc (beta particles) from 1–50 h. Antioxidant depletion in HDPE GM post irradiation was monitored by Std-OIT testing following ASTM D3895. Multiple-layer model was created to simulation the antioxidant depletion in HDPE GM. Another simulation was conducted with GEANT4 to mimic the HDPE GM under the *in situ* condition, which can predict the total dosage deposition in HDPE GM installed in LLW liners over a 1000-yr service life. Based on the dosage, the impact of radiation from LLW leachate on antioxidant depletion in HDPE GM can be estimated over 1000 yr using multiple-layer model.

#### **5.3.1 GEANT4 Monte Carlo Simulation Toolkit**

GEANT4 simulates the passage of particles though user-specified voxelized geometries. The standard physics package supports the transport of radioactive isotopes, with full transport and decay of subsequent daughter products and user-specified scoring of various physical quantities. For this study, the Monte Carlo particle transport toolkit GEANT4 version 9.6 (Agnostinelli et al. 2003) was used to simulate dose deposition from sealed sources of <sup>241</sup>Am and <sup>99</sup>Tc on HDPE GM for 1–50 h. Additionally, a simulation was created to simulate the radiation dosage in HDPE GM installed in LLW disposal facilities over 1000-yr service life.

# 5.3.1.1 Monte Carlo Model to Simulate Sealed Source Experiment

As a benchmark, the sealed-source experiments were simulated using GEANT4 to estimate dose deposition in HDPE GM. Sealed source was above a 21 cm  $\times$  21 cm HDPE layer in an environment of air (Fig. 5.2). The GM layer consisted of CH<sub>2</sub> with a density of 0.942 g/cm<sup>3</sup>. For the <sup>241</sup>Am simulation, the 2-mm-thick GM proximate to the source was voxelized to a 41  $\times$  41  $\times$  200 voxel grid, with a corresponding voxel size of 0.5 cm  $\times$  0.5 cm  $\times$  0.01 mm. The simulation of <sup>99</sup>Tc followed the same voxel size as <sup>241</sup>Am simulation.

Three-dimensional models of the sealed sources of <sup>241</sup>Am and <sup>99</sup>Tc were simulated in GEANT4 according to the nominal dimensions specified by the engineering documents provided by Eckert & Ziegler. The sealed source of <sup>241</sup>Am has a nominal activity of 1.85 MBq with an active diameter of 9.5 mm. The radiation foil consisted of an <sup>241</sup>Am and gold matrix with aluminum backing. For the <sup>241</sup>Am source, the depth of the active layer was adjusted within the manufacturer's quoted uncertainties to match the specified peak alpha energy of 4.7 MeV. The sealed source of <sup>99</sup>Tc has a nominal activity of 32.3 kBq with an active diameter of 16 mm.

#### 5.3.1.2 Monte Carlo Model to Simulate In Situ Condition

To investigate the dose deposition in HDPE GM installed within a LLW liner, a simulation was created to mimic HDPE GM exposed to LLW leachate for 1000 yr service life. The LLW reservoir geometry includes three layers: 21 cm  $\times$  21 cm layers consisting of water, HDPE, and sand layer in an environment of air. The water, GM and sand layers were 2 cm, 2 mm, and 10 cm thick, respectively (Fig. 5.3). The water layer was  $H_2O$  with a density of 1 g/cm<sup>3</sup>, the GM layer contains  $CH_2$  with a density of 0.942 g/cm<sup>3</sup>, and the sand layer was approximated using  $SiO_2$  with a density of 2.65 g/cm<sup>3</sup>. The GM layer was voxelized to a 21  $\times$  21  $\times$  100 voxel grid, with a corresponding voxel size of 1 cm  $\times$  1 cm  $\times$  0.02 mm.

The LLW leachate layer was a 10 cm × 10 cm × 2 cm region in the water layer with randomly distributed radioactive source particles. A net uranium concentration of 1500 µg/L was simulated with <sup>234</sup>U, <sup>235</sup>U, and <sup>238</sup>U in their natural abundances. The concentration of <sup>99</sup>Tc was assumed to be 29.6 Bq/L. Additionally, the LLW leachate layer also consisted of inorganic components (e.g., Ca, Na, K, and Mg) to replicate the field condition. For adequate dose statistics, 107 full decays of each specie was simulated, renormalized to dose-perdecay, and multiplied by the 1000-yr time-integrated activity of each isotope.

# 5.3.2 HDPE GM Exposed to Sealed Source

A commercially available 2-mm-thick smooth HDPE GM was used to study the effect of radiation on antioxidant depletion. HDPE GM sheet was mechanically pulverized and then extruded in a Dayton #6536 Model film-blowing machine to achieve different thicknesses. GM specimens with different thickness (approximately 0.04-mm, 0.1-mm, 0.2-mm, and 2-mm) were placed below the sealed source and irradiated to 1 h, 5 h, 10 h, 20 h, and 50 h.

# 5.3.3 OIT Measurement

Standard oxidation induction time was used measured to measure antioxidant depletion in HDPE GM with differential scanning calorimetry (DSC) following ASTM D3895 (Hsuan and Koerner 1998, Sangam and Rowe 2002, Gulec et al. 2004, Rowe et al. 2009). The following discussion is thus based on Std-OIT results, which are simply referred to as OIT. OIT is proportional to the amount of antioxidant remaining in the HDPE GM. OIT was measured using a TA Instruments Q100 DSC at the Soft Material Laboratory at the University of Wisconsin-Madison. The initial OIT value was 197 min for 2-mm-thick HDPE GM; however, some antioxidant depletion occurred during preparation of different thicknesses of HDPE film. HDPE GM samples were prepared using film-blowing equipment, which results in HDPE GM cooling down from 180 °C to room temperature. After the extrusion, the initial OIT decreased from 197 min to 185 min in 0.04-mm-thick GM samples, whereas the initial OIT decreased from 197 min to 191 min in 0.2-mm-thick GM samples (Table 5.1). The extrusion process has a relatively significant effect on antioxidant depletion in thinner GM specimen due to the larger surface area ratio. OIT tests were also conducted on specimens of HDPE GM post irradiation to determine the antioxidant depletion.

# 5.3.4 Multiple-Layer Model for Antioxidant Depletion in HDPE GM

A multiple-layer model is created to predict antioxidant depletion in HDPE GM after exposure to different dosage. Antioxidant depletion follows first-order degradation as a function of exposure dosage, as proposed by Mason et al. (1993):

$$OIT_D = OIT_0 \times e^{-KD}$$
 (1)

where  $OIT_D = OIT$  of specimen post irradiation,  $OIT_o = initial\ OIT$  for the specimen, k is the fitting parameter ( $k_\alpha$  and  $k_\beta$  for alpha and beta particles, respectively), D = dose.

Due to the limited penetration ability of alpha and beta particles, the HDPE GM exposed to alpha and beta radiation may have a radiation impact zone and an unimpacted zone, depending on specimen thickness (in Fig. 5.4a). The depth of the impact zones for alpha and beta radiation were determined using GEANT4 simulation. The dose depositions of alpha and beta radiation in HDPE GM can also be obtained using simulation with GEANT4 (in Fig. 5.4b). The impact zone was divided into thin layer, and thus the dose deposition was assumed to be uniform in each thin layer (e.g., 0.2 μm). The antioxidant depletion can be calculated in each thin layer with a known dosage using Eq. (1) using GEANT4 simulation. The total change of OIT in the impact zone can be calculated by adding ΔΟΙΤ<sub>i</sub> in each layer (Fig. 5.4c). Based on the thickness of the impacted zone and unimpacted zone (Fig. 5.4c), the overall OIT change in the specimen post irradiation can be calculated from the following equation:

$$OIT_{D} = \left[\sum_{i}^{n} (OIT - \Delta OIT_{i}) \times t + OIT \times t_{unexposed}\right] / t_{total}$$
 (2)

where  $OIT_D$  is the OIT of specimen post irradiation, n represents the number of thin layers,  $\Delta OIT_i$  is the change of OIT in each thin layer, t = the thickness of thin layer, t unimpacted is the thickness of unimpacted zone, and t total is the total thickness of the specimen.

Since the OIT test measures the bulk properties of specimen post irradiation, Eq. (2) builds a connection between multiple-layer model with sealed-source experiments. The fitting parameters ( $k_{\alpha}$  and  $k_{\beta}$ ) in Eq. (1) can be obtained using least-square fitting. Additionally, antioxidant depletion in HDPE GM exposed to LLW leachate can be calculated based on the multiple-layer model and GEANT4 simulation.

#### 5.4 RESULTS AND DISCUSSION

# 5.4.1 Dose Deposition in HDPE GM from Sealed Source

The results from MC simulation for the sealed sources of <sup>241</sup>Am (alpha particles) and the <sup>99</sup>Tc (beta particles) are shown in Fig. 5.5. The results indicate that physical dose deposition for both particles largely occurs on the superficial layers of the HDPE GM. For the <sup>241</sup>Am sealed source, a peak dose of approximately 0.22 µGy per decay is deposited at the surface of GM, with the dose profile decreasing monotonically with depth to a negligible dose below 28 µm. This depth corresponds to the maximum penetration for an alpha particle with approximately 4.7 MeV in HDPE. The <sup>99</sup>Tc sealed source simulation shows a peak dose of approximately 52 nGy per decay at the surface of the GM, decreasing to negligible values beyond 0.48 mm.

The dose deposition on HDPE GM exposed to sealed sources (e.g., <sup>241</sup>Am and <sup>99</sup>Tc) were calculated based on the total number of decays for 1 h, 5 h, 10 h, 20 h, and 50 h for <sup>241</sup>Am, as shown in Fig. 5.6. The alpha dose at the surface of HDPE GM reached approximately 50000 Gy after 50 h of exposure to the <sup>241</sup>Am sealed source (Fig. 5.6a), and the total dose due to beta radiation reached approximately 0.3 Gy after 50 h of exposure to the <sup>99</sup>Tc sealed source (Fig. 5.6b).

# 5.4.2 OIT Measurement Results

Antioxidant depletion post irradiation in HDPE of various thicknesses was determined by OIT (in Fig. 5.7). The OIT of thin HDPE GM (e.g., 0.04-mm, 0.1-mm, and 0.2-mm) decreased as the exposure time to <sup>241</sup>Am increased from 1 h to 50 h. The antioxidant depletion rate slowed as the exposure time increased. The OIT of the 0.04-mm-thick GM decreased from 185 min to 158 min after exposure to <sup>241</sup>Am for 50 h, whereas the OIT of the 2-mm-thick GM had negligible change after irradiation (Fig. 5.7a). Based on the GEANT4

model, the alpha particle carrying 4.7 MeV has a maximum penetration depth of approximately 28 µm in the HDPE GM. Thus, the alpha radiation only had a surficial influence on the HDPE GM. The effect of alpha radiation becomes negligible as the thickness of the GM increased to 2-mm thickness.

Similar results have been observed for the effect of beta radiation on HDPE GM, as shown in Fig. 5.7b. The OIT of 0.04-mm-thick GM decreased from 185 min to 174 min after exposure to <sup>99</sup>Tc for 50 h, whereas the OIT of 2-mm-thick GM did not change. The beta particles carrying 294 keV can penetrate 0.48 mm into HDPE GM. The beta particles have a deeper impact zone than that of alpha particles, but the total dosage for HDPE GM exposed to sealed source of <sup>99</sup>Tc was much lower than that exposed to sealed source of <sup>241</sup>Am. Thus, the effect of beta radiation on antioxidant depletion was smaller than the effect of alpha radiation due to limited dosage in the exposure test.

The decrease in OIT of the HDPE GM reflected the depletion of antioxidant due to irradiation with alpha and beta particles. Radiation can break the C-C or C-H bund, as proposed by Costa et al. (2008), Phillips (1988), Whyatt and Farnsworth (1989), Sohma et al. (1991), and Mason et al. (1993). Antioxidants in HDPE GM react with free radicals to form stable products and protect the HDPE GM from degradation. Thus, antioxidant was consumed in the HDPE GM during the irradiation.

As the thickness of the HDPE GM increased, the residual OIT became higher (Fig. 5.7), which indicates that the impact of alpha and beta radiation is limited to the surface of HDPE GM. The MC simulation indicated that the alpha particles from <sup>241</sup>Am can penetrate HDPE GM to approximately 28-µm depth, and beta particles from <sup>99</sup>Tc can penetrate HDPE GM to 0.48-mm depth. Alpha and beta particles thus only affect the surface of the HDPE GM. Consequently, the effect of alpha and beta radiation on antioxidant depletion becomes negligible as the thickness of the HDPE GM approaches to 2 mm.

Multiple-layer model was used to fit the antioxidant depletion in various thickness of HDPE specimen post irradiation with alpha radiation or beta radiation. The impact zone of alpha radiation was divided into 140 layers with a thickness of 0.2  $\mu$ m per layer, while the impact zone of beta radiation was divided into 96 layers with a thickness of 5  $\mu$ m per layer. The initial OITs were different for various thickness specimens due to extrusion process, as shown in Table 5.1. The parameter  $k_{\alpha}$  (7.93 × 10<sup>-6</sup>) and  $k_{\beta}$  (7.06 × 10<sup>-2</sup>) were obtained from least-square error fitting across all four thicknesses. The fitting curves are shown in Fig. 5.7.

# 5.4.3 Dose Deposition in HDPE GM under In Situ Condition

To investigate the long-term effect of radiation from LLW leachate, a MC simulation was created to mimic the *in situ* condition (Fig. 5.3). The deposition of individual species for a 1000-yr duty cycle are shown in Fig. 5.8. A peak dose of 2.42 Gy at the surface of HDPE GM is observed, with alpha particle decay comprising the majority of the dose. The alpha decay from <sup>234</sup>U and <sup>238</sup>U contribute to 1.21 Gy and 1.15 Gy, respectively. The remaining 0.06 Gy of dose is from <sup>235</sup>U and <sup>99</sup>Tc. The surface dose decreased sharply to approximately 0.1 Gy at 0.01-mm depth, beyond which the dose slowly decreased from 0.1 Gy at 0.01 mm to 0.04 Gy at 2-mm depth. Similar to the sealed source simulations, the rapid dose fall-off between surface and 0.01 mm corresponds to the maximum penetration depth of the alpha particles in the HDPE GM. The persistent low-dose tail throughout the depth of the GM is due to gamma photons produced from the subsequent decay of daughter products.

The dose profile of beta particles from <sup>99</sup>Tc were consistent with the sealed-source investigation, with a slower dose fall-off and higher penetration depth than the alpha particles. The negligible contribution from <sup>99</sup>Tc to the final dose profile was due to beta particles carrying low energy (294 keV), whereas the alpha particles emitted from uranium carries higher energy (exceeded 4.2 MeV). In the leachate simulation model, the total dosage form

alpha radiation (<sup>234</sup>U, <sup>235</sup>U and <sup>238</sup>U) was approximately 2.4 Gy at the surface of HDPE GM over the 1000-yr life cycle.

The low dosage deposition from LLW leachate in HDPE GM were due to (1) low radioactivity of radionuclides in LLW leachate and (2) the limited penetration capability of alpha and beta particles in leachate. Uranium and <sup>99</sup>Tc have relative long half-life time, resulting in low total decay over 1000-yr service life. The limited radioactivity in LLW leachate explains the low dose deposition on HDPE GM. Additionally, an alpha particle with 4.2 MeV (Alpha decay form <sup>238</sup>U) can transport through water with a range of approximately 20 µm, whereas a beta particle with 294 keV (Beta decay from <sup>99</sup>Tc) may penetrate approximately 0.5 mm in water (Turner 2007). Thus, only the radiation within a narrow zone adjacent to the GM can potentially reach the surface of the HDPE GM, which further weakens the effect of alpha and beta radiation from LLW leachate on HDPE GM. Therefore, the dose deposition on HDPE GM from LLW leachate is low over the evaluation period of 1000 yr evaluation period.

This simulation provided a conservative prediction due to simplified in the geometry. In the simulation, the geometry includes an HDPE GM layer sandwiched by layers of leachate and sand. In practice, a geotextile layer would overlap the HDPE GM and occupy the space above the HDPE GM. In addition, the leachate layer is located within the drainage layer, which consists of sand or gravel. The geotextile and drainage layer above the HDPE GM not only reduces the contact area between HDPE GM and LLW leachate, but also can shield the radiation from LLW leachate. Consequently, the actual dose deposition in HDPE GM by LLW leachate should be lower than 2.4 Gy.

Due to the low dosage deposition, the radiation from LLW leachate may have a limited effect on antioxidant depletion in HDPE GM. Multiple-layer model was used to calculate the antioxidant depletion in HDPE GM caused by radiation over the 1000-yr service life. The

parameters  $k_{\alpha}$  and  $k_{\beta}$  were applied to calculate the depletion of antioxidant due to alpha and beta radiation from LLW leachate, respectively. The OIT in HDPE decreased less than 0.1 min (shown in Fig. 5.9). Comparing with initial OIT (197 min) of the HDPE GM, the depletion of antioxidant caused by radiation from LLW leachate should be negligible over 1000 yr service life. Overall, alpha and beta radiation from LLW leachate had limited effect on antioxidant depletion in the HDPE GM. These results support the observation that antioxidant depletion rates in HDPE GM were no different in RSL and NSL, as described in Tian et al. (2014).

#### 5.5 CONCLUSION

This study investigated the effect of alpha and beta radiation from LLW leachate on antioxidant depletion in HDPE GM. A GEANT4 model was built to investigate the dosage deposition from sealed sources on HDPE GM. The HDPE GM specimens were exposed to sealed sources of <sup>241</sup>Am and <sup>99</sup>Tc to simulate the alpha and beta radiation from LLW leachate (e.g., <sup>234</sup>U, <sup>235</sup>U, <sup>238</sup>U and <sup>99</sup>Tc).

The simulation of sealed-source experimentation indicated that the alpha particles from <sup>241</sup>Am carrying 4.7 MeV can penetrate approximately 28 µm into 2-mm-thick HDPE GM and the beta particles from <sup>99</sup>Tc carrying 294 keV can penetrate approximately 0.48 mm into HDPE GM. Thus, the alpha and beta radiation can potentially affect the surface of HDPE GM.

The OIT for thin HDPE GM specimens (0.04 mm, 0.1 mm, and 0.2 mm) decreased with increasing exposure time. However, the radiation had negligible impact on 2-mm-thick HDPE GM. The physical experimentation agreed with Monte Carlo simulations in which the alpha and beta radiation only affect the surface of the HDPE GM. Multiple-layer model was created to simulate the antioxidant depletion in HDPE specimens post irradiation with alpha and beta particles.

Additionally, a GEANT4 Monte Carlo simulation was conducted to simulate the dose deposition in HDPE GM installed in LLW disposal facilities. The total dosage can potentially reach the surface was approximately 2.4 Gy over 1000-yr period. The low dose from LLW leachate would have limited effect on antioxidant depletion in HDPE GM. Based on multiple-layer model, antioxidant depletion in HDPE caused by radiation from LLW leachate was negligible (less than 0.1 min for OIT at the surface of HDPE GM) over a 1000-yr service life.

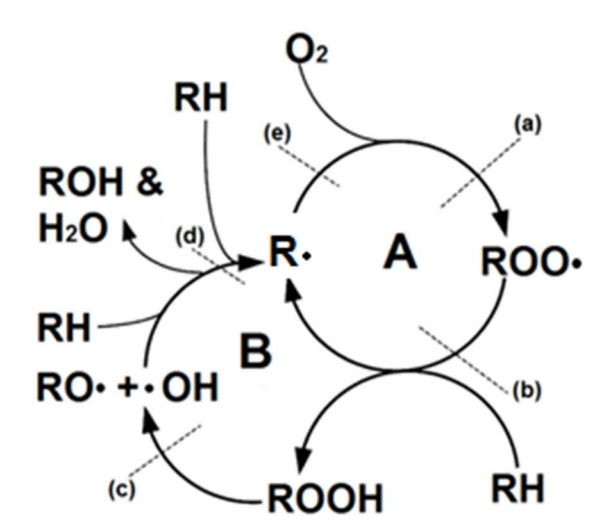
#### REFERENCE

- Abdelaal, F. and Rowe, K. (2015). Effect of high pH found in low-level radioactive waste leachates on the antioxidant depletion of a HDPE geomembrane. *Journal of Hazardous. Toxic, and Radioactive Waste*, 10.1061/(ASCE)HZ.2153-5515.0000262, D4015001.
- Agnostinelli et al. (2003). GEANT4-a simulation toolkit. *Nuclear Instruments and Methods in Physics Research A*, 506, 250–303.
- Bracco, P., Brach del Prever, E., Cannas, M., Luda, M., and Costa, L. (2006). Oxidation behaviour in prosthetic UHMWPE components sterilized with high energy radiation in a low oxygen environment. *Polymer Degradation and Stability*, 91(9), 2030–2038.
- Costa, L., Carpentieri, I., and Bracco, P. (2008). Post electron-beam irradiation oxidation of orthopaedic UHMWPE. *Polymer Degradation and Stability*, 93(9), 1695–1703.
- Czvikovszky, T. (2004). Degradation effects in polymers. *Proceeding of International Atomic Energy Agency Meeting,* Notre Dame, Indiana, U.S.
- Foose, G., Benson, C., and Edil, T. (2002). Comparison of solute transport in three composite liners. *Journal of Geotechnical and Geoenvironmental Engineering*, 128(5), 1–13.
- Grassie, N. and Scott, G. (1985). *Polymer Degradation and Stabilization*. Cambridge University Press, New York, USA, 222.
- Gulec, S., Edil, T., and Benson, C. (2004). Effect of acidic mine drainage on the polymer properties of an HDPE geomembrane. *Geosynthetic International*, 11(2), 60–72.
- Hamid, H. (2000). Handbook of polymer degradation, 2nd Ed., Dekker, New York.
- Hsuan, Y. and Koerner, R. (1998). Antioxidant depletion lifetime in high density polyethylene geomembranes. *Journal of Geotechnical and Geoenvironmental Engineering*, 124(6), 532–541.
- Mason, L., Doyle, T., and Reynolds, A. (1993). Oxidation induction time correlations with radiation dose and antioxidant concentration in EPR and XLPE Polymers. *Journal of Applied Polymer Science*, 50, 1493–1500.
- Peacock, A. (2000). *Handbook of Polyethylene: Structures, Properties and Application*. Marcel Dekker Inc., New York. 534pp.
- Phillips, D. (1988). Effect of radiation on poplymers. *Materials Science and Technology*, 4, 85–91.
- Powell, J., Abitz, R., Broberg, K., Hertel, W., and Johnston, F. (2011). Status and performance of the On-Site Disposal Facility Fernald Preserve, Cincinnati, Ohio. *Proceedings, Waste Management Symposia 2011*, WM Symposia, Ref. 11137, accessed via: http://www.wmsym.org/archives/2011/papers/11137.pdf.
- Rowe, R., Islam, M., and Hsuan, Y. (2009). Ageing of HDPE geomembrane exposed to air, water and leachate at different temperatures. *Geotextiles and Geomembranes*, 27, 137–151.
- Rowe, R., Islam, M., and Hsuan, Y. (2008). Leachate chemical composition effects on OIT depletion in an HDPE geomembrane. *Geosynthetics International*, 15(2), 136–151.

- Rowe, R. and Sangam, H. (2002). Durability of HDPE geomembranes. *Geotextiles and Geomembranes*, 20, 77–95.
- Saidi, F., Touze-Foltz, N., and Goblet, P. (2008). Numerical modelling of advective flow through composite liners in case of two interacting adjacent square defects in the geomembrane. *Geotextiles and Geomembranes*, 26(2), 196–204.
- Singh, A. (1999). Irradiation of polyethylene: Some aspects of crosslinking and oxidative degradation. *Radiation Physics and Chemistry*, 56, 375–380.
- Sohma, J., Chen, Q., Wu, X., Scholtyssek, G., Zachmann, G. (1991). MAS NMR studies on cross links induced by irradiation to polyethylene. *In: Proceeding of 7th Tihany Symposium Radiat. Chem.*, 281–288.
- Sugimoto, M., Shimada, A., Kudoh, H., Tamura, K., Seguchi, T. (2013). Product analysis for polyethylene degradation by radiation and thermal ageing. *Radiation Physics and Chemistry*, 82, 69–73.
- Take, W., Chappel, M., Brachman, R., and Rowe, R. (2007). Quantifying geomembrane wrinkles using aerial photography and digital image process. *Geosynthetics International*, 14(4), 219–227.
- Tian, K. (2012). Durability of high-density polyethylene geomembrane in low-level radioactive waste leachate. *MS thesis*, Univ. of Wisconsin-Madison, Madison, Wisconsin.
- Tian, K., Tinjum, J., Benson, C., and Edil, T. (2014). Antioxidant depletion in HDPE geomembranes exposed to low-level radioactive waste leachate. *Geo-Congress 2014 Technical Papers*, 1816–1825.
- Turner, J. (2007). *Atoms, Radiation, and Radiation Protection*. WILEY-VCH Verlag GmbH & Co. KGaA, Weinheim.
- Viebke, J., Elble, E., Ifwarson, M., and Gedde, U. (1994). Degradation of unstabilized medium-density polyethylene pipes in hot-water applications. *Polymer Engineering & Science*, 34(17), 1354–1361.
- Whyatt, G. and Farnsworth, R. (1989). The high pH chemical and compatibility of various liner materials. *Geosynthetic Testing for Waste Containment Applications*, ASTM STP 1081, Robert M. Koerner, editor, American Society for Testing and Materials, Philadelphia, 1990.
- U.S. EPA (U.S. Environmental Protection Agency). (2012). (http://www.epa.gov/radiation/larw/larw.html) (Jul. 16, 2014).

Table 5.1. Oxidation induction time of HDPE specimens with various thickness

Thickness (mm)	Initial OIT (min)
0.04	185 ± 1.2
0.1	189 ± 1.6
0.2	194 ± 0.8
2	197 ± 1.5



RH: Polyethylene polymer chain

R•: Reactive free radical ROO•: Hydroperoxy radical ROOH: Hydroperoxide

Fig. 5.1. Oxidation loops for polyethylene [modified from Grassie and Scott (1985) and Rowe and Sangam (2002)].

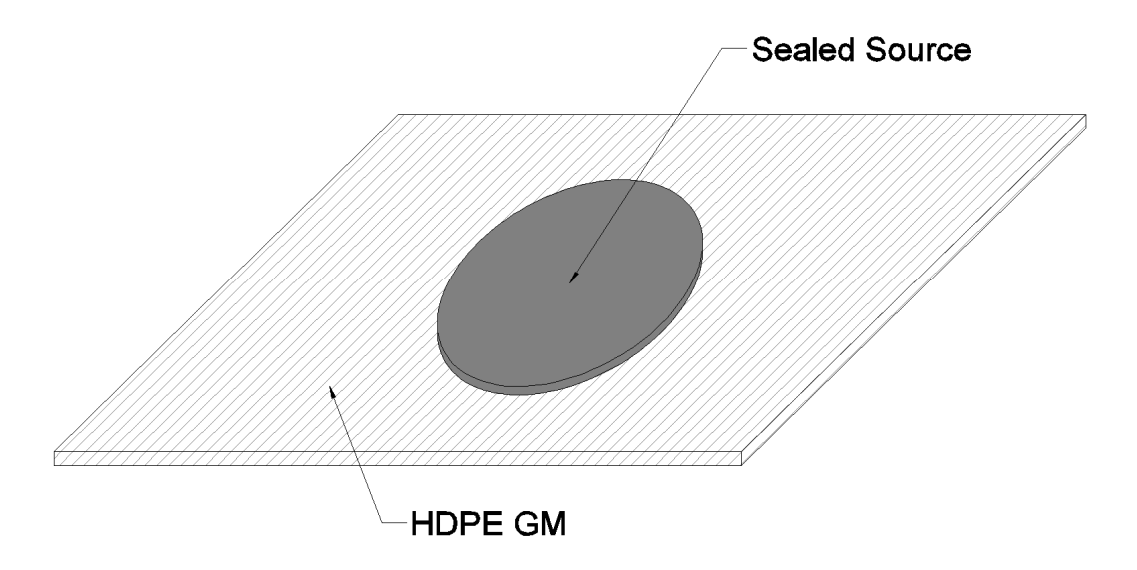


Fig. 5.2. GEANT4 Monte Carlo simulation geometry for sealed-source experiments (Note, the dimension of the sealed source was based on information provided by the manufacturer).

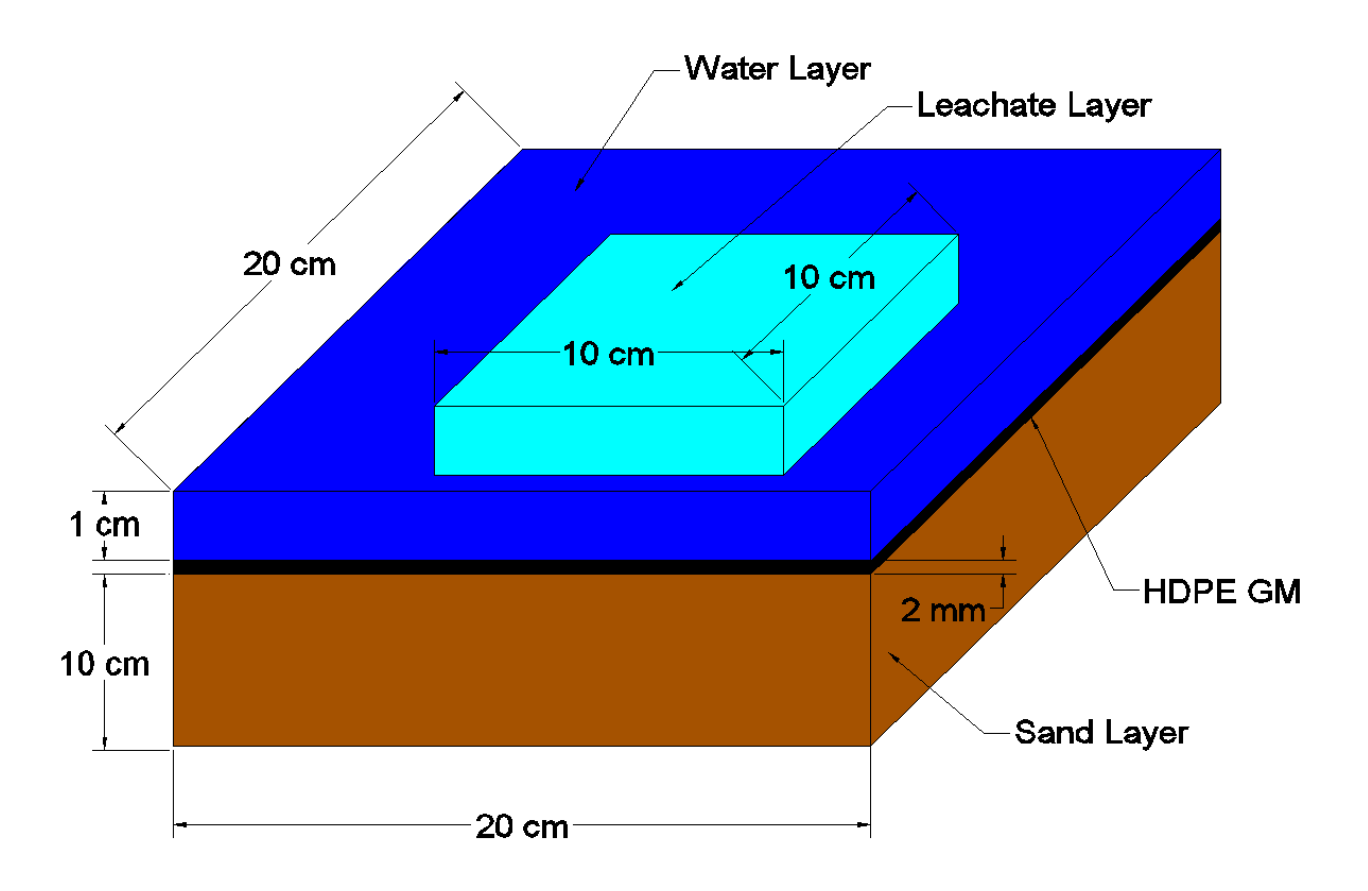


Fig. 5.3. GEANT4 Monte Carlo Simulation geometry for *in situ* condition, consisting of HDPE polymer sandwiched between water and sand. A region in the water is defined to be the source of particles.

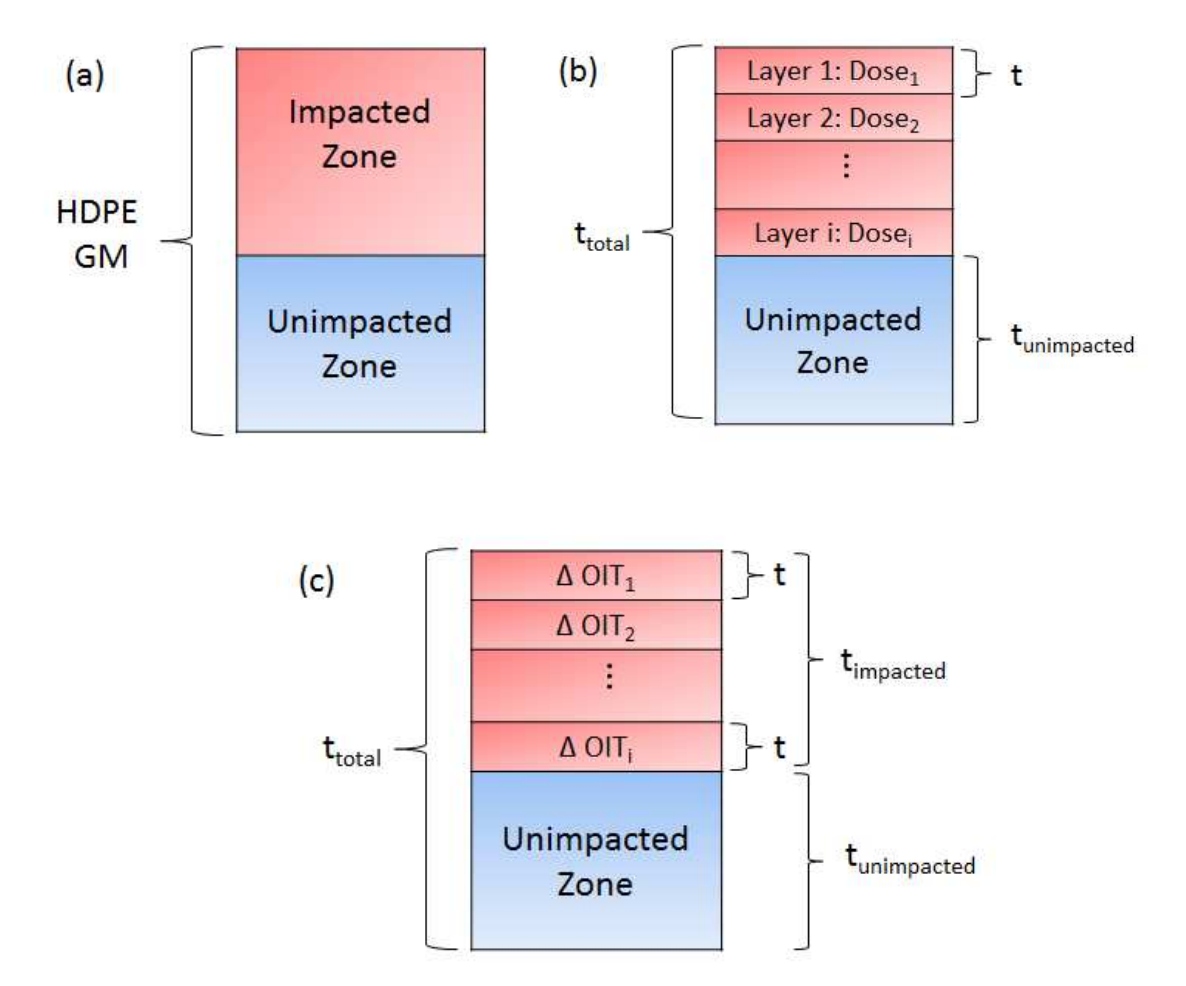
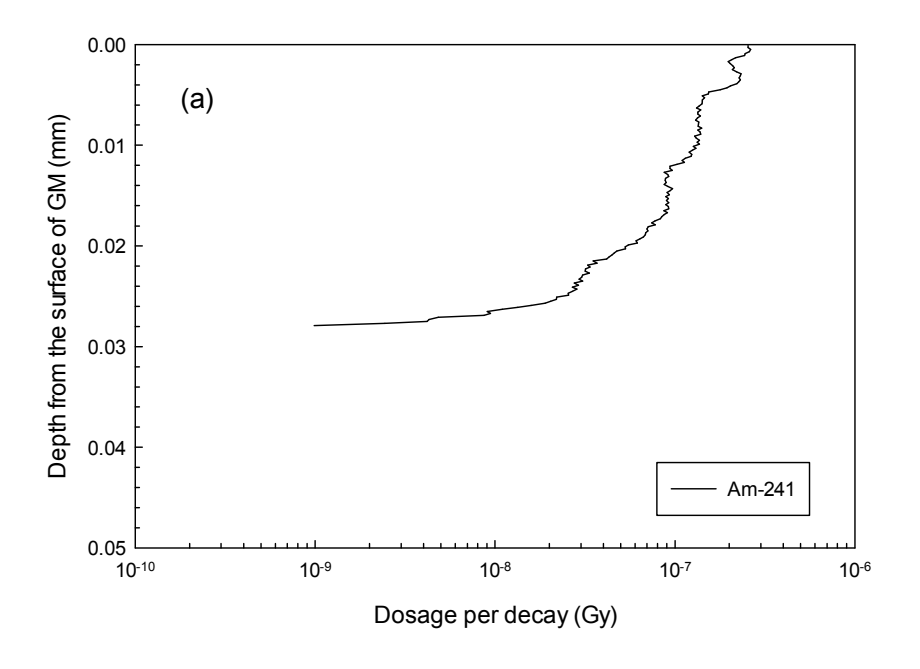


Fig. 5.4. Multiple-layer model for antioxidant depletion in HDPE GM exposure to radiation.



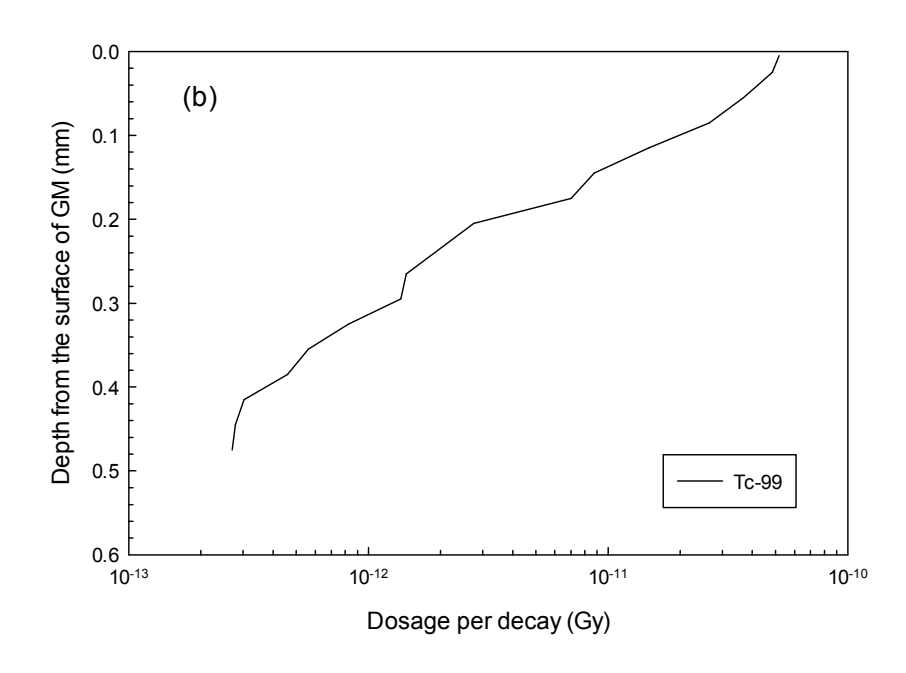


Fig. 5.5. Monte Carlo simulation for dose deposition in HDPE GM with sealed source of (a) Am-241 and (b) Tc-99 as a function of depth.

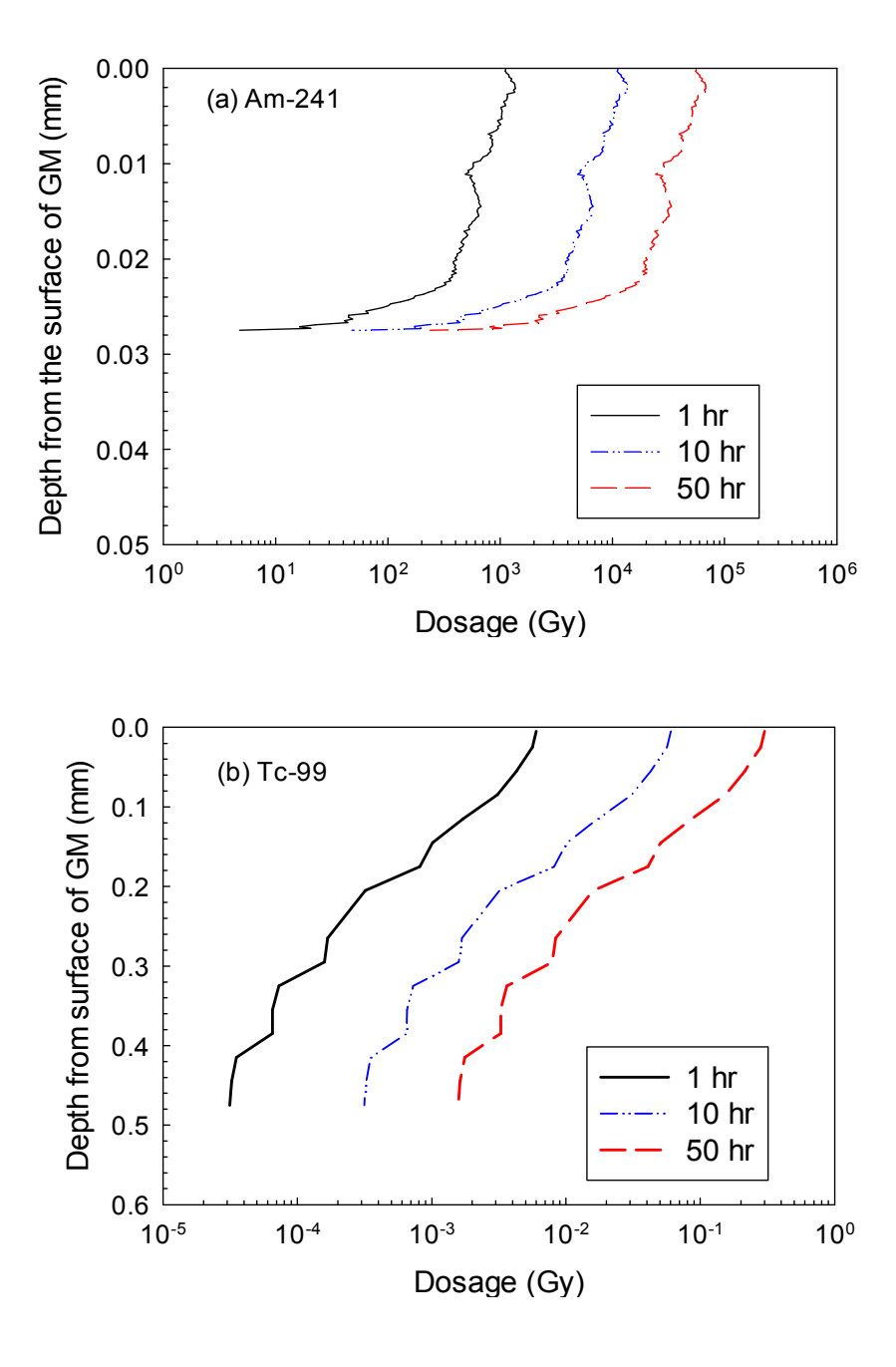


Fig. 5.6. Dose deposition in HDPE GM exposed to sealed source of 241Am sealed source (a) and 99Tc (b) for 1 h, 10 h, and 50 h.

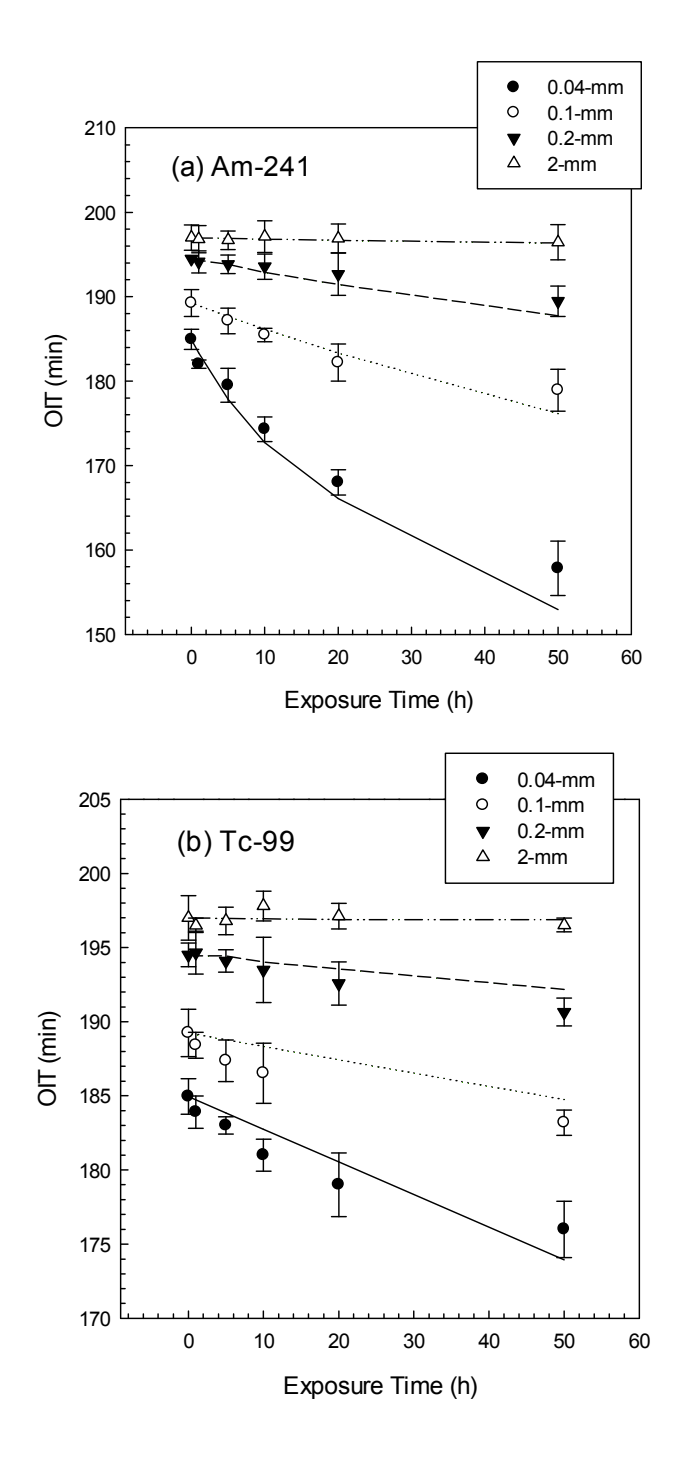


Fig. 5.7. Oxidation induction time of HDPE GM specimens exposed to sealed sources of (a) 241Am and (b) 99Tc, along with the fitting curve based on multiple-layer model. (Note: the error represents one standard deviation based on three measurements).

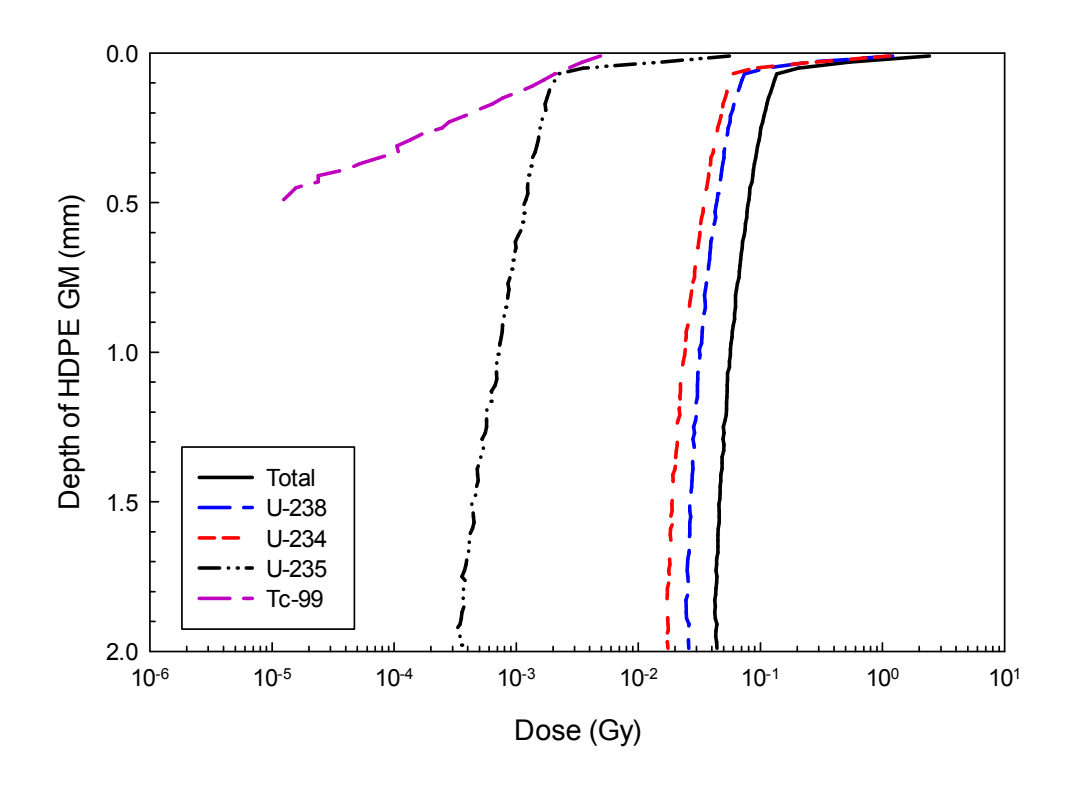
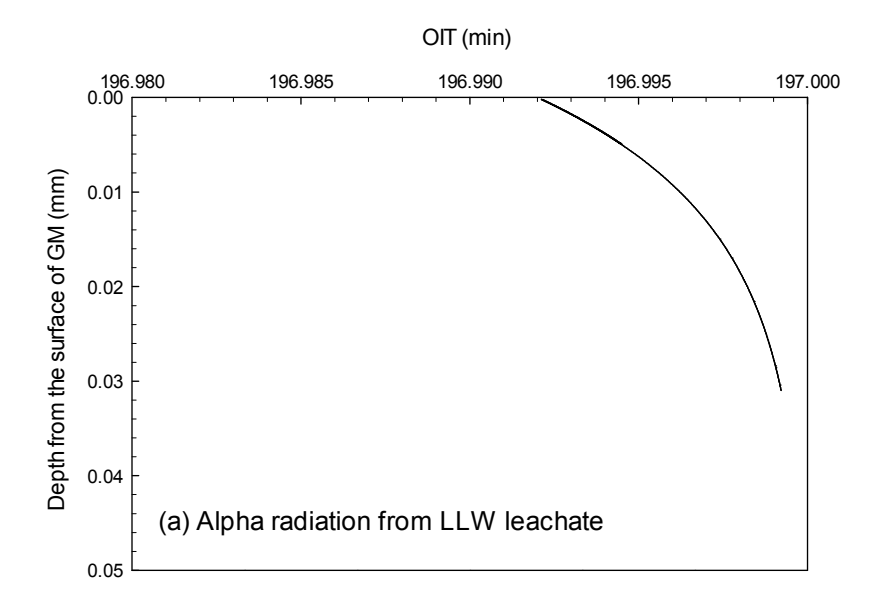


Fig. 5.8. Monte Carlo simulation for dosage deposition from low-level radioactive waste on HDPE GM over 1000 yr as a function of depth.



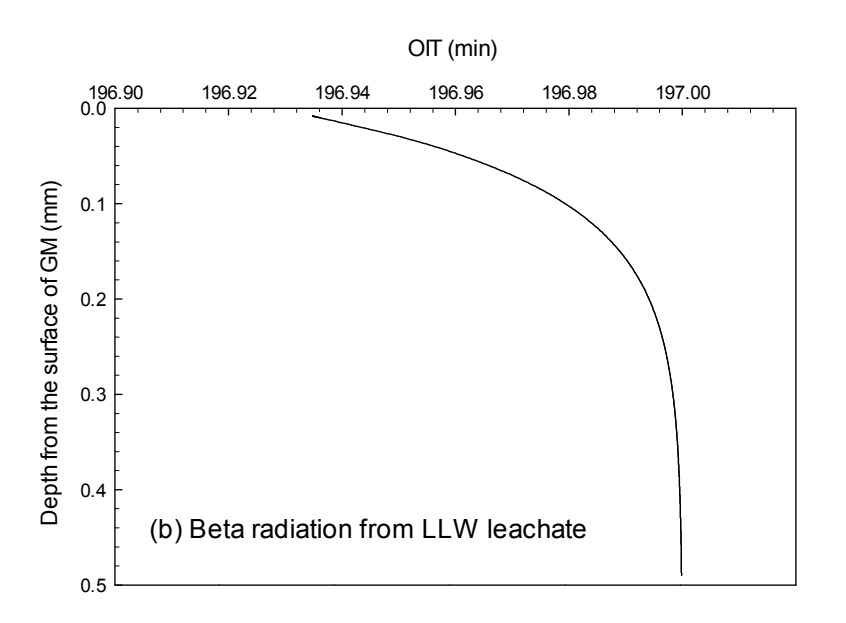


Fig. 5.9. Prediction of antioxidant depletion in HDPE GM over 1000-yr service life caused by (a) alpha radiation and (b) beta radiation.

# 6 BACKGROUND: COMPATIBILITY OF GEOSYNTHETIC CLAY LINER IN CONTAINMENT APPLICATION

# 6.1 INTRODUCTION

Geosynthetic clay liners (GCLs) consist of a thin layer of sodium bentonite (Na-B) sandwiched between two geotextiles. They are widely used in composite liner systems of waste disposal facilities due to their low hydraulic conductivity to water ( $k < 10^{10}$  m/s), ease of installation, and thinness (5–10 mm) compared to compacted clay liners. The Na-B layer in GCLs provides low hydraulic conductivity due to the osmotic swell of sodium montmorillonite (MMT), the primary clay mineral in bentonite. Water adsorbed by MMT is bound to the mineral surface and is essentially immobile, reducing the volume of flow-paths and making flow pathways more tortuous. However, osmotic swell of MMT only occurs when monovalent cations are in the exchange complex, and bound cations are subject to cation exchange, making MMT sensitive to the geochemical environment. Multivalent cations present in liquid (e.g., Ca, Mg, and Al) can replace monovalent cations in the exchange complex, resulting in reduced or eliminated osmotic swell of the bentonite (Jo et al 2001, 2005, Shackelford 2010, and Bouazza and Bowders 2010).

GCLs are often exposed to waste leachates with polyvalent cations and/or high ionic strength, such as municipal solid waste (MSW) leachate, and acid mine drainage, that result in decreased osmotic swell (Benson et al. 2008, Shackelford 2010, Bradshaw and Benson. 2014). The decreased swelling of clay increases the flow channel between particles and results in increased hydraulic conductivity. To prevent an increase in hydraulic conductivity in barrier scenarios, researchers have modified Na-B to improve the long-term hydraulic barrier performance of GCL (Onikata et al. 1999, Trauger and Darlington 2000, Schroeder et al. 2001, Kolstad et al. 2004a, Katsumi et al. 2008, Di Emidio et al. 2010). To improve hydraulic

behavior, bentonite modifications have focused on (1) intercalation of expandable organic molecules into MMT platelets to increase the total swell and (2) prevention of cation exchange by intercalating organic compounds.

This literature review primarily discusses the mechanism of hydraulic barrier behaviors of both conventional GCLs and modified GCLs based on laboratory study and simulated *in situ* condition (Jo et al 2001, 2005, Kolstad et al. 2004a,b, Lee and Shackelford 2005, Katsumi et al. 2008, Di Emidio et al. 2010). This information provides a background to understand hydraulic barrier behaviors for conventional and polymer-bentonite GCLs exposed to various leachate.

# **6.2 CONVENTIONAL BENTONITE**

Na-B is primarily composed of the MMT, which has large specific surface areas (as high as 850 m²/g), cation exchange capacities (80–150 meq/100g), and swelling capacities (Bouazza and Bowders 2010). MMT have two tetrahedral sheets that sandwich an octahedral layer sheet. Typically, the octahedral layer consists of aluminum (gibbsite-like) or magnesium (brucite-like) coordinated with four oxygen atoms and a hydroxyl ion, while the tetrahedral layer includes a silicon atom coordinated with oxygen. MMT displays extensive isomorphous substitution, including Mg²+ replacing Al³+ in the octahedral sheet and Al³+ replacing Si⁴+ in the tetrahedral layers, resulting in the overall structure carrying a negative charge imbalance (Bouazza and Bowders 2010). The negative charge is neutralized by exchangeable cations intercalated in the interlayer (e.g., Na⁺, Ca²+, and Mg²+). The species of exchangeable cations influences the swelling behavior of MMT.

#### **6.2.1 Swelling of Conventional Bentonite**

The swelling of MMT is due to water molecules that bind to the clay surface. The bound water is essentially immobile, behaving as if part of the solid phase with respect to the

effect on flow. The more water molecules bound to the clay surface, the narrower the flow-paths between the particles (McNeal and Coleman 1966, Mesri and Olson 1971). The fraction of bound water for MMT largely depends on numbers of layers of water molecules hydrating the exchangeable cations between the interlayer surfaces (Mitchell 1993).

The swell of the MMT can be characterized as crystalline and osmotic phase (Norrish and Quirk 1954, Mitchell 1993). Crystalline swelling occurs when strong hydration forces attract water to form one to four discrete layers of H<sub>2</sub>O molecules around the exchangeable cations and occurs regardless of cation valence (Slage et al. 1991, Bouazza and Bowders 2010). Osmotic swell occurs after crystalline swell and manifests as bound water driven into the interlayer by differences in the concentration gradient between bound monovalent cations, dissolved ions in the pore water, and negative surface charge of the clay (Norrish and Quirk 1954). When the exchangeable cations in the interlayer are multivalent cations, only crystalline swell occurs due to the increased electric static force between multivalent cations and negative charged interlayer (Slage et al. 1991, Bouazza and Bowders 2010). The exchangeability of bound cations is controlled by valence, atomic size, hydration energy, and relative concentration (Teppen and Miller 2005). For equivalent concentrations, the ranking from high to low affinity for bound cations in MMT is  $Fe^{3+} > Al^{3+} > Ca^{2+} > Mg^{2+} > K^+ > Na^+ > Ca^{2+} > Mg^{2+} > Mg^{2+$ Li<sup>+</sup> (Bouazza and Bowders 2010). Since osmotic swell is controlled by the prevalence of bound monovalent cations, the increased favorability for bound multivalent cations poses a concern for GCL containment applications. Low swell volume can enlarge the interparticles space and cause an increase of hydraulic conductivity.

Overall, two factors are required for osmotic swell to manifest and low hydraulic conductivity to occur: (1) the predominant exchange cations must be monovalent species (e.g., Li, Na) and (2) the ionic strength of the surrounding interparticle pore water should be lower than 300 mM (Norrish and Quirk 1954).

# 6.2.2 Compatibility Study of Conventional GCL

GCLs are widely used in containment applications to limit the migration of leachate (Shan and Daniel 1991, Shackelford et al. 2000). In containment applications, a conventional Na-B GCL is expected to exhibit osmotic swell and low hydraulic conductivity. However, chemical interactions between the bentonite and containment liquid have been shown to affect the hydraulic barrier performance of GCLs (Jo et al 2001, 2005, Shackelford 2010, Bouazza and Bowders 2010). GCLs applied in-situ are frequently exposed to leachates with high ionic strengths (e.g., municipal solid waste leachate) or that are predominate in multivalent cations (e.g., mine leachate). Previous studies have evaluated changes in hydraulic conductivity of GCLs under laboratory or *in situ* condition (Shan and Daniel 1991, Shackelford et al. 2000, Jo et al. 2001, 2005, Bradshaw and Benson 2014). *In situ* conditions can either limit the osmotic swell of MMT due to high ionic strength, or exchange of monovalent cations in the interlayer with multivalent cations, which eventually decreases swell and increases hydraulic conductivity of GCL (Shackelford et al. 2000, 2010, Jo et al. 2001, 2005).

Jo et al. (2001, 2005) and Lee and Shackelford (2005) conducted a series of tests to investigate how solutions with various concentrations and cation valences affect the swell and hydraulic conductivity of non-prehydrated GCLs. Falling-head hydraulic conductivity tests were conducted in flexible-wall permeameters with an effective stress of approximately 20 kPa according to ASTM D5084. Free swell tests were performed following ASTM D 5890. Fig. 6.1 displays swell index test results of bentonite with various concentrations of monovalent, divalent, and trivalent cations, and mixtures of monovalent and divalent cations (data from Jo et al. 2001, 2005, Kolstad et al. 2004b, and Lee and Shackelford 2005). Swelling behavior varied in the presence of monovalent versus multivalent cations. Na-B swelled more in monovalent solutions than in multivalent solutions of the same ionic strength.

As the concentration of monovalent species increased, swelling gradually decreased to the same level as multivalent cations with an ionic strength of 1000 mM. Swelling decreased rapidly in multivalent cation solutions as the ionic strength increased from 15 mM to 300 mM, and remained consistent to 1000 mM. Overall, the swelling of Na-B is dependent on valence at low concentration (< 100 mM), becoming less sensitive to valence effects after the concentration reaches 1000 mM or higher.

Fig. 6.2 shows results of hydraulic conductivity tests as a function of ionic strength. The hydraulic conductivities of GCLs exposed to monovalent solutions with concentrations less than 100 mM are similar to DI water (approximately 10<sup>-11</sup> m/s). Hydraulic conductivities of GCL in divalent solutions were less sensitive to different salt species. The hydraulic conductivities begin to increase sharply when the divalent cation concentration is higher than 10 mM. Compared to monovalent cations, divalent cations more drastically changed the hydraulic conductivity of GCLs. In high ionic strength solutions (1000 mM), hydraulic conductivity was higher than 10<sup>-7</sup> m/s regardless of valence.

Hydraulic conductivities of GCLs as a function of swell index are shown in Fig. 6.3. A strong inverse relationship exists between hydraulic conductivity and swelling. Significant increases in concentration and valence resulted in a decrease in swell behavior, which correlate to increased hydraulic conductivity. Therefore, the swell index test can be used as a quick indicator to predict hydraulic conductivity of GCLs exposed to various permeant solutions (Jo et al. 2001).

# 6.2.3 Compatibility of GCLs under *In Situ* Conditions

Previous studies have investigated GCL behaviors in the MSW liner system (Petrov and Rowe 1997, Ruhl and Daniel 1997). MSW is primarily composed of paper products, food waste, yard waste, glass, plastics, cardboard, and metal components (Tchobanoglous et al.

1993). The complexity of MSW influences the varying composition of MSW leachate. MSW leachate displayed a wide range of ionic strengths (40 to 620 mM), depending on waste site characteristics and landfill ages (Kolstad 2000).

Petrov and Rowe (1997) tested the effects of various permeant solutions on the hydraulic conductivity of GCLs. The permeant solutions included DI water, aqueous solutions with varying NaCl concentrations, a synthetic MSW leachate, and real MSW leachate. The main constituents of the synthetic MSW leachate were Na (1615 mg/L), K (354 mg/L), Ca (1224 mg/L), Mg (473 mg/L), acetic acid (4000 mg/L), propionic acid (3000 mg/L), and butyric acid (500 mg/L), with pH adjusted to 6.23 with NaOH. The major cations (Ca, Mg, Na, and K) were monitored to determine chemical stability. The hydraulic conductivity of GCLs exposed to synthetic MSW leachate was 8.7 x 10<sup>-11</sup> m/s, which was 5.5-times higher than those exposed to DI water. GCL thickness decreased when exposed to synthetic MSW leachate in comparison to GCLs exposed to DI water, due to compression of the interlayer space. Effluent monitoring showed retardation of the divalent cations, which was attributed to cation exchange of Ca2+ and Mg2+ for Na+ in the interlayer of MMT. Another comparative test was conducted to investigate the effect of pre-hydration on hydraulic conductivity. The hydraulic conductivity was 7.3 x 10<sup>-11</sup> m/s for GCLs exposed to synthetic MSW leachate following pre-hydration with DI water. Petrov and Rowe (1997) concluded that pre-hydration had an insignificant effect on the hydraulic conductivity of GCLs permeated with synthetic MSW leachate.

Ruhl and Daniel (1997) investigated the hydraulic conductivity of GCLs exposed to seven different permeant solutions. One of the permeant solutions was synthetic MSW leachate with the following constituents: Ca<sup>2+</sup> (1000 mg/L), sodium acetate (150 mM), acetic acid (150 mM), and salicylic acid (7 mM). The pH was adjusted to 4.4, while the effective stress was 35 kPa and hydraulic gradient ranged from 100 to 200. The hydraulic conductivity

of GCLs exposed to tap water ranged from 2.0 to 3.0 x 10<sup>-11</sup> m/s. After initial pre-hydration with tap water, the GCLs showed insignificant changes in hydraulic conductivity when exposed to synthetic MSW leachate. However, the GCLs permeated directly with synthetic MSW leachate yielded hydraulic conductivities between 10<sup>-8</sup> and 10<sup>-7</sup> m/s. The increased hydraulic conductivity was a consequence of exchange of Na<sup>+</sup> for Ca<sup>2+</sup> from the MMT. An insignificant increase in hydraulic conductivity of the GCL initially permeated with tap water was attributed to insufficient exposure time for cation exchange. Another GCL specimen was permeated with MSW leachate from a Midwestern landfill. The hydraulic conductivity was approximately 10<sup>-11</sup> m/s when permeated directly with MSW leachate, which is four orders of magnitude lower than the hydraulic conductivity of GCL directly exposed to synthetic MSW leachate. Ruhl and Daniel (1997) hypothesize that blockage of flow paths by suspended organic solids in the leachate resulted in the lower hydraulic conductivities.

# 6.3 MODIFIED BENTONITE

Recognizing the deficiencies of conventional GCLs, many researchers have focused on improving the performance of GCLs by modifying the bentonite with organic molecules (Onikata et al. 1999, Trauger and Darlington 2000, Schroeder et al. 2001, Kolstad et al. 2004a, Katsumi et al. 2008, Di Emidio et al. 2010). To improve hydraulic behavior, bentonite modifications have focused on maintaining osmotic swell through two methods: 1) intercalation of expandable organic molecules into MMT platelets to activate osmotic swell, and 2) prevention of cation exchange by intercalating organic compounds. The steps and materials used in creating several modified bentonites discussed in the following. Kondo (1996) and Onikata et al. (1999) created multi-swellable bentonites (MSBs) by mixing a dry Na-B with 15–45% propylene carbonate (PC) solution (by mass). The mixed materials were dried at 105 °C and then ground. The mixer can rely on the PC content to activate osmotic

swell, along with Na-B, thus it was named as MSB. Trauger and Darlington (2000) generated bentonite-polymer alloy (BPA) by *in situ* polymerization of an organic monomer within a Na-B slurry to form a bentonite-superabsorbent-polymer composite. Di Emidio (2010) created HYPER-clay (HC) by mixing dry bentonite with a solution containing 2% Nacarboxymethylcellulose (Na-CMC) (by mass). Similar to MSB, HC was oven dried at 105 °C and ground. Di Emidio et al. (2010, 2011) indicated that HC relies on Na-CMC to activate osmotic swell. Kolstad et al. (2004a) used dense prehydrated GCLs (DPH-GCLs), made by prehydrating Na-B to a water content of approximately 43% with a dilute aqueous solution containing Na-CMC and methanol, followed by subsequent densification. DPH-GCLs rely on two established mechanisms to improve performance compatibility: prehydration with a dilute solution (Shan and Daniel 1991, Ruhl and Daniel 1997, Vasko et al. 2001) and densification (Shackelford et al. 2000).

#### 6.3.1 Swell of Modified Bentonite

# 6.3.1.1 Activation of Osmotic Swell

The most common way to improve bentonite compatibility is intercalation of organic molecules into the MMT interlayers to activate osmotic swell. Onikata et al. (1996) intercalated PC within MMT to form MSB. X-ray diffraction (XRD) analysis of MSB showed increased d001 spacing to 1.4 nm corresponding to a monolayer of intercalated PC within the MMT interlayer, which results in increased swelling by expanding the space between adjacent MMT platelets (Onikata et al. 1996, 1999). Through Fourier transform infrared spectroscopy (FTIR) and thermogravimetric analysis (TGA), Onikata et al. (1999) observed that PC coordinates to interlayer cations through the hydration shells of the cations. Intercalated PC in MMT improved activation of osmotic swell in NaCl solutions up to 750 mM (Onikata et al. 1996), while the maximum solution strength allowing osmotic swelling in Na-B

was 300 mM (Norrish and Quirk 1954). MSB showed improved compatibility leading to osmotic swell with sodium solutions with strength between 300 mM and 750 mM.

Similar to PC intercalated to MMT, Na-CMC was shown by XRD to be intercalated into MMT to create HC and DPH-GCLs, and was hypothesized to act as an osmotic-swell activator (Schroeder et al. 2001, Kolstad et al. 2004a, Katsumi et al. 2008, Di Emidio et al. 2010). Trauger and Darlington (2000) reported an inter-platelet space for BPA of 0.35 nm to between 1.0 and 1.5 nm based on XRD analysis, which indicated that the polymer was intercalated in the bentonite interlayer. Trauger and Darlington (2000) hypothesized anionic polymer activated osmotic swell.

# 6.3.1.2 Locking of Bound Cations

Polyelectrolyte additives (e.g., Na-CMC and BPA) have functional groups that can potentially be adsorbed on MMT. The higher the molecular weight and number of functional groups, the greater the amount of polyelectrolyte was absorbed (Stumm 1992). Deng et al. (2006) investigated adsorption mechanisms of an anionic polyelectrolyte to MMT using FTIR. Based on experimental results, Deng et al. (2006) postulated that exchangeable cation bridging (ECB) was the dominant mechanism for polyelectrolyte adsorption to MMT. ECB was defined as anionic polyelectrolytes bound with exchange cations that serve to satisfy the negative charge of the MMT. Through ECB, the polyelectrolyte may form a shell to prevent MMT exposure to aggressive solutions, and can potentially "lock" the bound cations (Deng et al. 2006). Trauger and Darlinton (2000) also stated that BPA may lock Na<sup>+</sup> cations originally contained within MMT.

#### 6.3.2 Compatibility Study of Modified GCL.

Onikata and Kamon (1996) reported that swelling test results for MSB in DI water (20.0 mL/2 g) were similar to those of Na-B in DI water (24.0 mL/2 g). However, MSB swelled more

than three times more than Na-B in artificial seawater (32.0 mL/2 g versus 9.0 mL/2 g, respectively) (Onikata and Kamon 1996). Katsumi et al. (2008) compared long-term barrier performance between MSB and Na-B when permeated with aggressive leachate. The MSB was made by adding 25% PC to Na-B (Katsumi et al. 2008). Fig. 6.4 displays results of swell index tests conducted by Katsumi et al. (2008) at varying NaCl and CaCl<sub>2</sub> concentrations. Swell tests in DI water are plotted at 1 mM. MSB exhibited higher swelling than conventional Na-B in the NaCl solution with an ionic strength less than 800 mM. These results agreed with Onikata et al.'s (1996) observation that MSB shows active osmotic swell in monovalent solutions with concentrations up to 750 mM, whereas the conventional Na-B displays crystalline swelling when the monovalent solution concentration above 300 mM.

Fig. 6.5 shows hydraulic conductivities of MSB permeated with varying NaCl and CaCl<sub>2</sub> concentrations (derived from Katsumi et al. 2008). For comparison, data for conventional GCL permeated with similarly varied solutions are also shown in Fig. 6.5 (data derived from Jo. et al. 2001, 2005, Kolstad et al. 2004b, Lee and Shackelford 2005). Test results from GCLs permeated with DI water are plotted at 1 mM. The hydraulic conductivity tests on MSB had been conducted for up to 7 yr to reach chemical equilibrium (Katsumi et al. 2008). MSB and Na-B exhibited similar hydraulic conductivities (1.0 x 10<sup>-11</sup> m/s) when permeated with DI water. Katsumi et al. (2008) found that the hydraulic conductivity of MSB permeated with NaCl solutions with molar concentrations less than 1000 mM was of the same order of magnitude as those exposed to DI water. Na-B exhibited an increasing trend in hydraulic conductivity with NaCl concentrations exceeded 500 mM. MSB exhibited an increase in hydraulic conductivity of less than one order of magnitude (~6 x 10<sup>-11</sup> m/s) as CaCl<sub>2</sub> concentration increased from 50 to 500 mM. For conventional GCLs, Jo et al. (2001) observed a three order of magnitude increase in hydraulic conductivity for GCLs exposed to 100 mM CaCl<sub>2</sub> than for GCLs permeated with DI water. Consequently, MSB exhibited higher

resistance to divalent cations and ionic strength effects than conventional Na-B (Katsumi et al. 2008). Fig. 6.6 shows that swell index of MSB and conventional GCL decreases as ionic strength increases. However, the decrease of swell index for MSB caused an insignificant increase in hydraulic conductivity, whereas conventional GCL displayed a strong correspondence between swell index and hydraulic conductivity. Thus, these results illustrated that swell was a conservative indicator to predict the hydraulic conductivity of MSB (Katsumi et al. 2008).

In a brief summary, the MSB exhibits higher resistant to high ionic strength and divalent cation solutions than conventional GCL. The osmotic swelling ability of MSB increases from 300 mM (for a Na-B) to 750 mM when exposed to monovalent solutions. The hydraulic conductivity of MSB remains same magnitude to it exposed to DI water when exposed up to 500 mM CaCl<sub>2</sub>. Katsumi et al. (2008) indicate MSB is a long-term test reliable hydraulic barrier material.

Another type of modified GCL (DPH-GCL) was also tested by Katsumi et al. (2008) to investigate the long-term hydraulic conductivity. The results for DPH-GCLs permeated with CaCl<sub>2</sub> and DI water (plotted at 1 mM) are shown in Fig. 6.5. When permeated with DI water, DPH-GCL had an order of magnitude lower hydraulic conductivity (1.0 x 10<sup>-12</sup> m/s) than conventional GCL (1.0 x 10<sup>-11</sup> m/s). Moreover, DPH-GCL maintained a similar order of magnitude hydraulic conductivity (~10<sup>-12</sup> m/s) when permeated with solutions of NaCl and CaCl<sub>2</sub> with concentrations less than 1000 mM. For example, the hydraulic conductivity of the DPH-GCL permeated with 1000 mM molar CaCl<sub>2</sub> was between 1.1 x 10<sup>-12</sup> m/s and 1.5 x 10<sup>-12</sup> m/s. None of the DPH-GCL tests reached chemical equilibrium prior to termination due to the low hydraulic conductivity (Katsumi et al. 2008). Thus, the long-term behavior of DPH-GCL remains unknown.

Kolstad et al. (2004a) investigated hydraulic conductivity of DPH-GCLs exposed to aggressive leachate. The swell index of DPH-GCL in DI water was approximately 35 mL/2 g and decreased to 10 mL/2 g in 1 M CaCl<sub>2</sub>, similar to conventional GCLs (shown in Fig. 6.4). Kolstad et al. (2004a) reported that hydraulic conductivity of DPH-GCLs exposed to DI water, 1 M NaCl, 1 M CaCl<sub>2</sub>, and NaOH (pH = 13.1), were approximately 4.0 x 10<sup>-12</sup> m/s, and increased to 1.6 x 10<sup>-10</sup> m/s for HCl (pH = 1.2). In contrast, the hydraulic conductivity of the conventional GCL increased four orders of magnitude (~10<sup>-7</sup> m/s) for all permeants except NaOH (2.2 x 10<sup>-11</sup> m/s) as compared to permeation with DI water (1.2 x 10<sup>-11</sup> m/s). These results indicated little correspondence between hydraulic conductivity and swell index of DPH-GCLs. Kolstad et al. (2004a) concluded that swell index tests are not a valid index test to predict hydraulic behavior of DPH-GCLs (shown in Fig. 6.6).

Kolstad et al. (2004a) investigated the mechanism behind the lower hydraulic conductivity of DPH-GCL exposed to aggressive solutions. Low hydraulic conductivity of DPH-GCLs was hypothesized to be a result of intercalated Na-CMC, pre-hydration, and densification. To assess the effect of pre-hydration, a conventional GCL was prehydrated with DI water for 5.5 pore volumes of flow, then permeated with 1 M CaCl<sub>2</sub>. The hydraulic conductivity of the pre-hydrated GCL (1.0 x 10<sup>-10</sup> m/s) exposed to 1M CaCl<sub>2</sub> was 8100 times lower than that of a non-pre-hydrated GCL (8.1 x 10<sup>-7</sup> m/s), but 27 times higher than the DPH-GCL (3.7 x 10<sup>-12</sup> m/s) permeated with same solution.

To evaluate the effect of densification, an elevated effective stress (420 kPa) was applied to a conventional GCL to achieve the same porosity as a DPH-GCL (1.84). The hydraulic conductivity of densified GCLs exposed to 1 M CaCl<sub>2</sub> was 4.1 x 10<sup>-9</sup> m/s, which was 8.9 times lower than that of conventional GCL (4.0 x 10<sup>-8</sup> m/s) when permeated with the same leachate.

Assuming that the effects of prehydration and densification in reducing hydraulic conductivity were independent and multiplicative (Kolstad et al. 2004), the two factors were attributed to a 79400-times reduction in the hydraulic conductivity of a conventional GCL. However, initial comparative hydraulic conductivity testing with 1 M CaCl<sub>2</sub> by Kolstad et al. (2004a) showed hydraulic conductivity for DPH-GCLs approximately 219000-times lower than for conventional GCLs. After considering this reduction factor (79400), the hydraulic conductivity of conventional GCL exposed to 1000 mM was still approximately three-times higher than for the DPH-GCL. Kolstad et al. (2004a) hypothesized that the difference in reduction factors, after considering densification and pre-hydration, can be explained as a result of intercalated Na-CMC, differences in MMT content, or corresponding effects of prehydration and densification. Overall, intercalation of Na-CMC into Na-B was not the dominant factor for the improved hydraulic barrier performance of DPH-GCLs over conventional GCLs (Kolstad et al. 2004a).

Di Emidio et al. (2010) reported that swell index testing of HC with 4% Na-CMC (by mass) was sensitive to CaCl<sub>2</sub> concentration (shown in Fig. 6.4). HC exhibited identical swelling behavior when the CaCl<sub>2</sub> concentration was higher than 100 mM. A comparative hydraulic conductivity test by Di Emidio et al. (2010) permeated HC and Na-B with DI water, seawater, and 5 mM CaCl<sub>2</sub>. HC and Na-B exhibited comparable hydraulic conductivities when permeated with DI water, while the hydraulic conductivity of HC exposed to 5 mM CaCl<sub>2</sub> was two-times lower than that of Na-B. None of the tests had reach chemical equilibrium at termination due to limited testing time (80 days). CEC measurements exhibited were similar for HC and Na-B, leading Di Emidio et al. (2010) to conclude that Na-CMC cannot prevent cation exchange of initially bound cations.

Trauger and Darlington (2000) tested hydraulic barrier behavior of BPA. The hydraulic conductivity of the BPA was 4000-times lower than that of a conventional GCL when

permeated with artificial sea salt water (5 x  $10^{-12}$  m/s versus 2 x  $10^{-8}$  m/s, respectively). The BPA hydrated to a final water concent about 10 to 15 times greater to conventional GCL, which is attributed to the inclusion of superabsorbent polymer within BPA (Buchholz and Graham 1998)

# 6.3.3 Compatibility of GCLs under In Situ Conditions

To author's knowledge, limited information in the literature discusses about modified GCL performance when permeated with MSW leachate. Thus, the following review hydraulic conductivity testing by Shackelford et al (2010) to compare conventional and contaminant-resistant GCLs permeated with synthetic leachate to mimic the process water and acid drainage from a copper and zinc ore tailings site, with groundwater collected on-site used as a control. Limited information contaminate-resistant GCLs was provided in the paper. The hydraulic conductivity of both GCLs directly permeated with synthetic acid drainage leachate or process water was 2300-7600 times higher than when exposed to site groundwater. The increased hydraulic conductivities were due to the high ionic strength of synthetic acid drainage leachate (350 mM) and the predominance of divalent cations, which both limited the osmotic swelling of exchange cations within the interlayer. GCLs prehydrated with site groundwater provided a hydraulic conductivity 2-11 times lower than the GCLs from the non-pre-hydrated permeated test. Unexpectedly, the contaminant resistant GCL were no more resistant than conventional GCLs when permeated with acid drainage leachate.

# 6.4 SUMMARY

In summary, the modified GCL exhibited low hydraulic conductivity when permeated with higher ionic strength solution ( $\leq$  3 M), and high concentrated divalent cations ( $\leq$  1 M) solution. In contract, conventional GCLs exhibits orders-of magnitude increase hydraulic conductivity when exposed to solution with a ionic strength exceeded 300 mM and divalent

cations concentration ≥ 100 mM. Unlike the conventional GCL, a decoupling behavior between swell index and hydraulic conductivity displays in modified GCL (Kolstad et al. 2004a, and Katsumi et al. 2008), illustrating that other mechanisms, such as intercalated organic molecule, deification, or pre-hydration, play major roles to improve hydraulic barrier behavior of modified GCL. However, the example from Shackelford et al. (2010) illustrates that leachate-specific testing is needed to confirm that a GCL with conventional Na bentonite or polymer-modified bentonite will have low hydraulic conductivity.

#### REFERENCE

- Benson, C., Oren, A., and Gates, W. (2010). Hydraulic conductivity of two geosynthetic clay liners permeated with a hyperalkaline solution. *Geotextiles and Geomembranes*, 28(2) 206–218.
- Benson, C., Wang, X., Gassner, F., and Foo, D. (2008). Hydraulic conductivity of two geosynthetic clay liners permeated with an aluminum residue leachate. *GeoAmericas* 2008, International Geosynthetics Society.
- Bouzazza, A. and Bowders, J. (2010). *Geosynthetic clay liners for wastecontainment facilities*. CRC press/Balkema.
- Buchholz, F. and Graham, A. (1998). *Modern Superabsorbent Polymer Technology*. John Wiley and Sons, New York.
- Deng, Y., Dixon, J., and White, G. (2006). Bonding between polyacrylamide and smectite. *Colloids and Surfaces*, 281(1), 82–91.
- Di Emidio, G. (2010). Hydraulic and chemico-osmotic performance of polymer treated clays. *Ph.D. dissertation*, Ghent Univ., Belgium.
- Di Emidio, G., Van Impe, W., and Mazzieri, F. (2010). A polymer enhanced clay for impermeable geosynthetic clay liners. *Proceedings of Sixth International Conference on Environmental Geotechnics*, International Society for Soil Mechanics and Geotechnical Engineers, New Delhi, India, 963–967.
- Di Emedio, G., Van Impe, W., and Flores, V. (2011). Advances in geosynthetic clay liners: polymer enhanced clays. *GeoFrontiers 2011. Advances in Geotechnical Engineering,* American Society of Civil Engineers, Reston, USA, 1931–1940.
- Flynn, B. and Carter, G. (1998). Waterproofing material and method of fabrication thereof. US Patent Number: 6,537–676.
- Jo, H., Benson, C., Shackelford, C., Lee, J., and Edil, T. (2005). Long-term hydraulic conductivity of a non-prehydrated geosynthetic clay liner permeated with inorganic salt solutions. *J. of Geotech. and Geoenviron. Eng.*, 131(4), 405–417.
- Jo, H., Katsumi, T., Benson, C., and Edil, T. (2001). Hydraulic conductivity and swelling of non-prehydrated GCLs permeated with single species salt solutions. *J. of Geotech. and Geoenviron. Engr.*, 127(7), 557–567.
- Katsumi, T., Ishimori, Ho, Onikata, M., and Fukagawa, R. (2008). Long-term barrier performance of modified bentonite materials against sodium and calcium permeant solutions. *Geotextiles and Geomembranes*, 26(1), 14–30.
- Kolstad, D., Benson, C., and Edil, T. (2004a). Hydraulic conductivity and swell of nonprehydrated GCLs permeated with multi-species inorganic solutions. *J. of Geotech. and Geoenviron. Engr.*, 130(12), 1236–1249.
- Kolstad, D., Benson, C., Edil, T., and Jo, H. (2004b) Hydraulic conductivity of a dense prehydrated GCL permeated with aggressive inorganic solutions. *Geosynthetics International*, 11(3), 233–240.
- Kolstad, C. (2000). *Compatibility of GCL with multi-species inorganic solutions. M.S. Thesis*, University of Wisconsin-Madison.

- Lee, J. and Shackelford, C. (2005). Impact of bentonite quality on hydraulic conductivity of geosynthetic clay liners. *J. of Geotech. and Geoenviron. Engr.*, 131(1), 64–77.
- Lin, L. and Benson, C. (2000). Effect of wet-dry cycling on swelling and hydraulic conductivity of geosynthetic clay liners. *J. of Geotech. and Geoenviron. Engr.*, 126(1), 40–49.
- Lin, L., Katsumi, T., Kamon, M., Benson, C., Onikata, M., and Kondo, M. (2000). Evaluation of chemical-resistant bentonite for landfill barrier applications. *Annuls of Disas. Prev. Res. Inst.*, Kyoto Univ., No. 43 B-2, *525*–533.
- Mazzieri, F., Emidio, G., and Van Impe, P. (2010). Diffusion of calcium chloride in a modified bentonite: Impact on osmotic efficiency and hydraulic conductivity. *Clays and Clay Minerals*, 58(3), 351–363.
- Mazzieri, F. (2011). Impact of desiccation and cation exchange on the hydraulic conductivity of factory-prehydrated GCLs. *GeoFrontiers 2011. Advances in Geotechnical Engineering*, American Society of Civil Engineers, Reston, USA, 976–985.
- McNeal, B. and Coleman, N. (1966). Effect of solution composition on soil hydraulic conductivity. *Soil Sci. Soc. Am. Proc.*, 30, 308–312.
- Meer, S. and Benson, C. (2007). Hydraulic conductivity of geosynthetic clay liners exhumed from landfill final covers. *J. of Geotech. and Geoenviron. Engr.*, 133(5), 550–563.
- Mesri, G. and Olsen, R. (1971). Mechanisms controlling the permeability of clays. *Clays and Clay Minerals*, London, 19, 151–158.
- Mitchell, J. (1993). Fundamentals of soil behavior 2nd Ed. Wiley, New York, John Wiley & Sons, Inc.,
- Moore, D. and Reynolds, R. (1997). *X-ray Diffraction and the identification and analysis of clay minerals*. Oxford University Press.
- Norrish, K. and Quirk, J. (1954). Crystalline swelling of montmorillonite, use of electrolytes to control swelling. *Nature*, 173, 255–257.
- Onikata, M., Kondo, M., and Kamon, M. (1996). Development and characterization of a multiswellable bentonite. *Environmental Geotechnics*. Taylor and Francis, Rotterdam, 587–590.
- Onikata, M., Kondo, M., Hayashi, N., and Yamanaka, S. (1999). Complex formation of cation-exchanged montmorillonites with propylene carbonate: Osmotic swelling in aqueous electrolyte solutions. *Clays and Clay Minerals*, 47(5), 672–677.
- Petrov, R. and Rowe, R. (1997). Geosynthetic clay liner (GCL)-chemical compatibility by hydraulic conductivity testing and factors impacting its performance. *Canadian Geotechnical J.*, 34, 863–885.
- Ruhl, J. and Daniel, D. (1997). Geosynthetic clay liners permeated with chemical solutions and leachates. *J. of Geotech. and Geoenviron. Engr.*, 123(4), 369–381.
- Schroeder, C., Monjoie, A., Illing, P., Dosquet, D., and Thorez, J. (2001). Testing a factory-prehydrated GCL under several conditions. *Proceedings, Sardinia 2001, 8th International Waste Management and Landfill Symposium*, CISA Environmental Sanitary Engineering Centre, Cagliari, Italy, 187–196.

- Shackelford, C., Sevick, G., and Eykholt, G. (2010). Hydraulic conductivity of geosynthetic clay liners to tailings impoundment solutions. *Geotextiles and Geomembranes*, 28(2), 206–218
- Shackelford, C., Benson, C., Katsumi, T., Edil, T., and Lin, L. (2000). Evaluating the hydraulic conductivity of GCLs permeated with non-standard liquids. *Geotextiles and Geomembranes*, 18(23), 133–161.
- Shackelford, C. and Lee, J. (2003). The destructive role of diffusion on clay membrane behavior. *Clays and Clay Minerals*, 51(2), 187–197.
- Shan, H. and Daniel, D. (1991). Results of laboratory tests on a geotextile/bentonite liner material. *Geosynthetics 2001*, *Industrial Fabrics Assoc. International*, St. Paul, MN, 517–535.
- Slade, P., Quirk, J., and Norrish, K. (1991). Crystalline swelling of semectite samples in concentrated NaCl solutions in relation to layer charge. *Clays clay minerals*, 39, 234–238.
- Stumm, W. (1992). Chemistry of the Solid-Water Interface. John Wiley and Sons, New York.
- Stumm, W. and Morgan, J. (1996). *Aquatic Chemistry*, 3rd ed. Wiley, New York.
- Trauger R. and Darlington J. (2000). Next-generation geosynthetic clay liners for improved durability and performance. *TR-220*. Colloid Environmental Technologies Company, Arlington Heights, 2–14.
- Teppen, B. and Miller, D. (2005). Hydration energy determines isovalent cation exchange selectivity by clay minerals. *Soil Science Society America J.* 70, 31–34.
- Vasko, S., Jo, H., Benson, C., Edil, T., and Katsumi, T. (2001). Hydraulic Conductivity of Partially Prehydrated Geosynthetic Clay Liners Permeated with Aqueous Calcium Chloride Solutions. *Geosynthetics* 2001, Industrial Fabrics Assoc. International, St. Paul, MN, 685–699.

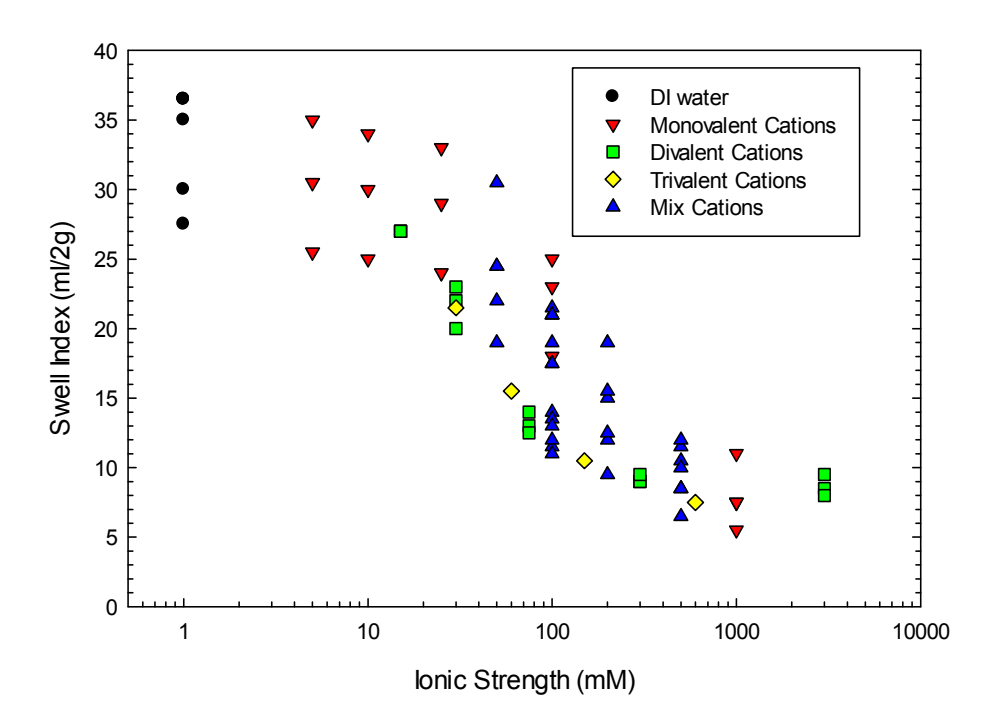


Fig. 6.1. Swelling index vs. Ionic Strength. (Mix cations include monovalent and divalent cations. Data derived from Jo et al. 2001, 2005; Kolstad et al. 2004b; Lee and Shackelford 2005.)

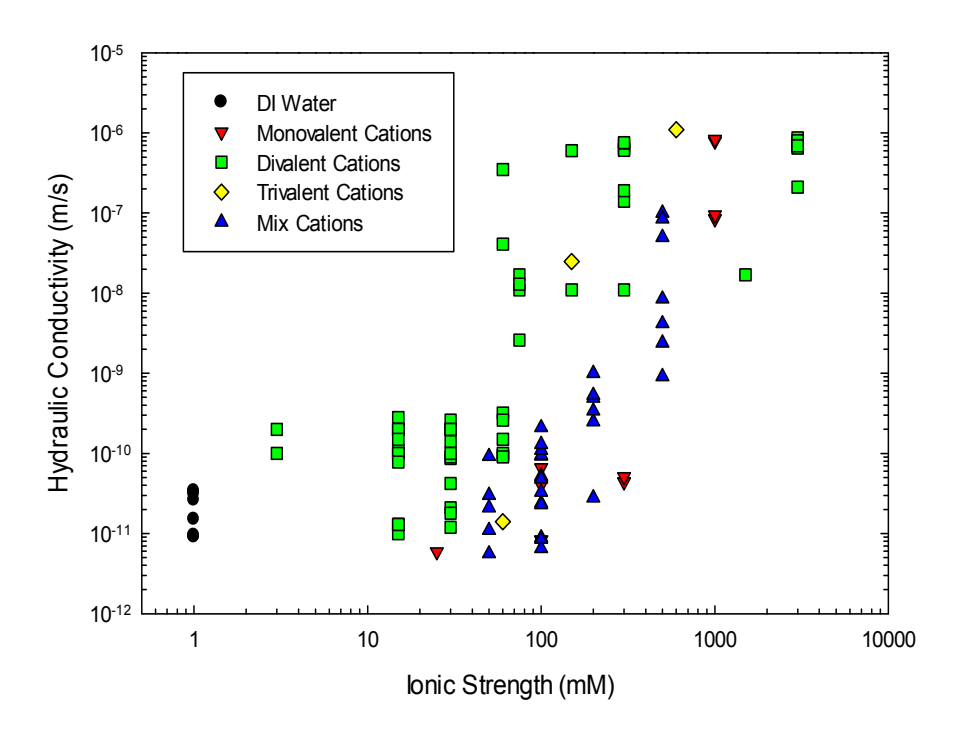


Fig. 6.2. Hydraulic conductivity of GCLs permeated with solutions of varying ionic strength and various valent cations. (Mix cations include monovalent and divalent cations. Data derived from Jo et al. 2001, 2005; Kolstad et al. 2004b; Lee and Shackelford 2005.)

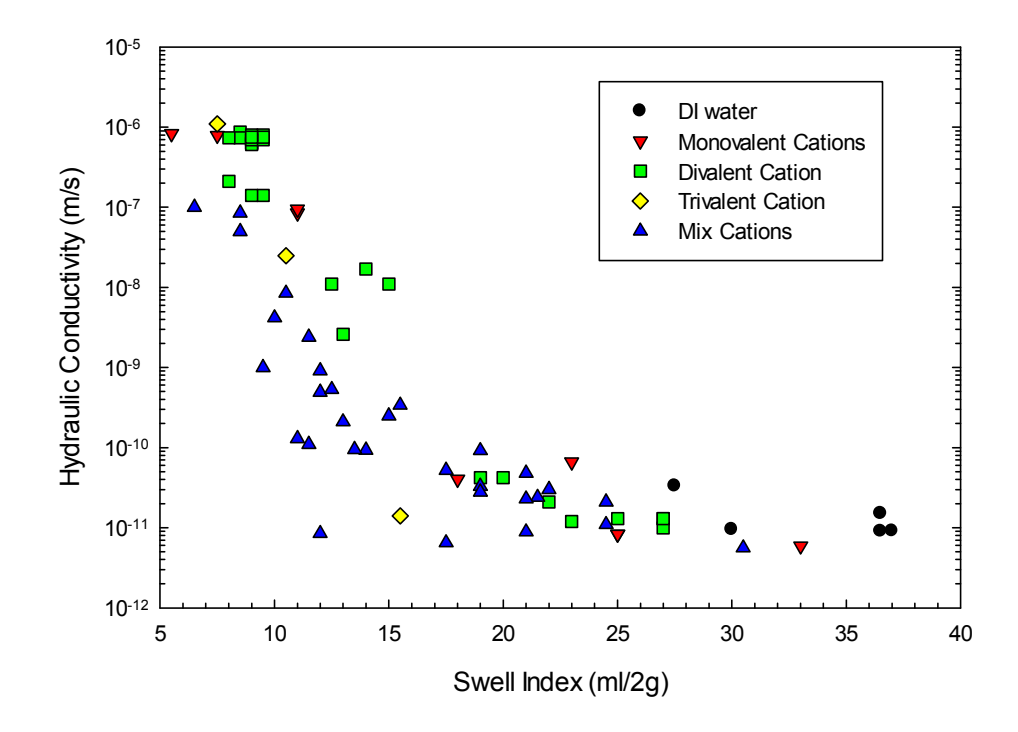


Fig. 6.3. Hydraulic conductivity of GCLs permeated with solutions of varying ionic strength versus swell index test of bentonite derived from the permeated GCLs. (Mix cations include monovalent and divalent cations. Data derived from Jo et al. 2001, 2005; Kolstad et al. 2004b; Lee and Shackelford 2005.)

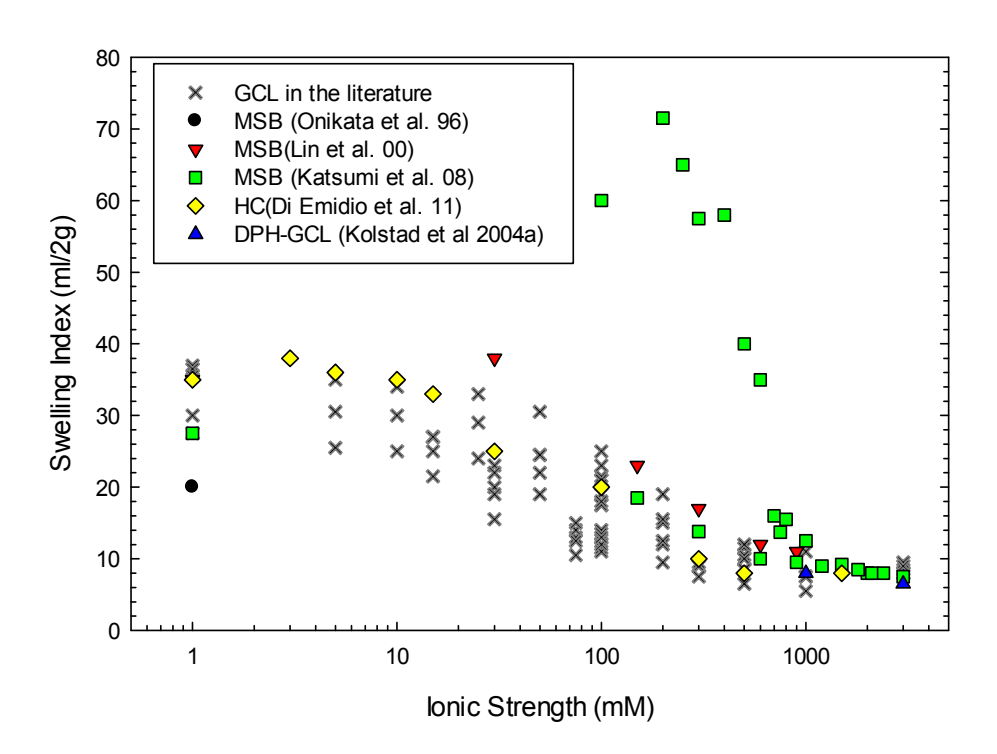


Fig. 6.4. Influence of ionic strength on the swell index of natural Na-bentonite and modified bentonites Literature data for Na-B GCLs are provided for comparison. (data derived from Jo et al. 2001, 2005; Kolstad et al. 2004b; Lee and Shackelford 2005.)

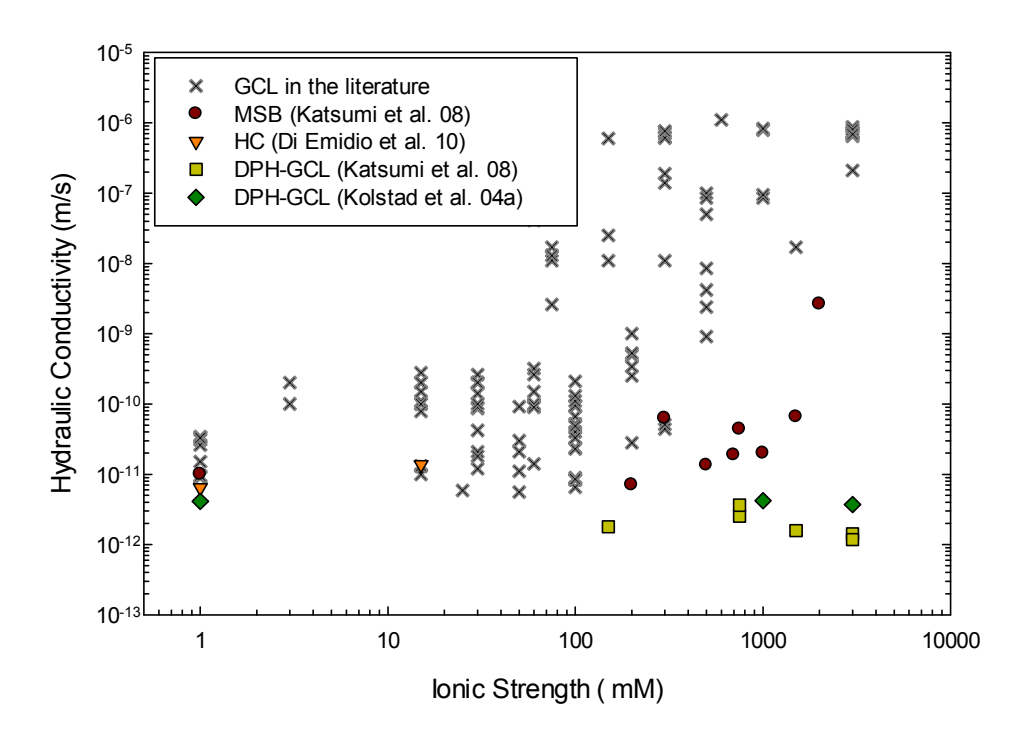


Fig. 6.5. Influence of ionic strength on the hydraulic conductivity of natural Na-bentonite and modified bentonites for hydraulic compatibility. Literature data for Na-B GCLs are provided for comparison. (data derived from Jo et al. 2001, 2005; Kolstad et al. 2004b; Lee and Shackelford 2005.)

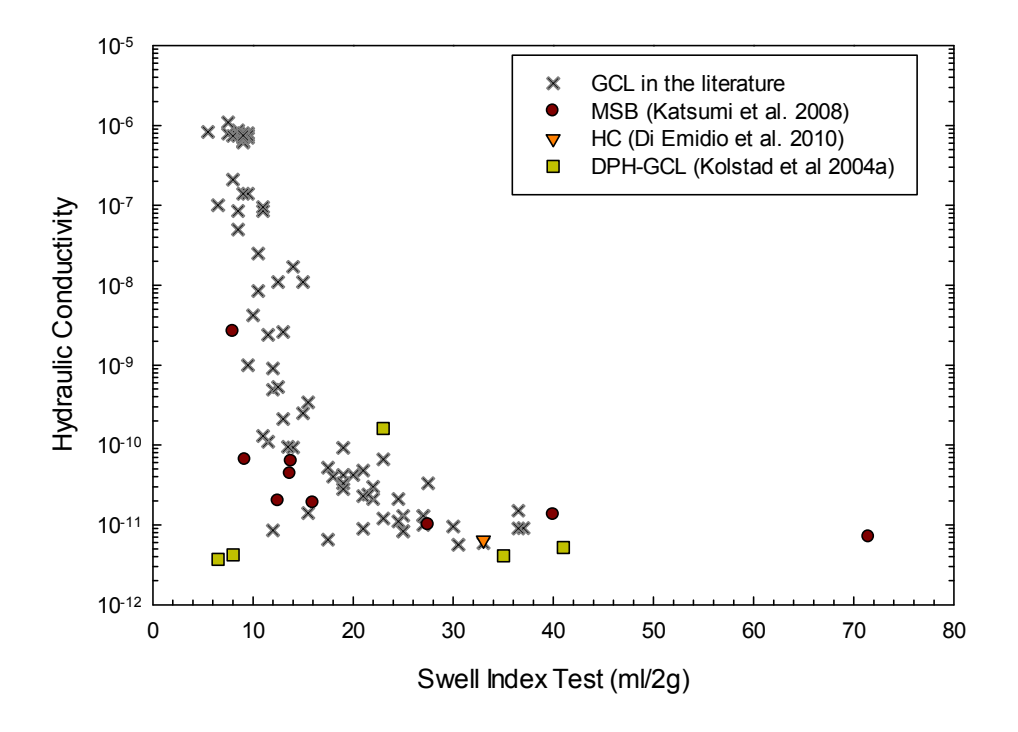


Fig. 6.6. Hydraulic conductivity versus swell index for natural Na-bentonite and modified bentonites. Literature data for Na-B GCLs are provided for comparison. (data derived from Jo et al. 2001, 2005; Kolstad et al. 2004b; Lee and Shackelford 2005.)

# 7 HYDRAULIC CONDUCTIVITY OF GEOSYNTHETIC CLAY LINERS PERMEATED WITH LOW-LEVEL RADIOACTIVE WASTE LEACHATE

ABSTRACT: Experiments were conducted to evaluate the hydraulic conductivity of geosynthetic clay liners (GCLs) to leachate characteristic of low-level radioactive waste (LLW) disposal facilities operated by the U.S. Department of Energy. Eight commercially available GCLs were evaluated. Two of the GCLs (CS and GS) contained conventional sodium bentonite (Na-B) and the others contained a polymer-bentonite mixture or composite (CPL. CPM, BPC, GPL, GPM, and GPH). All GCLs (except GPL and GPH) were permeated directly with two synthetic LLW leachates that are chemically identical, except one leachate was prepared without radionuclides (non-radioactive synthetic leachate, or NSL) and the other with radionuclides (radioactive synthetic leachate, or RSL). Control tests were conducted with deionized (DI) water. Hydraulic conductivities of the GCLs to RSL and NSL were identical. For the CS and GS GCLs, the hydraulic conductivity permeated with synthetic leachate gradually increased by a factor ranging between 5-25 times, relative to the hydraulic conductivity to DI water as divalent cations in the RSL or NSL replaced the native sodium in the bentonite. The CPL, GPL, and GPM GCLs with low to modest polymer loading (1.2–3.3%) had similar hydraulic conductivity as the conventional GCLs. In contrast, the CPM, GPH, and BPC GCLs with modest to high polymer loading (>5%) had hydraulic conductivity to all permeant liquids comparable to or lower than the hydraulic conductivity to DI water. Hydraulic conductivity of polymer-bentonite GCLs decreased as the polymer loading increased. A conceptual model is proposed of polymer hydrogel blocking the pore space in bentonite to maintain low hydraulic conductivity when GCLs are permeated with aggressive leachates

Keywords: bentonite, polymer, hydrogel, low-level radioactive waste, geosynthetic clay liner

## 7.1 INTRODUCTION

Geosynthetic clay liners (GCLs) are factory-manufactured hydraulic barriers consisting of a thin layer of sodium bentonite (Na-B) clay (~3-5 kg/m²) sandwiched between two geotextiles that are bonded by needle punching or stitching (Shackelford et al. 2000). Some GCLs also include a geomembrane bonded to the bentonite or laminated to the geotextile. GCLs are common elements in waste containment facilities due to their low hydraulic conductivity to water (typically < 10<sup>-10</sup> m/s) and ease of installation (Shackelford et al. 2000, Jo et al. 2001, 2005, Kolstad et al. 2004, Benson et al. 2010).

The effectiveness of GCLs is controlled primarily by the hydraulic conductivity of the Na-B in the GCL, which is predominately composed of the clay mineral montmorillonite (Shackelford et al. 2000, Jo et al. 2001, 2005, Kolstad et al. 2004, Bradshaw and Benson 2014). Osmotic swelling of the montmorillonite results in narrow and tortuous intergranular flow channels, resulting in low hydraulic conductivity of GCL (Mesri and Olson 1971, Jo et al. 2001, Kolstad et al. 2004). However, chemical interactions between the Na-B and waste leachate can limit osmotic swelling and result in increasing hydraulic conductivity. GCLs permeated with aggressive leachates having high ionic strength or a predominance of polyvalent cations can be orders of magnitude more permeable than GCLs permeated with deionized (DI) or tap water (Shan and Daniel 1991, Petrov and Rowe 1997, Ruhl and Daniel 1997, Shackelford et al. 2000, Jo et al. 2001, 2005, Vasko et al. 2001, Egloffstein 2002, Kolstad et al. 2004). GCLs containing polymer-modified bentonites have been proposed to be used for containment of more aggressive liquids (Onikata et al. 1996, 1999, Trauger and Darlington 2000, Ashmawy et al. 2002, Kolstad et al. 2004, Katsumi et al. 2008, Di Emidio et al. 2010, Scalia et al. 2014).

Hydraulic conductivity of GCLs to municipal solid waste (MSW) leachate has been studied by Petrov and Rowe (1997), Ruhl and Daniel (1997), Shan and Lai (2002), Guyonnet et al. (2009), and Bradshaw and Benson (2014). Studies with real MSW leachate show minimal impact on hydraulic conductivity (< 6 time increased to relative to DI water) because MSW leachate typically have modest ionic strength (typical < 80 mM) and a high ratio of monovalent to divalent cations (RMD), with Na<sup>+</sup> and NH<sub>4</sub><sup>+</sup> being the predominant cations (Bradshaw and Benson 2014). In contrast, low-level radioactive waste (LLW) leachate have abundance of divalent cations (e.g., Ca<sup>2+</sup> and Mg<sup>2+</sup>) and are more dilute than MSW leachates. LLW leachates also contain radionuclides. Consequently, the hydraulic conductivity of GCLs to LLW leachate cannot be inferred from past studies using MSW leachates.

This study evaluated the hydraulic conductivity of eight commercially available GCLs to synthetic LLW leachate. Two were conventional GCLs containing Na-B (CS and GS) and six GCLs containing polymer-bentonite mixtures or composites (CPL, CPM, GPL, GPM, GPH, and BPC) were used in this study [P = polymer, L, M and H = low (< 2%), medium (3–5%), high (> 10%) polymer loading]. Five of the six polymer-bentonites (P-B) GCLs were prepared by dry mixing Na-B and proprietary polymers, and the sixth contained the bentonite-polymer composite (BPC) described in Scalia et al. (2014). The GCLs were permeated with two synthetic leachates representative of LLW leachates encountered in lined on-site disposal facilities operated by the US Department of Energy (Tian 2012): radioactive synthetic leachate (RSL) and a non-radioactive synthetic leachate (NSL) chemically identical to RSL but without radionuclides.

#### 7.2 BACKGROUND

## 7.2.1 Effect of Ionic Strength and Cation Abundance

Previous studies conducted by Jo et al. (2001), (2005), Lee and Shackelford (2005), and Kolstad et al. (2004) indicated that swelling and hydraulic conductivity of GCLs are controlled by two dominate factors: 1) ionic strength and 2) relative abundance of monovalent and divalent cations (RMD).

Jo et al. (2001, 2005) reported that the high ionic strength solution inhibit the swelling of Na-B, resulting in high hydraulic conductivity of GCLs. The osmotic swelling Na-B reduced or turned to crystalline swell when exposed to aggressive salts solution (Norrish and Quirk 1954). For example, swell index of bentonite gradually decreased from approximately 30 mL/2 g to 10–12 mL/2 g as the ionic strength of monovalent salt solution increased from 5 mM to 1000 mM (Jo et al. 2001). The swelling of bentonite decrease to 10 mL/2 g in CaCl<sub>2</sub> with the ionic strength increased from 15 mM to 300 mM. The decreasing of swelling of bentonite resulted in increasing of hydraulic conductivity. GCLs displayed high hydraulic conductivity (~10<sup>-7</sup> m/s) to aggressive slat solution with ionic strength exceed 1000 mM.

Kolstad et al. (2004) further investigate how salts solution with a mixture of monovalent and divalent cations affect the swelling and hydraulic conductivity of Na-B GCLs. The relative abundance of monovalent and divalent cations is defined as RMD:

$$RMD = \frac{M_m}{\sqrt{M_d}}$$

where  $M_m$  is total molar concentration of monovalent cations; and  $M_d$  is total molar concentration of multivalent cations. For a given ionic strength, GCL permeated with solution with low RMD exhibited low swelling and high hydraulic conductivity (i.e., divalent cations is predominant in permeant solution). RMD had a greater influence for salt solution with low ionic strength (e.g., 50 mM), while concentration of salts became dominate factor at high

ionic strength (e.g., 500 mM). Thus, RMD is an important parameter to predict permeability of GCL when permeated with modest ionic strength leachate.

# 7.2.2 Composition of LLW Leachate

Tian (2012) summarized the composition of LLW leachate by analyzing leachate data collected by four LLW disposal facilities associated with U.S. department of energy. LLW leachate contains little organic carbon, inorganic macro-components and trace heavy metals that remain relatively constant over time. The LLW leachate includes major cations Ca (0.77–24.9 mM), Mg (0.20–30.2 mM), Na (0.19–38.13 mM), K (0.04–1.94 mM). Additionally, the LLW leachate contains radionuclides such as uranium (6.4–3060 μg/L), tritium (40–4260 Bg/L), and technetium-99 (0.3–28 Bg/L).

The ionic strength and RMD of LLW leachate were shown in Fig. 7.1, along with the MSW leachate data from Bradshaw and Benson (2014). The LLW leachate has dilute ionic strength and low RMD than MSW leachate. The high RMD of MSW is attributed to high concentration of Na<sup>+</sup> and NH<sub>4</sub><sup>+</sup> described in Bradshaw and Benson (2014), whereas LLW leachate has low RMD with divalent cation (e.g., Ca<sup>2+</sup> and Mg<sup>2+</sup>) being predominant major cations. Even the LLW leachate have modest ionic strength, the low RMD may affect the swelling and hydraulic conductivity of GCLs, as described in Kolstad et al. (2004).

## 7.2.3 Polymer-Bentonite

Polymer have been added to bentonite to provide resistant to aggressive leachate by increasing swell by intercalating organic molecules in the interlayer of montmorillonite (Onikata et al. 1996, 1999), or by clogging intergranular flow paths with super-swelling polymer (Scalia et al 2014). Using polymers to prevent cation exchange in bentonite has also been preferred, but has not been demonstrate of bentonite by adding polymer (Flynn et al. 1998, Trauger and Darlinton 2000).

Onikata et al. (1996, 1999) and Katsumi et al. (2008) used polymer to enhance swelling of Na-B in aggressive leachate by mixing a dry Na-B with 15-45% propylene carbonate (PC) solution (by mass) to created multi-swellable bentonite (MSB). The PC is intercalated in the interlayer of montmorillonite of MSB. Osmotic swell of MSB have been observed in NaCl solutions having an ionic strength up to 750 mM (Onikata et al. 1996), while the Na-montmorillonite can have osmotic swell with an ionic strength lower than 300 mM (Norrish and Quirk 1954). Katsumi et al. (2008) evaluated the long-term hydraulic conductivity of MSB with 25% PC and found that MSB exhibited higher swelling than conventional Na-B in NaCl solution, as that crystalline swelling was predominant when the ionic strength exceeded 800 mM. In CaCl<sub>2</sub> solutions with ionic strength exceeded 300 mM, the swelling MSB was similar to the swell index of calcium-bentonite (8-10 mL/2 g) (crystalline swelling only). Hydraulic conductivity of MSB permeated with NaCl solutions with concentration less than 1000 mM was approximately the same as the hydraulic conductivity to DI water (~10-11 m/s) (Katsumi et al. 2008), whereas the hydraulic conductivity of Na-B exhibited increased when the NaCl concentrations exceeded 500 mM. MSB also had hydraulic conductivity approximately 10<sup>-11</sup> m/s when permeated with 50 to 500 mM CaCl<sub>2</sub>, whereas conventional GCLs of Na-B have hydraulic conductivity orders of magnitude higher  $(\sim 10^{-8} \text{ m/s})$  for similar CaCl<sub>2</sub> (Jo et al. 2001).

Scalia et al. (2014) evaluated modified GCLs contained a bentonite-polymer composite (BPC) created by in-situ polymerization of acrylic acid with bentonite. The BPC had constant low hydraulic conductivity (<8 x 10<sup>-11</sup> m/s) when permeated with a range of aggressive leachate (200 mM CaCl<sub>2</sub>, 500 mM CaCl<sub>2</sub>, 1 M NaOH, or 1 M HNO<sub>3</sub>). Scalia et al. (2014) hypothesized that the low hydraulic conductivity was achieved because polymers detached from montmorillonite clogged intergranular flow paths in solutions, including those that prevented osmotic swelling.

GCLs containing polymer-modified bentonites may not be compatible with aggressive leachates. For example, Shackelford et al. (2010) conducted hydraulic conductivity tests on GCLs containing a "contaminant-resistant" polymer-modified bentonite using synthetic process water and acidic leachate from a mine waste disposal facility as the permeant liquid. The GCLs containing "contaminant-resistant" polymer-modified bentonite had hydraulic conductivity to synthetic process water or acidic leachate that was 2300-7600 times higher than the hydraulic conductivity to site groundwater.

## 7.3 MATERIALS AND METHODS

# 7.3.1 Geosynthetic Clay Liner (GCL)

Eight commercially available GCLs were evaluated in this study. Two of the GCLs contained conventional bentonite (CS and GS) and the others contained polymer-bentonite (CPL, CPM, GPL, GPM, GPH, and BPC). The CPL, CPM, GPL, GPM, and GPH GCLs contain a dry mixture of granule bentonites and proprietary polymers, whereas the BPC employs a bentonite-polymer composite created using the slurry polymerization process described in Scalia et al. (2014). Each GCL consists of granular material (bentonite granules, mixture of bentonite and polymer granules, or granules of bentonite-polymer composite) sandwiched between non-woven (top) and woven polypropylene (bottom) geotextile bonded by needle punching. Physical properties of the GCLs are summarized in Table 7.1.

The major mineral components in each bentonite, determined by X-ray diffraction, followed Scalia et al. (2014), are summarized in Table 7.2. Montmorillonite is the predominant mineral in each bentonite. Quartz, plagioclase, feldspar, oligoclase, illite, mica, and calcite are present in measureable quantities, and trace amounts of other minerals (orthoclase, siderite, clinoptilolite, and kaolinite) are also present. The mineralogy of the bentonite in GCLs are similar even though these GCLs were obtained from different

manufacturers. Granule size distribution were shown in Fig. 7.2. The GS, GPL, and GPM have similar graunle size distribution, whereas the CS, CPL, CPM and BPC have similar graunle size distribution.

Loss on ignition (LOI) determined via ASTM D7348 was used as an indicator of polymer loading in the bentonite. LOI of both conventional Na bentonites was 1.6%, which is attributed to loss of strongly bound water molecules (Grim 1968), decomposition of calcite or organic matter in bentonite. The LOI test is assumed to burn all polymer compound completely in bentonite, and thus the polymer loading were calculated based on the assumption that polymer additives only contained organic compound and can be burned completely. The CPL and GPL had low polymer loading (<2%), the GPM and CPM have modest polymer loading (3–5%), and GPH and BPC had polymer loading (>10%) [P = polymer, L, M, and H = low (<2%), medium (3–5%), high (>10%) polymer loading] (Table 7.1).

Mole fractions of the bound cations (BC) and the cation exchange capacity (CEC) for each bentonite are in Table 7.1. Na is predominant for cation in the exchange complex of all of the bentonites. BPC has a very high mole fraction of Na because a sodic polymer is used to manufacture this composite material (Scalia et al. 2014). The disagreement between BC and CEC of CPM measurement may be due to the polymer coating on the bentonite and prevent cation exchange, as the hypothesis proposed by Flynn et al. (1998).

The swell index test for each bentonite using ASTM D5890 is shown in Table 7.1. The P-B with low or modest polymer loading have a comparable swell index as the conventional bentonite, whereas the bentonites containing high polymer loading have much high swelling index due to swelling of the polymer additives.

## 7.3.2 Permeant Liquids

RSL, NSL, and DI water were used as permeant liquids. Constituents in RSL and NSL are summarized in Table 7.3. These leachate compositions were determined based on an analysis of leachate data from LLW disposal facilities operated by the US Department of Energy (Tian 2012). The RSL and NSL solutions were prepared by mixing salts of CaCl<sub>2</sub>, MgSO<sub>4</sub>, NaNO<sub>3</sub>, NaHCO<sub>3</sub>, Na<sub>2</sub>SO<sub>4</sub>, and KHCO<sub>3</sub> in Type II DI water. Additionally, trace metal components were added as sulfuric salts of Al, Fe, Mn, Zn, Ni, and Cu, and chloride salts of Ba. Uranium was added in synthetic leachate as uranyl acetate and [UO<sub>2</sub>(CH<sub>3</sub>COO)<sub>2</sub>·2H<sub>2</sub>O], <sup>99</sup>Tc was added as sodium pertechnetate (NaTcO<sub>4</sub>), and tritium added as water molecule. Average concentrations are used for each constituent, except for radionuclides, which are at the upper bound concentrations to represent worst-case conditions (Tian 2012). The concentrations of major cations and anions are adjusted to match charge balance and prevent precipitation. NSL has the same chemical composition as RSL, but without radionuclides. Trace elements and radionuclides in RSL and NSL account for less than 1% of the ionic strength. Inclusions of radionuclides altered the ionic strength and RMD cations by less than 0.03%. The ionic strength and RMD of RSL was shown in Fig. 7.1.

# 7.3.3 Hydraulic Conductivity Testing

Hydraulic conductivity tests on GCL specimens were conducted in flexible-wall permeameters using the falling headwater and constant tailwater method described in ASTM D6766. The GCLs were hydrated with permeant liquid in the permeameter for 48 h at an effective confining stress of 10 kPa. After hydration, the effective confining stress was increased to 20 kPa, and the average hydraulic gradient was set at approximately 130. Influent for the specimens was contained in 50 mL burettes sealed with parafilm to prevent

evaporation. Effluent was collected in 60 mL polyethylene bottles sealed with parafilm. One specimen each of CS, GS, CPL, CPM, GPM, BPC GCL was permeated with RSL and NSL. The GPL and GPH GCLs, which were tested later, were only permeated only with NSL. Control tests were conducted on all of the GCLs with DI water as permeant liquid.

## 7.3.4 Termination Criteria

All tests were conducted until meeting hydraulic and chemical termination criteria in ASTM D6766 along with an additional criterion for comparing concentrations of major cations in influent and effluent. The hydraulic conductivity termination criteria in D6766 require no temporal trend in the hydraulic conductivity measurements, hydraulic conductivity falling within 25% of the mean for three consecutive measurements, incremental effluent volume (Qout) within 25% of the incremental influent volume (Qin) for at least 3 measurements, and the ratio Q<sub>out</sub>/Q<sub>in</sub> exhibiting no temporal trend. The chemical termination criteria require no temporal trend in exhibit electrical conductivity (ECout) and that ECout fall within 10% of the electrical conductivity of the influent (ECin). In addition, for this study, the major cations concentrations in the effluent were required to fall within 10% of concentrations in the influent. The pH of the effluent (pHout) was required to have no temporal to fall within 10% of the pH in the influent (pH<sub>in</sub>). Additionally, the concentrations of major cations in influent and effluent were analyzed periodically for elemental concentrations by inductively coupled plasmaoptical emission spectroscopy (ICP-OES), as a supplement to determine chemical equilibrium. The concentration of major cations in the effluent were required to match the concentration in the influent within 10%.

## 7.3.5 Temporal Behavior and Chemical Analysis

Typical data from a hydraulic conductivity test is shown in Fig. 7.3a for the GS GCL.

The hydraulic conductivity increases approximately 10 times during the first 40 pore volume

of flow (PVF) due to chemical exchange processes. At approximately 40 PVF, the EC and pH of the effluent leveled off and fell within the range associated with the EC and pH termination criteria (Fig. 7.3b). However, the hydraulic conductivity continued to increase slowly (until 75 PVF), which reflects slow rate-limited cation exchange processes as described in Jo et al (2001, 2006).

A typical data record from a hydraulic conductivity test is shown in Fig. 7.4. Na concentrations in the effluent decreased rapidly for about 40 PVF and fell slowly within influent concentration until 80 PVF, which was due to slow rate-limit cation exchange process described in Jo et al. (2006). Oppositely, the concentrations of Ca, Mg, and K in the effluent increased over the same testing period until reaching inflow concentration. The observation suggested that Ca, Mg, and K were replacing Na in the bentonite. Comparison of Figs. 7.3 and 7.4 shows that hydraulic conductivity and major cations in inflow and effluent both reached equilibrium at approximately 80 PVF.

# 7.3.6 Freeze-Dry Method

To investigate the spatial distribution between polymer and bentonite under saturated condition, GCLs specimens were prepared though freeze-dry method (Soppirnath and Aminabhavi 2002, Schweins et al. 2003) and then taken image using scanning electron microscope (SEM) image. Freeze-dry prior to imaging to minimize disturbance of the clay fabric, polymer structure, and clay-polymer interactions established under saturated conditions. After permeation, the P-B GCL specimens were taken out from permeameters gently, removed the top geotextile, and trimmed to approximately 1 x 3 cm strip. Then the P-B specimens were frozen in liquid nitrogen immediately to and removed to Labconco-7740020 freeze-dry system to dry. The specimens froze in liquid nitrogen prevents crystallization of water molecules and the associated volume change that normally occurs

during transition from liquid to solid phase, which inhibit broken of the polymer structure. Drying the specimens under vacuum at low temperature (~ -70°C) impede the collapse of polymer structure due to release water molecules. SEM was used to taken image for the freeze-dry specimens to investigate the polymer-clay interaction and spatial distribution.

## 7.4 RESULTS AND DISCUSSION

A summary information of the tests results is reported in Table 7.4. The PVF reported in Table 7.4 are based on the initial pore volume. At the time this paper was prepared, the GCLs had been permeated for up to 2.3 yr with RSL and NSL. The CS, GS, CPL, and GPM GCLs permeated with RSL or NSL met the termination criteria in ASTM D6766. Additionally, the supplemental concentration criterion requiring that the concentrations of major cations in the influent and effluent fall within 10% (Jo et al. 2001, Bradshaw and Benson 2014). The GPL, CPM, GPH, and BPC GCLs had not met the termination criteria, and tests on these GCLs are still ongoing.

# 7.4.1 Effect of Leachate Chemistry on Hydraulic Conductivity

The comparison of hydraulic conductivities of the GCLs exposed to RSL or NSL are shown in Fig. 7.5. Essentially the same hydraulic conductivities were obtained using both leachates over a range of approximately two orders of magnitude and, all of the data fall within the band corresponding to a factor of 2, which Jo et al. (2001) indicated as the reproducibility of hydraulic conductivity tests on GCLs. The similarity in the hydraulic conductivities to RSL and NSL reflects the small impact of radionuclides on ionic strength and RMD of the leachate (both < 0.03%). Similar swell indexes were obtained with NSL and RSL for each Na-B or P-B (Fig. 7.6), which is consistent with the similar conductivities obtained with RSL and NSL. Based on these findings, RSL and NSL were determined

comparable in terms of their effect on hydraulic conductivity. Subsequent tests were conducted with NSL to reduce safety concerns and to simplify disposal of testing waste.

Hydraulic conductivity of GCLs permeated with RSL or NSL are compared to hydraulic conductivity to DI water in Fig. 7.7. Hydraulic conductivity of CS and GS conventional GCLs are approximately 5 to 25 times higher than the hydraulic conductivity to DI water. Hydraulic conductivity of the P-B GCLs fell into four categories. The GPM GCLs were 100 times more permeable to NSL than to DI water, and had the highest hydraulic conductivity of all. Hydraulic conductivity of the CPL and GPL GCLs permeated with RSL or NSL were comparable to conventional GCL, and approximate 5-25 times more permeable to RSL or NSL than to DI water. The CPM and GPH GCLs had the lowest hydraulic conductivity to RSL or NSL, and had essentially the same hydraulic conductivity as to DI water. The BPC had the lowest hydraulic conductivity of all GCLs (<10<sup>-11</sup> m/s for NSL, RSL, or DI) and was 1.4 to 2.5 times less permeable to NSL and RSL than to DI water. Fewer PVF passed through the CPM, GPH, and BPC GCLs than the conventional GCLs largely due to the very low flow rate associated with the very low flow hydraulic conductivity of the GCLs. Because so few PVF had passed through the CPM, GPH, and BPC GCLs, chemical equilibrium was not established. Longer-term testing of the GCLs is underway to ensure that the hydraulic conductivity represents chemical equilibrium.

# 7.4.2 Cation Exchange, Swelling, and Hydraulic Conductivity

The RSL and NSL leachate contain on abundance of divalent cations that have propensity to replace the monovalent Na<sup>+</sup> originally bound to the mineral surface. In NSL and RSL, the total molarity of divalent cations is 30% higher than for monovalent cations, and the total charge associated with the divalent cations is 2.6 times the charge associated with the monovalent cations. Cation exchange is evident in Fig. 7.4, where Na<sup>+</sup> is eluted due to

replacement by Ca<sup>2+</sup> and Mg<sup>2+</sup> in the leachate. The exchange complex after testing in CS, GS, CPL, and GPM GCLs is nearly devoid of monovalent cations, and almost completely composed of equal amounts of Ca<sup>2+</sup> and Mg<sup>2+</sup> (Table 7.5). Thus, cation exchange resulted in nearly a complete loss in swell by the end of testing, with swell index ranging between 10–12 mL/2 g for CS, GS, CPL, and GPM GCLs. Prior to permeation, the swell index in leachate ranged between 16–27 mL/2 g (average = 22 mL/2 g), and in DI water between 27–36 mL/2 g (average = 30 mL/2 g).

The conversion of the Na-B to Ca-Mg-B is responsible for the much higher hydraulic conductivity of the conventional Na-B to NSL and RSL, as shown in Fig. 7.7. The conventional Na-B GCLs are 10–25 times more permeable to NSL or RSL than to DI water. The GS conventional GCL has slightly lower hydraulic conductivity than the CS GCL due to finer bentonite granule size used in the CS GCL. The P-B GCLs with low to modest polymer loading (LOI < 5%, CPL, GPL, and GPM) with also have hydraulic conductivity that is 10–100 times higher than the hydraulic conductivity to DI water.

In contrast, the P-B GCLS with modest higher polymer loading (LOI > 6%, CPM, GPH, BPC) all had very low hydraulic conductivity to NSL or RSL, being comparable to or lower than the hydraulic conductivity to DI water. This suggests that a threshold in polymer loading exists beyond which the impact of cation exchange and bentonite swell are no longer important. For the GCLs evaluated in this study, the threshold in polymer loading is between 5.1% and 12.7% by mass based on LOI, as shown in Fig. 7.8. In contrast to conventional Na-B GCLs, the low hydraulic conductivities of the P-B GCLs must be due to a mechanism other than bentonite swelling.

## 7.4.3 Mechanism Controlling Polymer-Bentonite GCLs

The insensitivity of the hydraulic conductivity of the P-B GCLs to swell index suggests that the polymer is controlling the size and shape of pores rather than swelling of bentonite. For example, the swell index of Na-B in CS GCL was higher than P-B in CPM GCLs (Fig. 7.6), whereas the hydraulic conductivity of CS to RSL and NSL was approximately two orders of magnitude higher than CPM when permeated with RSL and NSL. This illustrated that the polymer controlled the size and shape of intergranular flow channels when reduction of swelling of bentonite occurred.

The eluent from hydraulic conductivity tests on the CPM GCL had higher viscosity than the permeant solutions, suggesting that polymer was eluted in the effluent. Adding the effluent into isopropanol resulted in white precipitation. FTIR analysis of white precipitation indicated the polymer matches 80% the anionic PAM, which suggests that the polymer in the CPM is anionic PAM. PAM is classified as hydrogel (Soppirnath and Aminabhavi 2002). The frame of hydrogel consists of polymer chains that have hydrophilic functional groups (e.g., carboxylic acid groups). Water molecules are attracted to the hydrophilic groups through hydrogen bonding. Additionally, PAM chain can connect with other chains through hydrogen bonding with water molecule, and as a result "longer polymer chain" are formed along with three-dimension structure. The swelling of P-B form the CPM GCL in DI water shown in Fig. 7.9a illustrates the formation of the hydrogel. The liquid-like glutinous hydrogel coats and binds to the bentonite particles.

In P-B GCL, the hydrogel is analogous to bentonite with osmotic swell. Similar to water molecules absorbed by bentonite, the water molecules bonded on hydrogel structures are immobile compared to free water in pore space. Thus, the hydrogel consisting polymer chains and bound water can block open pores, resulting in low hydraulic conductivities. While the hydrogel is a liquid-like glutinous material (Fig. 7.9a), to be effective in blocking flux, the

hydrogel must bind to mineral surface to prevent dissociation and elution through the pore space.

To investigate the interaction between polymer and bentonite, SEM image was taken for P-B from CPM GCLs permeated with DI water using freeze-dry method was shown in Fig. 7.9b. The polymer forms a three-dimensional net structure between bentonite granular. In a saturated system, the polymer frame binds water to form hydrogel occupied the pore space, as shown in Fig. 7.9a. The edge of the anionic polymer structure may attach to the mineral surface through electrostatic force. Deng et al. (2006) postulated that the mechanism for anionic PAM adsorption to montmorillonite basal surfaces was through exchangeable cation (e.g., Ca) bridging. Moreover, the edge surfaces of the clay minerals carrying positive charge may play a major role in anionic PAM adsorption (Black *et al.* 1965, Laird 1997, Heller and Keren 2003). Consequently, the anionic PAM can absorb on the surface of the bentonite to reduce the elution and clog the pore space effectively, resulting in low hydraulic conductivity of CPM GCL to leachate.

However, the polymer elution from CPM GCL reflects that binding between polymer and mineral due electrostatic force are not sufficient. Similar results had been reported by Scalia et al. (2014) that polymer eluted out from BPC GCLs when permeated with DI water or salt solutions. Polyelectrolyte with carbonyl group (e.g., anionic polyacrylate and anionic PAM) can interacted with divalent cations (e.g., Ca<sup>2+</sup>, Mg<sup>2+</sup>) in solutions, and thus neutralize the charge on the polymer chains (Schweins et al. 2003, 2006). Without the negative charge, the polymer can be flush out easily with permeant solutions. Thereby, the cations in the leachate may affect the binding between polymer chains and mineral surface. Further research is needed to investigate the polymer elution of P-B GCLs to determine the long-term compatibility.

A conceptual model of swelling of bentonite controlling hydraulic conductivity was shown in Fig. 7.10. The dry bentonite clusters can fully swell in DI water or dilute salts solutions and make narrow and tortuous flow channel, resulting in low hydraulic conductivity of GCL (Fig. 7.10b). However, the swelling of bentonite reduced when exposed to aggressive leachate with high ionic strength or predominated divalent cations, leading to open channels and increase hydraulic conductivity of GCLs (Fig. 7.10c).

For the P-B, even the Na-B shows lower swell when exposed to salt solution, the hydrogel can attach on bentonite cluster and help clogging the open channel in between bentonite particles (Fig. 7.11). The polymer can bind water to form glutinous hydrogel with three-dimension network (Fig. 7.11a). The bound water on hydrogel are immobilized and clog the pore space to reduce the advective flow in GCL (Fig. 7.11b). The anionic polymer chains attach on the mineral surface due to electrostatic force, which reduce the elution of polymer and form P-B composite. Thus, the P-B GCLs with modest to high polymer loading have low hydraulic conductive than conventional Na-B GCLs.

The hydraulic conductivity of P-B GCLs to RSL and NSL were highly depended on polymer loading. The P-B GCLs with low polymer loading (e.g., CPL and GPL) to RSL and NSL were no more resistant to RSL or NSL than conventional CS and GS GCLs, whereas P-B GCLs with high polymer loading (LOI > 6%) had consistent low hydraulic conductivity (Fig. 7.8). This observation indicated that P-B GCLs need sufficient polymer hydrogel to clog the open channels effectively. Without sufficient polymer hydrogel, bentonite may still have unclogged open channels that controlling the hydraulic conductivity of GCLs. Thus, a threshold in polymer loading exist to counteract impact of cation exchange of bentonite.

#### 7.5 CONCLUSION

Tests were conducted to evaluate hydraulic conductivity of geosynthetic clay liners (GCLs) used in low-level radioactive waste (LLW) disposal facilities composite liner systems. Tow conventional sodium-bentonite (Na-B) GCLs and six polymer-bentonite (P-B) GCLs were directly permeated with radioactive and non-radioactive synthetic leachates (RSL and NSL) that are chemically represent to LLW leachate. Control tests were conducted with deionized (DI) water.

- 1) Conventional CS and GS GCLs containing conventional Na-B are 10-25 times more permeable to LLW leachate than to the DI water due to replacement of native Na<sup>+</sup> in the bentonite by Ca2<sup>+</sup> and Mg<sup>2+</sup> in RSL and NSL, resulting in reducing osmotic swell and increase hydraulic conductivity.
- 2) Hydraulic conductivities and swelling of GCLs to NSL and RSL are indistinguishable. The similarity was due to small impact of radionuclides on ionic strength and RMD of the leachate (both < 0.03%). Testing with non-radioactive leachate is recommended to simplify health and safety concerns when investigating GCLs for LLW facilities.
- 3) P-B GCLs with polymer loading exceeded 5% by my mass as determined by loss on ignition (LOI) had hydraulic conductivity to LLW leachate comparable to hydraulic conductivity to DI water. The bentonite-polymer composite (BPC) GCL was slightly less permeable to LLW leachate than DI water.
- 4) The low hydraulic conductivity of P-B GCLs to RSL and NSL mechanism was hypothesized to be polymer hydrogel clogging. The hydrogel in P-B binds water to form three-dimension structures and clogs the pore space. Additionally, the polymer chains in hydrogel carrying negative charge groups (e.g., carbonyl acid groups) can absorbed on the mineral surface due to electrostatic force, reducing the flushing out of semi-liquid polymer.

P-B GCLs with polymer loading less than 4% by my mass as determined by LOI were no more resistant to RSL and NSL. Without sufficient polymer loading, the hydrogel are not enough to clog the all pore spaces induced by reduction of swelling of bentonite in leachate. As a result, the open intergranular channels become controlling the hydraulic conductivity in P-B GCL with load polymer loading. This suggests that a threshold in polymer loading exists beyond which the impact of cation exchange and bentonite swell are no longer important.

#### **REFERENCES**

- Ashmawy, A., Darwish, E., Sotelo, N., and Muhammad, N. (2002). Hydraulic performance of untreated and polymer-treated bentonite in inorganic landfill leachates. *Clays and Clay Minerals*, 50(5), 546–552.
- Benson, C., Oren, A., and Gates, W. (2010). Hydraulic conductivity of two geosynthetic clay liners permeated with a hyperalkaline solution. *Geotextiles and Geomembranes*, 28(2), 206–218.
- Black, A., Birkner, F., and Morgan, J. (1965) Destabilization of dilute clay suspensions with labeled polymers. *Journal of the American Water Works Association*, 57, 1547–1560.
- Bradshaw, S. and Benson, C. (2014). Effect of municipal solid waste leachate on hydraulic conductivity and exchange complex of geosynthetic clay liners, *J. Geotechnical and Geoenvironmental Engineering*, 140(4), 04013038.
- Deng, Y., Dixon, J., and White, G. (2006). Bonding between polyacrylamide and smectite. *Colloids and Surfaces*, 281(1), 82–91.
- Di Emidio, G., Van Impe, W., and Mazzieri, F. (2010). A polymer enhanced clay for impermeable geosynthetic clay liners. *Proc. Sixth International Conference on Environmental Geotechnics*, Balkema, Rotterdam, 963–967.
- Egloffstein, T. (2002). Bentonite as sealing material in geosynthetic clayliners-influence of the electrolytic concentration, the ion exchange and ion exchange with simultaneous partial desiccation on permeability. *Proc. International Symposium on Clay Geosynthetic Barriers*, H. Zanzinger, R. Koerner, and E. Gartung, eds., Balkema, Rotterdam, Netherlands, 141–153.
- Guyonnet, D., Touze-Foltz, N., Norotte, V., Pothier, C., Didier, G., Gailhanou, H., Blanc, P., and Warmont, F. (2009). Performance-based indicators for controlling geosynthetic clay liners in landfill applications. *Geotextiles and Geomembranes*, 27(5), 321–331.
- Heller, H. and Keren, R. (2003). Anionic polyacrylamide polymer adsorption by pyrophyllite and montmorillonite. *Clays and Clay Minerals*, 51(3), 334–339
- Jo, H., Benson, C., and Edil, T. (2006). Rate-limited cation exchange in thin bentonite barrier layers. *Canadian Geotechnical Journal*, 43, 370-391
- Jo, H., Benson, C., Lee, J., Shackelford, C., and Edil, T. (2005). Long-term hydraulic conductivity of a non-prehydrated geosynthetic clay liner permeated with inorganic salt solutions. *J. Geotechnical and Geoenvironmental Engineering*, 131(4), 405–417.
- Jo, H., Katsumi, T., Benson, C., and Edil, T. (2001). Hydraulic conductivity and swelling of non-prehydrated GCLs permeated with single species salt solutions. *J. Geotechnical and Geoenvironmental Engineering*, 127(7), 557–567.
- Kolstad, D., Benson, C., and Edil, T. (2004). Hydraulic conductivity and swell of nonprehydrated GCLs permeated with multispecies inorganic solutions. *J. Geotechnical and Geoenvironmental Engineering*, 130(12), 1236–1249.
- Katsumi, T., Ishimori, H., Onikata, M., and Fukagawa, R. (2008). Long-term barrier performance of modified bentonite materials against sodium and calcium permeant solutions. *Geotextiles and Geomembranes*, 26(1), 14–30.

- Lee, J. and Shackelford, C. (2005). Impact of bentonite quality on hydraulic conductivity of geosynthetic clay liners. *J. Geotechnical and Geoenvironmental Engineering*, 131(1), 64–77.
- Laird, D. (1997). Bonding between polyacrylamide and clay mineral surfaces. *Soil Science*, 162, 826–832.
- Mesri, G. and Olson, R. (1971). Mechanisms controlling the permeability of clays. *Clays and Clay Mineral*, 19, 151–158.
- Norrish, K. and Quirk, J. (1954). Crystalline swelling of montmorillonite, use of electrolytes to control swelling. *Nature*, 173, 255–257.
- Onikata, M., Kondo, M., and Kamon, M. (1996). Development and characterization of a multiswellable bentonite. *Environmental Geotechnics*. Taylor and Francis, Rotterdam, 587–590.
- Onikata, M., Kondo, M., Hayashi, N., and Yamanaka, S. (1999). Complex formation of cation-exchanged montmorillonites with propylene carbonate: Osmotic swelling in aqueous electrolyte solutions. *Clays and Clay Minerals*, 47(5), 672–677.
- Petrov, R. and Rowe, R. (1997). Geosynthetic clay liner (GCL) chemical compatibility by hydraulic conductivity testing and factors impacting its performance. *Canadian Geotechnical Journal*, 34, 863–885.
- Ruhl, J. and Daniel, D. (1997). Geosynthetic clay liners permeated with chemical solutions and leachates. *J. Geotechnical and Geoenvironmental Engineering*, 123(4), 369–381.
- Schweins, R., Lindner, P., Huber, K. (2003). Calcium induced shrinking of napa chains: a sans investigation of single chain behavior. *Macromolecules*, 36, 9564–9573
- Serizawa T., Wakita K., and Akashi M. (2002). Rapid deswelling of porous poly(N-isopropylacrylamide) hydrogels prepared by incorporation of silica particles. *Macromolecules*, 35, 10–12.
- Shackelford, C., Benson, C., Katsumi, T., Edil, T., and Lin, L. (2000). Evaluating the hydraulic conductivity of GCLs permeated with non-standard liquids. *Geotextiles and Geomembranes*, 18, 133–161.
- Scalia, J., Benson, C., Bohnhoff, G., Edil, T., and Shackelford, C. (2014). Long-term hydraulic conductivity of a bentonite-polymer composite permeated with aggressive inorganic solutions. *J. Geotechnical and Geoenvironmental Engineering*, 140(3), 04013025.
- Shackelford, C., Sevick, G., and Eykholt, G. (2010). Hydraulic conductivity of geosynthetic clay liners to tailings impoundment solutions. *Geotextiles and Geomembranes*, 28 (2), 206–218.
- Shan, H. and Daniel, D. (1991). Results of laboratory tests on a geotextile/bentonite liner material. *Proc. Geosynthetics* 1991, Industrial Fabrics Association International, St. Paul, MN, 517–535.
- Soppirnath, K. and Aminabhavi, T. (2002). Water transport and drug release study from cross-linked polyacrylamide grafted guar gum hydrogel microspheres for the controlled release application. *European Journal of Pharmaceutics and Biopharmaceutics*, 53(1), 87–98

- Trauger R. and Darlington J. (2000). Next-generation geosynthetic clay liners for improved durability and performance. *TR-220*. Colloid Environmental Technologies Company, Arlington Heights, 2–14.
- Tian, K. (2012). Durability of high-density polyethylene geomembrane in low-level radioactive waste leachate. *MS Thesis*, University of Wisconsin-Madison, Madison, Wisconsin.
- Vasko, S., Jo, H., Benson, C., Edil, T., and Katsumi, T. (2001). Hydraulic conductivity of partially prehydrated geosynthetic clay liners permeated with aqueous calcium chloride solutions. *Proc. Geosynthetics* 2001, Industrial Fabrics Association International (IFAI), Roseville, MN, 685–699.

Table 7.1. Polymer loading, swell index, and concentrations of bound cations in the exchange complex of bentonite in GCLs

001	Dry mass	LOI	Polymer	,		Mole Fraction of Bound Cations				
GCL	per area kg/m²	(%)	Loading (%)	DI (mL/2 g)	Na	К	Ca	Mg	(cmol <sup>+</sup> /kg)	
CS	3.6	1.6	N/A	36	0.45	0.04	0.29	0.12	71.3	
GS	3.7	1.6	N/A	32	0.42	0.03	0.31	0.10	73.2	
CPL	3.6	2.8	1.2	28	0.53	0.03	0.25	0.11	71.4	
GPL	3.7	3.5	1.9	28	0.57	0.02	0.33	0.04	72.1	
GPM	3.7	4.8	3.3	31	0.40	0.02	0.37	0.09	74.6	
CPM	3.6	6.6	5.1	27	0.14	0.01	0.13	0.04	89.6	
GPH		12.3	10.9	40	0.46	0.02	0.35	0.15	72.2	
BPC	4.8	11.0	12.7	45	0.75	0.01	0.09	0.04	91.5	

Note: Polymer loading is calculated based on loss on ignition per ASTM D7348. Swell index measured in DI water using ASTM D5890. Bound cations and CEC measured using ASTM D7503. N/A represents not applicable.

Table 7.2. Mineralogy of bentonite in GCLs (trc = trace amount)

Minaral Canatituanta	Relative Abundance (%)									
Mineral Constituents	CS	GS	CPL	GPL	CPM	GPM	GPH	BPC		
Montmorillonite	84	86	86	80	79	85	67	78		
Quartz	9	8	8	6	8	10	13	8		
Plagioclase, Feldspar, and Oligoclase	3	3	3	9	7	2	9	5		
Illite and Mica	1	-	1	trc	1	1	7	7		
Calcite	1	-	trc	trc	-	trc	3	-		
Other Minerals	2	3	2	5	5	2	1	2		

Note: The CPM, GPL, and GPH are modified from CS or GS respectively, therefore, the mineral compositions are assumed the same.

Table 7.3. Characteristics of synthetic LLW leachates used in the study

Major Cation Concentration		Trace Metal Concentrations (mM)					
Ca	4	As	As 0.001 Al				
Mg	6	Ва	0.002	Mn	0.01		
Na	7	Cu 0.0002 Ni		Ni	0.0003		
K	0.7	Fe	0.04	Sr	0.02		
Sulfate	7.5	Li	0.02	Zn	0.0005		
Chloride	8	Bulk Characteristics					
Nitrate	1.5	TOC (mg/L)					
Alkalinity	3.5	Eh (mV)					
Radionu	clides		7.2				
U-238 (µg/L)	1500	<sup>a</sup> loni	43.6				
H-3 (Bq/L)	4440		0.077				
Tc-99 (Bq/L)	29.6	PRMD (M <sup>1/2</sup> ) 0.0					

Notes: RMD =  $M_M/M_D^{0.5}$ , where  $M_M$  = the total molarity of divalent cations in the liquid (M) and  $M_D$  = total molarity of polyvalent cations in the liquid (M).

Table 7.4. Hydraulic conductivity of GCLs permeated with RSL, NSL, and DI water

			Total	Terr	minatio	n Crite	eria	Hydraulic Conductivity k (m/s)	
( = ( 1 )	Permeant Liquid	PVF	Test time (yr)	Hydraulic	EC	рН	Major Cations Conc.		<i>k/k</i> <sub>DI</sub>
	RSL	208	1.8	Yes	Yes	Yes	Yes	1.9x10 <sup>-10</sup>	8.6
CS	NSL	239	1.8	Yes	Yes	Yes	Yes	2.8x10 <sup>-10</sup>	12.7
	DI	12.8	0.3	Yes	No	No	No	2.2x10 <sup>-11</sup>	
	RSL	188	1.8	Yes	Yes	Yes	Yes	1.7x10 <sup>-10</sup>	20.2
GS	NSL	198	1.8	Yes	Yes	Yes	Yes	1.3x10 <sup>-10</sup>	15.5
	DI	7.5	0.3	Yes	No	No	No	8.4x10 <sup>-12</sup>	
	RSL	217	1.8	Yes	Yes	Yes	Yes	2.7x10 <sup>-10</sup>	24.5
CPL	NSL	170	1.8	Yes	Yes	Yes	Yes	1.2x10 <sup>-10</sup>	10.9
	DI	11.8	8.0	Yes	No	No	No	1.1x10 <sup>-11</sup>	
GPL*	NSL	74	0.9	Yes	No	No	No	9.6x10 <sup>-11</sup>	6.4
GFL	DI	30	0.7	Yes	No	No	No	1.5x10 <sup>-11</sup>	
	RSL	17	2.1	Yes	No	No	No	5.5x10 <sup>-12</sup>	1.6
CPM*	NSL	13	2.1	Yes	No	No	No	4.9x10 <sup>-12</sup>	1.5
	DI	12	1.7	Yes	No	No	No	3.2x10 <sup>-12</sup>	
	RSL	228	1.8	Yes	Yes	Yes	Yes	5.6x10 <sup>-10</sup>	73.7
GPM	NSL	140	1.8	Yes	Yes	Yes	Yes	7.5x10 <sup>-10</sup>	99.0
	DI	2.9	8.0	Yes	No	No	No	7.6x10 <sup>-12</sup>	
CDU*	NSL	9.6	0.4	Yes	No	No	No	3.8x10 <sup>-12</sup>	2.4
GPH*	DI	1.2	0.4	Yes	No	No	No	1.1x10 <sup>-12</sup>	
	RSL	16	2.3	Yes	No	No	No	2.7x10 <sup>-12</sup>	0.4
BPC*	NSL	239	2.3	Yes	No	No	No	4.9x10 <sup>-12</sup>	0.7
	DI	1.9	0.1	Yes	No	No	No	6.7x10 <sup>-12</sup>	

Note: \*Hydraulic conductivity tests are still being conducted. PVF= pore volume of flow, k =hydraulic conductivity.

Table 7.5. Swell index and concentrations of bound cations in the exchange complex

GCL Permeant Solution		Perme	II Index in ant Solution nL/2g)	Mole Fraction of Bound Cations after termination			
		Before	Termination	Na	K	Ca	Mg
CS	RSL	27	11	0.03	0.01	0.47	0.45
CS	NSL	27	10	0.01	0.02	0.45	0.52
GS	RSL	16	12	0.02	0.01	0.46	0.48
GS	NSL	16	11	0.04	0.03	0.42	0.49
CPL	RSL	22	10	0.03	0.02	0.43	0.47
CPL	NSL	22	11	0.01	0.02	0.46	0.49
CDM	RSL	20	12	0.02	0.01	0.43	0.47
GPM	NSL	21	10	0.02	0.02	0.40	0.52

Note: Before = original GCL before permeation, termination = GCLs after permeated with RSL or NSL.

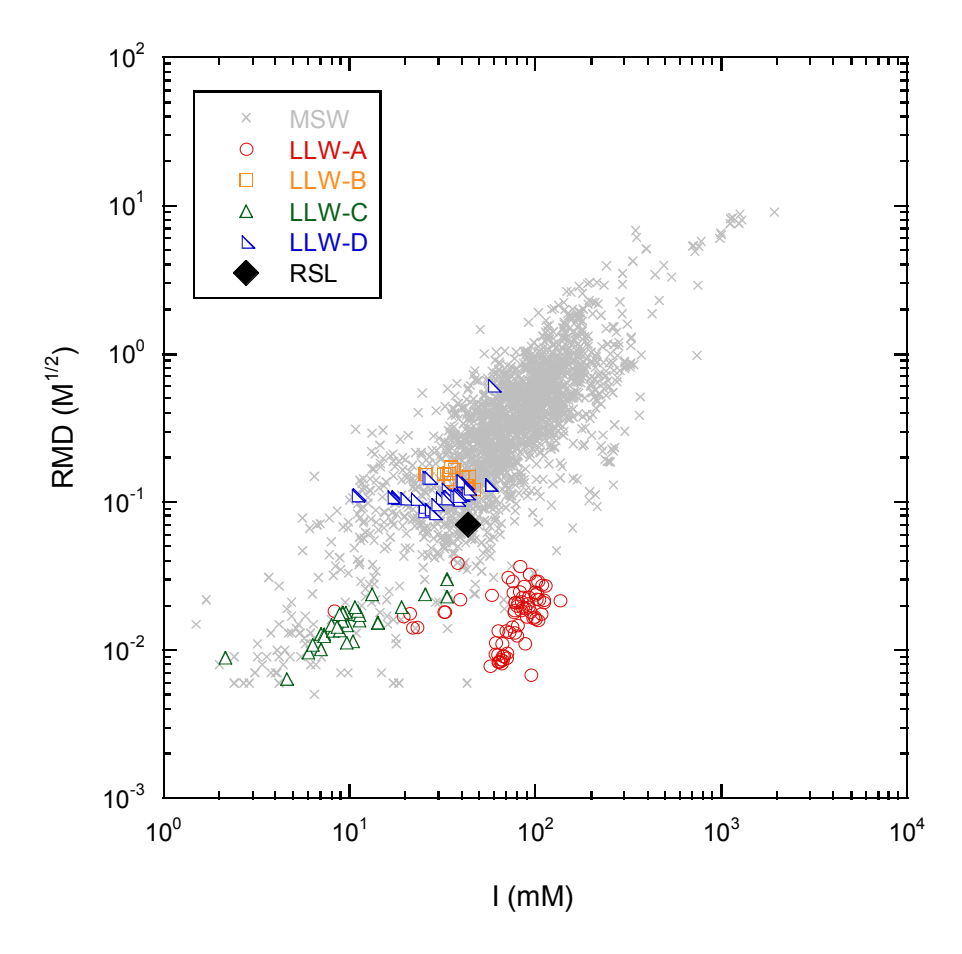


Fig. 7.1. RMD vs. ionic strength for LLW and MSW leachates. RSL is shown with diamond symbol.

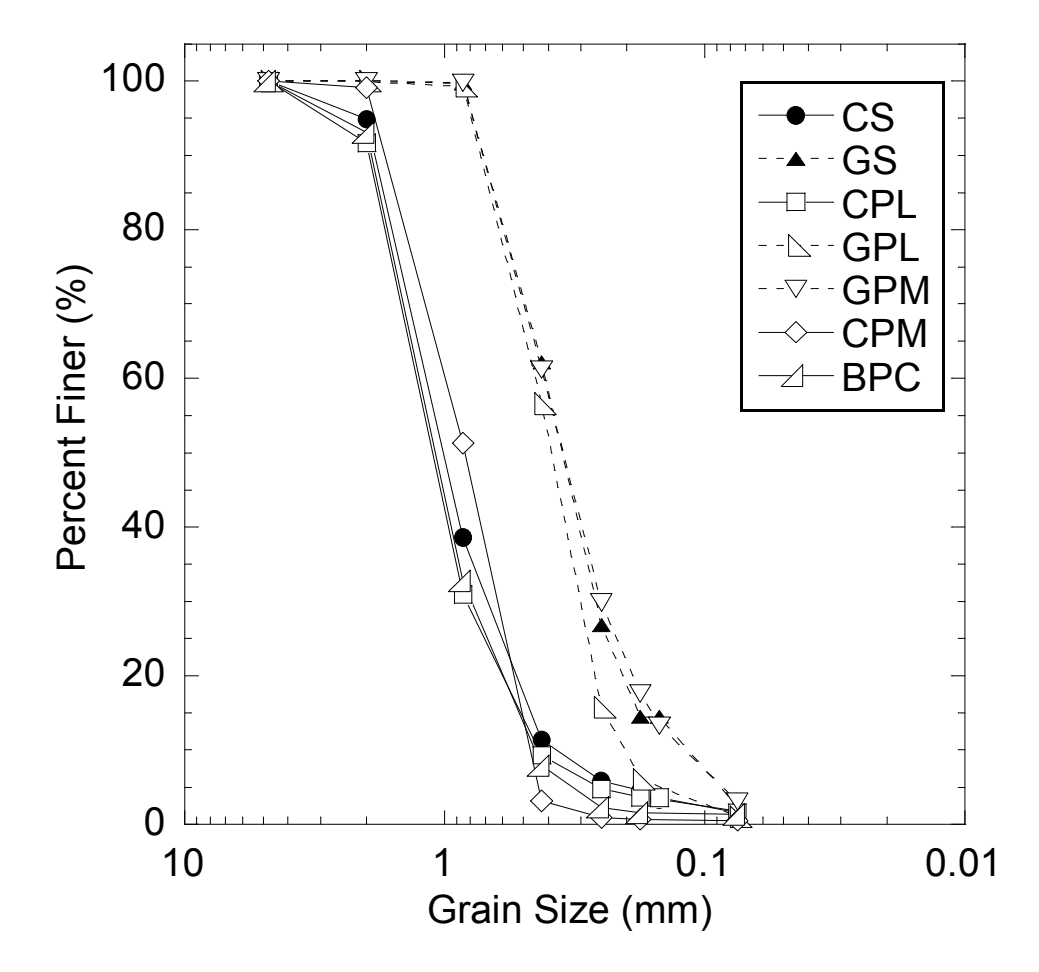


Fig. 7.2. Grain size distribution for GCLs used in this study. (the amount of GPH GCLs was not sufficient to conduct test for grain size distribution.)

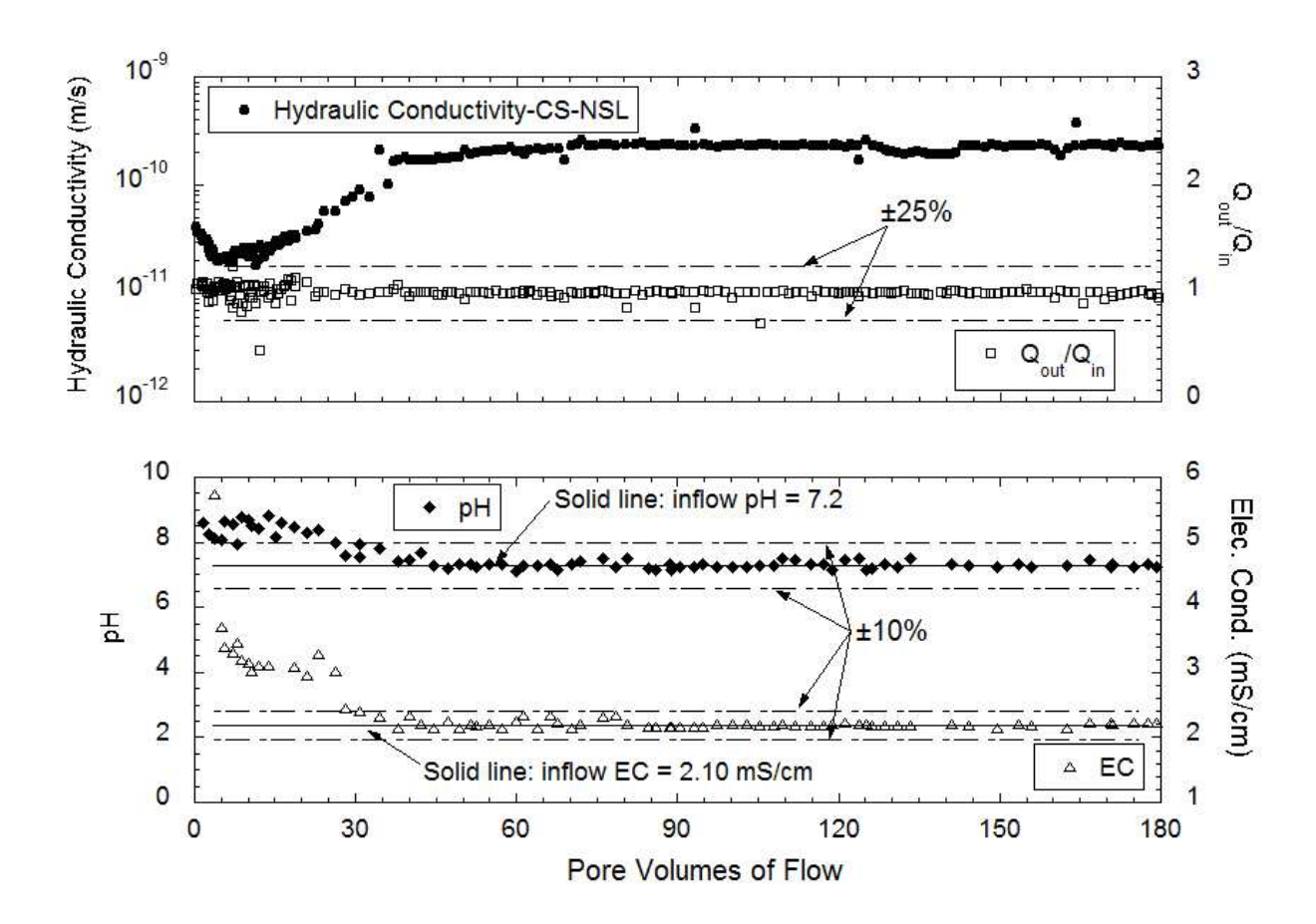


Fig. 7.3. Data from hydraulic conductivity test on CS GCL using NSL as the permeant liquid.

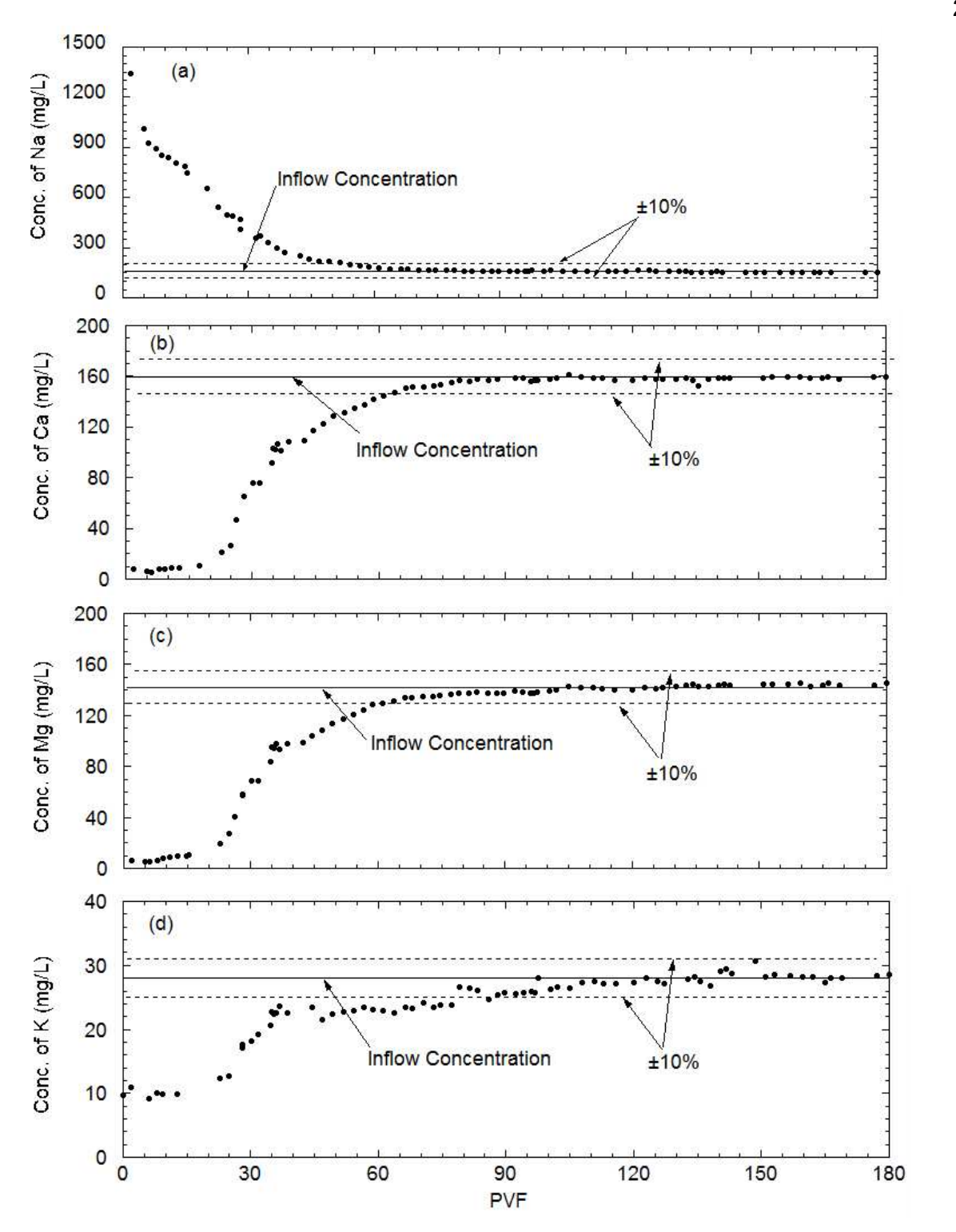


Fig. 7.4. Concentration of major cations in influent and effluent for test conducted with conventional CS GCL permeated with NSL: (a) Na, (b) Ca, (c) Mg, and (d) K.

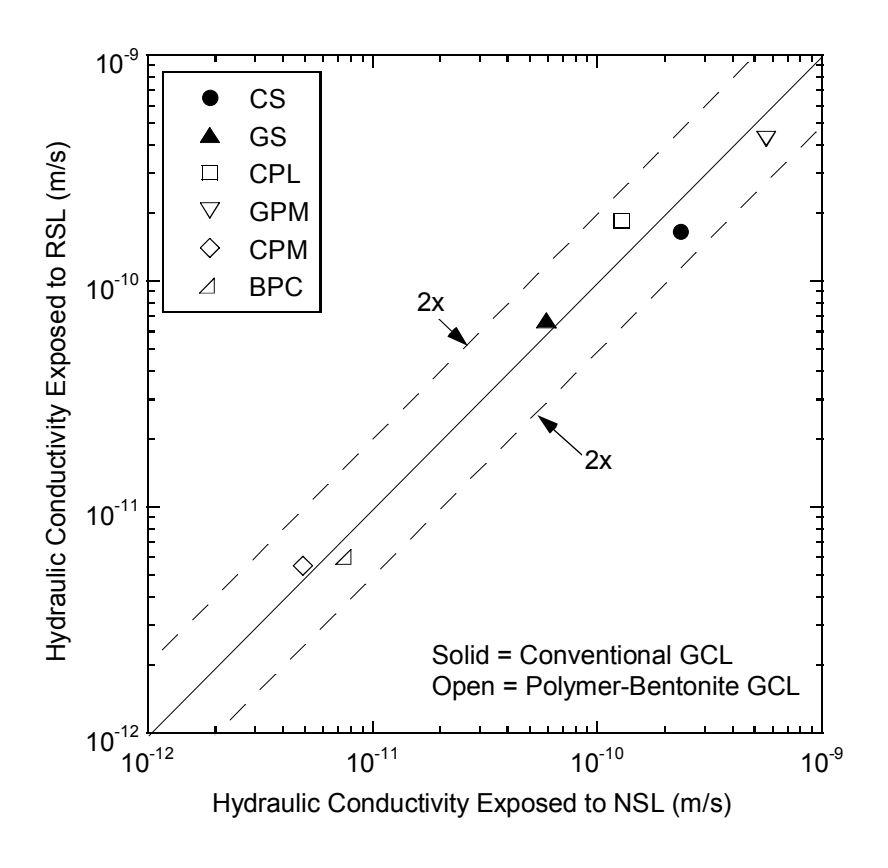


Fig. 7.5. Hydraulic conductivity of GCLs permeated with radioactive synthetic leachate (RSL) vs. hydraulic conductivity to non-radioactive synthetic leachate (NSL).

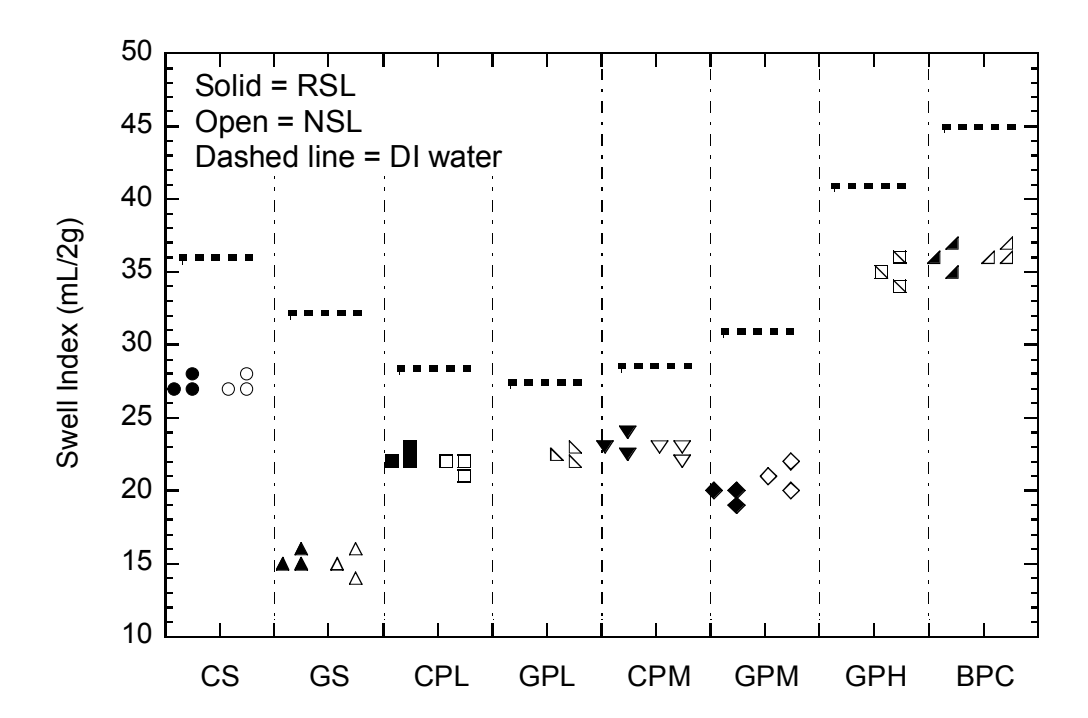


Fig. 7.6. Swell index of bentonite from each GCL in RSL, NSL, and DI water.

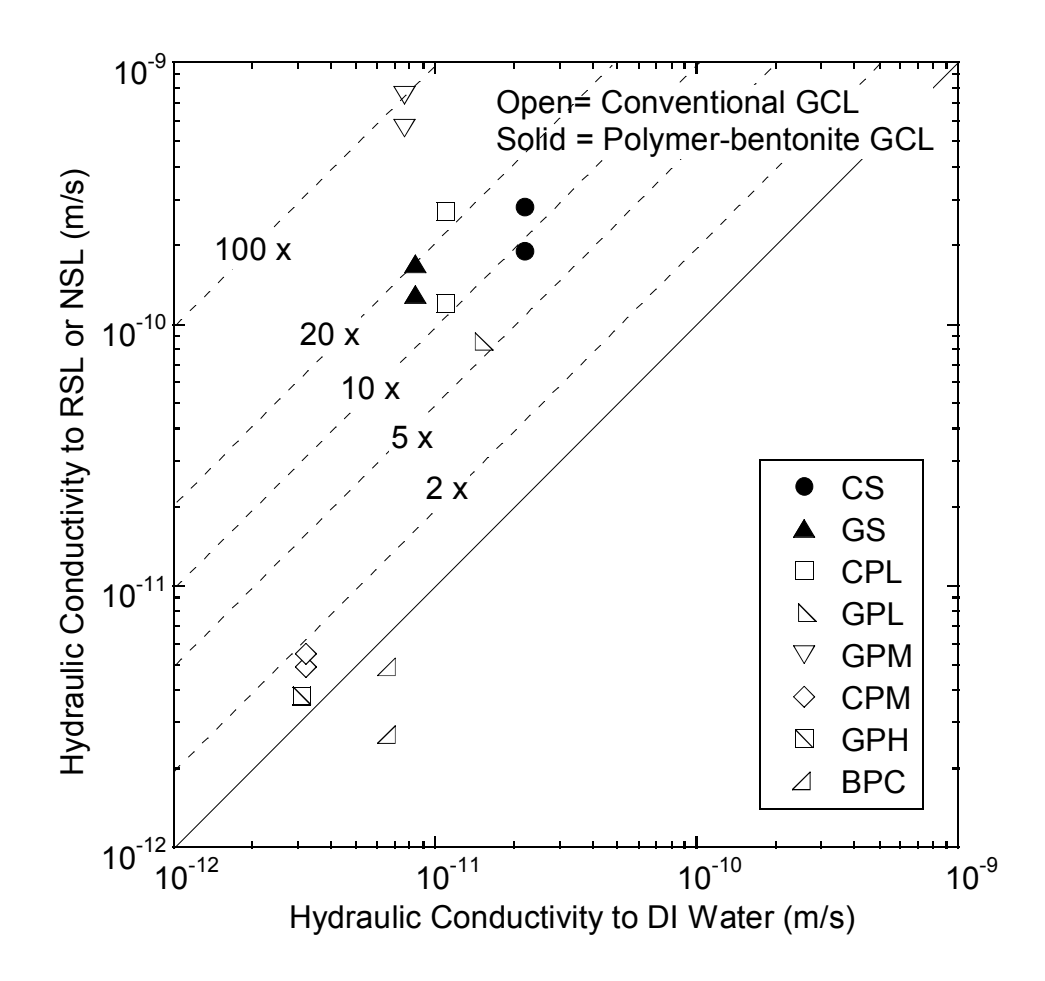


Fig. 7.7. Hydraulic conductivity of GCLs to RSL or NSL vs. hydraulic conductivity to DI water.

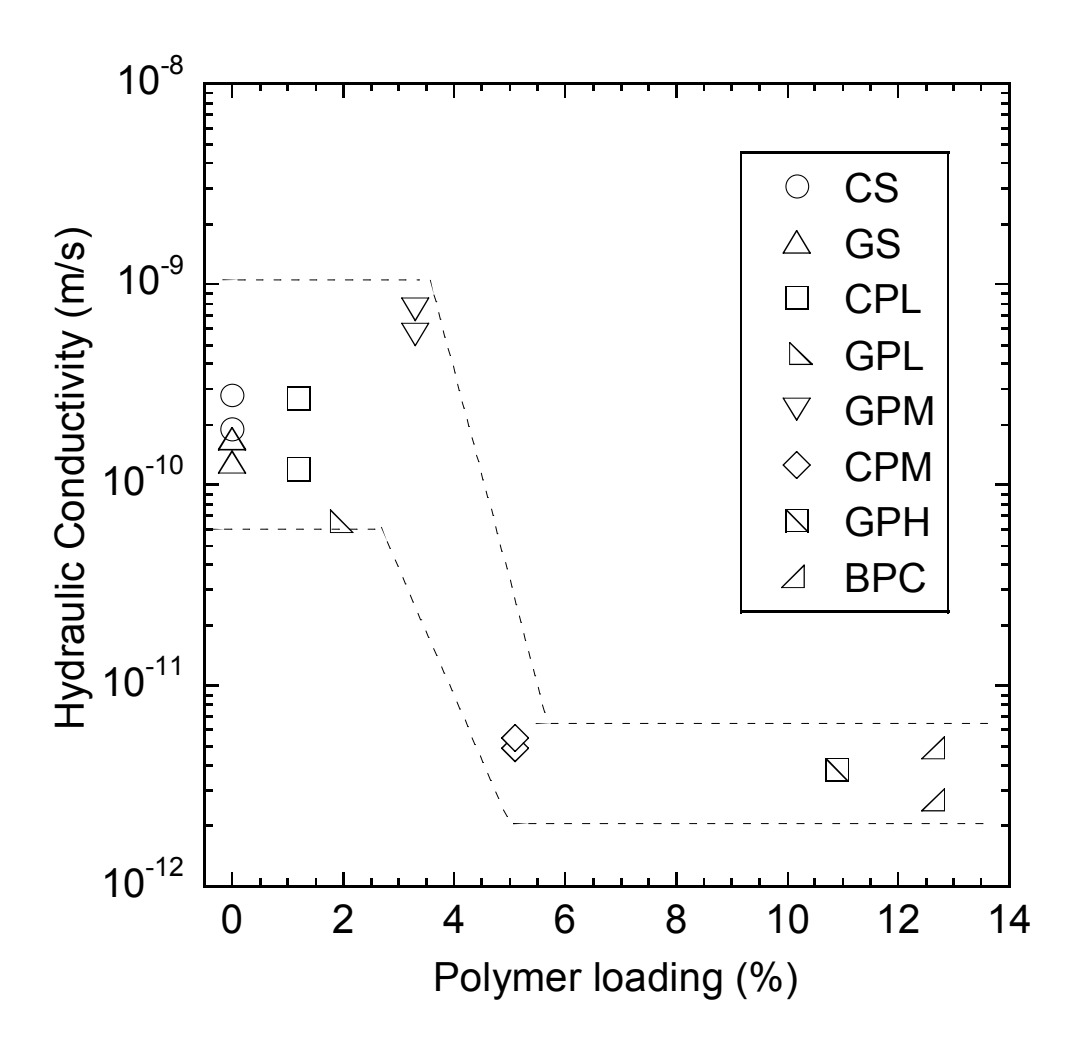


Fig. 7.8. Hydraulic conductivity of polymer-bentonite GCLs as a function of polymer loading.

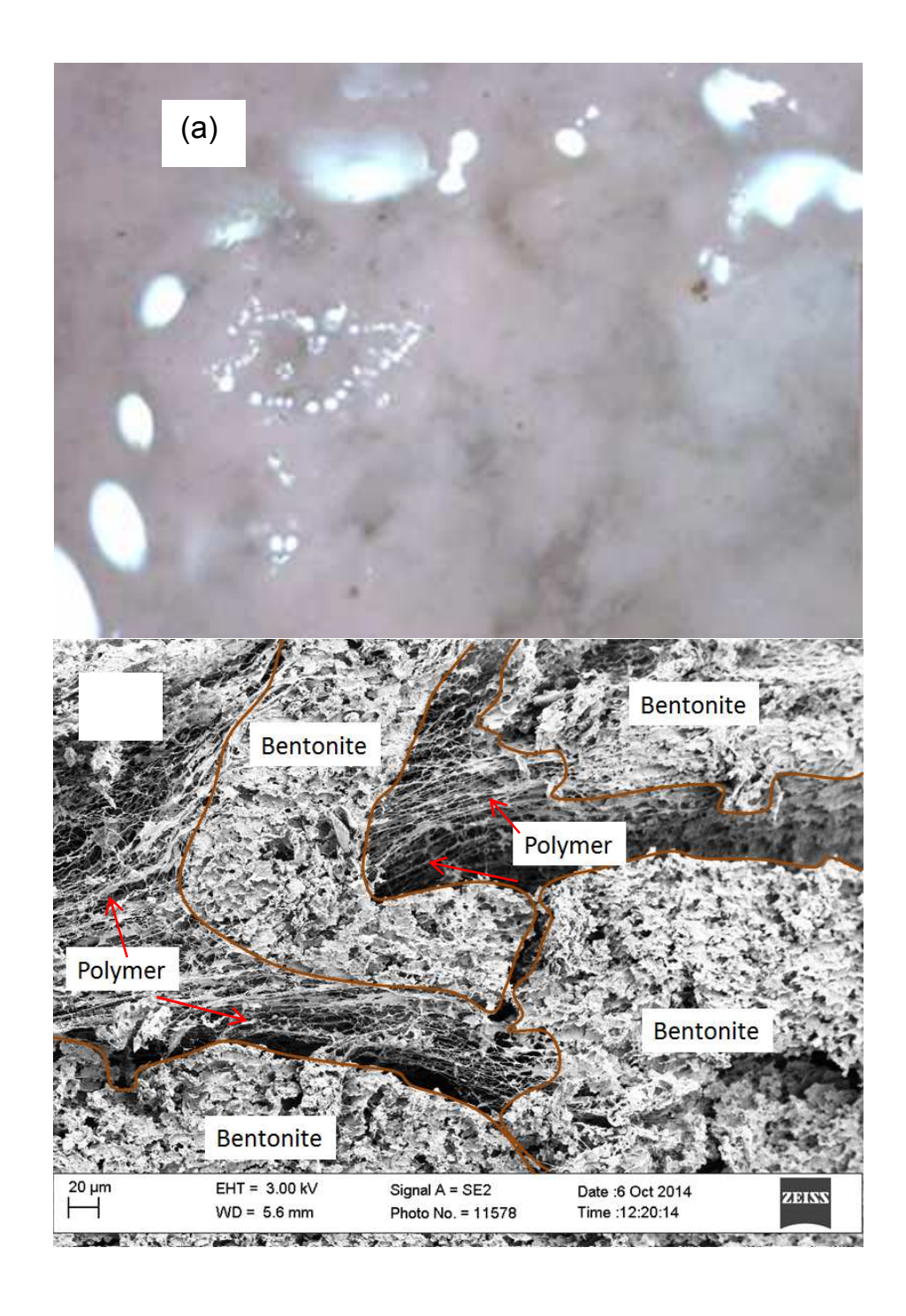
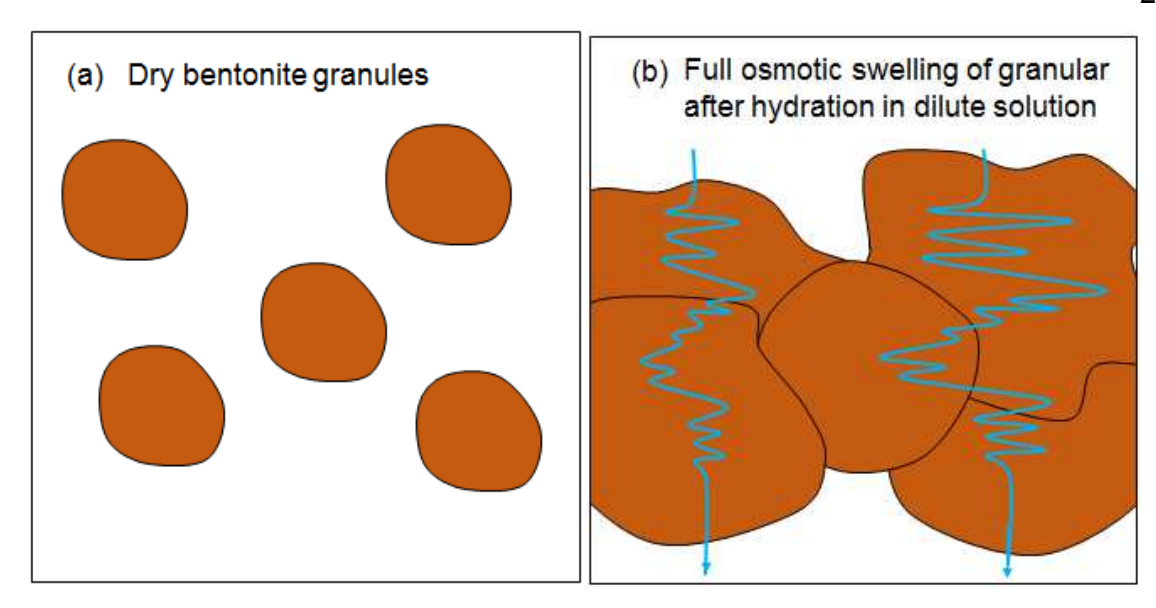


Fig. 7.9. Image of polymer-bentonite from CPM GCL at 20 x using optical microscope (a) and SEM image of freeze-dry polymer-bentonite from CPM permeated with DI water (b).



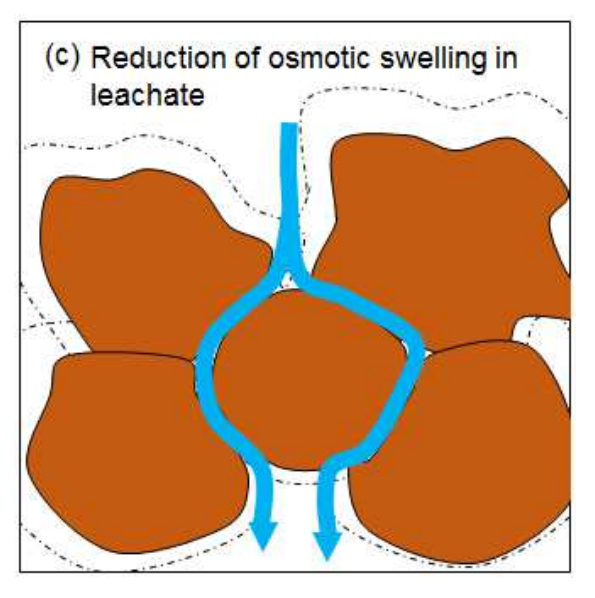
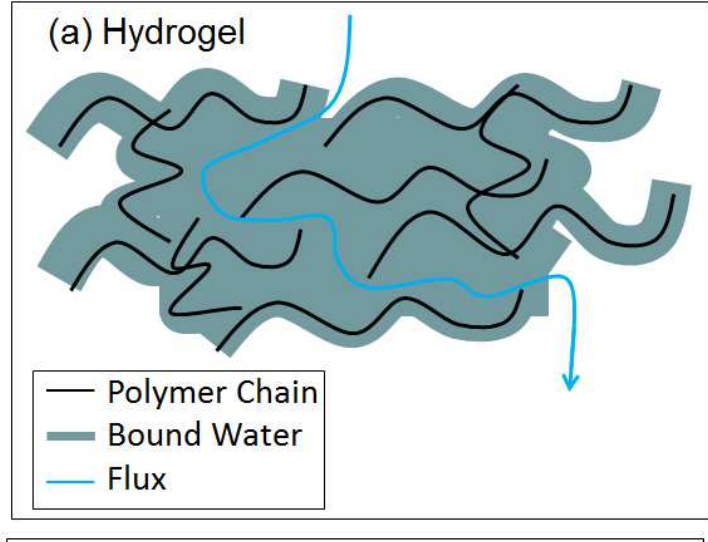


Fig. 7.10. Conceptual models for mechanism controlling hydraulic conductivity of sodium bentonite GCL: (a) bentonite granular, (b) osmotic swelling of sodium bentonite in dilute solution reduce flow between montmorillonite plate and decrease hydraulic conductivity.



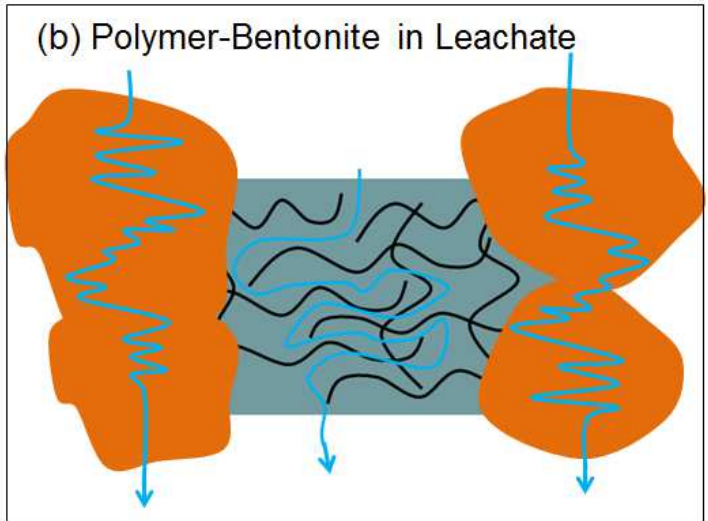


Fig. 7.11. Conceptual models for mechanism controlling hydraulic conductivity of polymerbentonite GCL: (a) hydrogel with bound water, (b) hydrogel clogs intergranular flow path and yields to low hydraulic conductivity when reduction of swell of bentonite in leachate.

# 8 EFFECT OF LOW-LEVEL RADIOACTIVE WASTE LEACHATE ON HYDRAULIC CONDUCTIVITY OF A GEOSYNTHETIC CLAY LINER

ABSTRACT: Experiments were conducted to evaluate how permeation with leachate from low-level radioactive waste (LLW) disposal facilities affects the hydraulic conductivity of a geosynthetic clay liner (GCL) with conventional sodium bentonite (CS). GCL specimens were permeated with radioactive and non-radioactive synthetic leachates (RSL and NSL) representative of leachates in LLW disposal facilities operated by the US Department of Energy. NSL is identical to RSL, but contains no radionuclides. Control tests were conducted with deionized (DI) water. GCLs permeated directly with RSL and NSL (no prehydration step) had essentially identical hydraulic conductivity (~ 3 x 10<sup>-10</sup> m/s) at 20 kPa effective stress, and were approximately 10 times more permeable to leachate than to DI water. Hydrating the GCL on a subgrade resulted in higher hydraulic conductivity at lower stresses, primarily due to a reduction in swell potential of the bentonite due to cation exchange from the subgrade. GCLs hydrated on subgrades exhibited preferential flow through localized areas. Increasing the confining stress from 20 to 450 kPa reduced the hydraulic conductivity approximately two orders of magnitude for both leachates, and eliminated preferential flow for GCLs hydrated on a subgrade prior to permeation.

#### 8.1 INTRODUCTION

Low-level radioactive waste (LLW) and mixed waste (MW) disposal facilities are operated by the US Department of Energy for long-term containment of wastes associated with clean up and decommissioning activities in the US nuclear weapons complex. These facilities employ multilayer barrier systems to control the flux of contaminants into the surrounding environment, including geosynthetic clay liner (GCLs). The long-term durability of GCLs and other geosynthetics used for barriers in contact with LLW leachate is of particular importance because the design life of LLW and MW barrier systems is required to be 1000 yr or longer.

GCLs are hydraulic barriers consisting of a thin layer of bentonite clay (~3–5 kg/m²) sandwiched between two geotextiles that are bonded by needle punching or stitching (Shackelford et al. 2000). Most GCLs contain conventional sodium bentonite (Na-B), but GCLs containing polymer-modified bentonites are available for special applications (Tian and Benson 2014). GCLs have low hydraulic conductivity to water (typically < 10<sup>-10</sup> m/s), but can be affected by chemical interactions between the bentonite and permeant solutions (Shackelford et al. 2000, Jo et al. 2001, Kolstad et al. 2004a, Benson et al. 2010). Chemical interactions that suppress swelling of the bentonite result in GCLs with higher hydraulic conductivity (Jo et al. 2001). Previous studies have shown that permeating GCLs with more aggressive leachates or leachates containing predominantly polyvalent cations reduces swelling of the bentonite and increases the hydraulic conductivity significantly (Petrov and Rowe 1997, Lin and Benson 2000, Shackelford et al. 2000, Jo et al. 2001, Kolstad et al. 2004a, b, Guyonnet et al. 2005, 2009).

Several studies have examined the hydraulic conductivity of GCLs permeated with real or synthetic municipal solid waste (MSW) leachates (Petrov and Rowe 1997, Rauen and Benson 2008, Bradshaw and Benson 2013). Rauen and Benson (2008) report that the hydraulic conductivity of GCLs exposed to actual MSW leachates is similar to the hydraulic conductivity of GCLs permeated with deionized water (DI), but also indicated that all of the studies they

evaluated were not conducted long enough to reach chemical equilibrium. In a very long-term study, Bradshaw and Benson (2013) show that the hydraulic conductivity of GCLs to MSW leachate is no more than a factor of 6 higher than the hydraulic conductivity to DI water under similar conditions. To date, however, no similar studies have been conducted to evaluate how LLW leachates affect the hydraulic conductivity GCLs.

This is the first study to evaluate how the hydraulic conductivity of conventional GCLs with Na-bentonite (named as CS in Chpater 7) is affected by permeation with LLW leachate. Tests were conducted on GCLs with radioactive and non-radioactive synthetic leachates using direct permeation and after prehydration on a typical subgrade at stresses ranging from 20 to 450 kPa.

#### 8.2 MATERIALS AND METHODS

# 8.2.1 Geosynthetic Clay Liner (GCL)

The GCL used in this study consists of granular Na-bentonite sandwiched between a non-woven geotextile (top) and a woven geotextile (bottom). Both geotextiles are polypropylene and are bonded together by needle punching. The GCL had an initial thickness = 5.1 mm, water content = 15.9%, and a swell index (SI) = 36 ml/2 g in DI water (per ASTM D 5890). Cation exchange capacity (CEC) of the bentonite in the GCL is 73.2 cmol<sup>+</sup>/kg,\_with the following bound cation mole fractions: Na (0.45), K (0.04), Ca (0.29), and Mg (0.12) (per ASTM D 7503). X-ray diffraction showed that montmorillonite is the major mineral component in the bentonite (84%), with other measureable quantities of quartz, plagioclase, feldspar, oligoclase, illite, mica, and calcite.

## 8.2.2 Permeant Liquids

Radioactive synthetic leachate (RSL), non-radioactive synthetic leachate (NSL), and DI water were used as permeant liquids. Constituents in RSL and NSL are summarized in Table 8.1. These leachate compositions were defined based on an analysis of leachate data from

lined LLW disposal facilities operated by the US Department of Energy (Tian 2012). The concentrations in Table 8.1 represent average concentrations for each constituent in the LLW database, except for radionuclides, which are near the upper bound concentrations reported by Tian (2012) and represent worst-case conditions. Non-radioactive synthetic leachate (NSL) has the same chemical composition as RSL, but does not have radionuclides. Trace metals and radionuclides in RSL and NSL account for less than 1% of the ionic strength. Exclusion of radionuclides alters the ionic strength (I) and relative abundance of monovalent and polyvalent cations (shown as RMD in Table 8.1) by less than 0.03%.

## 8.2.3 Hydraulic Conductivity Testing

Hydraulic conductivity tests on the GCL specimens were conducted in flexible-wall permeameters using the falling headwater - constant tailwater method described in ASTM D6766. GCL specimens were hydrated with the permeant liquid in the permeameter for 48 hr at an effective confining stress of 10 kPa and without a hydraulic gradient. After hydration, the effective confining stress was increased to 20 kPa and the hydraulic gradient was set at 150. Influent for the tests was contained in 50-mL burettes sealed with parafilm to prevent evaporation. Effluent was collected in 60-mL polyethylene bottles. The influent and effluent solutions were analyzed periodically for elemental concentrations by inductively coupled plasma-optical emission spectroscopy (ICP-OES) following USEPA Method 6010.

Equilibrium was defined using the hydraulic and chemical equilibrium criteria in ASTM D6766 along with an additional criterion for influent and effluent concentrations. The criteria in D6766 require no temporal trend in the hydraulic conductivity measurements, hydraulic conductivity falling within 25% of the mean for three consecutive measurements, incremental effluent volume ( $Q_{out}$ ) within 25% of the incremental influent volume ( $Q_{in}$ ) for at least 3 measurements, and the ratio  $Q_{out}/Q_{in}$  exhibiting no temporal trend. Chemical equilibrium is defined in D6766 as the electrical conductivity of the effluent ( $EC_{out}$ ) showing no temporal trend

and falling within 10% of the electrical conductivity of the influent (EC<sub>in</sub>). In addition, concentrations of major cations and pH of the effluent were required to be within 10% of those in the influent.

A typical data record from a hydraulic conductivity test with NSL is shown in Fig. 8.1. The hydraulic conductivity of the GCL decreased slowly during the first 5 pore volume of flow (PVF), and then increased appreciably until approximately 40 PVF due to cation exchange processes. At approximately 40 PVF, the EC and pH data meet the termination criteria However, after these criteria are met, the hydraulic conductivity continues to increase gradually until approximate 80 PVF, which is most likely due to slow rate-limited cation exchange processes as described in Jo et al. (2005, 2006).

Effluent concentrations for Na, Mg, and Ca for the same GCL specimen permeated with NSL are shown in Fig. 8.2. The solid horizontal lines represent the influent concentrations. Na concentrations in the effluent are substantially higher than in the influent during the early portions of the test, as soluble Na is eluted and bound Na is entrained in the effluent due to exchange reactions with Ca and Mg in the influent. The effluent Na concentration becomes comparable to the influent concentration around 80 PVF, which is similar to the PVF required to reach hydraulic equilibrium (80 PVF). In contrast, the concentrations Ca and Mg gradually increase in the effluent as the exchange reactions with Na are exhausted. The ultimate calcium concentration in the effluent is higher than the influent concentration, which may be due to dissolution of calcite as described in Bradshaw and Benson (2013).

## 8.2.4 Effective Stress

After the hydraulic conductivity tests reached chemical equilibrium, the effective stress was increased incrementally from 20 kPa to 100, 250, and 450 kPa to simulate increasing depth of waste on the liner, with the hydraulic conductivity being measured at each stress. GCL specimens were consolidated in the permeameter for 48 h after increasing the effective

confining stress before measuring the hydraulic conductivity. Before increasing the effective stress to next highest level, the GCL specimen was quickly and gently removed from the permeameter to determine the dimensions (thickness and diameter) and mass and then the test was quickly set up again. These properties were used to compute the pore volume of the GCL specimen at each stress, as summarized in Table 8.2.

#### 8.2.5 Subgrade Hydration

To simulate conditions in a LLW liner system more realistically, some of the GCL specimens were hydrated on subgrade soil prior to permeation with RSL. A subgrade was selected that represents a typical but slightly divalent cation pore water chemistry that might be encountered in practice based on the data reported by Scalia and Benson (2010) (Fig. 8.3). Batch tests were used to determine the pore water chemistry following the procedure described in ASTM D6141, as described in Scalia and Benson (2010). The following are pore water concentrations for the major cations: Na (0.73 mM), K (0.16 mM), Ca (0.99 mM), and Mg (0.68 mM).

GCL specimens were hydrated on the subgrade soil following the method described in Bradshaw and Benson (2013). Specimens of subgrade soil for GCL hydration were compacted at optimum water content in compaction molds following the procedure in ASTM D698. Each compacted subgrade specimen was extruded from the mold, and then a GCL specimen was placed on the top surface of the subgrade. The GCL specimen was overlain by a geomembrane disk and non-woven geotextile disk. The entire assembly was placed in a flexible-wall permeameter with the influent or effluent lines disconnected and with the cell pressure set at 10 kPa to mimic the stress applied by the leachate collection system. GCL specimens were hydrated using this method for 60 d, which yielded water contents between 65% and 68%.

#### 8.3 RESULTS AND DISCUSSION

GCL specimens were permeated directly with RSL, NSL, and DI water. GCL specimens hydrated on a subgrade were permeated with RSL. Summary information from the hydraulic conductivity tests is reported in Table 8.2. The PVF reported in Table 8.2 are based on the initial pore volume.

At the time this paper was prepared, the tests had been conducted for 0.1–1.8 yr. GCL specimens permeated directly with RSL and NSL met all of the termination criteria before the tests were terminated. The specimen permeated with DI water and the specimens hydrated on subgrades and permeated with RSL had not met the chemical termination criteria.

# 8.3.1 Hydraulic Conductivity

Hydraulic conductivities of the GCL specimens permeated with DI, NSL, and RSL at an effective stress of 20 kPa are shown in Fig. 8.4. Essentially the same hydraulic conductivities were obtained with NSL or RSL as the permeant liquid (~2-3 x 10<sup>-10</sup> m/s, Fig. 8.4 and Table 8.2), which reflects the small impact that radionuclides have on ionic strength and RMD of the leachate (both < 0.03%, Table 8.1). However, the hydraulic conductivities to RSL and NSL are approximately 10 times higher than the hydraulic conductivity to DI water (2.5 x 10<sup>-11</sup> m/s), which reflects the replacement of Na by multivalent cations, such as Ca and Mg in RSL or NSL, as well as the higher ionic strength of the leachate relative to DI water (Shackelford et al. 2000, Jo et al. 2001, Kolstad et al. 2004a, Benson et al. 2010).

The impact of cations in the NSL and RSL on swelling is shown in Fig. 8.5. Hydrating bentonite obtained from a new GCL in NSL or RSL results in SI of approximately 27 mL/2 g, whereas this same bentonite has SI = 36 mL/2 g in DI water. This reduction in swell is consistent with the higher hydraulic conductivities to RSL and NSL relative to DI water. The cation exchange that occurred during permeation is evident in the SI shown in Fig. 8.5 for conditions after permeation. The SI in DI water after permeation with NSL is just slightly above

the range typical of Ca-bentonite (8-10 mL/2 g, Jo et al. 2001, Kolstad et al. 2004a), indicating that permeation with NSL transformed the bentonite to a Ca-Mg form.

Bound cations on the surface of the bentonite from the GCL permeated with NSL are summarized in Table 8.3. Essentially all of the Na originally on the bentonite surface was replaced by Ca and Mg. SI of the bentonite when hydrated in NSL after permeation results in SI = 10.2 mL/2 g, just slightly lower that the SI in DI water, which is consistent with the swelling expected from a Ca-Mg bentonite.

# 8.3.2 Subgrade Hydration

Subgrade hydration was conducted to provide a more realistic scenario where the GCL would hydrate initially on the subgrade and subsequently would be contacted by leachate via permeation. Hydration prior to permeation has also been known to result in lower hydraulic conductivity to permeant liquids in some cases, a phenomenon known as the "prehydration effect" (Shackelford et al. 2000). Thus, subgrade hydration was explored to see if it would provide some degree of resistance to a change in hydraulic conductivity due to permeation by NSL or RSL. The GCL specimens hydrated on a subgrade were permeated with RSL; tests with NSL were considered un-necessary given the similarity in the major cations in both leachates and the similar hydraulic conductivities obtained by direct permeation with NSL and RSL.

Hydraulic conductivity to RSL at 20 kPa after subgrade hydration is shown in Fig. 8.4, The hydraulic conductivity to RSL after subgrade hydration is more than two orders of magnitude higher than the hydraulic conductivity obtained by direct permeation with RSL (in both replicate tests). Dye was added to the permeant liquid following the procedures proposed in Scalia and Benson (2010) to identify if preferential flow paths or sidewall leakage was occurring. The dye confirmed that preferential flow through the bentonite was occurring (Fig. 8.6). Similar dye stains were present on both GCL specimens used in the replicate tests.

Reduced swelling capacity of the bentonite after subgrade hydration is hypothesized as being responsible for the preferential flow. The SI in DI water after subgrade hydration was 21 mL/2 g, indicating that subgrade hydration had reduced the swelling capacity of the bentonite significantly (new bentonite = 36 mL/2 g, Fig. 8.5). SI of bentonite in RSL after subgrade hydration was 15.0 mL/2 g, or approximately 12 mL/2 g lower than the SI of new bentonite contacted with RSL (Fig. 8.5). Apparently, the Ca and Mg that replaced Na during subgrade hydration (Table 8.3) reduced the swelling capacity of the bentonite when it is first contacted with RSL. Consequently, some bentonite granules probably did not swell adequately, and preferential flow through the GCL occurred.

#### 8.3.3 Effect of Stress

The influence of effective stress on hydraulic conductivity of the GCL specimens permeated with RSL and NSL is shown in Fig. 8.7. The hydraulic conductivity decreased as the effective stress increased, and by 250 kPa the hydraulic conductivity to RSL and NSL was lower than the hydraulic conductivity to DI water at 20 kPa (2.5 x 10<sup>-11</sup> m/s). Thus, the impacts of cation exchange on hydraulic conductivity are reduced as the effective stress increases, and at high stress (>250 kPa) the reduction in void ratio due to the physical phenomenon (increasing stress) is dominant over increases in the size of pore spaces attributed to the chemical phenomenon (cation exchange).

High effective stress also eliminated preferential flow in the GCL hydrated on a subgrade. This GCL specimen was put back into the permeameter after inspection for dye-stained flow paths, re-equilibrated at 20 kPa, and then consolidated at an effective stress of 250 kPa. The hydraulic conductivity decreased to 2.5 x 10<sup>-11</sup> m/s, approximately three orders of magnitude (Fig. 8.7), and was comparable to the hydraulic conductivity obtained by direct permeation with RSL at 250 kPa. Apparently the preferential flow path was sealed by consolidation of the bentonite. Further investigation is planned to confirm this hypothesis.

#### 8.4 SUMMARY AND CONCLUSIONS

This study evaluated how the hydraulic conductivity of a geosynthetic clay liner (GCL) with conventional sodium bentonite is affected by permeation with liquids characteristic of leachate from low-level radioactive waste (LLW) disposal facilities operated by the US Department of Energy. GCL specimens were permeated with two synthetic leachates that were chemically identical, except one leachate was prepared without radionuclides (non-radioactive synthetic leachate) and the other with radionuclides (radioactive synthetic leachate). Control tests were conducted with deionized (DI) water. Tests were conducted by direct permeation with leachate or after hydrating the GCL on a subgrade. Effective stresses ranging from 20 to 450 kPa were employed to evaluate how the hydraulic conductivity may change as a LLW disposal facility is filled. The following conclusions are drawn based on the findings of this study:

The hydraulic conductivity of a GCL containing conventional Na bentonite gradually increases during permeation with synthetic LLW leachate. The final hydraulic conductivity is approximately 10 times higher than the hydraulic conductivity to DI water at an effective stress of 20 kPa.

Hydraulic conductivities of GCLs to non-radioactive and radioactive synthetic LLW leachate are essentially the same. Testing with non-radioactive leachate is recommended to simplify health and safety concerns when testing GCLs for LLW facilities.

Subgrade hydration results in bentonite with lower swell index and potentially higher hydraulic conductivity to leachate (approximately two orders of magnitude higher in this study at 20 kPa effective stress). The higher hydraulic conductivity is attributed to preferential flow through bentonite that does not swell sufficiently after subgrade hydration. Subgrade hydration cannot be assumed to be beneficial.

Increasing effective stress results in lower hydraulic conductivity regardless of whether the GCL is directly permeated or hydrated on a subgrade prior to permeation. In this study, the

hydraulic conductivity of GCLs permeated directly with leachate decreased by a factor of 50 times as the effective stress was increased from 20 to 450 kPa.

#### **REFERENCES**

- Benson, C., Oren, A., and Gates, W. (2010). Hydraulic conductivity of two geosynthetic clay liners permeated with a hyperalkaline solution. *Geotextiles and Geomembranes*, 28(2), 206–218.
- Bradshaw, S. and Benson, C. (2013). Effect of municipal solid waste leachate on hydraulic conductivity and exchange complex of geosynthetic clay liners, *J. Geotechnical and Geoenvironmental Engineering*, 04013038-1–17.
- Guyonnet, D., Gaucher, E., Gaboriau, H., Pons, C., Clinard, C., Norotte, V., and Didier, G. (2005). Geosynthetic clay liner interaction with leachate: Correlation between permeability, microstructure, and surface chemistry. *J. Geotechnical and Geoenvironmental Engineering*, 131(6), 740–749.
- Guyonnet, D., Touze-Foltz, N., Norotte, V., Pothier, C., Didier, G., Gailhanou, H., Blanc, P., and Warmont, F. (2009). Performance-based indicators for controlling geosynthetic clay liners in landfill applications. *Geotextiles and Geomembranes*, 27(5), 321–331.
- Jo, H., Katsumi, T., Benson, C., and Edil, T. (2001). Hydraulic conductivity and swelling of non-prehydrated GCLs permeated with single species salt solutions. *J. Geotechnical and Geoenvironmental Engineering*, 127(7), 557–567.
- Jo, H., Benson, C., Lee, J., Shackelford, C., and Edil, T. (2005). Long-term hydraulic conductivity of a non-prehydrated geosynthetic clay liner permeated with inorganic salt solutions. *J. Geotechnical and Geoenvironmental Engineering*, 131(4), 405–417.
- Jo, H., Benson, C., and Edil, T. (2006). Rate-limited cation exchange in thin bentonitie barrier layers, *Canadian Geotechnical J.*, 43, 370–391.
- Kolstad, D. Benson, C., and Edil, T. (2004a). Hydraulic conductivity and swell of nonprehydrated GCLs permeated with multispecies inorganic solutions. *J. Geotechnical and Geoenvironmental Engineering*, 130(12), 1236–1249.
- Kolstad, D., Benson, C., Edil, T., and Jo, H. (2004b). Hydraulic conductivity of a dense prehydrated GCL permeated with aggressive inorganic solutions. *Geosynthetics International*, *11*(*3*), 233–240.
- Lin, L., and Benson, C. (2000). Effect of wet-dry cycling on swelling and hydraulic conductivity of GCLs. *J. Geotechnical and Geoenvironmental Engineering*, 126(1), 40–49.
- Petrov, R. and Rowe, R. (1997). Geosynthetic clay liner (GCL) chemical compatibility by hydraulic conductivity testing and factors impacting its performance. *Canadian Geotechnical J.*, 34, 863–885.
- Rauen, T. L. and Benson, C. (2008). Hydraulic conductivity of a geosynthetic clay liner permeated with leachate from a landfill with leachate recirculation. *Proceedings GeoAmericas, International Geosynthetics Society (IGS)*, Jupiter, FL, 76–83.
- Scalia, J. and Benson, C. (2010). Preferential flow in geosynthetic clay liners exhumed from final covers with composite barriers. *Canadian Geotechnical J.*, 47(10), 1101–1111.
- Shackelford, C., Benson, C., Katsumi, T., Edil, T., and Lin, L. (2000). Evaluating the hydraulic conductivity of GCLs permeated with non-standard liquids. *Geotextiles and Geomembranes*, 18, 133–161.
- Tian, K. (2012). Durability of high-density polyethylene geomembrane in low-level radioactive waste leachate. MS Thesis, University of Wisconsin-Madison, Madison, Wisconsin.

Tian, K. and Benson, C. (2014). Hydraulic conductivity of geosynthetic clay liners exposed to low-level radioactive waste leachate. *Proceedings Waste Management '14*, WM Symposia Inc., Phoenix, AZ, 1–15.

Table 8.1. Characteristics of synthetic LLW leachates used in study

	ation & Anion rations (mM)	Trace Metal Concentrations (mM)					
Ca	4	As	0.001	Al	0.03		
Mg	6	Ва	0.002	Mn	0.01		
Na	7	Cu	0.0002	Ni	0.0003		
K	0.7	Fe	0.04	Sr	0.02		
Sulfate	7.5	Li	0.02	Zn	0.0005		
Chloride	8						
Nitrate	1.5	,	8				
Alkalinity	3.5		120				
Radio	Radionuclides		рН				
U-238 (µg/L) 1500		<sup>a</sup> lonic Strength, I (mM)			43.6		
H-3 (pCi/L) 120000							
Tc-99		b	RMD (M1/2)		0.077		
(pCi/L)	800	,					

Note: all and RMD in Table 8.1 for RSL. bRMD =  $M_M/M_D^{0.5}$ , where  $M_M$  = the total molarity of monovalent cations in the liquid (M) and  $M_D$  = total molarity of polyvalent cations in the liquid (M). Cationic strength = ionic strength computed without anion concentrations.

Table 8.2. Hydraulic conductivity of GCLs permeated with RSL, NSL, and DI water

Permeant	Hydration		Total Test	Termination Criteria		Effective	Hydraulic	Final Pore			
Liquid	1 -	PVF	time (yr)	Hydraulic	EC and pH	Major Cations Conc.	Stress (kPa)	Conductivity (m/s)	Volume (mL)		
							20	1.9x10 <sup>-10</sup>	40.5		
RSL	Direct	208	1.8	Yes	Yes	Vaa Vaa	Voc	100	6.1x10 <sup>-11</sup>	29.8	
KSL	Permeation	200	200	1.0	res	es Yes Yes	165	168	250	1.5x10 <sup>-11</sup>	22.3
							450		*		
		Direct 239		Yes	Yes	Yes	20	2.8x10 <sup>-10</sup>	38.2		
NSL	Direct		1.8				100	5.3x10 <sup>-11</sup>	28.1		
INOL	Permeation	239	1.0	165	165	165	250	1.7x10 <sup>-11</sup>	20.7		
							450	8.3x10 <sup>-12</sup>	15.5		
DI	Direct Permeation	3.8	0.1	Yes	No	No	20	2.5x10 <sup>-11</sup>	NA*		
RSL	Subgrade Hydration	18	0.1	Yes	No	No	20	2.5x10 <sup>-8</sup>	NA*		
RSL	Subgrade	35	0.3	Yes	No	No	20	3.1x10 <sup>-8</sup>	NA*		
KOL	Hydration	33	0.5	169	INU	INU	250	2.6x10 <sup>-11</sup>	NA*		

Note: \*Hydraulic conductivity tests are still being conducted.

Table 8.3. Mole fractions of bound cations of bentonite from GCL initially, after direct permeation with NSL, and after subgrade hydration

	Mole Fraction of Bound Cations in Exchange Complex						
Cation	Initial	After Direct	After Subgrade				
	IIIIIIai	Permeation with NSL	Hydration				
Na	0.45	0.01	0.40				
K	0.04	0.02	0.02				
Ca	0.29	0.45	0.38				
Mg	0.12	0.52	0.17				

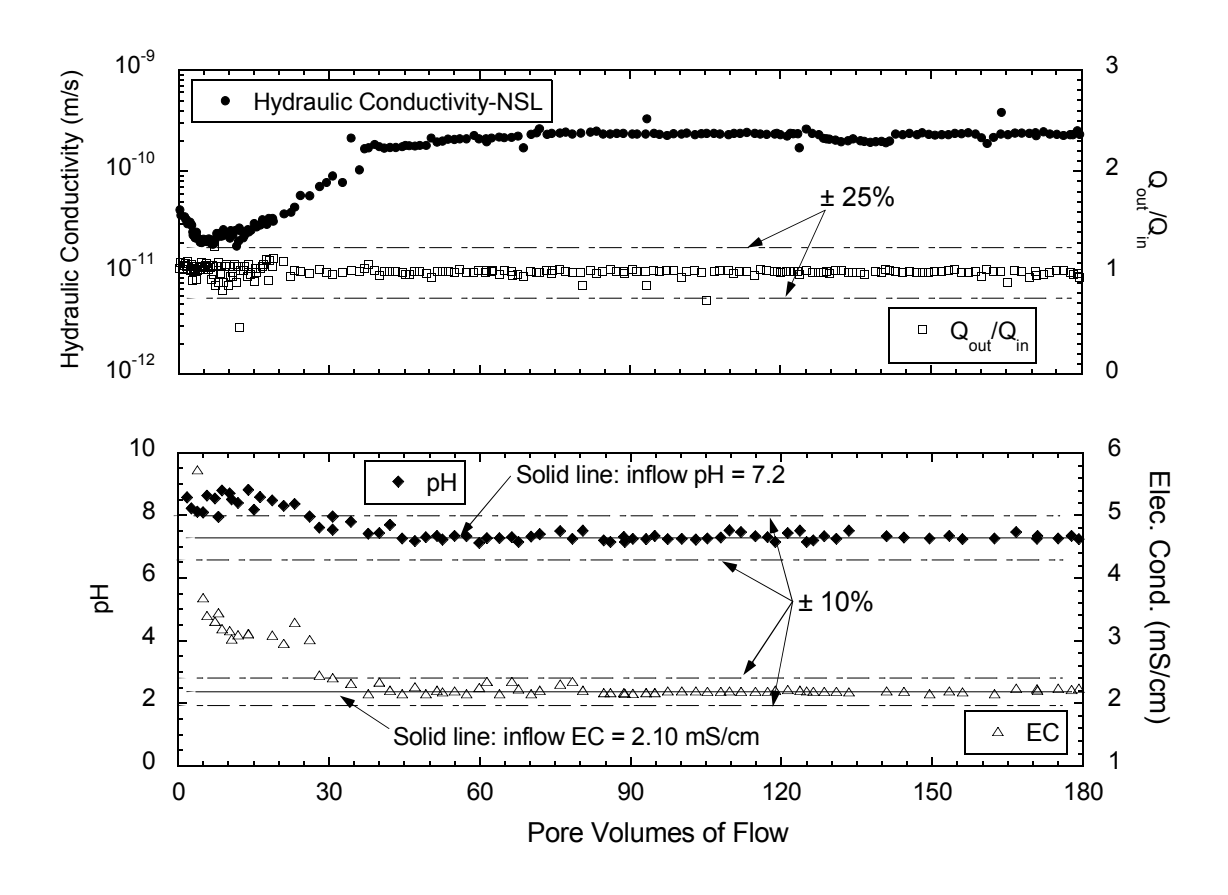


Fig. 8.1. Data from hydraulic conductivity test on GCL using NSL as the permeant liquid.

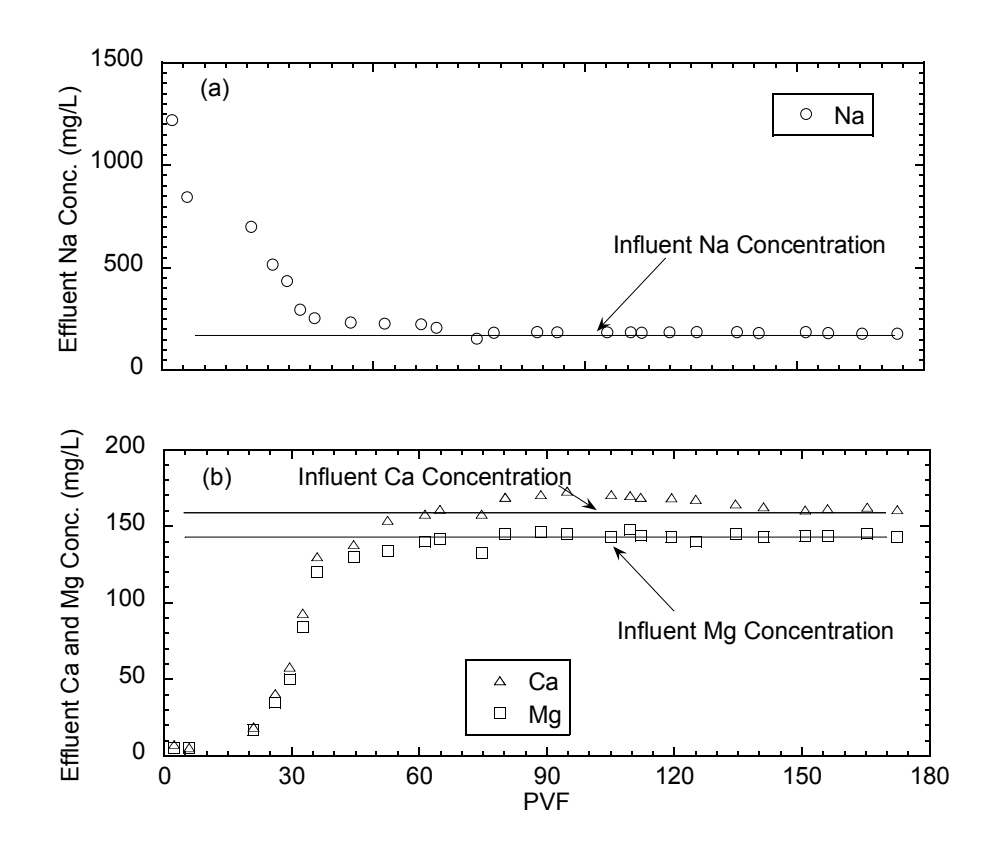


Fig. 8.2. Concentration of (a) Na and (b) Ca and Mg in effluent of GCL permeated with NSL.

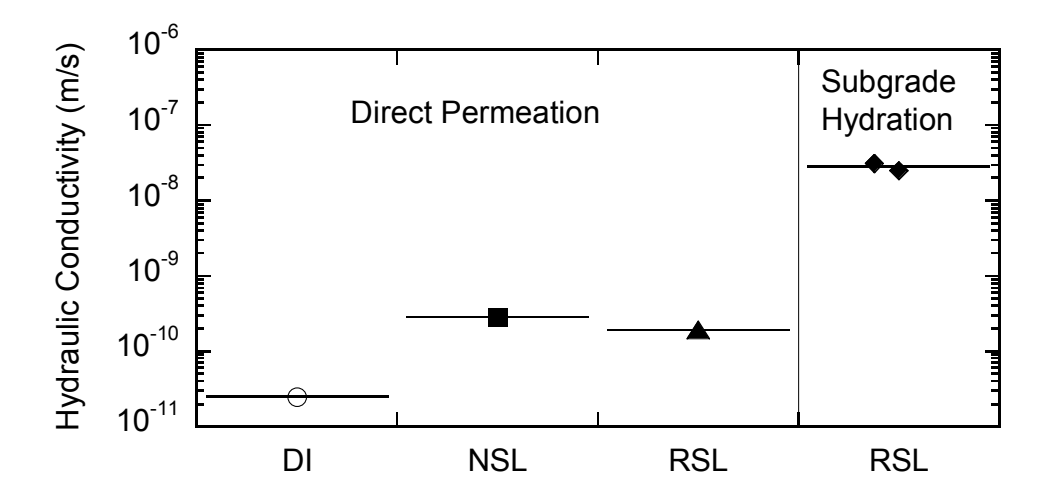


Fig. 8.3. Hydraulic conductivity of GCL to DI water, NSL, and RSL at 20 kPa effective stress after direct permeation or permeation after subgrade hydration.

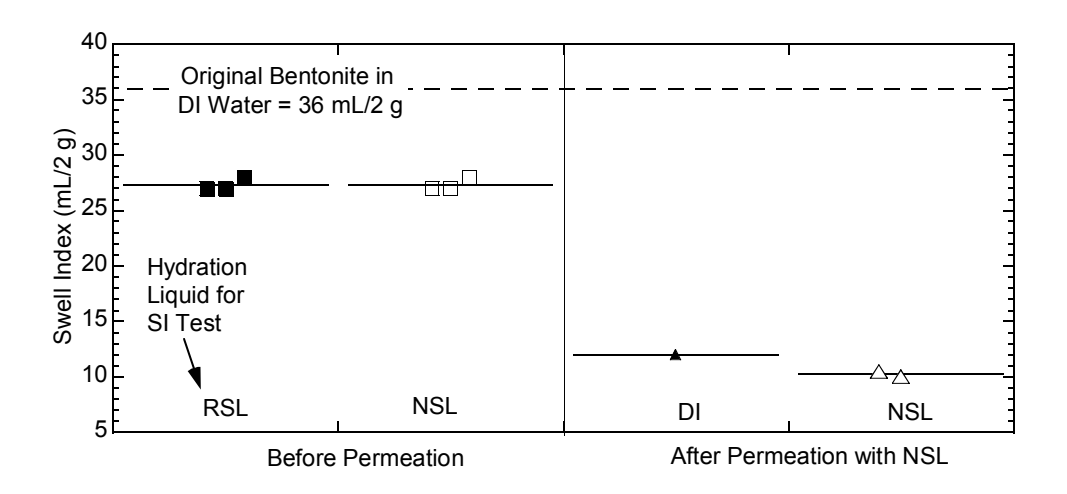


Fig. 8.4. Swell index of bentonite in DI water, NSL, and RSL before and after direct permeation with NSL.



Fig. 8.5. Dye marking preferential flow path in GCL specimen hydrated on subgrade and permeated with RSL.

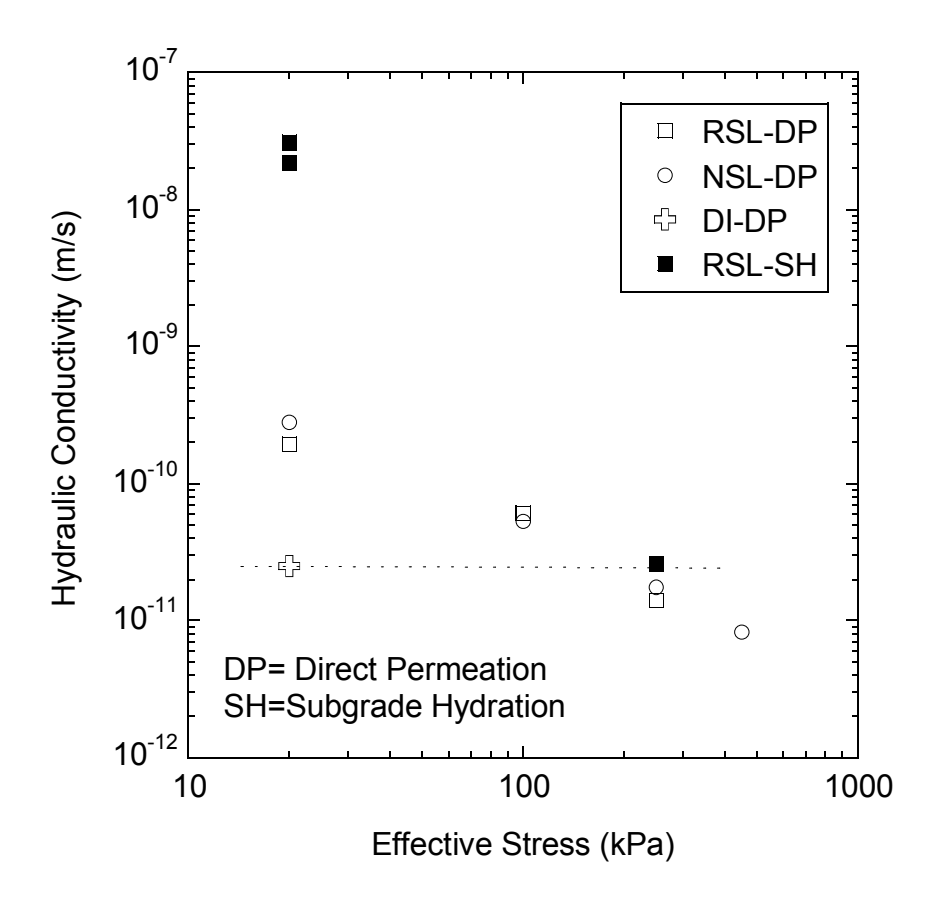


Fig. 8.6. Hydraulic conductivity vs. effective stress for GCL specimens directly permeated with DI, RSL, and NSL or permeated with RSL after subgrade hydration.